



Protecting America's Future

Y/LF-717, Rev 2
Docket No. 71-9315

Safety Analysis Report, Y-12 National Security Complex, Model ES-3100 Package with Bulk HEU Contents

Volume 2 Sections 3-8

Babcock & Wilcox Technical Services Y-12, LLC
Y-12 National Security Complex
P.O. Box 2009
Oak Ridge, Tennessee 37831

March 6, 2008

**Y-12
NATIONAL
SECURITY
COMPLEX**



MANAGED BY
BWXT Y-12, LLC
FOR THE UNITED STATES
DEPARTMENT OF ENERGY

UCN-13672 (11-03)

DISCLAIMER

This report was prepared as an account of work sponsored by an agency of the United States Government. Neither the United States Government nor any agency thereof, nor any of their employees, makes any warranty, express or implied, or assumes any legal liability or responsibility for the accuracy, completeness, or usefulness of any information, apparatus, product, or process disclosed, or represents that its use would not infringe privately owned rights. Reference herein to any specific commercial product, process, or service by trade name, trademark, manufacturer, or otherwise, does not necessarily constitute or imply its endorsement, recommendation, or favoring by the United States Government or any agency thereof. The views and opinions of authors expressed herein do not necessarily state or reflect those of the United States Government or any agency thereof.

**SAFETY ANALYSIS REPORT,
Y-12 NATIONAL SECURITY COMPLEX,
MODEL ES-3100 PACKAGE WITH BULK HEU CONTENTS**

Prepared by
Babcock & Wilcox Technical Services Y-12, LLC
Y-12 National Security Complex
P.O. Box 2009
Oak Ridge, Tennessee 37831
Managed by
Babcock & Wilcox Technical Services Y-12, LLC
for the
U. S. Department of Energy
under contract DE-AC05-00OR22800

March 6, 2008



APPROVALS

Y/LF-717, Rev. 2

**SAFETY ANALYSIS REPORT,
Y-12 NATIONAL SECURITY COMPLEX,
MODEL ES-3100 PACKAGE WITH BULK HEU CONTENTS**

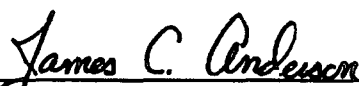
Approved by:



Walter I. North
Packaging Engineering Manager

3/4/08

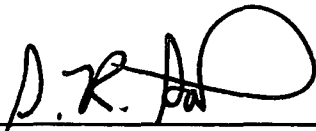
Date



James C. Anderson
Safety Analysis Report for Packaging Manager

3/4/08

Date



Steven R. Sanders
HEU Disposition and Uranium Supply Program Manager

3/4/08

Date



CONTENTS

	Page
APPROVALS	iii
FIGURES	xi
TABLES	xiii
ABBREVIATIONS	xvii
REVISION LOG	xix
1. GENERAL INFORMATION	1-1
1.1 INTRODUCTION	1-1
1.2 PACKAGE DESCRIPTION	1-1
1.2.1 Packaging	1-4
1.2.2 Containment System	1-7
1.2.3 Contents	1-10
1.2.4 Operational Features	1-23
1.3 GENERAL REQUIREMENTS FOR ALL PACKAGES	1-23
1.3.1 Minimum package size	1-23
1.3.2 Tamper-indicating feature	1-23
1.4 APPENDICES	1-27
1.4.1 PACKAGE CERTIFICATION DRAWING	1-29
1.4.2 EQUIPMENT SPECIFICATION JS-YMN3-801580-A002, <i>ES-3100 DRUM ASSEMBLY</i>	1-43
1.4.3 EQUIPMENT SPECIFICATION JS-YMN3-801580-A001, <i>ES-3100 CONTAINMENT VESSEL</i>	1-53
1.4.4 EQUIPMENT SPECIFICATION, JS-YMN3-801580-A003, <i>MANUFACTURING PROCESS SPECIFICATION FOR CASTING KAOLITE</i> <i>1600™ INTO THE ES-3100 SHIPPING PACKAGE</i>	1-67
1.4.5 EQUIPMENT SPECIFICATION, JS-YMN3-801580-A005, <i>CASTING</i> <i>CATALOG NO. 277-4 NEUTRON ABSORBER FOR THE ES-3100</i> <i>SHIPPING PACKAGE</i>	1-87
1.4.6 PACKAGE CATEGORY DETERMINATION	1-127
1.4.7 HEU OXIDE MATERIAL SPECIFICATION AS PROVIDED BY Y-12 HIGHLY ENRICHED URANIUM DISPOSITION PROGRAM OFFICE	1-131
1.4.8 DETAILED ENGINEERING DRAWINGS	1-135
1.4.9 DESIGN ANALYSES AND CALCULATIONS, DAC-PKG-801624-A001, MIXING WEIGHTS AND ELEMENTAL COMPOSITION OF 277-4 NEUTRON POISON USED IN THE ES-3100	1-179
1.4.10 PYROPHORICITY OF URANIUM METAL	1-207
SECTION 1 REFERENCES	1-227
2. STRUCTURAL EVALUATION	2-1
2.1 DESCRIPTION OF STRUCTURAL DESIGN	2-2
2.1.1 Discussion	2-2
2.1.2 Design Criteria	2-5

CONTENTS

	Page
2.1.3 Weights and Centers of Gravity	2-15
2.1.4 Identification of Codes and Standards for Package Design	2-15
2.2 MATERIALS	2-19
2.2.1 Material Properties and Specifications	2-19
2.2.2 Chemical, Galvanic, or Other Reactions	2-19
2.2.3 Effects of Radiation on Materials	2-26
2.3 FABRICATION AND EXAMINATION	2-27
2.3.1 Fabrication	2-27
2.3.2 Examination	2-29
2.4 LIFTING AND TIE-DOWN STANDARDS FOR ALL PACKAGES	2-31
2.4.1 Lifting Devices	2-31
2.4.2 Tie-Down Devices	2-32
2.5 GENERAL CONSIDERATIONS	2-32
2.5.1 Evaluation by Test	2-32
2.5.2 Evaluation by Analysis	2-35
2.6 NORMAL CONDITIONS OF TRANSPORT	2-36
2.6.1 Heat	2-38
2.6.2 Cold	2-40
2.6.3 Reduced External Pressure	2-41
2.6.4 Increased External Pressure	2-41
2.6.5 Vibration	2-44
2.6.6 Water Spray	2-46
2.6.7 Free Drop	2-47
2.6.8 Corner Drop	2-48
2.6.9 Compression	2-48
2.6.10 Penetration	2-50
2.7 HYPOTHETICAL ACCIDENT CONDITIONS	2-51
2.7.1 Free Drop	2-54
2.7.2 Crush	2-64
2.7.3 Puncture	2-70
2.7.4 Thermal	2-71
2.7.5 Immersion—Fissile Material	2-80
2.7.6 Immersion—All Packages	2-81
2.7.7 Deep Water Immersion Test	2-81
2.7.8 Summary of Damage	2-81
2.8 ACCIDENT CONDITIONS FOR AIR TRANSPORT OF PLUTONIUM	2-96
2.9 ACCIDENT CONDITIONS FOR FISSILE MATERIAL PACKAGES FOR AIR TRANSPORT	2-96
2.9a SPECIAL FORM	2-96
2.9b FUEL RODS	2-96
2.10 APPENDICES	2-97
2.10.1 ES-3100 CONTAINMENT VESSEL ASME CODE EVALUATION	2-99
2.10.2 IMPACT ANALYSES OF ES-3100 DESIGN CONCEPTS USING BOROBOND AND CAT 277-4 NEUTRON ABSORBERS	2-157
2.10.3 KAOLITE PROPERTIES	2-463
2.10.4 CATALOG 277-4 PROPERTIES	2-535

CONTENTS

	Page
2.10.5 BOROBOND4 PROPERTIES	2-645
2.10.6 RECOMMENDED RANDOM VIBRATION AND SHOCK TEST SPECIFICATIONS FOR CARGO TRANSPORTED ON SST AND SGT TRAILERS	2-659
2.10.7 TEST REPORT OF THE ES-3100 PACKAGE, VOLUME 1 - MAIN REPORT, ORNL/NTRC-013/V1, REV. 0, SEPTEMBER 10, 2004	2-677
2.10.8 THE ES-3100 TEST REPORT; VOL. 3, APPENDIX K - TU-4 DATA SHEETS	2-809
2.10.9 PACKAGING MATERIALS OUTGASSING STUDY FINAL REPORT	2-853
SECTION 2 REFERENCES	2-893
3. THERMAL EVALUATION	3-1
3.1 DISCUSSION	3-1
3.1.1 Design Features	3-3
3.1.2 Content's Decay Heat	3-4
3.1.3 Summary Tables of Temperatures	3-6
3.1.4 Summary Tables of Maximum Pressures	3-14
3.2 SUMMARY OF THERMAL PROPERTIES OF MATERIALS	3-17
3.2.1 Material properties	3-17
3.2.2 Component Specifications	3-18
3.3 GENERAL CONSIDERATIONS	3-18
3.3.1 Evaluation by Analysis	3-18
3.3.2 Evaluation by Test	3-18
3.3.3 Margins of Safety	3-24
3.4 THERMAL EVALUATION UNDER NORMAL CONDITIONS OF TRANSPORT	3-28
3.4.1 Heat and Cold	3-28
3.4.2 Maximum Normal Operating Pressure	3-30
3.4.3 Maximum Thermal Stresses	3-30
3.5 HYPOTHETICAL ACCIDENT THERMAL EVALUATION	3-32
3.5.1 Initial Conditions	3-32
3.5.2 Fire Test Conditions	3-33
3.5.3 Maximum Temperatures and Pressure	3-35
3.5.4 Accident Conditions for Fissile Material Packages for Air Transport	3-39
3.6 APPENDICES	3-41
3.6.1 THERMAL EVALUATION OF THE ES-3100 SHIPPING CONTAINER FOR NCT AND HAC (CONCEPTUAL DESIGN WITH BOROBOND4 NEUTRON ABSORBER)	3-43
3.6.2 THERMAL EVALUATION OF THE ES-3100 SHIPPING CONTAINER FOR NCT AND HAC (FINAL DESIGN WITH CATALOG 277-4 NEUTRON ABSORBER)	3-83
3.6.3 THERMAL STRESS EVALUATION OF THE ES-3100 SHIPPING CONTAINER DRUM BODY ASSEMBLY FOR NCT (FINAL DESIGN WITH CATALOG 277-4 NEUTRON ABSORBER)	3-123
3.6.4 CONTAINMENT VESSEL PRESSURE DUE TO NORMAL CONDITIONS OF TRANSPORT FOR THE PROPOSED CONTENTS	3-147

CONTENTS

	Page
3.6.5 CONTAINMENT VESSEL PRESSURE DUE TO HYPOTHETICAL ACCIDENT CONDITIONS FOR THE PROPOSED CONTENTS	3-155
3.6.6 SILICONE RUBBER THERMAL PROPERTIES FROM THERM 1.2 DATABASE	3-163
SECTION 3 REFERENCES	3-165
4. CONTAINMENT	4-1
4.1 DESCRIPTION OF THE CONTAINMENT BOUNDARY	4-2
4.1.1 Containment Boundary	4-2
4.1.2 Special Requirements for Plutonium	4-4
4.2 GENERAL CONSIDERATIONS	4-4
4.2.1 Type A Fissile Packages	4-4
4.2.2 Type B Packages	4-4
4.3 CONTAINMENT UNDER NORMAL CONDITIONS OF TRANSPORT (TYPE B PACKAGES)	4-6
4.4 CONTAINMENT UNDER HYPOTHETICAL ACCIDENT CONDITIONS (TYPE B PACKAGES)	4-8
4.5 LEAKAGE RATE TESTS FOR TYPE B PACKAGES	4-10
4.6 APPENDICES	4-11
4.6.1 DETERMINATION OF A_2 FOR THE ES-3100 PACKAGE WITH HEU CONTENTS	4-13
4.6.2 CALCULATION OF THE ES-3100 CONTAINMENT VESSEL'S REGULATORY REFERENCE AIR LEAKAGE RATES	4-23
SECTION 4 REFERENCES	4-35
5. SHIELDING EVALUATION	5-1
5.1 DESCRIPTION OF SHIELDING DESIGN	5-1
5.1.1 Design Features	5-1
5.1.2 Summary Table of Maximum Radiation Levels	5-1
5.2 SOURCE SPECIFICATION	5-1
5.3 DOSE RATE ANALYSIS MODELS	5-3
5.3.1 Packaging Model Conservative Features	5-7
5.3.2 Photon model for 36-kg HEU metal content	5-9
5.3.3 Neutron model for 36-kg HEU metal content	5-11
5.3.4 Photon model for 24-kg HEU oxide content	5-11
5.3.5 Neutron model for 24-kg HEU oxide content	5-11
5.4 SHIELDING EVALUATION	5-11
5.5 APPENDICES	5-15
5.5.1 ORIGEN INPUT DATA FROM TABLE 5.3	5-17
5.5.2 CSASN AND ICE INPUT FROM TABLE 5.8	5-19
5.5.3 MORSE ROUTINES AND INPUT DATA	5-21
SECTION 5 REFERENCES	5-39

CONTENTS

	Page
6. CRITICALITY EVALUATION	6-1
6.1 DESCRIPTION OF THE CRITICALITY DESIGN	6-1
6.1.1 Design Features	6-1
6.1.2 Summary of the Criticality Evaluation	6-2
6.1.3 Criticality Safety Index	6-4
6.2 PACKAGE CONTENTS	6-5
6.2.1 Fissile Material Contents	6-5
6.2.2 Convenience Cans, Teflon and Polyethylene Bottles, and 277-4 Canned Spacers	6-32
6.2.3 Packing Materials	6-32
6.2.4 Package Content Loading Restrictions	6-33
6.3 GENERAL CONSIDERATIONS	6-34
6.3.1 Model Configuration	6-35
6.3.2 Material Properties	6-52
6.3.3 Computer Codes and Cross-Section Libraries	6-54
6.3.4 Demonstration of Maximum Reactivity	6-66
6.4 SINGLE PACKAGE EVALUATION	6-67
6.4.1 Solid HEU Metal of Specified Geometric Shapes	6-68
6.4.2 HEU Solid Metal of Unspecified Geometric Shapes or HEU Broken Metal	6-74
6.4.3 HEU Oxide	6-75
6.4.4 UNH Crystals	6-77
6.5 EVALUATION OF PACKAGE ARRAYS UNDER NORMAL CONDITIONS OF TRANSPORT	6-78
6.5.1 Solid HEU Metal of Specified Geometric Shapes	6-78
6.5.2 HEU Solid Metal of Unspecified Geometric Shapes or HEU Broken Metal	6-81
6.5.3 HEU Oxide	6-82
6.5.4 UNH Crystals	6-82
6.6 EVALUATION OF PACKAGE ARRAYS UNDER HYPOTHETICAL ACCIDENT CONDITIONS	6-83
6.6.1 Solid HEU Metal of Specified Geometric Shapes	6-83
6.6.2 HEU Solid Metal of Unspecified Geometric Shapes or HEU Broken Metal	6-84
6.6.3 HEU Oxide	6-85
6.6.4 UNH Crystals	6-85
6.7 FISSILE MATERIAL PACKAGES FOR AIR TRANSPORT	6-86
6.7.1 Results for Solid HEU, One Piece per Convenience Can	6-86
6.7.2 Results for TRIGA Fuel Elements, Three Pieces per Convenience Can	6-90
6.7.3 Results for HEU Broken Metal, More Than One Piece per Convenience Can	6-93
6.7.4 Conclusions	6-95
6.8 BENCHMARK EXPERIMENTS	6-95
6.8.1 Applicability of Benchmark Experiments	6-95
6.8.2 Details of Benchmark Calculations	6-96
6.8.3 Bias Determination	6-96
6.9 APPENDICES	6-97
6.9.1 FISSILE CONTENT MODELS	6-99
6.9.2 HAC PACKAGE MODEL	6-105
6.9.3 PACKAGE MATERIAL COMPOSITIONS	6-117

CONTENTS

	Page
6.9.4 QUALIFICATION OF A NEUTRON ABSORBER MATERIAL FOR THE ES-3100	6-149
6.9.5 MISCELLANEOUS INFORMATION AND DATA	6-161
6.9.6 ABRIDGED SUMMARY TABLES OF CRITICALITY CALCULATION RESULTS	6-165
6.9.7 INPUT LISTINGS OF ES-3100 CALCULATION MODELS FOR SELECT CASES	6-301
SECTION 6 REFERENCES	6-503
7. PACKAGE OPERATIONS	7-1
7.1 PACKAGE LOADING	7-1
7.1.1 Preparation for Loading	7-1
7.1.2 Loading of Contents	7-3
7.1.3 Preparation for Transport	7-7
7.2 PACKAGE UNLOADING	7-10
7.2.1 Receipt of Package from Carrier	7-10
7.2.2 Removal of Contents	7-11
7.3 PREPARATION OF EMPTY PACKAGE FOR TRANSPORT	7-12
7.4 OTHER OPERATIONS	7-12
SECTION 7 REFERENCES	7-13
8. ACCEPTANCE TESTS AND MAINTENANCE PROGRAM	8-1
8.1 ACCEPTANCE TESTS	8-1
8.1.1 Visual Inspections and Measurements	8-3
8.1.2 Weld Examinations	8-4
8.1.3 Structural and Pressure Tests	8-5
8.1.4 Leakage Tests	8-5
8.1.5 Component and Material Tests	8-6
8.1.6 Shielding Tests	8-6
8.1.7 Thermal Tests	8-6
8.1.8 Miscellaneous Tests	8-7
8.2 MAINTENANCE PROGRAM	8-7
8.2.1 Structural and Pressure Tests	8-7
8.2.2 Leakage Tests	8-7
8.2.3 Component and Material Tests	8-9
8.2.4 Thermal Tests	8-9
8.2.5 Miscellaneous Tests	8-9
SECTION 8 REFERENCES	8-11

FIGURES

	Page
1.1. Schematic of the ES-3100 shipping package	1-2
1.2. Exploded view of the ES-3100 package with bulk HEU contents	1-3
1.3. Containment boundary of the ES-3100 shipping package	1-8
1.4. Typical shipping configurations inside the ES-3100 containment vessel	1-18
1.5. TRIGA fuel element	1-24
2.1. Containment vessel calculated stress locations	2-12
2.2. ES-3100 shipping package center of gravity locations	2-16
2.3. ES-3100 vibration testing arrangement	2-45
2.4. Water spray test arrangement for Test Unit -4	2-46
2.5. NCT free drop test on Test Unit-4	2-48
2.6. Compression test on Test Unit-4	2-49
2.7. Penetration test damage on Test Unit-4	2-50
2.8. 9-m drop test arrangement for all test units	2-54
2.9. 9-m drop test damage on Test Unit-4	2-56
2.10. Cumulative damage from 9-m drop and crush testing on Test Unit-2	2-58
2.11. Test Unit-3 damage from 1.2 and 9-m drop tests	2-59
2.12. 1.2 and 9-m drop test damage on Test Unit-1	2-61
2.13. 1.2 and 9-m drop test damage to Test Unit-5	2-63
2.14. Cumulative damage following 9-m crush on Test Unit-1	2-65
2.15. Cumulative damage following 9-m crush test on Test Unit-3	2-67
2.16. Cumulative damage from 9-m drop and crush testing on Test Unit-4	2-68
2.17. Cumulative damage from 9-m drop and crush testing on Test Unit-5	2-70
2.18. 28° oblique and horizontal puncture tests on Test Unit-1	2-72
2.19. 40° oblique puncture test on Test Unit-1	2-72
2.20. Horizontal puncture test over Test Unit-1's containment vessel flange	2-73
2.21. Horizontal CG puncture test on Test Unit-2	2-73
2.22. 24.6° oblique puncture test on Test Unit-3	2-74
2.23. Vertical puncture test on Test Unit-4	2-74
2.24. Horizontal puncture test over Test Unit-5's containment vessel flange	2-75
2.25. Visual comparison of the cumulative damage on the crush side surface after the three drop tests (from top to bottom: Test Unit-1, analytical results with BoroBond, analytical results with Cat 277-4)	2-84
2.26. Visual comparison of the cumulative damage on the rigid surface side after the four drop tests (from left to right: Test Unit-2, analytical results with BoroBond, analytical results with Cat 277-4)	2-87
2.27. Visual comparison of the cumulative damage on the crush plate side after the three drop tests (from left to right: Test Unit-2, analytical results with BoroBond, analytical results with Cat 277-4)	2-87
2.28. Visual comparison of the cumulative bottom damage after the three drop tests (from top to bottom: Test Unit-3, analytical results with BoroBond, analytical results with Cat 277-4) ...	2-89
2.29. Visual comparison of the cumulative lid damage after the three drop tests (from top to bottom: Test Unit-3, analytical results with BoroBond, analytical results with Cat 277-4) ...	2-90
2.30. Visual comparison of the cumulative damage after the three drop tests (from left to right: Test Unit-4, analytical results with BoroBond, analytical results with Cat 277-4)	2-92
2.31. Containment vessel markings at assembly (swivel hoist ring removed prior to testing)	2-95
2.32. Containment vessel marking after compliance testing	2-95
3.1. MSC.Patran axisymmetric finite element model of the ES-3100 shipping container with BoroBond 4—nodal locations of interest (elements representing air not shown for clarity). ...	3-6
3.2. Test units preheat arrangement.	3-25
3.3. Test unit insertion into furnace.	3-25

FIGURES

	Page
3.4. Test unit removal from furnace.	3-26
3.5. Test unit cool down and monitoring arrangement.	3-26
5.1. Cylindrical calculational model of the ES-3100 shipping package for NCT	5-6
5.2. ES-3100 HEU metal content radial (top view) geometric models	5-10
6.1. R/Z section view of ES-3100 single-unit packaging model	6-37
6.2. R/Z section view at bottom of ES-3100 single-unit packaging showing KENO V.a geometry units 1001–1003, and 1006 (partial)	6-38
6.3. R/Z section view at center of the ES-3100 single-unit packaging showing KENO V.a geometry units 1006 (partial), 1007, and 1008 (partial)	6-39
6.4. R/Z section view of near top of the ES-3100 single-unit packaging showing KENO V.a geometry units 1008 (partial) and 1010–1016	6-40
6.5. R/Z section view at the top of the ES-3100 single-unit packaging showing KENO V.a geometry units 1016–1019	6-41
6.6. R/Z section view of ES-3100 array packaging model	6-42
6.7. R/Z section view at the bottom of the ES-3100 array packaging showing KENO V.a geometry units 1001–1003, and 1006 (partial)	6-43
6.8. R/Z section view at the center of the ES-3100 array packaging showing KENO V.a geometry units 1006 (partial), 1007, and 1008 (partial)	6-44
6.9. R/Z section view of near top of the ES-3100 array packaging showing KENO V.a geometry units 1008 (partial) and 1010–1016	6-45
6.10. R/Z section view at the top of the ES-3100 array packaging showing KENO V.a geometry units 1016–1019	6-46
6.11. Model 1.	6-50
6.12. Model 2.	6-50
6.13. Model 3.	6-50
6.14. Model 4	6-51
6.15. Model 5	6-51
6.16. Model 6	6-51
6.16a. $k_{eff} + 2\sigma$ versus pitch for triangular arrangement of content in CV	6-70
6.16b. $k_{eff} + 2\sigma$ versus triangular pitch over range of CV moderation	6-71
6.16c. $k_{eff} + 2\sigma$ as a function of uranium weight fraction and moderation	6-71
6.17. K_{eff} vs. enrichment (wt % ^{235}U) for HEU ranging from 7 to 10 kg	6-88
6.18. K_{eff} vs. stainless steel shell radius (cm) for 7 kg HEU with enrichments ranging from 19 to 100 wt % ^{235}U	6-88
6.19. K_{eff} vs. Kaolite shell radius (cm) for 7 kg HEU with enrichments ranging from 19 to 100 wt % ^{235}U	6-89
6.20. K_{eff} vs. shell radius (cm) for dry and water-saturated Kaolite for 7 kg HEU at 100% enrichment	6-89
6.21. K_{eff} vs shell radius (cm) for 10.4 kg core of UZrH_x with stainless steel or Kaolite shell	6-90
6.22. K_{eff} vs. core radius (cm) for homogenized core of UZrH_x , 500 g polyethylene, and Kaolite where the Kaolite water content ranges from the dry to the water-saturated condition	6-91
6.23. k_{eff} vs. excess water from Kaolite for fissile core blanketed with a variable thickness Kaolite shell.	6-92
6.23b. k_{eff} vs. excess water from Kaolite for UZrH_x and U_3O_8 -Al contents	6-93
6.23c. k_{eff} vs. Excess water from Kaolite for UZrH_x , UO_2 -Mg, and UO_2 contents	6-93
6.24. K_{eff} vs. excess water from Kaolite for core of 1–7 kg enriched HEU broken metal at 100% enrichment, core blanketed with a variable thickness Kaolite shell	6-94
6.25. K_{eff} vs. excess water from Kaolite for core 20% enriched HEU broken metal (0.6–7 kg ^{235}U), core blanketed with a variable thickness Kaolite shell	6-94

TABLES

	Page
1.1. Uranium concentration limits	1-10
1.2. Bounding uranium isotopic concentrations in oxide	1-10
1.3. Authorized content ^a and fissile mass loading limits ^{b, c} for ground transport	1-15
1.3a. Authorized content and fissile mass loading limits ^{a, b} for air transport	1-16
1.4. TRIGA fuel specifications	1-25
2.1. Proposed HEU contents for shipment in the ES-3100	2-2
2.2. Category designations for Type B packages	2-7
2.3. Summary of load combinations for normal and hypothetical accident conditions of transport	2-10
2.4. Containment vessel allowable stress	2-11
2.5. Allowable stress intensity (S_m) for the containment boundary construction materials of construction	2-11
2.6. ES-3100 containment boundary design evaluation allowable stress comparisons	2-13
2.7. ES-3100 packaging material specifications	2-14
2.8. Packaging weights for various ES-3100 shipping package arrangements	2-17
2.9. Compliance test unit weights	2-19
2.10. Calculated center of gravity for the various ES-3100 shipping arrangements	2-20
2.11. Applicable codes and standards for Category I packaging	2-21
2.12. Mechanical properties of the metallic components of the drum assembly	2-22
2.13. Mechanical properties of the lid fastening components for the drum assembly	2-23
2.14. Mechanical properties of the cast refractory insulation	2-23
2.15. Mechanical properties of containment vessel O-rings	2-23
2.16. Mechanical properties of the metallic components of the containment boundary	2-24
2.17. Mechanical properties of the cast neutron absorber	2-25
2.18. Summary of NCT – 10CFR71.71 tests for ES-3100 package	2-34
2.19. Summary of HAC – 10CFR71.73 tests for ES-3100 package	2-34
2.20. Summary of temperatures and pressures for NCT	2-37
2.21. ES-3100 containment boundary evaluation for both hot and cold conditions	2-42
2.22. NCT ES-3100 containment boundary stress compared to the allowable stress at reduced and increased external pressures	2-43
2.23. Test and analysis summary for the ES-3100 package	2-52
2.24. Recorded height damage to Test Unit-4 from 1.2-m and 9-m drop testing	2-55
2.25. Recorded diametrical damage to Test Unit-4 from 1.2-m and 9-m drop tests	2-55
2.26. Recorded diametrical damage to Test Unit-2 from NCT and HAC drop testing	2-57
2.27. Recorded flat contour damage to Test Unit-2 from NCT and HAC drop testing	2-57
2.28. Recorded height damage to Test Unit-2 from NCT and HAC drop testing	2-57
2.29. Recorded height damage to Test Unit-3 from 1.2-m and 9-m drop testing	2-59
2.30. Recorded diametrical damage to Test Unit-3 from 1.2-m and 9-m drop testing	2-59
2.31. Recorded height damage to Test Unit-1 from 1.2-m and 9-m drop testing	2-60
2.32. Recorded diametrical damage to Test Unit-1 from 1.2-m and 9-m HAC drop testing	2-60
2.33. Recorded flat contour damage to Test Unit-1 from 1.2-m and 9-m drop testing	2-61
2.34. Recorded height damage to Test Unit-5 from 1.2-m and 9-m drop testing	2-62
2.35. Recorded diametrical damage to Test Unit-5 from 1.2-m and 9-m HAC drop testing	2-62
2.36. Recorded flat contour damage to Test Unit-5 from 1.2-m and 9-m drop testing	2-63
2.37. Recorded height damage to Test Unit-1 from the 9-m crush test	2-64
2.38. Recorded diametrical damage to Test Unit-1 from the 9-m crush test	2-64

TABLES

	Page
2.39. Recorded flat contour damage to Test Unit-1 from the 9-m crush test	2-65
2.40. Recorded height damage to Test Unit-3 from the 9-m crush test	2-66
2.41. Recorded flat contour damage to Test Unit-3 from the 9-m crush test	2-66
2.42. Recorded diametrical damage to Test Unit-3 from the 9-m crush test	2-66
2.43. Recorded height damage to Test Unit-4 from the 9-m crush test	2-67
2.44. Recorded diametrical damage to Test Unit-4 from the 9-m crush test	2-68
2.45. Recorded height damage to Test Unit-5 from the 9-m crush test	2-69
2.46. Recorded diametrical damage to Test Unit-5 from the 9-m crush tests	2-69
2.47. Recorded flat contour damage to Test Unit-5 from the 9-m crush test	2-69
2.48. 1-m (40-in.) puncture drop test description and results	2-71
2.49. Thermax temperature indicating patches for test units	2-75
2.50. Maximum HAC temperatures recorded on the test packages' interior surfaces	2-78
2.51. HAC ES-3100 containment boundary stress compared to the allowable stress	2-80
2.52. Diametrical damage comparison of Test Unit-1 with analytical predictions	2-83
2.53. Flat contour damage comparison of Test Unit-1 with analytical results	2-83
2.54. Cumulative analytical 12° slapdown drop tests maximum effective plastic strain results	2-85
2.55. Diametrical damage comparison of Test Unit-2 with analytical predictions	2-86
2.56. Flat contour damage comparison of Test Unit-2 with analytical predictions	2-86
2.57. Cumulative analytical side drop test maximum effective plastic strain results	2-88
2.58. Diametrical damage comparison of Test Unit-3 with analytical predictions	2-88
2.59. Cumulative analytical corner drop test maximum effective plastic strain results	2-91
2.60. Diametrical damage comparison of Test Unit-4 with analytical predictions	2-92
2.61. Cumulative analytical top drop test maximum effective plastic strain results	2-93
2.62. ES-3100 test package weights before and after 10 CFR 71.73(c)(4) HAC thermal testing	2-93
3.1. Isotopic mass and weight percent for the HEU contents	3-4
3.2. Decay heat for 35.2 kg of HEU content (watts)	3-5
3.3. Maximum "quasi steady-state" temperatures during NCT for the ES-3100 shipping container with various content heat loads—Kaolite density of 19.4 lb/ft ³ and BoroBond4	3-7
3.4. Maximum "quasi steady-state" temperatures during NCT for the ES-3100 shipping container with various content heat loads—Kaolite density of 30 lb/ft ³ and BoroBond4	3-8
3.5. ES-3100 shipping container maximum steady-state temperatures with Cat 277-4	3-9
3.6. ES-3100 shipping container maximum "quasi steady-state" temperatures during NCT with various content heat loads and Cat 277-4	3-10
3.7. ES-3100 shipping container HAC maximum temperatures	3-12
3.8. ES-3100 shipping container HAC maximum temperatures	3-13
3.9. Maximum HAC temperatures recorded on the test packages' interior surfaces	3-14
3.10. Total pressure inside the containment vessel at 87.81°C (190.06°F)	3-15
3.11. Total pressure inside the containment vessel at 123.85°C (254.93°F)	3-17
3.12. Thermal properties of the materials used in the thermal analysis	3-19
3.13. Mechanical properties of the materials used in the static stress analyses	3-20
3.14. Packaging material technical specifications	3-21
3.15. Component allowable service temperature and pressure	3-23
3.16. Summary of results of evaluation for the ES-3100 under NCT	3-27
3.17. Summary of results of evaluation under HAC for the ES-3100 shipping arrangement using bounding case parameters	3-27
3.18. ES-3100 test package weights before and after 10 CFR 71.73(c)(4) HAC thermal testing	3-35

TABLES

	Page
3.19. Thermax temperature indicating patches for test units	3-36
3.20. Predicted temperature adjustments (°F) for containment vessel due to HAC	3-38
3.21. Predicted temperatures of the containment vessel due to HAC	3-38
4.1. Containment requirements of transport for Type B packages	4-1
4.2. Summary of the containment vessel design and fabrication acceptance basis	4-1
4.3. Isotopic mass and weight percent for the HEU contents	4-5
4.4. Activity, A ₂ value, and number of A ₂ proposed for transport	4-5
4.5. Regulatory leakage criteria for NCT	4-7
4.6. Containment vessel verification tests criteria for NCT	4-7
4.7. Regulatory leakage criteria for HAC	4-9
4.8. Containment vessel design verification tests for HAC	4-9
5.1. Calculated external dose rates for the ES-3100 package with 36 kg of HEU metal contents ...	5-2
5.2. Calculated external dose rates for the ES-3100 package with 24 kg of HEU oxide contents ...	5-2
5.3. Radioisotope specification for all ES-3100 package analysis source calculations with HEU content and other nuclides per HEU unit weight	5-3
5.4. Photon source for one gram of HEU for all contents	5-4
5.5. Neutron source for one gram of HEU for all contents	5-4
5.6. Geometric data for the shielding analysis models of the ES-3100 shipping package as shown in Fig. 5.1 for NCT	5-5
5.7. Detector locations relative to the drum for NCT and to the containment vessel for HAC	5-7
5.8. Shielding model material specifications for the ES-3100 package with HEU content	5-8
5.9. ANSI standard photon flux-to-dose-rate conversion factors	5-12
5.10. ANSI standard neutron flux-to-dose-rate conversion factors	5-13
6.1a. Summary of criticality evaluation for solid HEU metal cylinders and bars	6-6
6.1b. Summary of criticality evaluation for solid HEU metal slugs	6-10
6.1c. Summary of criticality evaluation for solid HEU metal of unspecified geometric shapes characterized as broken metal	6-13
6.1d. Summary of criticality evaluation for HEU product and skull oxide	6-20
6.1e. Summary of criticality evaluation for UNX crystals and unirradiated TRIGA reactor fuel elements	6-24
6.2a. HEU fissile material mass loading limits for surface-only modes of transportation	6-29
6.2b. HEU fissile material mass loading limits for air transport mode of transportation	6-30
6.3. Deformation of 18.37-in.-diam ES-3100 drum projected by finite element analysis Case "3100 RUN1HL Lower Bound Kaolite May 2004"	6-48
6.4. Material compositions used in the ES-3100 calculation models	6-55
7.1. Replacement parts for the ES-3100 packaging	7-2
8.1. Acceptance tests for the drum assembly	8-2
8.2. Acceptance tests for the containment vessel assembly	8-3

ABBREVIATIONS

ALARA	as low as reasonably achievable
AM	as-manufactured
ANC	Average Net Count
ANSI	American National Standards Institute
AS	allowable stress
ASME	American Society of Mechanical Engineers
ASTM	American Society for Testing and Materials
Cat 277-4	Thermo Electron Corporation (corporate name changed to Shieldwerx) Catalog No. 277-4™ (or Cat. No. 277-4)
CD	capacity discharge
CERCA	Compagnie pour l'Étude et la Realisation de Combustibles Atomiques
CFR	Code of Federal Regulations
CMTR	certified material test report
CoC	Certificate of Compliance
CSI	criticality safety index
CV	containment vessel
CVA	containment vessel arrangement
DOE	U.S. Department of Energy
DOT	U.S. Department of Transportation
EPDM	ethylene-propylene-diene monomer
ETP	explicit triangular pack
FEA	finite element analysis
H/X ratio	hydrogen-to-fissile isotope ratio
HAC	Hypothetical Accident Conditions
HEU	highly enriched uranium
IAEA	International Atomic Energy Agency
k_{eff}	calculated neutron multiplication factor
LOD	loss on drying
LTL	lower tolerance limit
M.S.	margin of safety
MNOP	maximum normal operating pressure
MOCFR	moisture fraction inside the containment vessel
MOIFR	moisture fraction of the package external to the containment vessel
NCT	Normal Conditions of Transport
NLF	neutron leakage fraction
NRC	U.S. Nuclear Regulatory Commission
NTRC	National Transportation Research Center
OECD	Organization for Economic Cooperation and Development
ORNL	Oak Ridge National Laboratory
PGNAA	Prompt Gamma-ray Neutron Activation Analysis
ppb	parts per billion
ppm	parts per million
QA	quality assurance
QCPI	Quality Certification and Procurement
RCSB	Rackable Can Storage Box
SAR	safety analysis report
SCALE	Standardized Computer Analysis for Licensing Evaluation

ABBREVIATIONS

s_i	standard error
SRS	Savannah River Site
SS304	type 304 stainless steel
SST/SGT	Safe-Secure Trailer/Safeguards Transporter
TGA	thermogravimetric analysis
TI	transport index
TID	tamper-indicating device
TS	test sample
UNH	uranyl nitrate hexahydrate
UNX	uranyl nitrate crystals
USL	upper subcritical limit
VF	Volume Fraction
Y-12	Y-12 National Security Complex

REVISION LOG

Date	SAR Revision No.	Description	Affected Pages
2/25/05	0	Original issue	All
8/15/05	0, Page Change 1	Page changes resulting from <i>Responses to Request for Additional Information #1, Y/LF-747.</i>	title page, iv, xxiii, 1-4, 1-145, 2-2, 2-3, 2-6, 2-31, 2-32, 2-33, 2-34, 2-57, 2-59, 2-61, 2-107, 2-125, 2-131, 2-171, 2-173, 2-181, 2-183, 2-185, 2-186, 2-189, 2-367, 2-458, 2-675, 8-8, 8-9, 8-31
2/6/06	0, Page Change 2	Page changes resulting from <i>Responses to Request for Additional Information #2, Y/LF-761.</i>	All Sections
3/20/06	0, Page Change 3	Page changes resulting from <i>Responses to Request for Additional Information #3, Y/LF-764.</i>	1.38, 1.48, Appendix 1.4.1, 2-120, Table 6.4
5/8/06	0, Page Change 4	Added polyethylene bottles and nickel alloy cans as convenience containers for authorized HEU contents. (CoC Revision 1)	Various pages in chapters 1, 2, 3 and 4.
8/21/06	0, Page Change 5	Revised equipment specifications for Kaolite and 277-4 neutron absorber. (CoC Revision 3)	Appendices 1.4.4 and 1.4.5.

REVISION LOG

Date	SAR Revision No.	Description	Affected Pages
11/15/06	1	<p>Updated definition of pyrophoric uranium.</p> <p>Evaluated air transport.</p> <p>Revised criticality safety calculations to remove bias correct factors.</p> <p>Added a CSI option of 3.2.</p> <p>Increased mass of off-gassing material allowed in containment vessel.</p> <p>Increased carbon concentration in HEU contents.</p> <p>Increased Np-237 concentration in HEU contents.</p> <p>Added uranium zirconium hydride and uranium carbide as contents (TRIGA fuel).</p> <p>Revised equipment specifications for 277-4 neutron absorber. (CoC Revision 3)</p>	All Sections
3/29/07	1, Page Change 1	Updated definition of TRIGA fuel for air transport and added TRIGA-related criticality safety cases.	title pages, viii, xi, xx, 1-12, 1-13, 1-20, 6-30, 6-54, 6-64, 6-66, 6-87, 6-119, 6-240 to 6-286, 6-385 to end
5/31/07	1, Page Change 2	Revised SAR in response to RAIs dated May 9, 2007 in reference to CoC Revision 4	title pages, xiii, xx, Section 1 and Section 6
6/30/07	1, Page Change 3	Revised SAR in response to RAIs dated May 9, 2007 in reference to CoC Revision 5	title pages, table of contents, Section 1, and Section 7
7/31/07	1, Page Change 4	Removed oxidation as an option for treating pyrophoric uranium metal	title pages, xx, 1-12, 1-201, 1-203, 1-212, 2-26, 7-4
8/28/07	1, Page Change 5	Modified TRIGA fuel definition to include fuel pellets with cladding	title page, xx, 1-13, 1-17, 2-4, 6-29, 6-30a, 6-66c, 6-66d, 6-73, 6-87, 6-119a

REVISION LOG

Date	SAR Revision No.	Description	Affected Pages
10/10/07	1, Page Change 6	<ul style="list-style-type: none"> -Revised criticality safety calculations to remove bias correction factors. -Added a CSI option of 3.2. -Increased mass of off-gassing material in containment vessel to allow Teflon bottles. -Increased carbon and moisture concentration in HEU contents. -Increased Np-237 concentration in HEU contents. -Revised equipment specifications for 277-4 neutron absorber. -Details of alloys of uranium in contents definition. -More precise specification of maximum fissile mass in calculations (changed from 36 kg to 35.2 kg). 	<ul style="list-style-type: none"> Table 6.2a and supporting calculations. Table 6.2a and supporting calculations. Figure 1.4, page 1-15, and Appendices 3.6.4 and 3.6.5. Pages 1-10 and 1-11, Table 6.2a and pages 6-31 and 6-52. Pages 5-1 to 5-4, and supporting calculations. Pages 1-83 and 1-97. Page 1-12. Administrative change affecting many pages. Removed round-off. No new calculations.

REVISION LOG

Date	SAR Revision No.	Description	Affected Pages
3/6/08	2	<p>-Add the following contents for ground transport:</p> <ul style="list-style-type: none"> • HEU oxides (U₃O₈-Al and UO₂-Mg) • Research reactor fuel elements or components (clad U-Al, U₃O₈-Al, UO₂, or UO₂-Mg) <p>-Add the following contents for air transport:</p> <ul style="list-style-type: none"> • HEU oxides (UO₂, UO₂-Mg, U₃O₈, and U₃O₈-Al) • Broken HEU bulk metal and uranium-aluminum alloy of unspecified geometric form • Research reactor fuel elements or components (clad U-Al, U₃O₈-Al, UO₂, or UO₂-Mg) 	<p>1-10 through 1-17, 1-20, 1-22, 2-1, 2-2, 2-4, 2-5, 2-15, 2-17, 2-18, 2-25, 2-26, 3-15 through 3-17, 3-22, 3-147, 3-149, 3-151 through 3-155, 3-157 through 3-161, 4-2, 6-1, 6-2, 6-4, 6-5, 6-30 through 6-34, 6-51, 6-56, 6-69, 6-78, 6-83, 6-87, 6-92, 6-93, 6-95, 6-119, 6-128 through 6-130, 6-168, 6-282 through 6-286, 6-303 through 6-305, and 6-488 through 6-501.</p>

3. THERMAL EVALUATION

Design analysis, similarity, and full-scale testing (see Sect. 2) have demonstrated that the ES-3100 shipping package is in compliance with the applicable requirements of Title 10 Code of Federal Regulations (CFR) 71 (10 CFR 71) when used to ship highly enriched uranium (HEU) having a maximum gross weight up to 35.2 kg (77.60 lb). The ES-3100 has a nominal gross shipping weight that ranges from 146.88 kg (323.79 lb) to 187.81 kg (414.05 lb) for the empty and maximum weight containment vessel configurations shown in Table 2.8, respectively.

3.1 DISCUSSION

The drum assembly of the shipping package is defined as the structure that maintains the position of and provides the impact and thermal barrier surrounding the containment boundary. Preserving the location of the containment boundary within the packaging prevents reduction of the shielding and subcriticality effectiveness. The drum assembly for the ES-3100 consists of an internally flanged Type 304L stainless-steel 30-gal modified drum with two Type 304L stainless-steel inner liners, one filled with noncombustible cast refractory insulation and impact limiter and one filled with noncombustible cast neutron poison; a stainless-steel top plug with noncombustible cast refractory insulation; silicone rubber pads; silicon bronze hex-head nuts; and a stainless-steel lid and bottom (Drawing M2E801580A031, Appendix 1.4.8). The nominal weight of these components is 131.89 kg (290.76 lb).

The drum's diameters (inner diameter of 18.25 in.) and corrugations meet the requirements of Military Standard, MS27683-7. All other dimensions are controlled by Drawing M2E801580A004 (Appendix 1.4.8). Modifications to the drum from MS27683-7 include the following: (1) the overall height was increased; (2) the drum was fabricated with two false wire open ends; and (3) a 0.27-cm (12-gauge, 0.1046-in.)-thick concave cover was welded to the bottom false wire opening (Drawing M2E801508A005, Appendix 1.4.8). Four 0.795-cm (0.313-in.)-diam equally spaced holes are drilled in the top external sidewall to prevent a pressure buildup between the drum and inner liner. The holes are filled with a plastic plug to provide a moisture barrier for the cast refractory insulation during Normal Conditions of Transport (NCT). The cavity created by the inner liners is a three-tiered volume with a 37.52-cm (14.77-in.) inside diameter 13.26 cm (5.22 in.) deep, a 21.84-cm (8.60-in.) inside diameter 5.59 cm (2.20 in.) deep, and an additional 15.85-cm (6.24-in.) inside diameter 78.31-cm (30.83 in.) deep. The volume between the drum and mid liner is filled with a lightweight noncombustible cast refractory material called Kaolite 1600 (Thermal Ceramics, Appendix 2.10.3). The material is composed of portland cement, water, and vermiculite and has an average density of 358.8 kg/m³ (22.4 lb/ft³). The procedure for manufacturing and documenting the insulation, JS-YMN3-801580-A003 (Appendix 1.4.4), is referenced on Drawings M2E801580A002 and M2E801580A008 (Appendix 1.4.8) for the drum body weldment and top plug weldment, respectively. The insulation has a maximum continuous service temperature limit of 871 °C (1600 °F) due to the presence of the vermiculite and portland cement. The volume between the most internal liner and the mid liner is filled with a noncombustible cast neutron poison (absorber) material called Cat 277-4 from Thermo Electron Corporation. The material is composed of aluminum, magnesium, calcium, boron, carbon, silicone, sulfur, sodium, iron, and water. The final mixture will have an average density of 1681.9 kg/m³ (105 lb/ft³). The procedure for manufacturing and documenting this material, JS-YMN3-801580-A005 (Appendix 1.4.5), is referenced on Drawing M2E801580A002 (Appendix 1.4.8). This neutron poison material has a maximum continuous service temperature limit of 150.0 °C (302 °F). At this temperature,

the moisture inside the Cat 277-4 material remains an integral part of the composite material, and moisture content loss is negligible.

The top plug is fabricated in accordance with Drawing M2E801580A008 (Appendix 1.4.8), with an overall diameter of 36.50 cm (14.37 in.) and a height of 13.41 cm (5.28 in.). The plug's rim, bottom sheet, and top sheet are fabricated from 0.15-cm (16-gauge, 0.0598-in.)-thick Type 304/304L stainless-steel sheet per ASME SA240. Four lifting inserts are welded into the top sheet for loading and unloading operations. The internal volume of the top plug assembly is filled with Kaolite 1600 in accordance with JS-YMN3-801580-A003 (Appendix 1.4.4).

Three silicone rubber pads complete the drum assembly. One pad is placed on the bottom of the most inward liner to support the containment vessel during transport. Another pad is placed on the top shelf of the mid liner to support the top plug during transport. The final plug is placed over the top of the containment vessel lid and closure nut interface. The pads are molded to the shapes as defined on Drawing M2E801580A009 (Appendix 1.4.8). The material is silicone rubber with a Shore A durometer reading of 22 ± 5 .

The ES-3100 package is evaluated for a maximum heat source of 0.4 W (Sect. 1.2.3.7); however, no active cooling systems or specific thermal design features are required. A lightweight cast refractory insulation between the inner liner and the drum provides thermal protection of the contents from external heat sources.

Thermal criteria are applied to the package in accordance with 10 CFR 71 for NCT and Hypothetical Accident Conditions (HAC). These requirements specify that each package design provide containment, shielding, and criticality safety at temperatures ranging from -40 to 38°C (-40 to 100°F) with full insolation. Also, in accordance with *Packaging and Transportation of Radioactive Material* [10 CFR 71.43(g)], a package must be designed, constructed, and prepared for transport so that in still air at 38°C (100°F) and in the shade no accessible surface of a package would have a temperature exceeding 50°C (122°F) in a nonexclusive use shipment, or 85°C (185°F) in an exclusive use shipment. In addition, each package will experience no significant reduction in effectiveness as the result of being exposed to a thermal radiation environment of 800°C (1475°F) for 30 min with an emissivity coefficient of at least 0.9.

The maximum internal pressures and thermal stresses for both NCT and HAC are discussed and calculated (Sects. 3.4.2, 3.4.3, and 3.5.3) for use in the structural evaluation. The calculated pressures are well below the design pressures of the package components, and the effect of thermal stresses on the package is negligible (Sects. 2.6.1.2 and 2.7.4.2).

Compliance with the NCT thermal requirements is shown by analysis (Sect. 3.3.1). Since the components to be shipped have a maximum decay heat load of 0.4 W, a thermal analysis was conducted for the ES-3100 package (Appendix 3.6.2). Since the decay heat load is so meager, the maximum predicted temperature of the entire package, while stored at 38°C (100°F) in the shade, is 38.52°C (101.33°F) [Table 3.5]. The analysis shows that no accessible surface of the package would have a temperature exceeding 50°C (122°F). Therefore, the requirement of 10 CFR 71.43(g) would be satisfied. If the package is exposed to solar radiation at 38°C (100°F) in still air, the conservatively calculated temperatures at the top of the drum, center of containment vessel lid, and on the containment vessel near the O-ring sealing surfaces are 117.72°C (243.89°F), 87.81°C (190.06°F), and 87.72°C (189.90°F), respectively (Sect. 3.4.2 and Table 3.6). For conservatism, the O-ring sealing surface temperature will be assumed to be 87.81°C (190.06°F). At the low-temperature range and neglecting

decay heating, the package components would stabilize at -40°C (-40°F), which is within normal operating limits of the packaging materials (Sect. 2.2).

Five full-scale packages were subjected to the HAC thermal test following the drop, crush and puncture tests (Sects. 2.7.1 through 2.7.3). All of these test packages were exposed to a thermal radiation environment of $>800^{\circ}\text{C}$ ($>1475^{\circ}\text{F}$) for well over 30 min in a furnace. Other temperature conditions before and during the thermal testing are given in *Test Report of the ES-3100 Package* for the furnace, test packages, and package supports. The maximum temperature recorded during the tests on the external surface of any of the containment vessels was 127.2°C (261°F). This containment vessel maximum temperature reading is the highest value shown in Table 3.9. This temperature was recorded on Test Units-4 and -5 on the containment vessel sealing lid. The maximum internal temperature adjacent to the O-rings was 116°C (241°F). Temperature adjustments are then added to the containment vessel's maximum recorded temperature to correct for measuring accuracy, internal decay heating, insolation heating during cool down, location of crush plate damage, neutron poison substitution, thermal capacitance difference between mockups and actual contents, and material density variations. Detailed discussion of each temperature adjustment is provided in Sect. 3.5.3. Since Test Unit-5 was tested with a mock-up that represented the lightest proposed content, no temperature correction was needed for mass differences. The containment vessel's recorded temperature values were lower on all other test units, which consisted of much heavier mock-up contents.

3.1.1 Design Features

The drum assembly for the ES-3100 consists of an internally flanged Type 304L stainless-steel 30-gal modified drum with two Type 304L stainless-steel inner liners, one filled with noncombustible cast refractory insulation and impact limiter and one filled with noncombustible cast neutron poison; a stainless-steel top plug with noncombustible cast refractory insulation, silicone rubber pads, silicon bronze hex-head nuts, and a stainless-steel lid and bottom (Drawing M2E801580A031, Appendix 1.4.8). The drum's diameter (inner diameter of 18.25 in.) and corrugations meet the requirements of Military Standard, MS27683-7. All other dimensions are controlled by Drawing M2E801580A004 (Appendix 1.4.8). Modifications to the drum from MS27683-7 include the following: (1) the overall height was increased; (2) the drum was fabricated with two false wire open ends; and (3) a 0.27-cm (12-gauge, 0.1046-in.)-thick concave cover was welded to the bottom false wire opening (Drawing M2E801508A005, Appendix 1.4.8). Four 0.795-cm (0.313-in.)-diam equally spaced holes are drilled in the top external sidewall to prevent a pressure buildup between the drum and inner liner. The cavity created by the inner liners is a three-tiered volume with a 37.52-cm (14.77-in.) inside diameter 13.26 cm (5.22 in.) deep, a 21.84-cm (8.60-in.) inside diameter 5.59 cm (2.20 in) deep, and an additional 15.85-cm (6.24-in.) inside diameter 78.31 cm (30.83 in.) deep. Drum and inner liner wall thickness is 0.15 cm (16 gauge, 0.0598 in.).

The volume between the drum and mid liner is filled with a lightweight noncombustible cast refractory material called Kaolite 1600 (Thermal Ceramics, Appendix 2.10.3). The material is composed of portland cement, water, and vermiculite and has an average density of 358.8 kg/m^3 (22.4 lb/ft^3). The procedure for manufacturing and documenting the insulation, JS-YMN3-801580-A003 (Appendix 1.4.4), is referenced on Drawings M2E801580A002 and M2E801580A008 (Appendix 1.4.8) for the drum body weldment and top plug weldment, respectively.

The volume between the most internal liner and the mid liner is filled with a noncombustible cast neutron poison material from Thermo Electron Corporation (Cat 277-4). The material is composed of aluminum, magnesium, calcium, boron, carbon, silicone, sulfur, sodium, iron, and water. This mixture will have an average density of 1681.9 kg/m^3 (105 lb/ft^3). The procedure for manufacturing and

documenting this material, JS-YMN3-801580-A005 (Appendix 1.4.5), is referenced on Drawing M2E801580A002 (Appendix 1.4.8).

Three silicone rubber pads complete the drum assembly. One pad is placed on the bottom of the most inward liner to support the containment vessel during transport. Another pad is placed on the top shelf of the mid liner to support the top plug during transport. The final plug is placed over the top of the containment vessel lid and closure nut assembly. Pads are molded to the shapes as defined on Drawing M2E801580A009 (Appendix 1.4.8) using silicone rubber with a Shore A durometer reading of 22 ± 5 .

3.1.2 Content's Decay Heat

The maximum decay heat and radioactivity of the contents (Sect. 4) are based on a maximum of 35.2 kg of HEU in the isotopic and mass distribution at fabrication as shown in Table 3.1.

Table 3.1. Isotopic mass and weight percent for the HEU contents ^a

Nuclide	Weight percent	Mass (g)
²³² U	0.000004	0.001408
²³³ U	0.600000	211.200000
²³⁴ U	2.000000	704.000000
²³⁵ U	54.895996	19,323.390592
²³⁶ U	40.000000	14,080.000000
²³⁸ U	0.000000	0.000000
Transuranic	0.004000	1.408000
²³⁷ Np	2.500000	880.000000
Total	100.000000	35,200.000000

^a Weight percent values of individual isotopes are those that generate the largest activity within the allowable ranges presented in Sect. 1.2.3.

Using the ORIGEN-S program for determining decay heat values and predicting the isotopic decay patterns from 0 to 70 years from original fabrication, the following decay heat loads are predicted and shown in Table 3.2. Isotopic mass distribution has been calculated in Sect. 4 and shown in Table 2 of Appendix 4.6.1. The maximum decay heat load is rounded up from 0.3954 to 0.4 W, and 0.4 W is used in subsequent analyses for temperature predictions. Contributions from the transuranics and ²³⁷Np at the bottom of Table 3.2 remain constant for the time period evaluated. The decay heat per gram value used for the transuranic isotopes was an average of the decay heat values for ²³⁸Pu, ²³⁹Pu, ²⁴⁰Pu, ²⁴¹Pu, ²⁴²Pu and ²⁴¹Am.

Table 3.2. Decay heat for 35.2 kg of HEU content (watts)

Decay Heat (Watts per gram)	Isotope	DECAY TIME								
		0 years	5 years	10 years	20 years	30 years	40 years	50 years	60 years	70 years
1.7920E-02	Pb-210	0.0000E+00	2.5360E-12	1.9556E-11	1.4635E-10	4.5799E-10	1.0156E-09	1.8547E-09	3.0280E-09	4.5294E-09
2.6280E+03	Pb-212	0.0000E+00	4.7733E-05	5.3284E-05	4.9583E-05	4.4773E-05	4.0703E-05	3.6781E-05	3.3302E-05	3.0157E-05
2.8650E+02	Bi-210	0.0000E+00	2.5008E-11	1.9280E-10	1.4339E-09	4.5175E-09	1.0003E-08	1.8312E-08	2.9848E-08	4.4570E-08
2.4500E+05	Bi-212	0.0000E+00	4.2147E-04	4.6984E-04	4.3875E-04	3.9729E-04	3.5929E-04	3.2578E-04	2.9503E-04	2.6705E-04
1.4420E+02	Po-210	0.0000E+00	3.4726E-10	2.6806E-09	1.9902E-08	6.2751E-08	1.3911E-07	2.5486E-07	4.1327E-07	6.1939E-07
5.1130E+03	Rn-222	0.0000E+00	7.2355E-09	2.8942E-08	1.1555E-07	2.5990E-07	4.6077E-07	7.1995E-07	1.0331E-06	1.4075E-06
1.8230E+03	Ra-223	0.0000E+00	1.1907E-08	4.5091E-08	1.6416E-07	3.3642E-07	5.4602E-07	7.8557E-07	1.0463E-06	1.3210E-06
5.4700E+03	Ra-224	0.0000E+00	8.6260E-04	9.6272E-04	9.0111E-04	8.1639E-04	7.3783E-04	6.6774E-04	6.0459E-04	5.4760E-04
2.8380E+01	Ra-225	0.0000E+00	5.9942E-07	1.2947E-06	2.5895E-06	3.8842E-06	5.1730E-06	6.4737E-06	7.7325E-06	9.0512E-06
2.8600E-02	Ra-226	0.0000E+00	6.3026E-09	2.5170E-08	1.0068E-07	2.2553E-07	4.0071E-07	6.2624E-07	9.0009E-07	1.2243E-06
1.5200E-02	Ra-228	0.0000E+00	3.1241E-15	1.0485E-14	3.1241E-14	5.4992E-14	7.9599E-14	1.0442E-13	1.2946E-13	1.5449E-13
2.0290E+03	Ac-225	0.0000E+00	3.4282E-05	6.2564E-05	1.2513E-04	1.8769E-04	2.4983E-04	3.1239E-04	3.7453E-04	4.3709E-04
3.5000E-02	Ac-227	0.0000E+00	1.6165E-10	6.1483E-10	2.2253E-09	4.5656E-09	7.4402E-09	1.0687E-08	1.4204E-08	1.7924E-08
1.7460E+04	Ac-228	0.0000E+00	4.3760E-13	1.4701E-12	4.3760E-12	7.6949E-12	1.1161E-11	1.4652E-11	1.8143E-11	2.1659E-11
1.1250E+03	Th-227	0.0000E+00	1.2065E-08	4.5869E-08	1.6630E-07	3.4130E-07	5.5434E-07	7.9781E-07	1.0609E-06	1.3413E-06
2.6850E+01	Th-228	0.0000E+00	8.2427E-04	9.1879E-04	8.5830E-04	7.7889E-04	7.0327E-04	6.3900E-04	5.7850E-04	5.2178E-04
6.0870E-03	Th-229	0.0000E+00	3.8569E-05	5.5025E-05	1.0992E-04	1.6456E-04	2.1984E-04	2.7384E-04	3.2912E-04	3.8440E-04
5.8220E-04	Th-230	0.0000E+00	5.6970E-06	1.1353E-05	2.2747E-05	3.4100E-05	4.5494E-05	5.6970E-05	6.8037E-05	7.9513E-05
5.7940E+02	Th-231	0.0000E+00	4.5568E-05	4.5568E-05	4.5568E-05	4.5568E-05	4.5568E-05	4.5568E-05	4.5568E-05	4.5568E-05
2.6590E-09	Th-232	0.0000E+00	5.4281E-12	1.0894E-11	2.1787E-11	3.2681E-11	4.3425E-11	5.4281E-11	6.5512E-11	7.6368E-11
9.5900E+00	Th-234	0.0000E+00	0.0000E+00	0.0000E+00	0.0000E+00	0.0000E+00	0.0000E+00	0.0000E+00	0.0000E+00	0.0000E+00
1.4390E-03	Pa-231	0.0000E+00	1.3457E-07	2.6942E-07	5.3940E-07	8.0910E-07	1.0760E-06	1.3457E-06	1.6154E-06	1.8823E-06
5.2710E+01	Pa-233	0.0000E+00	0.0000E+00	0.0000E+00	0.0000E+00	0.0000E+00	0.0000E+00	0.0000E+00	0.0000E+00	0.0000E+00
7.0800E-01	U-232	9.9686E-04	9.4702E-04	9.0216E-04	8.1743E-04	7.3967E-04	6.6989E-04	6.0709E-04	5.4927E-04	4.9744E-04
2.8070E-04	U-233	5.9280E-02	5.9278E-02	5.9278E-02	5.9275E-02	5.9273E-02	5.9270E-02	5.9268E-02	5.9265E-02	5.9263E-02
1.7910E-04	U-234	1.2609E-01	1.2609E-01	1.2609E-01	1.2609E-01	1.2608E-01	1.2608E-01	1.2608E-01	1.2607E-01	1.2607E-01
6.0000E-08	U-235	1.1594E-03	1.1594E-03	1.1594E-03	1.1594E-03	1.1594E-03	1.1594E-03	1.1594E-03	1.1594E-03	1.1594E-03
2.0000E-06	U-236	2.4656E-02	2.4656E-02	2.4656E-02	2.4656E-02	2.4656E-02	2.4656E-02	2.4656E-02	2.4656E-02	2.4656E-02
8.5111E-09	U-238	0.0000E+00	0.0000E+00	0.0000E+00	0.0000E+00	0.0000E+00	0.0000E+00	0.0000E+00	0.0000E+00	0.0000E+00
1.1580E-01	transuranic	1.6306E-01	1.6306E-01	1.6306E-01	1.6306E-01	1.6306E-01	1.6306E-01	1.6306E-01	1.6306E-01	1.6306E-01
2.0100E-05	Np-237	1.7688E-02	1.7688E-02	1.7688E-02	1.7688E-02	1.7688E-02	1.7688E-02	1.7688E-02	1.7688E-02	1.7688E-02
	Total watts	3.9293E-01	3.9517E-01	3.9542E-01	3.9530E-01	3.9514E-01	3.9500E-01	3.9489E-01	3.9480E-01	3.9473E-01

3.1.3 Summary Tables of Temperatures

3.1.3.1 NCT Summary Tables

The ES-3100 shipping container has been conservatively evaluated empty of all containment vessel internal components for NCT. Prior to the change of neutron absorber from BoroBond4 to Cat 277-4, parameters, such as Kaolite 1600 density, BoroBond4 thermal conductivity, and decay heat loads, were varied to encompass the range of potential variations in material properties. The available thermal conductivity information on BoroBond4 was limited to moderate temperatures in the range of -3.89°C (25°F) to 40°C (104°F) [Eagle-Picher presentation excerpts sent to Gerry Byington via e-mail from Jim Hall on March 12, 2004]. Using the available thermal conductivity data for BoroBond4, thermal analyses for NCT and HAC have been performed and are documented in DAC-PKG-801699-A001 (summarized in Appendix 3.6.1). Nodal locations for temperatures presented are shown in Fig. 3.1. Based on the results reported in the above document and shown in Tables 3.3 and 3.4, it was determined that the higher temperatures occurred when the lowest density of the Kaolite 1600 was used. Therefore, subsequent analysis using the proposed Cat 277-4 neutron absorber during NCT uses a Kaolite 1600 density of 19.4 lb/ft^3 . The results for the steady state condition at 38°C (100°F) in the shade, and the transient condition of applying solar insolation are shown in Tables 3.5 and 3.6 for the proposed configuration (package with Cat 277-4 neutron absorber).

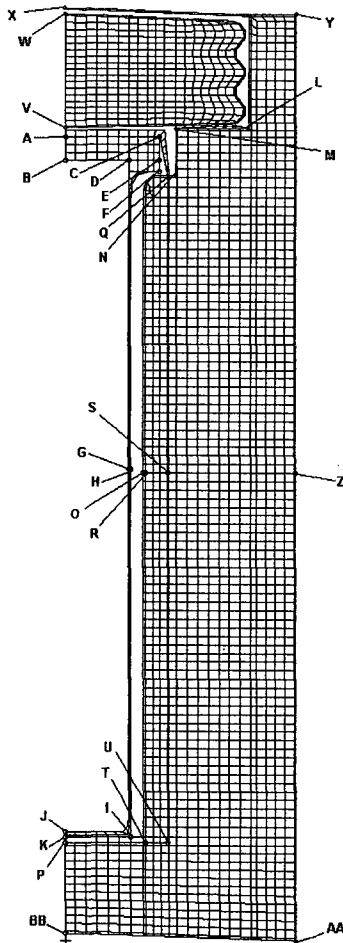


Fig. 3.1. MSC.Patran axisymmetric finite element model of the ES-3100 shipping container with BoroBond 4—nodal locations of interest (elements representing air not shown for clarity).

Table 3.3. Maximum “quasi steady-state” temperatures during NCT for the ES-3100 shipping container with various content heat loads—Kaolite density of 19.4 lb/ft³ and BoroBond4

Node ^a	Location	Maximum “quasi steady-state” temperature, °C (°F)			
		0 W	0.4 W	20 W	30 W
A	CV lid, top, center	88.30 (190.95)	88.62 (191.52)	103.84 (218.91)	111.35 (232.42)
B	CV lid, bottom, center	88.28 (190.90)	88.60 (191.48)	103.90 (219.03)	111.45 (232.62)
C	CV lid, top, outer	88.32 (190.97)	88.63 (191.54)	103.61 (218.50)	111.00(231.80)
D	CV flange at interface, inner ^b	88.24 (190.83)	88.56 (191.41)	103.87 (218.96)	111.42 (232.55)
E	CV flange at interface, outer ^b	88.25 (190.84)	88.56 (191.41)	103.77 (218.78)	111.27 (232.28)
F	CV flange, bottom, outer	88.24 (190.82)	88.55 (191.39)	103.75 (218.75)	111.25 (232.24)
G	CV shell, mid-height, inner	83.04 (181.47)	83.61 (182.50)	110.50 (230.89)	123.46 (254.23)
H	CV shell, mid-height, outer	83.04 (181.47)	83.61 (182.50)	110.49 (230.88)	123.45 (254.21)
I	CV bottom, outer	83.36 (182.04)	83.75 (182.74)	102.58 (216.64)	111.99 (233.59)
J	CV bottom, center, inner	88.37 (182.07)	83.76 (182.77)	102.70 (216.86)	112.17 (233.91)
K	CV bottom, center, outer	88.37 (181.07)	83.76 (182.77)	102.69 (216.84)	112.15 (233.87)
L	Drum liner, plug cavity, outer	98.72 (209.70)	98.80 (209.85)	102.63 (216.73)	104.58 (220.24)
M	Drum liner, plug cavity, inner	94.43 (201.97)	94.58 (202.24)	101.92 (215.46)	105.65 (222.16)
N	Drum liner, CV flange cavity, outer	89.43 (192.97)	89.63 (193.34)	99.83 (211.70)	105.01 (221.02)
O	Drum liner, CV cavity, mid-height, inner	83.12 (181.62)	83.43 (182.18)	98.63 (209.54)	106.40 (223.52)
P	Drum liner, CV cavity, bottom, inner	83.62 (182.52)	83.96 (183.13)	100.36 (212.65)	108.60 (227.48)
Q	Borobond4, top, outer	88.82 (191.88)	89.04 (192.27)	99.65 (211.38)	105.04 (221.07)
R	Borobond4, mid-height, inner	83.12 (181.62)	83.43 (182.18)	98.63 (209.53)	106.39 (223.51)
S	Borobond4, mid-height, outer	83.03 (181.46)	83.33 (182.00)	97.91 (208.23)	105.36 (221.65)
T	Borobond4, bottom, inner	83.55 (182.39)	83.85 (182.93)	98.58 (209.45)	106.03 (222.86)
U	Borobond4, bottom, outer	83.51 (182.31)	83.80 (182.83)	97.82 (208.07)	104.90 (238.82)
V	Drum plug liner, bottom, center	112.01 (233.62)	112.05 (233.69)	113.95 (237.11)	114.90 (238.82)
W	Drum plug liner, top, center	92.09 (197.77)	92.31 (198.16)	102.93 (217.27)	108.26 (226.87)
X	Drum lid, top, center	118.01 (244.42)	118.03 (244.45)	118.77 (245.79)	119.15 (246.47)
Y	Drum lid, top, outer	107.33 (225.19)	107.34 (225.22)	108.22 (226.80)	108.67 (227.60)
Z	Drum, mid-height, outer	92.27 (198.08)	92.30 (198.14)	93.81 (200.86)	94.58 (202.24)
AA	Drum bottom, outer	91.70 (197.06)	91.74 (197.13)	93.61 (200.49)	94.54 (202.18)
BB	Drum bottom, center	88.82 (191.88)	88.93 (192.07)	93.84 (200.91)	96.30 (205.35)

^a See Fig. 3.1.

^b Approximate location of the CV O-rings.

Table 3.4. Maximum “quasi steady-state” temperatures during NCT for the ES-3100 shipping container with various content heat loads—Kaolite density of 30 lb/ft³ and BoroBond4

Node ^a	Location	Maximum “quasi steady-state” temperature, °C (°F)			
		0 W	0.4 W	20 W	30 W
A	CV lid, top, center	86.56 (187.81)	86.88 (188.38)	102.98 (215.74)	109.59 (229.26)
B	CV lid, bottom, center	86.56 (187.80)	86.88 (188.38)	102.16 (215.90)	109.71 (229.47)
C	CV lid, top, outer	86.54 (187.78)	86.86 (188.34)	101.89 (215.41)	109.31 (228.75)
D	CV flange at interface, inner ^b	86.47 (187.64)	86.79 (188.21)	102.09 (215.77)	109.67 (229.40)
E	CV flange at interface, outer ^b	86.44 (187.59)	86.76 (188.16)	102.00 (215.61)	109.53 (229.15)
F	CV flange, bottom, outer	86.42 (187.56)	86.74 (188.13)	101.99 (215.58)	109.51 (229.12)
G	CV shell, mid-height, inner	81.52 (178.74)	82.09 (179.76)	109.01 (228.21)	121.98 (251.57)
H	CV shell, mid-height, outer	81.52 (178.74)	82.09 (179.76)	109.00 (228.19)	121.97 (251.55)
I	CV bottom, outer	81.32 (178.37)	81.71 (179.08)	100.57 (213.02)	109.99 (229.99)
J	CV bottom, center, inner	81.37 (178.47)	81.77 (179.18)	100.73 (213.31)	110.21 (230.38)
K	CV bottom, center, outer	81.37 (178.47)	81.77 (179.18)	100.72 (213.29)	110.19 (230.34)
L	Drum liner, plug cavity, outer	97.74 (207.93)	97.82 (208.07)	101.65 (214.96)	103.59 (218.47)
M	Drum liner, plug cavity, inner	92.91 (199.23)	93.06 (199.50)	100.40 (212.72)	104.13 (219.43)
N	Drum liner, CV flange cavity, outer	87.69 (189.84)	87.90 (190.21)	98.09 (208.57)	103.27 (217.43)
O	Drum liner, CV cavity, mid-height, inner	81.30 (178.35)	81.61 (178.90)	96.82 (206.27)	104.13 (219.43)
P	Drum liner, CV cavity, bottom, inner	81.52 (178.74)	81.86 (179.35)	98.30 (208.94)	106.56 (223.80)
Q	Borobond4, top, outer	87.36 (189.25)	87.58 (189.64)	98.19 (208.74)	103.57 (218.43)
R	Borobond4, mid-height, inner	81.30 (178.35)	81.61 (178.90)	98.81 (206.26)	104.58 (220.24)
S	Borobond4, mid-height, outer	81.37 (178.46)	81.66 (178.99)	96.24 (205.23)	103.69 (218.64)
T	Borobond4, bottom, inner	81.67 (179.01)	81.98 (179.56)	96.73 (206.12)	104.19 (219.55)
U	Borobond4, bottom, outer	81.78 (179.21)	82.07 (179.72)	96.11 (205.00)	103.23 (217.81)
V	Drum plug liner, bottom, center	111.30 (232.35)	111.34 (232.42)	113.25 (235.85)	114.21 (237.57)
W	Drum plug liner, top, center	90.70 (195.26)	90.92 (195.66)	101.53 (214.76)	106.87 (224.36)
X	Drum lid, top, center	117.74 (243.93)	117.75 (243.96)	118.50 (245.30)	118.88 (245.98)
Y	Drum lid, top, outer	107.04 (224.68)	107.06 (224.71)	107.94 (226.29)	108.39 (227.10)
Z	Drum, mid-height, outer	91.86 (197.36)	91.90 (197.41)	93.42 (200.15)	94.18 (201.53)
AA	Drum bottom, outer	91.00 (195.79)	91.04 (195.86)	92.92 (199.26)	93.87 (200.96)
BB	Drum bottom, center	87.21 (188.97)	87.31 (189.15)	92.26 (198.07)	94.74 (202.54)

^a See Fig. 3.1.

^b Approximate location of the CV O-rings.

**Table 3.5. ES-3100 shipping container maximum steady-state temperatures with Cat 277-4
(100°F ambient temperature, no insolation)**

Node map ^a	Node coordinates (in.)			Maximum "quasi steady-state" temperature (°F)		
	No.	r	z	0.4 W	20 W	30 W
	2	0.000	4.505	100.83	134.54	150.15
	255	3.180	21.528	100.75	131.57	146.21
	351	4.300	21.528	100.71	129.45	142.87
	474	4.300	37.535	100.46	117.90	125.67
	494	7.325	37.525	100.32	110.87	115.19
	536	7.385	42.755	100.21	105.50	107.19
	3655 ^c	9.185	21.528	100.28	107.58	109.92
	3780 ^c	9.185	42.755	100.21	105.29	106.89
	3807 ^c	0.000	0.320	100.43	114.39	120.08
	3865 ^c	9.185	0.008	100.32	108.97	111.97
	3880	3.178	4.505	100.74	130.48	144.23
	3888	4.300	4.505	100.71	128.60	141.42
	4721	3.500	35.275	100.59	124.08	134.90
	4740	4.300	35.275	100.57	122.92	133.15
	4746 ^c	0.000	43.065	100.20	104.99	106.43
	6158	0.000	37.579	100.57	123.14	133.42
	6339	0.000	42.859	100.25	107.42	110.04
	6359 ^b	2.530	36.075	100.80	133.51	148.56
	6365 ^b	3.425	36.075	100.79	133.33	148.28
	6369	3.750	35.525	100.79	133.27	148.20
	6385	3.750	37.175	100.78	132.85	147.58
	6389	2.310	5.025	100.97	141.27	160.06
	6398	0.000	4.775	100.96	140.91	159.55
	6399	0.000	5.025	100.96	140.94	159.60
	6574	2.530	21.528	101.33	157.70	183.56
	6647	0.000	36.075	100.80	133.56	148.63
6715	0.000	37.135	100.79	133.40	148.40	

^a See Figs. 8 through 11 in Appendix 3.6.2 for details of node locations.

^b Approximate location of the CV O-ring.

^c These nodes are at the accessible surfaces of the package (i.e., the drum, drum lid, and drum bottom plate).

Table 3.6. ES-3100 shipping container maximum “quasi steady-state” temperatures during NCT with various content heat loads and Cat 277-4 (100°F ambient temperature, with insolation)

Node map ^a	Node coordinates (in.)			Maximum “quasi steady-state” temperature (°F)			
	No.	r	z	0 W	0.4 W	20 W	30 W
	2	0.000	4.505	180.59	181.23	210.15	224.69
	255	3.180	21.528	179.33	179.93	207.32	221.43
	351	4.300	21.53	179.59	180.14	204.73	217.27
	474	4.300	37.54	198.88	199.20	212.72	219.58
	494	7.325	37.53	207.40	207.56	214.4	217.87
	536	7.385	42.76	226.44	226.49	228.31	229.24
	3655	9.185	21.528	198.09	198.15	200.81	202.16
	3780	9.185	42.755	223.47	223.51	225.13	225.95
	3807	0.000	0.320	190.48	190.70	199.84	204.43
	3865	9.185	0.008	195.87	195.97	199.91	201.90
	3880	3.178	4.505	180.72	181.28	206.65	219.52
	3888	4.300	4.505	181.03	181.55	205.08	217.01
	4721	3.500	35.275	189.45	189.90	209.53	219.47
	4740	4.300	35.275	190.56	190.98	209.37	218.68
	4746	0.000	43.065	243.86	243.89	245.32	246.03
	6158	0.000	37.579	198.42	198.84	217.12	226.32
	6339	0.000	42.859	233.98	234.06	237.32	238.95
	6359 ^b	2.530	36.075	189.28	189.90	217.07	230.51
	6365 ^b	3.425	36.075	189.27	189.88	216.88	230.23
	6369	3.750	35.525	189.23	189.85	216.79	230.12
	6385	3.750	37.175	189.39	190.00	216.57	229.72
	6389	2.310	5.025	179.94	180.70	215.75	233.27
	6398	0.000	4.775	179.99	180.76	215.52	232.92
	6399	0.000	5.025	179.99	180.76	215.55	232.96
	6574	2.530	21.528	179.27	180.35	229.19	252.87
	6647	0.000	36.075	189.40	190.02	217.24	230.72
	6715	0.000	37.14	189.44	190.06	217.14	230.54

^a See Figs. 8 through 11 in Appendix 3.6.2 for details of node locations.

^b Approximate location of the CV O-ring.

3.1.3.2 HAC Temperature Summary Tables

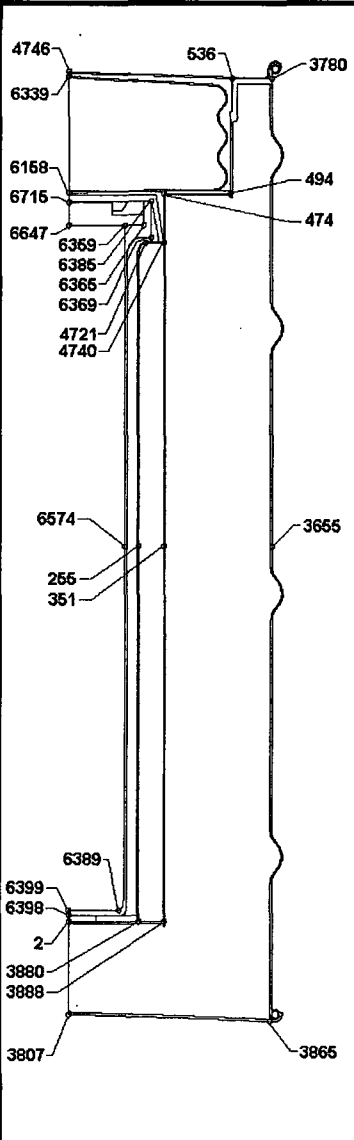
In order to predict the maximum temperature for the packaging components during HAC, a transient thermal analyses was performed on the finite element model of the ES-3100 shipping container (undamaged configuration) to simulate HAC as prescribed by 10 CFR 71.73(c)(4). A 30-min fire of 800°C (1475°F) was simulated by applying natural convection and radiant exchange boundary conditions to all external surfaces of the drum (assuming the drum is in a horizontal orientation) with content heat loads of 0, 0.4, 20, and 30 W. There are no heat flux boundary conditions simulating insolation applied to the model before and during the 30-minute fire. The initial temperature distribution within the package having content heat loads of 0.4, 20, and 30 W is obtained from their respective steady-state analyses (Table 3.5). The initial temperature distribution within the package having no content heat load (0 W) is assumed to be at a uniform temperature equal to the ambient temperature of 38°C (100°F). The content heat load is simulated by applying a uniform heat flux to the internal surfaces of the elements representing the containment vessel.

Following the 30-min fire transient analyses, 48-h cool-down transient thermal analyses are performed using the temperature distribution at the end of the fire as the initial temperature distribution. During post-fire cool-down, natural convection and radiant exchange boundary conditions are applied to all external surfaces of the drum (assuming the drum is in a horizontal orientation). Additionally, cases are analyzed in which insolation is included during the post-fire cool-down. For the cases in which insolation is applied to the model during cool-down, insolation is applied during the first 12-h period following the 30-min fire, and then alternated (off, then on) as was done for NCT.

Based on the previous analysis of the ES-3100 package using BoroBond4 (Appendix 3.6.1), it was noted that using the low-end density of Kaolite 1600 results in higher containment vessel temperatures than using the high-end density of Kaolite 1600. For this reason, the NCT and HAC thermal analyses were run using a density of 19.4 lb/ft³. Similarly, the low-end density of the Cat 277-4 material (100 lb/ft³) was also used in these analyses. However, while using these low-end densities will result in higher temperatures to the containment vessel, using the high-end densities for these two materials will result in higher temperature differences from the baseline case. Thus, HAC runs are also made for heat loads of 0, 0.4, 20, and 30 W using a Kaolite 1600 density of 30 lb/ft³ and a Cat 277-4 density of 110 lb/ft³.

The maximum temperatures calculated for the ES-3100 shipping container for HAC are summarized in Table 3.7 for the analyses using a Kaolite 1600 density of 19.4 lb/ft³ and a Cat 277-4 density of 100 lb/ft³. The maximum temperatures calculated for the ES-3100 shipping container for HAC are summarized in Table 3.8 for the analyses using a Kaolite 1600 density of 30 lb/ft³ and a Cat 277-4 density of 110 lb/ft³. The thermal analyses that use the low-end density values for Kaolite 1600 and Cat 277-4 achieve the higher package temperatures (see Table 3.7).

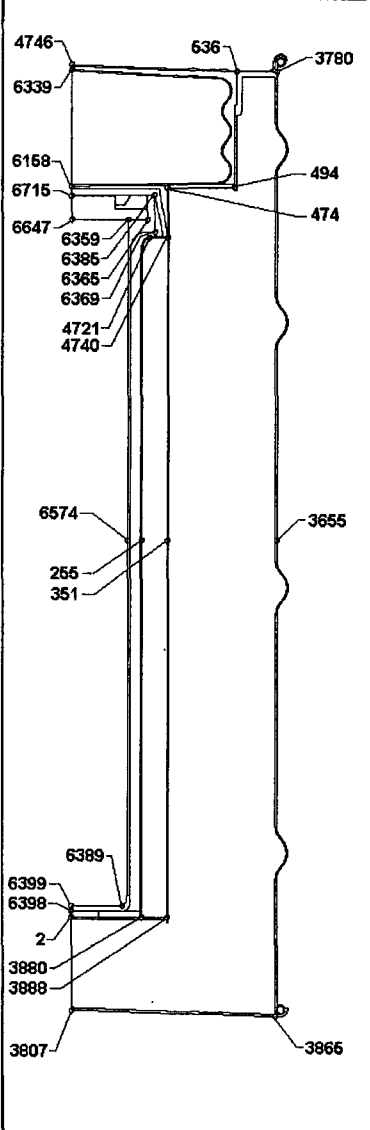
**Table 3.7. ES-3100 shipping container HAC maximum temperatures
(Kaolite 1600 density of 19.4 lb/ft³ and Cat 277-4 density of 100 lb/ft³)**

Node map	Node coordinates (in.)			HAC maximum temperature (°F)									
	No.	r	z	0 W		0.4 W		20 W		30 W			
				Insolation during cool-down?		Insolation during cool-down?		Insolation during cool-down?		Insolation during cool-down?			
				No ^b	Yes	No	Yes	No	Yes	No	Yes		
	2	0.000	4.505	225.5	232.1	226.2	232.8	255.5	261.7	269.5	275.7		
4746	536	3780	255	3.180	21.528	194.5	212.5	195.2	213.2	223.8	241.3	237.8	255.3
6339	351	4.300	21.528	195.8	211.9	196.4	212.5	222.3	237.8	234.8	250.3		
6168	474	4.300	37.535	392.9	395.0	393.2	395.4	407.6	409.7	414.2	416.3		
6715	494	7.325	37.525	671.2	672.0	671.4	672.3	679.1	680.0	682.5	683.3		
6647	536	7.385	42.755	1380.4	1380.4	1380.4	1380.4	1380.9	1380.9	1381.1	1381.1		
6369	3655	9.185	21.528	1457.8	1457.8	1457.8	1457.8	1458.0	1458.0	1458.1	1458.1		
6385	3780	9.185	42.755	1427.8	1427.8	1427.9	1427.9	1428.1	1428.1	1428.2	1428.2		
6365	3807	0.000	0.320	1454.5	1454.5	1454.5	1454.5	1454.9	1454.9	1455.0	1455.0		
6369	3865	9.185	0.008	1470.1	1470.1	1470.1	1470.1	1470.1	1470.1	1470.2	1470.2		
4721	3880	3.178	4.505	230.6	236.4	231.2	237.0	257.1	262.5	269.4	274.8		
4740	3888	4.300	4.505	236.9	241.7	237.5	242.3	261.5	266.1	272.9	277.5		
4746	4721	3.500	35.275	245.7	252.8	246.2	253.3	266.8	273.8	276.6	283.6		
6158	4740	4.300	35.275	258.4	263.5	258.8	264.0	278.1	283.1	287.1	292.1		
6339	4746	0.000	43.065	1448.0	1448.0	1448.0	1448.0	1448.2	1448.2	1448.3	1448.3		
6359 ^a	6158	0.000	37.579	308.7	311.6	309.1	312.0	328.3	331.2	337.3	340.2		
6365 ^a	6339	0.000	42.859	1335.1	1335.1	1335.2	1335.2	1336.4	1336.4	1336.9	1336.9		
6369	6359 ^a	2.530	36.075	236.7	247.6	237.3	248.3	266.2	276.6	279.8	289.9		
6385	6365 ^a	3.425	36.075	236.6	247.6	237.3	248.3	266.0	276.4	279.5	289.7		
6389	6369	3.750	35.525	236.5	247.6	237.2	248.2	265.8	276.2	279.3	289.5		
6398	6385	3.750	37.175	237.3	248.2	237.9	248.8	266.1	276.4	279.4	289.5		
3880	6389	2.310	5.025	219.0	227.4	219.9	228.2	255.3	263.1	272.2	279.9		
3888	6398	0.000	4.775	219.7	227.9	220.5	228.7	255.6	263.3	272.5	280.0		
3807	6399	0.000	5.025	219.7	227.9	220.5	228.7	255.6	263.3	272.5	280.0		
	6574	2.530	21.528	196.1	214.9	197.3	216.0	246.7	263.8	269.9	286.5		
	6647	0.000	36.075	237.2	248.0	237.9	248.6	266.8	277.0	280.4	290.4		
	6715	0.000	37.135	237.4	248.1	238.0	248.8	266.8	277.0	280.4	290.4		

^a Approximate location of the CV O-ring.

^b Baseline case for ΔT comparisons.

**Table 3.8. ES-3100 shipping container HAC maximum temperatures
(Kaolite 1600 density of 30 lb/ft³ and Cat 277-4 density of 110 lb/ft³)**

Node map	Node coordinates (in.)			HAC maximum temperature (°F)							
	No.	r	z	0 W		0.4 W		20 W		30 W	
				Insolation during cool-down?		Insolation during cool-down?		Insolation during cool-down?		Insolation during cool-down?	
				No ^b	Yes	No	Yes	No	Yes	No	Yes
	2	0.000	4.505	209.9	218.9	210.6	219.6	240.4	248.8	254.6	262.8
	255	3.180	21.528	185.5	207.7	186.1	208.4	215.1	236.6	229.3	250.6
	351	4.300	21.528	185.6	207.4	186.2	208.0	212.3	233.3	225.0	245.9
	474	4.300	37.535	342.9	345.5	343.3	345.9	358.1	360.7	365.0	367.5
	494	7.325	37.525	596.3	597.4	596.5	597.6	604.7	605.8	608.3	609.4
	536	7.385	42.755	1366.8	1366.8	1366.8	1366.8	1367.4	1367.4	1367.6	1367.6
	3655	9.185	21.528	1452.8	1452.8	1452.8	1452.8	1453.0	1453.0	1453.1	1453.1
	3780	9.185	42.755	1420.8	1420.8	1420.8	1420.8	1421.0	1421.0	1421.2	1421.2
	3807	0.000	0.320	1449.4	1449.4	1449.4	1449.4	1449.8	1449.8	1449.9	1449.9
	3865	9.185	0.008	1467.3	1467.3	1467.3	1467.3	1467.4	1467.4	1467.4	1467.4
	3880	3.178	4.505	213.1	221.4	213.7	222.0	240.0	247.9	252.5	260.3
	3888	4.300	4.505	217.0	224.4	217.6	225.0	242.1	249.1	253.8	260.7
	4721	3.500	35.275	228.0	237.5	228.5	238.0	249.7	259.0	259.7	269.0
	4740	4.300	35.275	236.5	243.8	236.9	244.3	256.7	263.9	266.0	273.2
	4746	0.000	43.065	1441.8	1441.8	1441.8	1441.8	1442.0	1442.0	1442.1	1442.1
	6158	0.000	37.579	277.3	281.8	277.8	282.3	297.5	302.0	306.7	311.2
	6339	0.000	42.859	1299.5	1299.5	1299.6	1299.6	1301.1	1301.1	1301.7	1301.7
	6359 ^a	2.530	36.075	225.1	237.3	225.8	237.9	254.7	266.1	268.3	279.6
	6365 ^a	3.425	36.075	225.0	237.3	225.7	237.9	254.5	266.0	268.1	279.3
	6369	3.750	35.525	224.9	237.2	225.6	237.8	254.3	265.8	267.9	279.2
	6385	3.750	37.175	225.5	237.6	226.2	238.3	254.6	266.1	268.0	279.2
	6389	2.310	5.025	205.3	215.9	206.2	216.8	242.0	251.9	259.2	268.9
	6398	0.000	4.775	205.8	216.3	206.7	217.1	242.2	252.0	259.2	268.8
	6399	0.000	5.025	205.8	216.3	206.7	217.1	242.2	252.0	259.3	268.8
	6574	2.530	21.528	187.8	209.1	189.0	210.2	238.9	258.4	262.4	281.3
	6647	0.000	36.075	225.6	237.7	226.3	238.3	255.2	266.5	268.9	280.0
	6715	0.000	37.135	225.8	237.8	226.4	238.4	255.2	266.5	268.9	280.0

^a Approximate location of the CV O-ring.

^b Baseline case for ΔT comparisons.

Table 3.9. Maximum HAC temperatures recorded on the test packages' interior surfaces

Temperature patch location ^a	ES-3100 Test Unit				
	1	2	3	4	5
	°C (°F)	°C (°F)	°C (°F)	°C (°F)	°C (°F)
Top plug bottom	149 (300)	163 (325)	177 (350)	177 (350)	177 (350)
Inner liner					
Flange step wall	135 (275)	163 (325)	135 (275)	135 (275)	135 (275)
BoroBond4 step	107 (225)	135 (275)	107 (225)	177 (350) ^b	121 (250)
Adjacent to CV body wall high	99 (210)	99 (210)	99 (210)	99 (210)	104 (219)
Adjacent to CV body wall middle	99 (210)	93 (199)	116 (241)	93 (199)	99 (210)
Bottom flat portion	104 (219)	99 (210)	99 (210)	127 (261)	110 (230)
Containment boundary					
Lid (external top)	116 (241)	110 (230)	116 (241)	127 (261)	127 (261)
Lid (internal)	104 (219)	104 (219)	110 (230)	110 (230)	116 (241)
Flange (external)	116 (241)	110 (230)	110 (230)	116 (241)	121 (250)
Flange (internal)	104 (219)	99 (210)	116 (241) ^b	104 (219)	116 (241)
Body wall mid height	99 (210)	88 (190)	99 (210)	82 (180)	93 (199)
Bottom end cap (center)	99 (210)	99 (210)	88 (190)	110 (230)	99 (210)
Mock-up					
Side top	82 (180)	77 (171)	77 (171)	77 (171)	99 (210)
Side middle	77 (171)	77 (171)	77 (171)	77 (171)	93 (199)
Side bottom	77 (171)	77 (171)	77 (171)	77 (171)	88 (190)

^a Refer to figures for exact locations and to Tables 5.3 through 5.7 in ORNL/NTRC-013, Vol. 1 for recorded values.

^b Temperature indicating patch may have been damaged due to impact with surrounding structure.

3.1.4 Summary Tables of Maximum Pressures

3.1.4.1 Maximum NCT Pressures

Table 3.10 summarizes the results from Appendix 3.6.4 in which the pressure of the containment vessel when subjected to the tests and conditions of NCT per 10 CFR 71.71 has been determined for the most restrictive containment vessel arrangements (CVAs) shipped in the ES-3100. The most restrictive CVAs are those in which the void volume inside the containment vessel is minimized based on content volumes and those CVAs that carry the largest mass of items that offgas at the predicted temperatures during NCT. Several convenience container heights are proposed for shipment (Fig. 1.4). Shipping configurations will use these containers in any configuration as long as it does not exceed the HEU weight limit and form and does not exceed the height constraint of the containment vessel. However, in

Table 3.10. Total pressure inside the containment vessel at 87.81°C (190.06°F) ^a

CVA	n _a (lb-mole)	n _v (lb-mole)	n _{po} (lb-mole)	n _{bo} (lb-mole)	n _{tf} (lb-mole)	n _T (lb-mole)	P _T (psia)
1	3.0855E-04	1.0057E-05	0.0000E+00	0.0000E+00	0.0000E+00	3.1861E-04	17.786
2	3.0826E-04	1.0047E-05	0.0000E+00	0.0000E+00	0.0000E+00	3.1831E-04	17.786
3	3.0227E-04	9.8522E-06	0.0000E+00	0.0000E+00	0.0000E+00	3.1212E-04	17.786
4	2.9252E-04	9.5344E-06	0.0000E+00	0.0000E+00	0.0000E+00	3.0205E-04	17.786
5	1.9163E-05	5.8795E-04	0.0000E+00	0.0000E+00	0.0000E+00	6.0711E-04	17.786
6	2.0206E-04	6.5858E-06	0.0000E+00	0.0000E+00	0.0000E+00	2.0865E-04	17.786
7	5.6450E-06	1.7320E-04	0.0000E+00	0.0000E+00	2.2296E-05	2.0114E-04	20.004
8	This configuration is bounded by CVA #3						
9	This configuration is bounded by CVA #4 ^b						
10	This configuration is bounded by CVA #4						

^a This assumes that the internal convenience cans, polyethylene or Teflon FEP bottles, and Cat 277-4 spacer cans are sealed.

^b Although CVA #9 may slightly exceed the height of the combined three 25.4 cm (10 in.) can height (CVA #4), the open-ended cans and contents produce a larger void volume and thereby lower overall pressure inside the containment vessel.

order to determine the worst-case shipping configuration, the arrangements that minimize the void volume inside the containment vessel are analyzed as follows:

1. one shipment will contain six cans with external dimensions of 10.8 cm (4.25 in.) diameter by 12.38 cm (4.875 in.) high cans;
2. one shipment will contain five cans with external dimensions of 10.8 cm (4.25 in.) diameter by 12.38 cm (4.875 in.) high cans and four can spacers;
3. one shipment will contain three cans with external dimensions of 10.8 cm (4.25 in.) diameter by 22.23 cm (8.75 in.) high and three can spacers;
4. one shipment will contain three cans with external dimensions of 10.8 cm (4.25 in.) diameter by 25.4 cm (10 in.) high;
5. one shipment will contain six nickel cans with external dimensions of 7.62 cm (3.00 in.) diameter by 12.07 cm (4.75 in.) high;
6. one shipment will contain three polyethylene bottles with external dimensions of 12.54 cm (4.94 in.) diameter by 22.1 cm (8.7 in.) high;
7. one shipment will contain three teflon bottles with external dimensions of 11.91 cm (4.69 in.) diameter by 23.88 cm (9.4 in.) high;
8. one shipment will contain a brazed assembly of two cans with final external dimensions of 10.8 cm (4.25 in.) diameter by 44.46 cm (17.50 in.) high. An empty can with external dimensions of 10.8 cm (4.25 in.) diameter by 22.23 cm (8.75 in.) high will be placed on top of the 44.46 cm (17.50 in.) high can;

9. one shipment will contain fuel rods, or tubes, or plates greater than 43.18 cm (17.00 in.) in length. These items are bundled together and protected on both ends with an open-ended can with external dimensions of ≤ 12.7 cm (5.0 in.) diameter by ≤ 22.23 cm (8.75 in.) high. Total assembly height will be ≤ 77.47 cm (30.5 in.). If space is available inside the containment vessel, stainless-steel metal scrubbers will be added on the bottom and top of this assembly or an empty can will be placed on top of this partially canned assembly; and
- 10 one shipment will contain three cans brazed together with external dimensions of 4.25-in. diameter by ~ 30 in. high.

These arrangements are shown in Fig. 1.4. To determine the ES-3100's maximum normal operating pressure, the following assumptions have been used in the calculations:

1. The HEU contents are loaded into convenience cans, and convenience cans are placed inside the containment vessel at standard temperature (T_{amb}) and pressure (P) [25°C (77°F) and 101.35 kPa (14.7 psia)] with air at a maximum relative humidity of 100%;
2. The convenience cans and bottles are assumed to be sealed to minimize the void volume inside the containment vessel;
3. Convenience can and bottle geometry does not change during pressure increase inside containment vessel;
4. If metal convenience cans are used, the total amount of polyethylene bagging and lifting slings is limited to 500 g per containment vessel shipping arrangement;
5. All offgassing material (polyethylene bagging or bottles, Teflon bottles, silicone pads, lifting slings) is limited to 1490 g for containment vessel arrangement #7 and 845 g for containment vessel arrangement #6; and
6. Containment vessel arrangements that utilize closed convenience cans with a diameter greater than 10.8 cm (4.25 in.) will not contain any materials that off gas at the temperatures associated with Normal Conditions of Transport (NCT).

3.1.4.2 Maximum HAC Pressures

Table 3.11 summarizes the results from Appendix 3.6.5 in which the pressure of the containment vessel when subjected to the tests and conditions of HAC per 10 CFR 71.73 has been determined for the most restrictive CVAs shipped in the ES-3100. The shipping configurations discussed in Sect. 3.1.4.1 are evaluated for HAC. To determine the maximum pressure generated inside the ES-3100's containment vessel due to HAC conditions, the following assumptions have been used in the calculations:

1. The initial pressure inside the containment vessel is the maximum normal operating pressure shown in Table 3.10 for each CVA at ambient temperature;
2. The convenience cans and bottles are assumed to be sealed in order to minimize the void volume inside the containment vessel;
3. Convenience can and bottle geometry does not change during pressure increase inside containment vessel or because of damage from compliance testing;

4. If metal convenience cans are used, the total amount of polyethylene bagging and lifting slings is limited to 500 g per containment vessel shipping arrangement;
5. All offgassing material (polyethylene bagging or bottles, Teflon bottles, silicone pads, lifting slings) is limited to 1490 g for containment vessel arrangement #7 and 845 g for containment vessel arrangement #6; and
6. Containment vessel arrangements that utilize closed convenience cans with a diameter greater than 10.8 cm (4.25 in.) will not contain any materials that off gas at the temperatures associated with Hypothetical Accident Conditions (HAC).

The above assumptions are very conservative because the convenience cans buckle and deform significantly under an external pressure differential of one atmosphere as demonstrated during the helium leak checking. When the convenience cans deform inward under external pressure, additional void volume is created, thereby reducing the overall pressure inside the containment vessel. However, quantitative data on this structural deformation of the convenience cans has not been measured, and repeatability of the deformation is not predictable. Therefore, convenience can geometry is assumed not to change for the calculation of pressure inside the containment vessel.

Table 3.11. Total pressure inside the containment vessel at 123.85°C (254.93°F) ^a

CVA	n_{MNOP} (lb-mole)	n_{po} (lb-mole)	n_{bo} (lb-mole)	n_{if} (lb-mole)	n_T (lb-mole)	P_T (psia)
1	3.8549E-04	1.3458E-05	3.1529E-04	0.0000E+00	7.1424E-04	43.852
2	3.8514E-04	1.7302E-05	3.1529E-04	0.0000E+00	7.1773E-04	44.108
3	3.7765E-04	1.1535E-05	3.1529E-04	0.0000E+00	7.0448E-04	44.151
4	3.6547E-04	7.6901E-06	3.1529E-04	0.0000E+00	6.8845E-04	44.585
5	7.3457E-04	0.0000E+00	3.1529E-04	0.0000E+00	1.0499E-03	33.827
6	2.5245E-04	0.0000E+00	5.3284E-04	0.0000E+00	7.8529E-04	73.625
7	2.4337E-04	0.0000E+00	3.1529E-04	2.2296E-05	5.8096E-04	63.545
8	This configuration is bounded by CVA #3					
9	This configuration is bounded by CVA #4 ^b					
10	This configuration is bounded by CVA #4					

^a This assumes that the internal convenience cans, polyethylene or Teflon FEP bottles, and Cat 277-4 spacer cans are sealed.

^b Although CVA #9 may slightly exceed the height of the combined three 25.4 cm (10 in.) can height (CVA #4), the open-ended cans and contents produce a larger void volume and thereby lower overall pressure inside the containment vessel.

3.2 SUMMARY OF THERMAL PROPERTIES OF MATERIALS

3.2.1 Material properties

Thermal properties at various temperatures for the stainless steel used in the fabrication of the drum, noncombustible cast refractory (Kaolite 1600), noncombustible neutron poison (BoroBond 4 or Cat 277-4), silicone rubber pads, and air are listed in Table 3.12. Properties used to evaluate thermal stresses due to differences in coefficient of thermal expansion are listed in Table 3.13.

3.2.2 Component Specifications

Component specifications are listed in Tables 3.14 and 3.15.

3.3 GENERAL CONSIDERATIONS

Thermal evaluation of the package design for NCT was performed by analysis. Evaluation of the package design for HAC was performed by a combination of testing and analysis.

3.3.1 Evaluation by Analysis

A description of the method and calculations used to perform the thermal and thermal stress analyses of the package for NCT and HAC is presented in detail in Appendices 3.6.1, 3.6.2 and 3.6.3.

3.3.2 Evaluation by Test

Full-scale testing of five ES-3100 test units was conducted in accordance with 10 CFR 71.73 for HAC. A single full-scale ES-3100 (TU-4) was assembled and subjected to both NCT testing and the sequential tests specified in 10 CFR 71.73(c). The furnace used for thermal testing was the No. 3 furnace at Timken Steel Company in Latrobe, Penn., which is a gas-fired furnace. This furnace employs "pulsed" fire burners, in which the natural gas flow rate is varied based on furnace controller demands, but the flow of air through the burners is constant, even when no gas is flowing. This ensures a very rich furnace atmosphere capable of supporting any combustion of package materials of construction.

Oxygen content was not monitored in stack gases of the furnace because it was not anticipated that any of the package's materials of construction were combustible. There was some burning of the silicone pads which are placed between the inner liner and the top plug of the package.

The most significant change to the definition of the HAC thermal test in the current 10 CFR 71 is the requirement for calculation purposes to base convective heat input on "that value which may be demonstrated to exist if the package was exposed to the fire specified." This is not especially significant for this package because it was tested in the gas-fired furnace with burners placed in an attitude which produced a strong convective swirl. Careful examination of the thermal test data indicates that the total heat imparted to the packages was significantly greater than the required total heat specified in 10 CFR 71.73(c)(4).

Table 3.12. Thermal properties of the materials used in the thermal analysis

Material	Temperature (°F)	Thermal conductivity (Btu/h-in.-°F)	Density (lbm/in. ³)	Specific heat (Btu/lbm-°F)	Emissivity
Stainless steel	-279.67	0.443 ^a	0.285 ^a	0.065 ^a	0.22 ^a
	-99.67	0.607	—	0.096	—
	260.33	0.799	—	0.123	—
	620.33	0.953	—	0.133	—
	980.33	1.088	—	0.139	—
	1340.33	1.223	—	0.146	—
	1700.33	1.348	—	0.153	—
	2240.33	1.526	—	0.163	—
Kaolite 1600	68	0.0093 ^b	0.011 ^c	0.2 ^d	—
	212	0.0091	—	—	—
	392	0.0081	—	—	—
	572	0.0072	—	—	—
	1112	0.0082	—	—	—
Neutron poison (Cat 277-4)	-31	0.0457 ^e	0.0579 ^f	0.125 ^e	—
	73.4	0.0485	—	0.186	—
	140	0.04	—	0.239	—
	212	0.0295	—	0.242	—
	302	0.0305	—	0.291	—
Neutron poison (BoroBond4)	25	0.0450 ^g	0.0683 ^g	0.2160 ^g	—
	77	0.0576	—	—	—
	100	0.0632	—	—	—
	104	0.0642	—	—	—
Silicone rubber	—	0.0161 ^h	0.047 ^h	0.300 ^h	1.0 ⁱ
Air	-9.67	1.074 × 10 ⁻³ ^a	4.064 × 10 ⁻⁵ ^{a,j}	0.240 ^a	—
	80.33	1.266 × 10 ⁻³	—	0.241	—
	170.33	1.445 × 10 ⁻³	—	0.241	—
	260.33	1.628 × 10 ⁻³	—	0.242	—
	350.33	1.796 × 10 ⁻³	—	0.244	—
	440.33	1.960 × 10 ⁻³	—	0.246	—
	530.33	2.114 × 10 ⁻³	—	0.248	—
	620.33	2.258 × 10 ⁻³	—	0.251	—
	710.33	2.393 × 10 ⁻³	—	0.254	—
	800.33	2.523 × 10 ⁻³	—	0.257	—
	890.33	2.644 × 10 ⁻³	—	0.260	—
	980.33	2.759 × 10 ⁻³	—	0.263	—
	1070.33	2.870 × 10 ⁻³	—	0.265	—
	1160.33	2.985 × 10 ⁻³	—	0.268	—
	1250.33	3.096 × 10 ⁻³	—	0.270	—
1340.33	3.212 × 10 ⁻³	—	0.273	—	
1520.33	3.443 × 10 ⁻³	—	0.277	—	

^a F. P. Incropera and D. P. DeWitt, *Fundamentals of Heat and Mass Transfer*, 2nd edition, John Wiley & Sons, New York, 1985.

^b Hsin Wang, *Thermal Conductivity Measurements of Kaolite*, ORNL/TM-2003/49 (Appendix 2.10.3).

^c Based on a baked density of 19.4 lbm/ft³ (0.011 lbm/in.³). Specification JS-YMN3-801580-A003 (Appendix 1.4.4) requires a baked density of 22.4 ± 3 lbm/ft³. Using a lower value for the Kaolite density results in higher temperatures on the containment vessel because the heat capacity of the Kaolite is minimized—allowing more heat to flow to the containment vessel; therefore, the thermal analyses are performed using a low-end density of 19.4 lbm/ft³. The HAC analyses also consider a high-end density of 30 lbm/ft³.

^d FAX communication from J. W. Breuer of Thermal Ceramics, Engineering Department, August 11, 1995.

^e Hsin Wang, *Thermophysical Properties of Heat Resistant Shielding Material*, ORNL/TM-2004/290 (Appendix 2.10.4). Specific heat values are presented in MJ/m³-K in ORNL/TM-2004/290—converted to mass-based units using a density of 105 lbm/ft³.

^f Based on a cured density of density of 100 lbm/ft³ (0.0579 lbm/in.³). B. F. Smith and G. A. Byington, *Mechanical Properties of 277-4*, Y/DW-1987, January 19, 2005 (Appendix 2.10.4), presents a range of measured densities between approximately 100 and 110 lbm/ft³ for Catalog No. 277-4. Therefore, in order to minimize the heat capacity of the material and allow more heat to be transferred to the containment vessel, the lower-bound value is used. The HAC analyses also consider a high-end density of 110 lbm/ft³.

^g E-mail communication with presentation attachment, Jim Hall (Eagle-Picher) to Jerry Byington (BWXT Y-12), 3/12/2004.

^h THERM 1.2, thermal properties database by R. A. Bailey.

ⁱ Conservatively modeled as 1.0.

^j Constant density value evaluated at 100°F.

Table 3.13. Mechanical properties of the materials used in the static stress analyses

Material	Temperature (°F)	Modulus of Elasticity (psi)	Poisson's Ratio	Density (lbm/in. ³)	Coefficient of thermal expansion (in./in./°F)
Stainless steel	-40	28.6×10^6 ^a	0.29 ^b	0.285 ^d	8.2×10^{-6} ^e
	100	28.14×10^6	—	—	8.6×10^{-6}
	200	27.6×10^6	—	—	8.9×10^{-6}
	300	27.0×10^6	—	—	9.2×10^{-6}
Kaolite	—	29,210 ^c	0.01 ^c	0.013 ^f	5.04×10^{-6} ^g
Neutron absorber (Cat 277-4)	-40	1.991×10^6 ^h	0.33 ^h	0.0608 ^h	7.056×10^{-6} ⁱ
	-4	—	—	—	7.222×10^{-6}
	32	—	—	—	7.222×10^{-6}
	70	0.984×10^6	0.28	—	—
	100	0.403×10^6	0.25	—	—
	104	—	—	—	7.000×10^{-6}
	140	—	—	—	6.444×10^{-6}
	176	—	—	—	5.778×10^{-6}
	212	—	—	—	5.389×10^{-6}
	248	—	—	—	5.056×10^{-6}
	284	—	—	—	4.889×10^{-6}
	302	—	—	—	4.833×10^{-6}

^a ASME Boiler and Pressure Vessel Code, Sect. II, Part D, Subpart 2, Tables TE-1, B column, and TM-1.

^b R. A. Bailey, *Strain - A Material Database*, Lawrence Livermore National Laboratory, 1989.

^c The Poisson's Ratio of Kaolite is assumed to be a small value of 0.01 (Appendix 2.10.2).

^d F. P. Incropera and D. P. DeWitt, *Fundamentals of Heat and Mass Transfer*, 2nd edition, John Wiley & Sons, New York, 1985.

^e *Metallic Materials and Elements for Aerospace Vehicle Structures*, MIL-HDBK-5H, May 1986.

^f Specification JS-YMN3-801580-A003 (Appendix 1.4.4) requires a baked density of 22.4 ± 3 lbm/ft³.

^g E-mail communication, Ken Moody (Thermal Ceramics, Inc.) to Paul Bales (BWXT Y-12), December 9, 2004.

^h B. F. Smith and G. A. Byington, *Mechanical Properties of 277-4*, Y/DW-1987, January 19, 2005 (Appendix 2.10.4).

ⁱ W. D. Porter and H. Wang, *Thermophysical Properties of Heat Resistant Shielding Material*, ORNL/TM-2004/290, Oak Ridge National Laboratory, Oak Ridge, Tenn., December 2004 (Appendix 2.10.4). Coefficient of thermal expansion at each temperature taken as the maximum of values for Runs #2, #3, and #5.

Table 3.14. Packaging material technical specifications

Component	Specifications
<i>Drum assembly</i>	
Drum washers	1.375 OD × 0.812 ID × 0.25-in. thick, 300 Series stainless steel
Drum threaded weld studs	5/8-11 × 7/8 long, fabricated per ASME SA-193, using Type 304/304L stainless-steel per ASME 479
Drum hex nuts	5/8-11 UNC-2B, silicon bronze C65100, ASTM F-467
Drum lid weldment	Modified 30-gal, 16-gauge (MS27683-61) lid, type 304 or 304L stainless steel; and a 11-gauge thick sheet, type 304 or 304L stainless steel, ASME SA-240
Drum weldment	Modified 30-gal, 16-gauge (MS27683-7), type 304 or 304L stainless steel, ASME SA-240, manufactured per Drawing M2E801580A004 (Appendix 1.4.8)
Drum plugs	Nylon plastic plug, Micro Plastic, Inc.
<i>Impact limiter, insulation enclosure, neutron absorber, and drum packing material</i>	
Insulation and impact limiter (not removable)	Lightweight cast refractory insulation, Kaolite 1600, 358.8 kg/m ³ (22.4 lb/ft ³) density, cast in stainless-steel shells in the drum and top plug
Neutron absorber	Cat 277-4, 1681.9 +240/-80 kg/m ³ (105 +15/- 5 lb/ft ³) density
Top plug (removable)	Type 304 or 304L stainless steel, ASME SA-240 (body), ASME SA-79 (lifting inserts),
Inner liners	Type 304 or 304L stainless steel, ASME SA-240 (body), ASME SA-79 (modified angle)
Aluminum tape	
Silicone pads	Silicone rubber, 22 ± 5 Shore A, color black/gray
<i>Containment boundary</i>	
Containment vessel plug	Part # 04-2126, Modified VCO threaded plug, brass
Containment vessel swivel hoist ring	3052T56, Swivel hoist ring, alloy steel (not used for shipment)

Table 3.14. Packaging material technical specifications

Component	Specifications
Containment vessel	<p>Method 1: Type TP304L stainless steel ASME SA-312 (welded or seamless pipe body); type F304L, stainless steel, ASME SA-182 (flange, and end cap); type 304, stainless steel, ASME SA-479 (sealing lid), Nitronic 60 SST per ASME SA-479, UNS-S21800 (closure nut)</p> <p>Method 2: Type F304L stainless ASME SA-182 (body, flange, and end cap); type 304, stainless steel, ASME SA-479 (sealing lid), Nitronic 60 SST per ASME SA-479, UNS-S21800 (closure nut)</p> <p>All components per <i>ASME Boiler and Pressure Vessel Code</i>, Sect. II, Part D, Table 2A</p>
Containment vessel O-rings	Elastomer, ethylene propylene, normal service temperature range of -40 to 150°C, Specification M 3BA712A14B13F17 in ASTM D-2000, per OO-PP-986, Rev. D
Containment vessel lid assembly retaining ring	Part # WSM-400-S02, type 302 stainless steel
Containment vessel O-ring lubricant	Clear dimethyl siloxane polymer
Containment vessel closure nut lubricant	Krytox #240AC
Containment vessel body dowel pins	0.2501/0.2503 OD × 0.50 long, 18-8 stainless steel
<i>Containment vessel packing material</i>	
Convenience cans	Stainless steel or tin plated carbon steel with stainless-steel can handles and nylon coated stainless-steel wire, or passivated nickel
Silicone rubber pads	Silicone rubber, 22 ±5 Shore A, color black/gray
Spacers	Stainless-steel can filled with Cat 277-4
Bottles	Polyethylene, glass, or Teflon FEP
Bagging	Polyethylene
Metal scrubbers	Stainless steel, McMaster Carr Part # 7361T13

Table 3.15. Component allowable service temperature and pressure

Component	Allowable service temperature range °C (°F)	Allowable pressure range kPa (psia)
<i>Drum assembly</i>		
Stainless-steel drum and lid	-40 to 871 (-40 to 1600) ^a	48.3 (7)
Silicon bronze nuts	-40 to 871 (-40 to 1600) ^a	N/A
Stainless-steel washers	-40 to 871 (-40 to 1600) ^a	N/A
Stainless-steel mid liner	-40 to 350 (-40 to 176.7)	N/A
Stainless-steel inner liner	-40 to 350 (-40 to 176.7)	N/A
Stainless-steel top plug weldment	-40 to 871 (-40 to 1600) ^a	
Kaolite 1600	-40 to 871 (-40 to 1600) ^a	N/A
Cat 277-4	-40 to 150 (-40 to 302) ^b	N/A
Silicone rubber pads	-40 to 232 (-40 to 450)	N/A
<i>Containment vessel</i>		
Stainless-steel body and sealing lid	-40 to 427 (-40 to 800) ^c	149.62 (21.7) external 699.82 (101.5) internal
Nitronic 60 closure nut	-40 to 427 (-40 to 800) ^c	149.62 (21.7) external 699.82 (101.5) internal
Stainless-steel retaining ring	-40 to 427 (-40 to 800) ^c	N/A
Dowel pins	-40 to 427 (-40 to 800) ^c	N/A
Brass VCO fitting (Viton O-rings)	-40 to 204 (-40 to 400) ^d	N/A
Ethylene propylene O-rings	-40 to 150 (-40 to 302) ^d	5.52 × 10 ³ (800) with no backing rings
Containment vessel silicone pads	-40 to 232 (-40 to 450)	N/A

^a This limit is established by the proximity of the Kaolite 1600 material.

^b This limit is established based on criticality limits of moisture loss.

^c This limit is established by the *ASME Boiler and Pressure Vessel Code*.

^d This limit is provided by the *Parker O-Ring Handbook* for each material's continuous service limit.

Compliance with ASTM E-2230-02, *Standard Practice for Thermal Qualification of Type B Packages for Radioactive Materials* (ASTM E-2230-02), was accomplished by the method described in Sect. 7.3 of this standard. This standard is in general agreement with Paragraph 2.2.1 (“Steady-state Method of Compliance”) of SG 140.1 entitled *Combination Test Analysis/ Method Used to Demonstrate Compliance to DOE Type B Packaging Thermal Test Requirements (30 Minute Fire Test)*. The data from each of the thermal tests, as shown in the test report, show that five of the six thermocouple-instrumented exterior surfaces of each package reached temperatures well in excess of 800°C (1475°F) during the 30-min thermal testing. Similarly, all other surfaces of the furnace, including the support stand, exceeded 800°C (1475°F) during the timed portion of the thermal test. For the test specified in the regulations, regardless of the amount of heat input by convection, radiation, or conduction, the maximum temperature the skin of the package could reach would be 800°C (1475°F). That is, the source of the heat in the regulatory-specified test is at 800°C (1475°F). Heat can only be transferred from a hotter source to a colder source. Thus, regardless of the mode of heat transfer, the greatest temperature a specimen exposed to the 10 CFR 71.73,(c)(4) thermal test can attain is 800°C (1475°F). The thermal performance of the packaging components as an assembled unit has been demonstrated through full-scale tests. Actual tests and procedures followed are described in Sect. 4.5 of ORNL/NTRC-013, Vol. 1. Figures 3.2 through 3.5 show the general testing arrangements.

Since full-scale testing in accordance with 10 CFR 71.73 for HAC was conducted on prototypical packages. No analyses were conducted to show compliance with the HAC thermal test. However, to determine the thermal impacts of (1) an internal heat source, (2) application of insulation during cool down, (3) thermal capacitance differences between test mock-ups and actual contents, and (4) the change in neutron absorbing material, analyses were conducted and are summarized in Appendices 3.6.1 and 3.6.2. Further discussion of these issues is found in Sect. 3.5.3.

3.3.3 Margins of Safety

Tables 3.16 and 3.17 summarize the results of thermal analysis and testing in accordance with NCT and HAC regulatory requirements. Margins of safety have not been calculated. However, the calculated results are compared with the allowable limits for individual components. Based on these results, the ES-3100 components are well below the allowable limits concerning temperature, stress, and pressure during transportation.

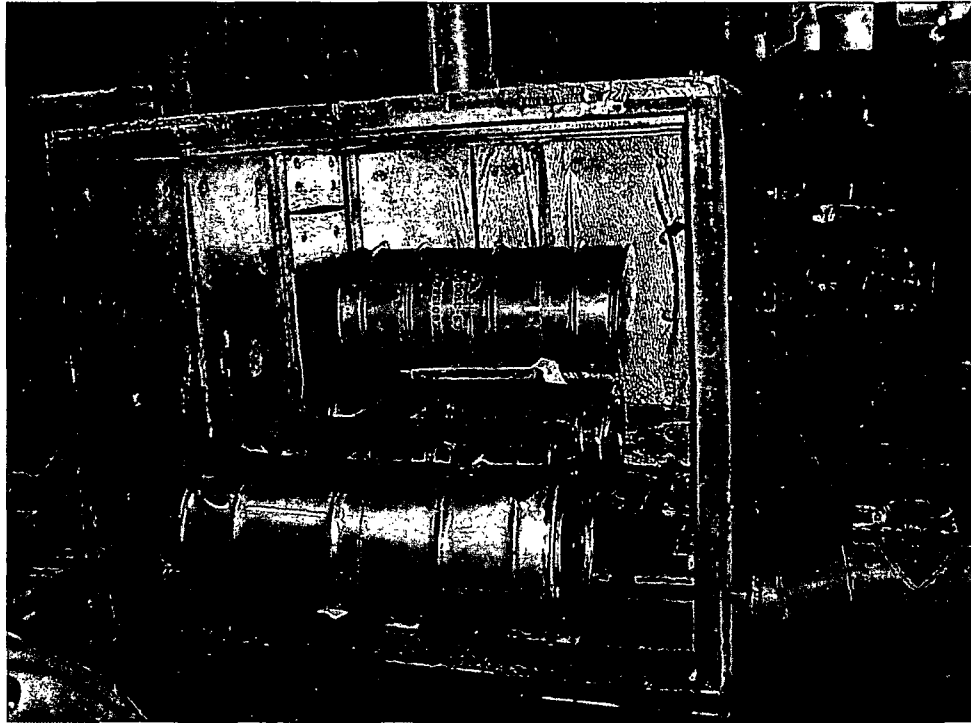


Fig. 3.2. Test units preheat arrangement.

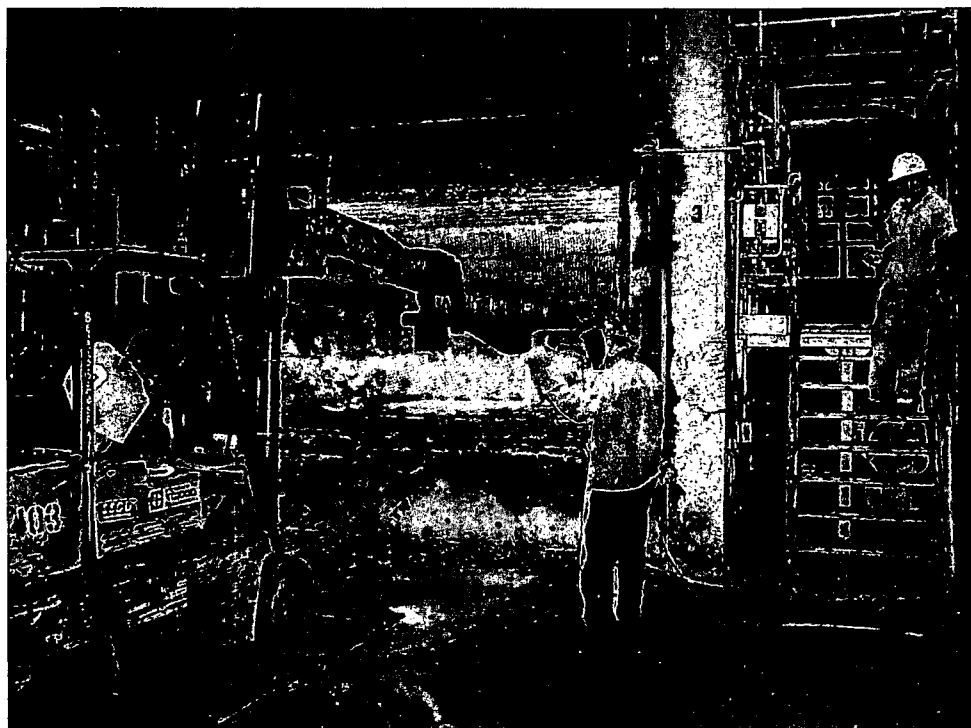


Fig. 3.3. Test unit insertion into furnace.

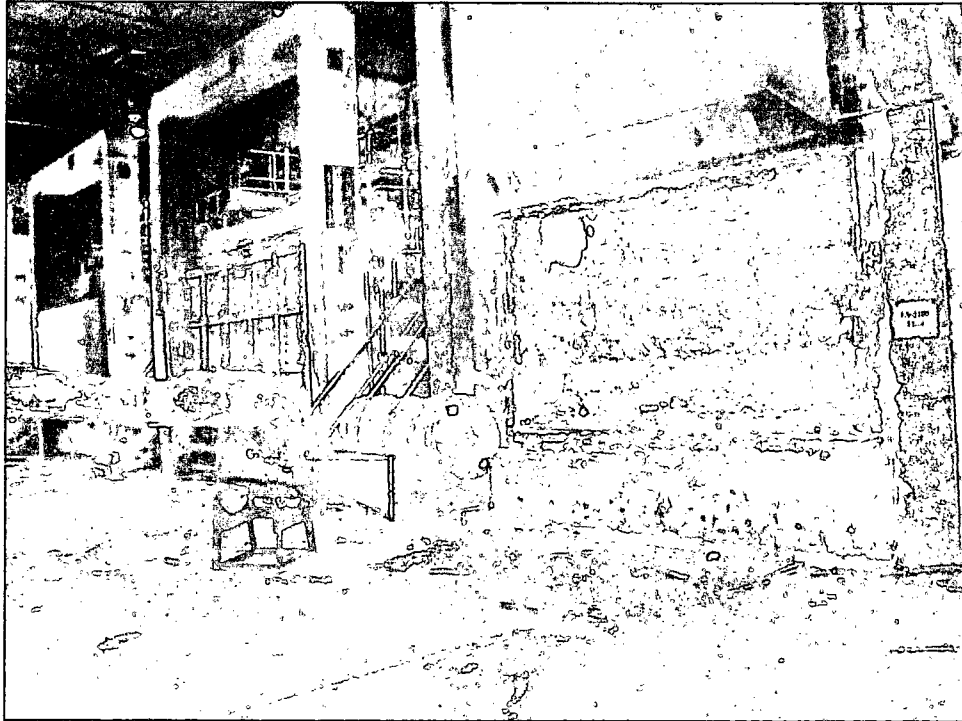


Fig. 3.4. Test unit removal from furnace.

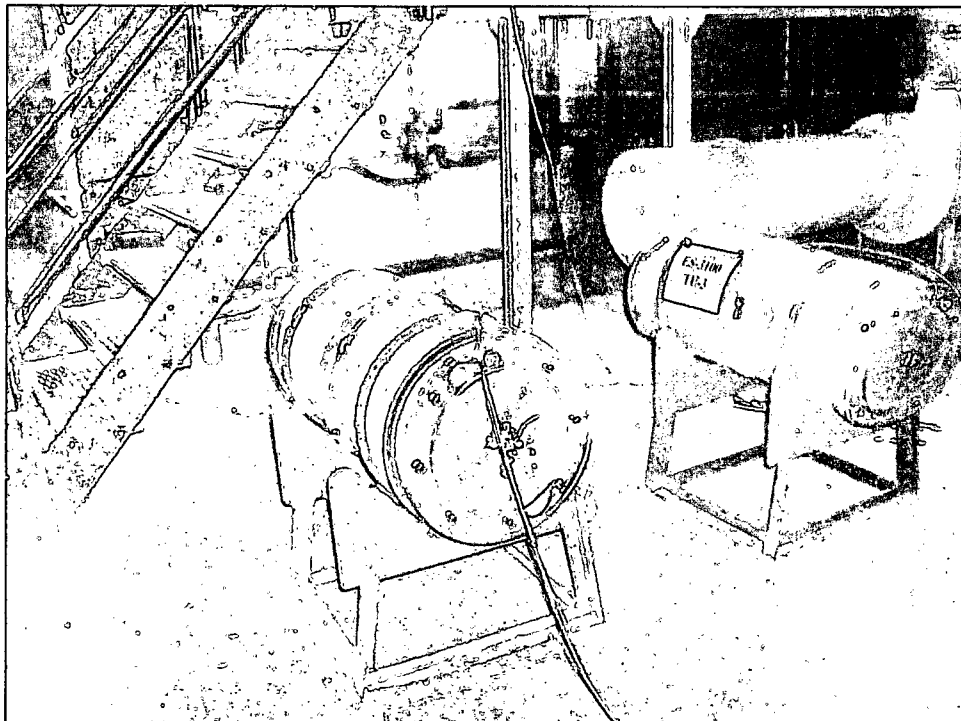


Fig. 3.5. Test unit cool down and monitoring arrangement.

Table 3.16. Summary of results of evaluation for the ES-3100 under NCT

Conditions	Calculated results	Allowable limit	SARP reference
Minimum package temperature, °C (°F)	-40 (-40)	-40 (-40)	Sect. 3.4.1
Maximum drum assembly stress due to cold conditions per 10 CFR 71.71(c)(2), kPa (psia)	61,150 (8,869)	132,379 (19,200)	Appendix 3.6.3
Minimum containment vessel pressure, kPa (psia)	76.74 (11.13)	0.0 (0.0)	Sect. 3.4.1
Maximum drum temperature with insolation, °C (°F)	117.72 (243.89) ^a	N/A	Appendix 3.6.2 Sect. 3.4.1
Maximum drum assembly stress due to hot conditions per 10 CFR 71.71(c)(1), kPa (psia)	66,934 (9,708)	132,379 (19,200)	Appendix 3.6.3
Containment vessel temperature with insolation, °C (°F)	87.81 (190.06) ^a	427 (800) ^b	Appendix 3.6.2 Sect. 3.4.1
Maximum O-ring temperature, °C (°F)	87.81 (190.06)	150 (302) ^c	Appendix 3.6.2 Sect. 3.4.1
Maximum containment vessel pressure, kPa (psia)	137.92 (20.004) ^d	801.2 (116.2) ^e	Appendix 3.6.4 Sect. 3.4.2

^a Appendix 3.6.2.

^b ASME Boiler and Pressure Code, Sect. II, Part D, maximum allowable temperature for Sect. III, Div. 1, Subsection NB vessel.

^c Maximum O-ring seal life up to 150°C (302°F) for continuous service (*Parker O-ring Handbook*, Fig. 2-24).

^d Appendix 3.6.4.

^e Appendix 2.10.1 allowable limit.

Table 3.17. Summary of results of evaluation under HAC for the ES-3100 shipping arrangement using bounding case parameters

Condition	Results	Design limits	SARP references
Maximum adjusted containment vessel temperature during testing, °C (°F)	152.22 (306.00)	426.67 (800) ^a	Sect. 3.5.3
Maximum containment vessel pressure during testing, kPa (psia)	507.63 (73.625) ^b	801.2 (116.2) ^c	Appendix 3.6.5 Sect. 3.5.3
Maximum adjusted O-ring temperature, °C (°F)	141.22 (286.20)	150 (302) ^d	Sect. 3.5.3

^a ASME Boiler and Pressure Code, Sect. II, Part D, maximum allowable temperature for Sect. III, Div. 1, Subsection NB vessel.

^b Appendix 3.6.5.

^c Appendix 2.10.1 at 148.89°C (300°F).

^d Maximum O-ring seal life up to 150°C (302°F) for continuous service (*Parker O-ring Handbook*, Fig. 2-24).

3.4 THERMAL EVALUATION UNDER NORMAL CONDITIONS OF TRANSPORT

3.4.1 Heat and Cold

The ambient temperature requirement for NCT is 38°C (100°F). The 35.2 kg of HEU shipped in the ES-3100 package generates a maximum bounding heat load of 0.4 W. The insolation heat flux stipulated in 10 CFR 71.71(c)(1) was used in the calculations. If the package is exposed to solar radiation at 38°C (100°F) in still air, the conservatively calculated temperatures at the top of the drum, on the top surface of the containment vessel, and on the containment vessel near the O-ring sealing surfaces, are 117.72, 87.81, and 87.72°C (243.89, 190.06, 189.90°F), respectively, for the ES-3100. Nevertheless, these temperatures are within the service limits of all packaging components, including the O-rings. The normal service temperature range of the O-rings used in the containment boundary is -40 to 150°C (-40 to 302°F), in accordance with B&PVC, Sect. III; thus, the seal will not be affected by this maximum normal operating temperature.

Using the temperatures calculated for the conditions of 10 CFR 71.71(c)(1), Appendix 3.6.4 predicts that the maximum normal operating pressure inside the containment vessel will be 137.92 kPa (20.004 psia). The design absolute pressure of the containment vessel is 801.17 kPa (116.2 psia), and the hydrostatic test pressure is 1135.57 kPa (164.7 psia). Thus, increasing the internal pressure of the containment vessel to a maximum of 137.92 kPa (20.004 psia) during NCT would have no detrimental effect. Stresses generated in the containment vessel at this pressure are insignificant compared to the materials of construction allowable stress. Table 2.20 provides a summary of the pressure and temperature for the various shipping configurations. As discussed in Sect. 2.6.1.4, the containment vessel and vessel closure nut stresses for these pressure conditions are below the allowable stress values.

Summarizing 10 CFR 71.43(f), the tests and conditions of NCT shall not substantially reduce the effectiveness of the packaging to withstand HAC sequential testing. The effectiveness of the ES-3100 to withstand HAC sequential testing is not diminished through application of the tests and conditions stipulated in 10 CFR 71.71. The justification for this statement is provided by physical testing of both the ES-2M and ES-3100 test packages. Due to the similarities in design, fabrication, and material used in construction of both the ES-2M and the ES-3100 package, the Kaolite 1600 physical characteristics will hold true for both designs. The integrity of the Kaolite 1600 is not significantly affected by the NCT vibration and 1.2-m (4-ft) drop tests.

Prior to testing the ES-2M design (a similarly constructed shipping package), each test unit was radiographed to determine the integrity of the Kaolite 1600 impact and insulation material. Following casting of the material inside the drum, some three-dimensional curving cracks were seen in some packages near the top thinner sections from the bottom of the liner to the bottom drum edge. After vibration testing, radiography of the ES-2M Test Unit-4 showed that the lower half of the impact limiter was broken into small pieces (Byington 1997). To evaluate these findings, Test Unit-4 was reassembled and subjected to HAC sequential testing (Byington 1997). After vibration and impact testing, many three-dimensional curving cracks were seen around the impact areas, and the inner liner was also visibly deformed. Nevertheless, temperatures at the containment boundary were also similar to other packages not subjected to vibration testing prior to HAC testing. No leakage of water was recorded following immersion. Also, Test Unit-4 of the ES-3100 shipping package was subjected to the full NCT test battery including vibration.

Following these tests, the containment vessel of the ES-2M Test Unit-4 was removed, and a full body helium leak check was performed. The test unit passed the leak-tight criteria in accordance with ANSI N14.5-1997. The containment vessel was then reassembled into the previously tested drum

assembly and subjected to the complete HAC testing. Based on the success of this unit and the similar design of the ES-2M, it can be concluded that vibration normally incident to transport does not reduce the effectiveness of the ES-3100 packaging during HAC testing. The ES-3100 has been tested to determine the effectiveness of the package following a sequential NCT 1.2-m (4-ft) drop test and HAC test battery. Throughout all of the vibration and structural testing, the effectiveness of the Kaolite 1600 material as an impact limiter and thermal insulation was not substantially reduced.

Since the components to be shipped have an assumed decay heat load of 0.4 W, a thermal analysis was conducted for the ES-3100 package with and without full solar insolation. The package was analyzed using the ABAQUS/Standard computer code, and the finite element geometry was constructed for each model using MSC.Patran 2004. The predicted temperature, while stored at 38°C (100°F) in the shade, for the drum lid center and the containment vessel flange near the inner O-ring, is 37.89°C (100.20°F) and 38.22°C (100.80°F), respectively. The analysis shows that no accessible surface of the package would have a temperature exceeding 50°C (122°F). Therefore, the requirement of 10 CFR 71.43(g) would be satisfied for either transportation mode (exclusive use or nonexclusive use).

Also, in accordance with 10 CFR 71.71(c)(2), the containment vessel pressure must be calculated at -40°C (-40°F). Given the initial conditions of temperature, relative humidity, no silicone rubber or polyethylene bag offgassing, the pressure is calculated as follows:

$$P_1 @ 25^\circ\text{C} = P_a + P_v + P_{fo},$$

where,

$$\begin{aligned} P_a &= 98.15 \text{ kPa (14.236 psia)} && \text{(Appendix 3.6.4)} \\ P_v &= 3.20 \text{ kPa (0.464 psia)} && \text{(Appendix 3.6.4)} \\ P_{fo} &= 0 && \text{(no offgassing, Appendix 3.6.4)} \end{aligned}$$

At -40°C (-40°F), the partial pressure of the water vapor is conservatively assumed to be zero. Therefore, the final pressure of the mixture at -40°C (-40°F) is calculated according to the ideal gas law based solely on the partial pressure of the air.

$$\frac{P_1 V_1}{T_1} = \frac{P_2 V_2}{T_2}$$

where,

$$\begin{aligned} P_1 &= 98.15 \text{ kPa (14.236 psia)} \\ T_1 &= 25^\circ\text{C (298.15 K)} \\ T_2 &= -40^\circ\text{C (233.15 K)} \\ V_1 &= V_2 \end{aligned}$$

rearranging and solving for P_2 ,

$$\begin{aligned} P_2 &= P_1 (T_2/T_1) \\ &= (98.15)(233.15/298.15) \\ P_2 &= 76.76 \text{ kPa (11.13 psia).} \end{aligned}$$

The cold condition for NCT specified in 10 CFR 71.71 is an ambient temperature in still air and shade of -40°C (-40°F). The 35.2 kg (77.60 lb) of HEU contents in the ES-3100 package generates a maximum bounding decay heat load of 0.4 W. However, in accordance with Regulatory Guide 7.8, the thermal effects of this internal heat source are neglected during evaluation of the package performance at

-40°C (-40°F). When exposed to this condition, the package component temperatures will stabilize over time at a temperature approaching -40°C (-40°F). The package has been examined for use at -40°C (-40°F) (Sect. 2.6.2). No detrimental effects on the package structure or sealing capability result from this minimum temperature requirement. The normal service temperature range of the O-rings used in the containment boundary is -40 to 150°C (-40 to 302°F), in accordance with the *Parker O-ring Handbook*; thus, the seal will not be affected by this minimum package temperature in accordance with 10 CFR 71.71(c)(2). Leak testing conducted on Test Unit-2 to the leak tight criteria stipulated by ANSI N14.5-1997 following compliance testing provides justification of the above statements.

3.4.2 Maximum Normal Operating Pressure

The stainless-steel drum and cast refractory system will not pressurize as a result of temperature increases because of four ventilation holes (0.795 cm [0.313 in.] in diameter) drilled in the drum side wall 3.81 cm (1.5 in.) from the flanged top and equally spaced around the drum. The holes are filled with nylon plugs, but they are not hermetically sealed. The inner liner encapsulating the noncombustible neutron poison (Cat 277-4) will not pressurize as a result of temperature increases because of three ventilation holes (0.635 cm [0.25 in.] in diameter) and a slot (1.63 cm [0.64 in.] in width and 4.17 cm [1.64 in.] in length) drilled into this inner liner. These features are covered during transport with aluminum tape to prevent contamination of the neutron poison. This tape does not represent a hermetic seal.

The maximum normal operating pressure is defined in 10 CFR 71.4 as the maximum gauge pressure that would develop in the containment system in a period of one year under the heat conditions specified in 10 CFR 71.71(c)(1). The internal pressure developed under these conditions in the ES-3100 containment vessel is calculated in Appendix 3.6.4 for the most restrictive containment vessel configurations. For conservatism, the decay heat of 0.4 W was used for the maximum internal heat load in evaluating the package for NCT. The maximum calculated internal absolute pressure in the containment vessel with solar insolation and the bounding case parameters is 137.92 kPa (20.004 psia). This pressure incorporated the offgassing from the silicone rubber pads, polyethylene bottles, teflon bottles, and polyethylene bagging and assumes that the containment vessel is assembled at ambient temperature and pressure at 100% relative humidity. The heat-transfer capability of the packaging is not degraded due to gap creation caused by differences in the fabrication material's coefficient of thermal expansion. Modeling assumed nominal gaps and position based on the engineering drawings of Appendix 1.4.8.

Little or no hydrogen gas is generated inside the containment vessel due to thermal- or radiation-induced decomposition of the water vapor, polyethylene bagging and bottles, or teflon bottles.

3.4.3 Maximum Thermal Stresses

The temperature of the package under NCT will vary from a low of -40°C (-40°F) throughout the package to a maximum of 117.72 and 87.81°C (243.89 and 190.06°F) (Appendix 3.6.2) on the surface of the drum and the containment vessel, respectively (Sect. 3.4.1). The slow temperature increase or decrease experienced in normal conditions between these limits will result in an essentially uniform temperature change throughout the package. All materials of construction are within this operating temperature range (Table 3.15). Thermal stresses due to differences in thermal expansion are insignificant, as discussed in Sects. 2.6.1.2 and 2.6.2.

Most of the components of the packaging are completely unrestrained. Therefore, any thermal stresses in the packaging components as the temperature varies between the extremes listed above will

have no effect on the ability of the packaging to maintain containment, shielding integrity, and nuclear subcriticality. The maximum stresses due to pressure under NCT for the containment vessel are given in Tables 2.21 and 2.22. These values are significantly below the allowable stresses for the packaging components. The Kaolite 1600 insulation and Cat 277-4 materials are poured and cast in place during the fabrication of the drum weldment (Drawing M2E801508A002, Appendix 1.4.8). This situation produces a zero gap between these materials and the bounding drum and inner liners. Due to differences in coefficients of thermal expansion, some radial and axial interference is expected due to thermal growth or contraction of the inner liners. These radial and axial interferences and induced stresses are calculated in Appendix 3.6.3. The results show that the stresses induced are minimal and do not reduce the effectiveness of the drum assembly.

The containment vessel, which is Type 304L austenitic (iron-nickel-chromium) stainless steel, is designed and fabricated in accordance with Sects. III SubSect. NB and IX of the *ASME Boiler and Pressure Vessel Code* (B&PVC Sect. III and B&PVC Sect. IX). The two sealing surfaces of each containment boundary are joined together by torquing the closure nut inside the containment vessel body to 162.7 ± 6.8 N·m (120 ± 5 lbf·ft). The O-ring material is ethylene-propylene elastomer.

The design temperature range of the containment vessel is -29 to 148.89°C (-20 to 300°F) (Appendix 2.10.1). However, the package has been evaluated to -40°C (-40°F) (Sect. 2.6.2). The thermal properties of the stainless-steel container body, lid, and closure nut are not critical at these temperatures. The O-ring seal is important for the containment properties of the containment vessel. The normal service temperature range for the elastomer O-ring is -40 to 150°C (-40 to 302°F) for continuous service and up to 165°C (329°F) for 72 h (*Parker O-ring Handbook*). The maximum adjusted HAC temperature of the ES-3100 containment vessel was based upon the thermal testing results in the vicinity of the O-rings. The maximum temperature recorded in the vicinity of the ES-3100 O-rings (241°F) is shown in Table 3.9. As shown in Sect. 3.5.3, the maximum temperature for the containment vessel at the O-ring location was adjusted for the ES-3100 package to 141.22°C (286.20°F). Hence, no damage would be expected to the O-rings during HAC.

The test packages were all preheated to above 38°C (100°F) prior to being placed in the furnace, which was heated to over 800°C (1475°F). As noted in the test report (Appendix 2.10.7), the temperatures recorded on the containment vessels of all the test units were fairly uniform, both vertically and circumferentially. The maximum temperature variation on the containment vessels was $\sim 50^\circ\text{F}$ (from the test temperatures reported in Table 3.9). No damage would be expected on the containment vessel from thermal stresses resulting from a temperature differential of this magnitude. This conclusion is based on the guidelines given in B&PVC, Sect. III. Thermal stress is defined as a self-balancing stress produced by a nonuniform distribution of temperature (Paragraph NB-3213.13 of B&PVC, Sect. III). This paragraph further states that there are two types of thermal stresses: general thermal stress and local thermal stress. An example of a general stress is that produced by an axial temperature distribution in a cylindrical shell (Paragraph NB-3213.9). This general stress is further classified (Paragraph NB-3213.9) as a secondary stress (that is, a normal stress or a shear stress developed by the constraint of adjacent materials or by self-constraint of the structure). Paragraph NB-3213.9 further states that the basic characteristic of a secondary stress is that it is self-limiting. Local yielding and minor distortions can satisfy the conditions that cause the stress to occur, and failure from a single application would not be expected. An example of a local thermal stress is a small hot spot in the wall of a pressure vessel (Paragraph NB-3213.13). Local thermal stress is associated with almost complete suppression of the differential expansion and thus produces no significant distortion. Such stresses are considered only from a fatigue standpoint. Fatigue will not result from a one-time cyclic event such as an accidental fire.

Following the thermal test, the volume between the O-rings on the five containment vessels (Sect. 2.7.4) was then leak tested and met the air leak-rate criterion of 10^{-4} ref-cm³/s. Following the O-ring leak check, the five containment vessels were drilled and tapped for full body helium leak testing. All five containment vessels passed the leak rate criteria for leaktightness per ANSI N14.5-1997. The containment vessels were then submerged under a pressure equivalent to 0.9 m (3 ft) of water for 8 h, with no leakage noted. (Sect. 2.7.5). Visual inspection following testing and disassembly also indicated that no distortion or damage occurred in the containment vessel wall, sealing lid, closure nut, O-rings, or sealing surfaces. These tests and observations demonstrate that thermal stresses produced during testing did not affect the containment capability of the containment vessel.

3.5 HYPOTHETICAL ACCIDENT THERMAL EVALUATION

3.5.1 Initial Conditions

Five full-scale packages were tested in the sequence shown in Table 2.19. Each ES-3100 test package was subjected to the 1.2-m (4-ft) drop test in accordance with 10 CFR 71.71(c)(5) prior to the sequential HAC tests in accordance with 10 CFR 71.73 (free drop, crush, puncture, thermal, and immersion tests). One of these units (Test Unit-4) had previously completed the tests and conditions stipulated in 10 CFR 71.71(c)(5) through (c)(10), excluding (c)(8). Two different mock-up configurations were used to represent the minimum and maximum proposed shipping weight and to simulate various center of gravity locations. The structural and thermal interface between the mock-up component and the containment vessel was designed to match that of the actual hardware proposed for transport. Based on LS-DYNA-3D drop simulations (Appendix 2.10.2) the five test units with their associated test weights represent the worst drop orientations for the ES-3100 package. Test Unit-5 used a near replicate of the lightest weight contents for its mock-up component. NCT free-drop, 9 m (30 ft) free drop, 9 m (30 ft) crush and puncture tests were made as specified in 10 CFR 71.71(c)(1), and 73(c)(1) through (c)(3) on all five full-scale test packages prior to thermal testing. The results of this testing are discussed in Sects. 2.7.1, 2.7.2, and 2.7.3. The 1.2-m (4-ft), 9-m (30-ft) drop and crush test orientations were as follows: two tests with the long axis of drum at an oblique angle of 12° to impact surface; a center of gravity over the corner of the drum lid; a drop with the long axis of drum parallel with the impact surface; and a vertical drop on to the drum's lid. The subsequent 40-in. puncture drops were made at various orientations as shown in Table 2.19.

Prior to the thermal test, each test unit was preheated to the maximum temperature extreme in accordance with 10 CFR 71.73(b)(1). Since the containment vessels were initially assembled at ~101.35 kPa (14.7 psia) at 25°C (77°F), the initial internal containment vessel pressure was ~105.70 kPa (15.33 psia) at 38°C (100°F) using the ideal gas law. In accordance with 10 CFR 71.73(b)(1), the internal pressure should be that calculated for the maximum normal operating pressure or 137.92 kPa (20.004 psia). This slight pressure differential has little or no effect on the thermal test results. The maximum decay heat load of the contents is calculated to be 0.4 W based on 35.2 kg of HEU. Analysis of the ES-3100 package after thermal HAC tests both with and without the decay heat load has been performed. The maximum projected temperature differential between the two packages following furnace exposure, as calculated in Appendix 3.6.2, would be 0.4°C (0.7°F) at the top center of the containment vessel lid, 0.4°C (0.7°F) at the containment vessel flange near the O-rings, 0.45°C (0.8°F) at the containment vessel bottom center, and 0.6°C (1.1°F) at the containment vessel mid body. These temperature differentials are representative for both the Kaolite 1600 densities evaluated.

3.5.2 Fire Test Conditions

Full-scale testing in accordance with 10 CFR 71.73 for HAC was conducted on prototypical packages. Therefore, no analyses were conducted to show compliance with the HAC thermal test. However, analyses were conducted and are discussed in Sect. 3.5.3 to determine the thermal impacts of an internal heat source, application of insolation during cool down, location of crush plate impact on test unit, and thermal capacitance differences between test hardware and proposed shipping hardware.

Full-scale testing of five ES-3100 test units was conducted in accordance with 10 CFR 71.73(c)(4) for HAC. A single full-scale ES-3100 test unit (TU-4) was assembled and subjected to both NCT and to the sequential tests specified in 10 CFR 71.73(c). The furnace used for thermal testing was the No. 3 Furnace at Timken Steel Company in Latrobe, Penn., which is a gas-fired furnace. Oxygen content in stack gases from the furnace were not monitored because it was not anticipated that any of the package's materials of construction were combustible. There was some burning of the silicone pads which are placed between the inner liners and the top plugs of the packages. However, it should be noted that this furnace employs "pulsed" fire burners. This type of burner is unique in that the natural gas flow rate is varied based on furnace controller demands, but the flow of air through the burners is constant, even when no gas is flowing, thereby ensuring a very rich furnace atmosphere capable of supporting any combustion of package materials of construction.

The most significant change to the definition of the HAC thermal test in the current 10 CFR 71 is the requirement for calculation purposes to base convective heat input on "that value which may be demonstrated to exist if the package was exposed to the fire specified." This is not especially significant for this package because it was tested in the gas-fired furnace with burners placed in an attitude which produced a strong convective swirl. Careful examination of the thermal test data indicates that the total heat imparted to the packages was significantly greater than the required total heat specified in 10 CFR 71.73(c)(4). Compliance with ASTM E-2230-02, *Standard Practice for Thermal Qualification of Type B Packages for Radioactive Materials*, was accomplished by the method described in Sect. 7.3 of this standard. This standard is in general agreement with Paragraph 2.2.1 ("Steady-state Method of Compliance") of SG 140.1 entitled *Combination Test Analysis/ Method Used to Demonstrate Compliance to DOE Type B Packaging Thermal Test Requirements (30 Minute Fire Test)*.

Prior to the beginning of the thermal test, the furnace was characterized for temperature and heat recovery times. The support stand was welded to a large steel plate which had been placed on the floor of the furnace prior to heating. This steel plate acted as the radiating surface at the bottom of the furnace, as well as providing the ability to hold the test stand rigidly in place. Before heating the furnace, workers practiced loading and unloading test packages from the cold furnace to ensure that the furnace door would not remain open >90 s during each loading. In fact, the maximum time the door was open during any loading was 64 s. As discussed in *Test Report of the ES-3100 Package (Appendix 2.10.7)*, six thermocouples were affixed to the drum assembly's exterior surface. Metal retainer clips were welded to the exterior surface to hold the thermocouples in place. The thermocouple tips were inserted underneath the metal clips, and the wire was wrapped around the metal clip. To eliminate any radiant heat exchange between the thermocouples and the furnace walls, the tips and metal clips were covered with a ceramic coating. Three thermocouples were mounted on each of the walls of the furnace, as well as on the furnace floor, on the furnace door, and three thermocouples were mounted on the test stand.

A minimum of 24 h prior to the beginning of all testing, the furnace was turned on with a set-point temperature of 871°C (1600°F). Following each test, the furnace set point was adjusted to 871°C (1600°F) for at least 45 min prior to the beginning of the next test. The furnace control data recorder ran continuously for the entire duration of the preheat cycle test. Each test unit was preheated to

over 38°C (100°F) by placing the packages in an environmental chamber. The environmental chamber was heated by a torpedo-type kerosene space heater controlled by a mechanical bulb thermostat with a control range of 38 to 93°C (100 to 200°F). The environmental chamber is a welded steel frame with fiberglass insulation panels. It was heated from the bottom with four floor register vents located around the perimeter and a 20.32-cm (8-in.)-diam manual dampened center venting stove pipe.

The set point temperature of the environmental chamber was monitored and adjusted for the duration of the preheat cycle. Initially, the thermostat was set to 66°C (150°F) for ~23 h. The thermostat set point was then reduced to 43°C (110°F) for the remainder of the preheat cycle (24 h). All packages were preheated for at least 47 h. No test package was loaded into the furnace until 15 of the 18 thermocouples monitoring the furnace had a reading of 800°C (1475°F) or higher. All packages were placed in the preheated furnace on the support stand with the long axis positioned horizontally, and the package lid facing toward a furnace side wall. During the testing of each package, the thermocouple temperature data recorder was set to record every 15 s.

These packages were exposed to the radiation environment for a minimum of 30 min after all functioning furnace thermocouples and at least five of the six test package exterior surface thermocouples reached a temperature of 800°C (1475°F). During the testing, the package thermocouple temperature data were recorded every 15 s.

After each test, the furnace was allowed to reheat for a minimum of 45 min after obtaining the set point temperature before testing the next unit. The furnace control temperature data recorder ran continuously for the duration of the preheat. No test package was loaded into the furnace until all functioning thermocouples on the furnace walls and support stand had again reached a temperature of 800°C (1475°F) or higher.

All units were tested in a horizontal attitude with the top end of the package facing to the right side wall of the furnace and the 0° mark on the drum facing the floor of the furnace. The data from each of the thermal tests, as shown in the test report, show that at least four of the six external drum thermocouples reached temperatures well in excess of 800°C (1475°F) and remained above 800°C (1475°F) during the 30-min thermal testing. Similarly, all other surfaces of the furnace, including the support stand, exceeded 800°C (1475°F) during the timed portion of the thermal test. For the test specified in the regulations, regardless of the amount of heat input by convection, radiation, or conduction, the maximum temperature the skin of the package could reach would be 800°C (1475°F). That is, the source of the heat in the regulatory specified test is at 800°C (1475°F). Heat can only be transferred from a hotter source to a colder source. Thus, regardless of the mode of heat transfer, the greatest temperature a specimen exposed to the 10 CFR 71.73,(c)(4) thermal test can attain is 800°C (1475°F). Therefore, the fact that these test packages attained temperatures well in excess of 800°C (1475°F) is an excellent indication that the thermal tests performed not only met the requirements of 10 CFR 71.73(c)(4) but actually exceeded them markedly. The results of these tests are provided in the test report (Appendix 2.10.7).

Each test package was removed from the furnace and placed in an area where it was not exposed to artificial cooling. As the furnace door was opened for each test unit, flaming or smoking was visible at the tamper indicating device (TID) holes in the drum/lid interface. Flaming continued on some of the packages for a short duration; the longest flame duration was 22 min after removal from the furnace. Smoke was also visible from each of the packages and continued after flames were no longer visible. The packages continued to smoke between 12 and 60 min after removal from the furnace. All the packages were allowed to cool naturally to room temperature. The post-thermal testing weights of each unit are summarized in Table 3.18. The drums were disassembled, and the damage was photographed. Each package was visually inspected, and the condition of the package and any observations were recorded.

**Table 3.18. ES-3100 test package weights before and after 10 CFR 71.73(c)(4)
HAC thermal testing**

Test Unit	Pre-test ^a weight kg (lb)	Post-test ^a weight kg (lb)	Thermal test weight loss kg (lb)	BoroBond4 original weight ^b kg (lb)	Water weight in BoroBond4 ^c kg (lb)	Water loss percent ^d (%)
1	202.3 (446)	202.3 (446)	0.0 (0)	20.7 (45.64)	4.91 (10.82)	0.00
2	202.8 (447)	202.8 (447)	0.0 (0)	20.5 (45.19)	4.86 (10.72)	0.00
3	203.7 (449)	203.2 (448)	0.45 (1)	20.5 (45.19)	4.87 (10.74)	9.31
4	201.8 (445)	201.4 (444)	0.45 (1)	20.4 (44.97)	4.84 (10.66)	9.38
5	157.4 (347)	156.9 (346)	0.45 (1)	20.6 (45.42)	4.89 (10.77)	9.29

^a Data from ORNL/NTRC-013.

^b Weight of BoroBond4 and water obtained from casting data. (ES-3100 Weldments 2004)

^c This weight is based on TGA measurements and calculation showing that the minimum water percent is 23.71%.

^d All weight loss attributed to loss of water in BoroBond4.

3.5.3 Maximum Temperatures and Pressure

The five test unit's previously subjected to both NCT and HAC drop testing were thermal tested in accordance with 10 CFR 71.73(c)(4). To determine the maximum temperatures reached during thermal testing, temperature indicating patches were placed at various locations throughout the test package at assembly. The temperature range for each patch used is identified in Table 3.19. When the temperature of an indicator was reached, the color would change to black (i.e., blackout temperature). The range of possible blackout temperatures of the patches was from 51.67 to 260°C (125 to 500°F). For Test Units-1 through -5, Table 3.19 defines the number and location of the temperature indicating patches.

Since the structural and thermal interface between the various mock-ups and containment vessels is the same as the actual hardware, the use of steel mock-ups to simulate the contents is not expected to affect the results of the thermal test significantly. The total maximum weight of the test packages ranged from 157.4 kg (347 lb) to 203.7 kg (449 lb). The ES-3100 package has a nominal gross shipping weight that ranges from 146.88 kg (323.79 lb) to 187.81 kg (414.05 lb) for the minimum and maximum weight containment vessel configurations shown in Table 2.8, respectively. However, the effect on temperature is evaluated in the following paragraphs due to thermal capacitance differences between the mock-up and the actual contents.

Table 3.19. Thermax temperature indicating patches for test units

Patch Location	Internal surface	External surface	Temperature range °C (°F)	Test report figure ^a
Inner liner of drum assembly		17 (Full Range)	52–260 (125–500)	5.30
Top plug weldment		4 (Full Range)	52–260 (125–500)	5.31
Containment vessel body flange	8 (4B & 4C)	8 (4B & 4C)	“B” 77–127 (171–261) “C” 132–182 (270–360)	5.28
Containment vessel body (end cap and cylinder)		5 (B)	“B” 77–127 (171–261)	5.28
Containment vessel sealing lid	4 (B)	4 (B)	“B” 77–127 (171–261)	5.29
Test mock-up components		6 (B)	“B” 77–127 (171–261)	5.26 & 5.27

^a ORNL/NTRC-013, Volume 1.

As previously stated, temperature indicators (patches) were placed on the surface of each containment vessel, inner liner, and mock-up component. The blackout temperatures that occurred during thermal testing are recorded for each test unit; the maximum blackout temperatures are listed in Table 3.9. A maximum blackout temperature of 116°C (241°F) was recorded in the vicinity of the O-rings on the containment vessel of Test Unit-5. As discussed below, this temperature will be conservatively adjusted to correlate the test conditions to shipping conditions with decay heat and solar insolation. The blackout temperatures are increased to account for (1) the temperature interval between blackout dots; (2) the ambient temperature of the package prior to insertion into the furnace; (3) the temperature increase due to the effects of applying solar insolation during post-HAC thermal test cool down; (4) the temperature increase due to the decay heat load of the actual contents being shipped; (5) effects of crushing at different locations along the body of the shipping package; (6) thermal capacitance difference in the proposed contents and hardware used during testing; (7) temperature difference occurring when using Borobond4 and Cat 277-4; and (8) temperature difference resulting from variations in Kaolite 1600 and Cat 277-4 material densities.

The initial adjustment for the blackout reading is an increase of 6.11°C (11.0°F) from the patch that blacked out. The highest blackout reading indicates that the actual temperature is somewhere between the highest temperature indicated and the next higher temperature.

The second adjustment compensates for thermal testing at package soak temperatures less than the maximum temperature of 38°C (100°F). In the case of the ES-3100 package, each test unit was thermally soaked to over 38°C (100°F) prior to insertion into the furnace. Therefore, there is no temperature adjustment required.

The third adjustment is a temperature increase to represent the effect of insolation heat flux on the package immediately following the conclusion of the thermal HAC test. Analyses of the ES-3100 package after thermal HAC tests both with and without insolation have been performed. Results from these analyses indicate an increase of ~5.94°C (10.7°F) at the containment vessel top (node 6715), ~6.06°C (10.9°F) at the containment vessel O-ring (node 6359), ~10.44°C (18.8°F) at the containment vessel mid body (Node 6574), and ~4.56°C (8.2°F) at the containment vessel bottom (node 6399), as a result of applying insolation following HAC thermal testing. These increases are extracted from Tables 3.7 and 3.8. The most pronounced effect of applying the insolation heat flux was that it increased

the time required to cool the package to NCT type conditions. Nevertheless, the influence of insolation is included in the adjustments to the blackout temperatures.

The fourth temperature adjustment considered is the temperature increase due to the decay heat load of the actual contents being shipped. A maximum decay heat load of 0.4 W is calculated as the bounding case for 35.2 kg of HEU. HAC analysis of the ES-3100 package both with and without the decay heat load has been performed, with the results shown in Tables 3.7 and 3.8. The maximum projected temperature increase during HAC due to a 0.4-W heat source, as calculated in Appendix 3.6.2, would be $\sim 0.39^{\circ}\text{C}$ (0.7°F) at the containment vessel's top (node 6715), $\sim 0.39^{\circ}\text{C}$ (0.7°F) at the containment vessel's O-ring (node 6359), $\sim 0.6^{\circ}\text{C}$ (1.1°F) at the containment vessel's mid body (node 6574), and $\sim 0.45^{\circ}\text{C}$ (0.8°F) at the containment vessel bottom (node 6399).

The fifth temperature adjustment considered is the temperature increase to the containment vessel based on the location of impact from the 500 kg (1100 lb) crush plate. Based on the differences in location of the crush plate between Test Units-1 and -2, crushing the shipping package with the center of gravity of the plate directly above the containment vessel flange increases the containment vessel temperature on average $\sim 6.11^{\circ}\text{C}$ (11°F).

The sixth adjustment compensates for the shipment of only 3 kg of HEU rather than the steel mock-ups. The higher content weight was used for testing to cover the possibility of shipping larger components without retesting. The larger content weight gave conservative structural deformation test results to the drum assembly than would the actual shipping weight. One effect, however, of using the larger test mass could be to reduce the containment vessel's temperature rise during the thermal test because the mock-up acts like a heat sink. In order to eliminate this temperature adjustment, a mock-up of the lightest proposed shipment was used in Test Unit-5. The structural and thermal interface between the mock-up components and the containment vessel was designed to match that of the actual shipping hardware, thereby providing the same conductive heat path for thermal testing. As shown by the test results, both the containment vessel and mock-up components of Test Unit-5 recorded higher temperatures than the other test units. This supports the theory that the heavier mock-ups act as heat sinks for the containment vessel. Therefore, by testing the 3.6-kg (8-lb) mock-up representing the lightest assembly to be shipped, a more accurate prediction of actual temperatures reached during thermal testing was achieved. No further temperature adjustments due to differences in mock-up weight are needed.

The seventh temperature adjustment compensates for conducting the HAC compliance tests with BoroBond4 and substituting Cat 277-4 for the production shipping containers. This adjustment is determined by using an undamaged package and subjecting it to a thermal environment representative of that required by 10 CFR 71.73(c)(4). Based on the analytical results shown in Appendix 3.6.2, the containment vessel in a package using Cat 277-4 would be from 2.5°F to 8°F cooler than a package with BoroBond4. Conservatively, the temperatures will not be adjusted due to the neutron poison change.

The eighth and final temperature adjustment compensates for material density variation in the Kaolite 1600 and Cat 277-4 material during HAC compliance tests. Again, this temperature adjustment was predicted for an undamaged package using the finite element method. Based on the analytical results shown in Appendix 3.6.2 (Tables 3.7 and 3.8), the containment vessel temperature was predicted to be $\sim 6.4^{\circ}\text{C}$ (11.6°F) higher at the containment vessel's top (node 6715), $\sim 6.4^{\circ}\text{C}$ (11.6°F) higher at the containment vessel's O-ring (node 6359), $\sim 4.6^{\circ}\text{C}$ (8.3°F) higher at the containment vessel's mid body, and $\sim 7.72^{\circ}\text{C}$ (13.9°F) at the containment vessel's bottom (node 6399) when the lower density values for Kaolite 1600 and the neutron poison were used. Since actual compliance testing was conducted with

these densities on the high side, the above adjustments must be added to the containment vessel temperatures.

Table 3.20 summarizes the numerous temperature adjustments needed for the containment vessel.

Table 3.20. Predicted temperature adjustments (°F) for containment vessel due to HAC

Node ^a	Analytical Temperature Adjustments								Total Temp Adjustment
	1	2	3	4	5	6	7	8	
6715	11.00	0.00	10.70	0.70	11.00	0.00	0.00	11.60	45.00
6359	11.00	0.00	10.90	0.70	11.00	0.00	0.00	11.60	45.20
6574	11.00	0.00	18.80	1.10	11.00	0.00	0.00	8.30	50.20
6399	11.00	0.00	8.20	0.80	11.00	0.00	0.00	13.90	44.90

^a See Figs. 8 through 11 in Appendix 3.6.2 for details of node locations.

Table 3.21 shows the results of adding the eight temperature adjustments previously discussed to the black-out temperatures for the containment vessel with the 3.6-kg (8-lb) mock-up (Test Unit-5). These adjusted temperatures would not adversely affect the stainless-steel components or the O-ring materials of the containment vessel.

Table 3.21. Predicted temperatures of the containment vessel due to HAC (°F)

Node ^a	Analytical temperature adjustments (°F)	Maximum blackout temperature on Test Unit-5 (°F)	Final predicted CV temperature (°F)
6715	45.00	261	306.00
6359	45.20	241	286.20
6574	50.20	199	249.20
6399	44.90	210	254.90

^a See Figs. 8 through 11 in Appendix 3.6.2 for details of node locations.

To determine the maximum pressure inside the containment vessel as a result of thermal testing, the average adjusted gas temperature must be calculated based on the above results. The approach used is to divide the containment vessel volume into three distinct equal regions and then average the three together. The first volume is represented by the gas adjacent to the containment vessel lid and flange region and the top convenience can. Based on the temperature recorded near the O-rings [116.11°C (241°F)] and the temperature recorded on the external surface of the convenience can [98.89°C (210°F)], the average temperature of the gas in this region is 107.50°C (225.50°F). Using the temperature adjustment of 25.11°C (45.20°F) for this region, the adjusted average temperature in the first region is 132.61°C (270.70°F). The second volume is represented by the gas adjacent to the second

convenience can from the top. Based on the temperature recorded on the containment vessel wall and convenience can [92.78°C (199°F)], the average temperature of gas in this region is 92.78°C (199°F). Using the temperature adjustment of 27.89°C (50.20°F) for this region, the adjusted average temperature in the second region is 120.67°C (249.20°F). The third and final volume is represented by the gas adjacent to the bottom convenience can. Again based on the convenience can temperature [87.78°C (190°F)] and the containment vessel end cap temperature [98.89°C (210°F)], the average temperature of gas in this region is 93.33°C (200°F). Using the temperature adjustment of 24.94°C (44.90°F) for this region, the adjusted average temperature in the third region is 118.28°C (244.90°F). Averaging these three temperatures, an average adjusted gas temperature of 123.85°C (254.93°F) is determined for the containment vessel.

As shown in Appendix 3.6.5, the maximum adjusted average gas temperature and pressure in the containment vessel during accident conditions was calculated to be 123.85°C (254.93°F), and 507.63 kPa (73.625 psia), respectively.

The maximum adjusted temperature on the surface of the containment vessel, adjacent to the O-rings, was 141.22°C (286.20°F). This is well within the design range for the packaging. The full body helium leak test on all test units following thermal testing meets the "leaktight" criteria in accordance with ANSI N14.5-1997. Visual inspection following testing and unloading indicated that no distortion or damage occurred in the containment vessel wall, sealing lid, closure nut, O-rings, or sealing surfaces. No water was visible inside the containment vessel following the 0.9-m (3-ft) water immersion test or the 15-m (50-ft) water immersion test on Test Unit-6.

The ES-3100 package satisfies the requirements of 10 CFR 71.73 for transport of the 35.2-kg (77.60-lb) arrangements shown in Table 2.8. Section 2.7 has additional details to support this conclusion.

3.5.4 Accident Conditions for Fissile Material Packages for Air Transport

The expanded fire test conditions specified in 10 CFR 71.55(f)(1)(iv) for fissile material package designs for air transportation was not conducted. The issue of subcriticality is addressed in Section 6 with content mass limits as addressed in Section 1 for air transport.

3.6 APPENDICES

Appendix	Description
3.6.1	THERMAL EVALUATION OF THE ES-3100 SHIPPING CONTAINER FOR NCT AND HAC (CONCEPTUAL DESIGN WITH BOROBOND4 NEUTRON ABSORBER)
3.6.2	THERMAL EVALUATION OF THE ES-3100 SHIPPING CONTAINER FOR NCT AND HAC (FINAL DESIGN WITH CATALOG 277-4 NEUTRON ABSORBER)
3.6.3	THERMAL STRESS EVALUATION OF THE ES-3100 SHIPPING CONTAINER DRUM BODY ASSEMBLY FOR NCT (FINAL DESIGN WITH CATALOG 277-4 NEUTRON ABSORBER)
3.6.4	CONTAINMENT VESSEL PRESSURE DUE TO NORMAL CONDITIONS OF TRANSPORT FOR THE PROPOSED CONTENTS
3.6.5	CONTAINMENT VESSEL PRESSURE DUE TO HYPOTHETICAL ACCIDENT CONDITIONS FOR THE PROPOSED CONTENTS
3.6.6	SILICONE RUBBER THERMAL PROPERTIES FROM THERM 1.2 DATABASE

Appendix 3.6.1

**THERMAL EVALUATION OF THE ES-3100 SHIPPING CONTAINER FOR NCT AND HAC
(CONCEPTUAL DESIGN WITH BOROBOND4 NEUTRON ABSORBER)**

Appendix 3.6.1

THERMAL EVALUATION OF THE ES-3100 SHIPPING CONTAINER FOR NCT AND HAC (CONCEPTUAL DESIGN WITH BORBOND4 NEUTRON ABSORBER)

INTRODUCTION

Thermal analyses of the ES-3100 shipping container are performed to determine the temperature distribution within the packaging during Normal Conditions of Transport (NCT) as specified in 10 CFR 71.71(c)(1).^[1] Transient thermal analyses are performed by treating the problem as a cyclic transient with the incident heat flux due to solar radiation applied and not applied in alternating 12-hour periods.

Additionally, thermal analyses of the ES-3100 shipping container are performed to determine the thermal response of the packaging to Hypothetical Accident Conditions (HAC) as specified in 10 CFR 71.73(c)(4).^[1] Since physical testing of the ES-3100 shipping container will be conducted with no internal heat source or insulation during cool-down, temperature increases due to internal heat loads of 0.4, 20, and 30 W as well as temperature increases due to the application of insulation during cool-down following the HAC fire are calculated. Although earlier revisions of 10 CFR 71 specifically state that insulation does not need to be evaluated before, during, or after HAC, the current version of 10 CFR 71 and associated guidance are unclear regarding the need for consideration following HAC testing. Since the Nuclear Regulatory Commission (NRC) has taken the position that insulation must be considered and evaluated following fire testing, analyses are conducted to determine the effect of insulation following the HAC fire on the ES-3100 shipping container. The predicted temperature increases may be used to adjust physical test data for those loads not included in the tests.

FINITE ELEMENT MODEL DESCRIPTION

A two-dimensional axisymmetric (r-z) finite element model of the ES-3100 shipping container is constructed using MSC.Patran (2004, Version 12.0.044)^[2] for evaluation for NCT. The actual contents of the ES-3100 shipping container are not specifically modeled—instead, the content source heat load (if desired) is modeled by applying a uniform heat flux to the inner surfaces of the containment vessel. This is a conservative approach in that package temperatures will not be reduced in a transient analysis by the heat capacity of the contents. A schematic of the finite element model is presented in Figure 1. The model consists of five materials: stainless steel (drum, liners, and containment vessel), Kaolite, Borobond4, silicone rubber, and air in the gaps between the drum liner and containment vessel and between the drum liner and top plug. Thermal properties of the materials used in the analysis are presented in Table 1.

Heat is transferred to the model from the contents (i.e., decay heat of the contents) via heat flux boundary conditions applied to the inner surface of the elements representing the containment vessel. Additionally, solar heat fluxes are applied to the model during NCT and HAC post-fire cool-down via heat flux boundary conditions. The heat applied to the model via the boundary conditions is transferred through the model via conduction and thermal radiation. Heat is rejected from the external surfaces of the model via natural convection and thermal radiation boundary conditions.

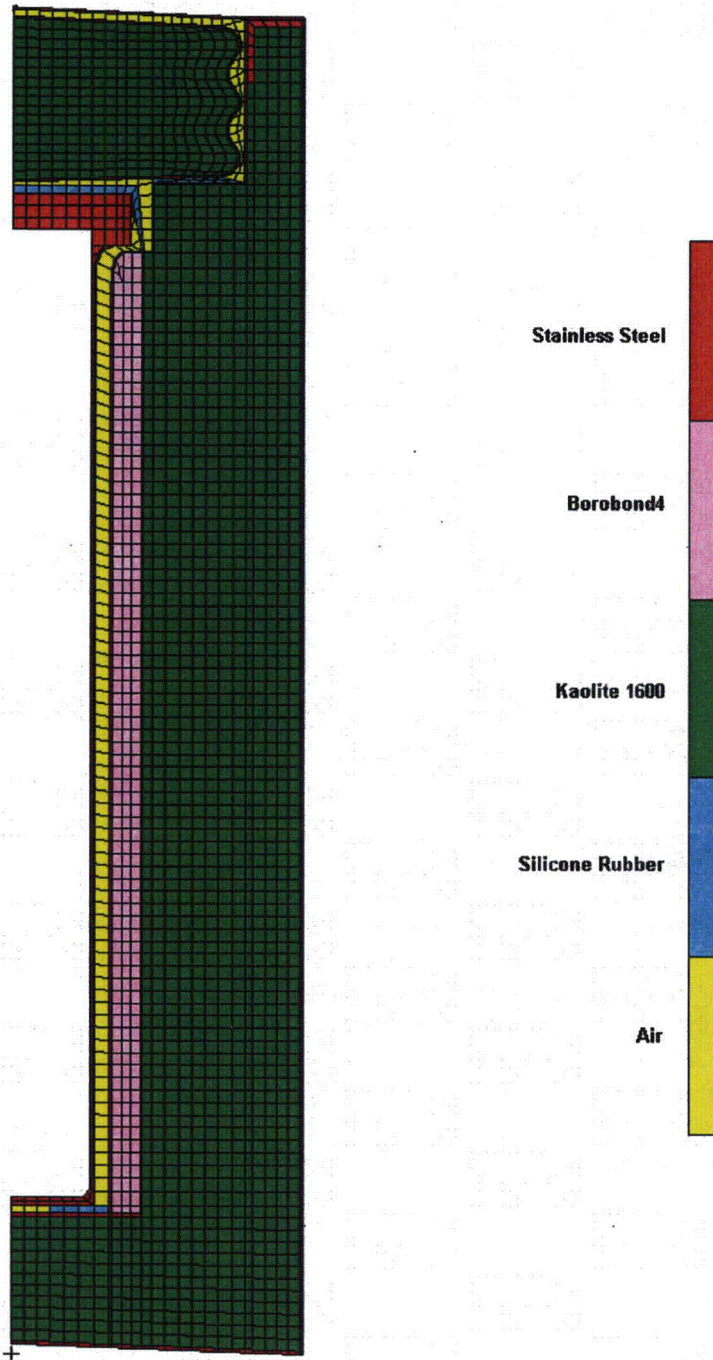


Figure 1. MSC.Patran axisymmetric finite element model of the ES-3100 shipping container.

Table 1. Thermal properties of the materials used in the thermal analysis.

Material	Temperature (°F)	Thermal conductivity (Btu/h-in.-°F)	Density (lbm/in. ³)	Specific heat (Btu/lbm-°F)	Emissivity
Stainless steel	-279.67	0.443 ^(a)	0.285 ^(a)	0.065 ^(a)	0.22 ^(a)
	-99.67	0.607	—	0.096	—
	260.33	0.799	—	0.123	—
	620.33	0.953	—	0.133	—
	980.33	1.088	—	0.139	—
	1340.33	1.223	—	0.146	—
	1700.33	1.348	—	0.153	—
	2240.33	1.526	—	0.163	—
Kaolite 1600	68	0.0093 ^(b)	0.011 ^(c)	0.2 ^(d)	—
	212	0.0091	—	—	—
	392	0.0081	—	—	—
	572	0.0072	—	—	—
	1112	0.0082	—	—	—
Borobond4	25	0.0450 ^(f)	0.0683 ^(f)	0.2160 ^(f)	—
	77	0.0576	—	—	—
	100	0.0632	—	—	—
	104	0.0642	—	—	—
Silicone rubber	—	0.0161 ^(g)	0.047 ^(g)	0.300 ^(g)	1.0 ^(h)
Air	-9.67	1.074×10 ^{-3(a)}	4.064×10 ^{-5(a),(i)}	0.240 ^(a)	—
	80.33	1.266×10 ⁻³	—	0.241	—
	170.33	1.445×10 ⁻³	—	0.241	—
	260.33	1.628×10 ⁻³	—	0.242	—
	350.33	1.796×10 ⁻³	—	0.244	—
	440.33	1.960×10 ⁻³	—	0.246	—
	530.33	2.114×10 ⁻³	—	0.248	—
	620.33	2.258×10 ⁻³	—	0.251	—
	710.33	2.393×10 ⁻³	—	0.254	—
	800.33	2.523×10 ⁻³	—	0.257	—
	890.33	2.644×10 ⁻³	—	0.260	—
	980.33	2.759×10 ⁻³	—	0.263	—
	1070.33	2.870×10 ⁻³	—	0.265	—
	1160.33	2.985×10 ⁻³	—	0.268	—
	1250.33	3.096×10 ⁻³	—	0.270	—
1340.33	3.212×10 ⁻³	—	0.273	—	
1520.33	3.443×10 ⁻³	—	0.277	—	

- Notes:
- (a) F. P. Incropera and D. P. DeWitt, *Fundamentals of Heat and Mass Transfer*, 2nd edition, John Wiley & Sons, New York, 1985.
 - (b) Hsin Wang, *Thermal Conductivity Measurements of Kaolite*, ORNL/TM-2003/49.
 - (c) Based on a baked density of 19.4 lbm/ft³ (0.011 lbm/in³). Specification JS-YMN3-801580-A003 requires a baked density of 22.4 ± 3 lbm/ft³. Using a lower value for the Kaolite density results in higher temperatures on the containment vessel because the heat capacity of the Kaolite is minimized—allowing more heat to flow to the containment vessel; therefore, the thermal analyses are performed using a low-end density of 19.4 lbm/ft³. The HAC analyses also consider a high-end density of 30 lbm/ft³.
 - (d) FAX communication from J. W. Breuer of Thermal Ceramics, Engineering Department, August 11, 1995.
 - (e) W. D. Porter and H. Wang, *Thermophysical Properties of Heat Resistant Shielding Material*, ORNL/TM-2004/290, ORNL, Dec. 2004. Specific heat values are presented in MJ/m³-K in ORNL/TM-2004/290—converted to mass-based units using a density of 105 lbm/ft³.
 - (f) Data via email from Jim Hall (Eagle-Picher) to Jerry Byington (BWXT Y-12), March 12, 2004.
 - (g) THERM 1.2, thermal properties database by R. A. Bailey.
 - (h) Conservatively modeled as 1.0.
 - (i) Constant density value evaluated at 100°F.

MODELED HEAT TRANSFER MECHANISMS

The heat transfer mechanisms included in the thermal model such as thermal radiation, natural convection, and insolation (solar heat flux) are described in detail in the following sections.

Heat Transfer Between Package Exterior and Ambient

The heat transfer between the exterior of the package and the ambient (or fire) is modeled as a combination of radiant heat transfer and natural convection. The heat transfer due to radiant exchange with the environment is calculated as:^[3]

$$q''_{\text{rad}} = \sigma F_e (T_s^4 - T_a^4), \quad (1)$$

where σ = Stefan-Boltzmann constant,
 F_e = overall exchange factor,
 T_s = container outer surface temperature (absolute), and
 T_a = ambient or fire temperature (absolute).

The overall interchange factor is calculated as:^[3]

$$F_e = \left[\frac{1}{\frac{1}{\varepsilon_p} + \frac{A_p}{A_s} \left(\frac{1}{\varepsilon_s} - 1 \right)} \right], \quad (2)$$

where ε_p = emissivity of package surface,
 A_p = surface area of the package,
 A_s = surface area of the surroundings, and
 ε_s = emissivity of surroundings.

For NCT and the cool-down period following the HAC fire, the area of the surroundings is assumed to be much larger than the surface area of the package; therefore, Eq. 2 reduces to:

$$F_e \approx \varepsilon_p. \quad (3)$$

An emissivity value of 0.22,^[4] which is typical of clean stainless steel, is assumed for the outer surfaces of the drum during NCT and during the cool-down period following the HAC fire. In reality, the outer surfaces of the drum will have a much higher emissivity following the HAC fire; therefore, this assumption is conservative.

During the HAC fire, the area of the surroundings is assumed to be approximately equal to the surface area of the drum; therefore, Eq. 2 reduces to:

$$F_e = \left[\frac{1}{\frac{1}{\varepsilon_p} + \frac{1}{\varepsilon_s} - 1} \right] \quad (4)$$

During the HAC 30-minute fire, an emissivity of 0.8 is assumed for the drum, and an emissivity of 0.9 is assumed for the fire per the guidance of 10 CFR 71.74(c)(4).^[1] This results in an overall exchange factor of 0.7347 during the HAC fire using Eq. 4.

The natural convection heat transfer from the package surface to the ambient air is calculated as:

$$q''_{\text{convection}} = h(T_s - T_a) \quad (5)$$

where, h = natural convection heat transfer coefficient,
 T_s = container outer surface temperature, and
 T_a = ambient or fire temperature.

During the NCT transient thermal analyses and the steady-state thermal analyses (used to obtain the starting temperature distribution in the package for NCT and HAC when a content heat load is present), the shipping container is assumed to be in an upright (vertical) orientation. The top of the drum is modeled as a heated horizontal flat plate facing up using the following correlation:^[5]

$$h = \left(\frac{k}{L} \right) C_1 Ra^{C_2} \quad (6)$$

where, k = thermal conductivity of air,
 L = characteristic length (= $D/4$ per Ref. 5),
 D = diameter of the package,
 Ra = Rayleigh number,
 C_1 = constant (see Table 2), and
 C_2 = constant (see Table 2).

The Rayleigh number in Eq. 6 is defined as:

$$Ra = \frac{g \beta \Delta T L^3}{\nu \alpha} \quad (7)$$

where, g = acceleration of gravity,
 β = coefficient of thermal expansion,
 ΔT = temperature difference,
 ν = kinematic viscosity [μ/ρ],
 μ = absolute viscosity,
 α = thermal diffusivity [$k/(\rho C_p)$],
 ρ = density of air, and
 C_p = specific heat of air.

The properties of air used in the natural convection calculations are presented in Table 3.

Table 2. Coefficients for natural convection correlations.

Coefficient	Rayleigh Number Range	Value
C ₁	2.6×10 ⁴ < Ra < 1.0×10 ⁷	0.54
	1.0×10 ⁷ < Ra < 3.0×10 ¹⁰	0.15
C ₂	2.6×10 ⁴ < Ra < 1.0×10 ⁷	0.25
	1.0×10 ⁷ < Ra < 3.0×10 ¹⁰	1/3
C ₃	Ra < 1.0×10 ⁹	0.680
	Ra > 1.0×10 ⁹	0.825
C ₄	Ra < 1.0×10 ⁹	0.670
	Ra > 1.0×10 ⁹	0.387
C ₅	Ra < 1.0×10 ⁹	0.25
	Ra > 1.0×10 ⁹	1/6
C ₆	Ra < 1.0×10 ⁹	4/9
	Ra > 1.0×10 ⁹	8/27
C ₇	Ra < 1.0×10 ⁹	1
	Ra > 1.0×10 ⁹	2
C ₈	1.0×10 ⁴ < Ra < 1.0×10 ⁹	0.53
	1.0×10 ⁹ < Ra < 1.0×10 ¹²	0.13
C ₉	1.0×10 ⁴ < Ra < 1.0×10 ⁹	0.25
	1.0×10 ⁹ < Ra < 1.0×10 ¹²	1/3

Source: *MSC.Patran Thermal User's Guide, Volume 1: Thermal/Hydraulic Analysis*, MSC Software Corporation, Santa Ana, CA 92702, 2003.

Table 3. Properties of air used in natural convection calculations.

Temperature (K)	Thermal Conductivity (W/m-K)	Density (kg/m ³)	Specific heat (J/kg-K)	Absolute viscosity (N-s/m ²)	Coefficient of thermal expansion (K ⁻¹)
250	22.3×10 ⁻³	1.3947	1006	159.6×10 ⁻⁷	4.00×10 ⁻³
300	26.3×10 ⁻³	1.1614	1007	184.6×10 ⁻⁷	3.33×10 ⁻³
350	30.0×10 ⁻³	0.9950	1009	208.2×10 ⁻⁷	2.86×10 ⁻³
400	33.8×10 ⁻³	0.8711	1014	230.1×10 ⁻⁷	2.50×10 ⁻³
450	37.3×10 ⁻³	0.7740	1021	250.7×10 ⁻⁷	2.22×10 ⁻³
500	40.7×10 ⁻³	0.6964	1030	270.1×10 ⁻⁷	2.00×10 ⁻³
550	43.9×10 ⁻³	0.6329	1040	288.4×10 ⁻⁷	1.82×10 ⁻³
600	46.9×10 ⁻³	0.5804	1051	305.8×10 ⁻⁷	1.67×10 ⁻³
650	49.7×10 ⁻³	0.5356	1063	322.5×10 ⁻⁷	1.54×10 ⁻³
700	52.4×10 ⁻³	0.4975	1075	338.8×10 ⁻⁷	1.43×10 ⁻³
750	54.9×10 ⁻³	0.4643	1087	354.6×10 ⁻⁷	1.33×10 ⁻³
800	57.3×10 ⁻³	0.4354	1099	369.8×10 ⁻⁷	1.25×10 ⁻³
850	59.6×10 ⁻³	0.4097	1110	384.3×10 ⁻⁷	1.18×10 ⁻³
900	62.0×10 ⁻³	0.3868	1121	398.1×10 ⁻⁷	1.11×10 ⁻³
950	64.3×10 ⁻³	0.3666	1131	411.3×10 ⁻⁷	1.05×10 ⁻³
1000	66.7×10 ⁻³	0.3482	1141	424.4×10 ⁻⁷	1.00×10 ⁻³
1100	71.5×10 ⁻³	0.3166	1159	449.0×10 ⁻⁷	9.09×10 ⁻⁴

Source: F. P. Incropera and D. P. DeWitt, *Fundamentals of Heat and Mass Transfer*, 2nd ed., John Wiley & Sons, New York, 1985.

During the NCT transient thermal analyses and the steady-state thermal analyses, the sides of the drum are modeled as a vertical flat plate using the following correlation.^[5]

$$h = \left(\frac{k}{L} \right) \left[C_3 + \frac{C_4 Ra^{C_5}}{\left(1 + \left[\frac{0.492}{Pr} \right]^{9/16} \right)^{C_6}} \right]^{C_7}, \quad (8)$$

where L = characteristic length = the drum height,
 C₃ = constant (see Table 2),
 C₄ = constant (see Table 2),
 C₅ = constant (see Table 2),
 C₆ = constant (see Table 2),
 C₇ = constant (see Table 2), and
 Pr = Prandtl number [(C_p × μ)/k].

The bottom of the drum is conservatively modeled as adiabatic during the NCT transient analyses and the steady-state analyses.

During the HAC 30-minute fire and the post-fire cool-down, the shipping container is assumed to be in a horizontal orientation (as it is during furnace testing). As such, the top and bottom of the drum are modeled as vertical flat plates using Eq. 8 having a characteristic length, L, equivalent to the drum diameter, and the sides of the drum are modeled as a horizontal cylinder using the following correlation:^[5]

$$h = \left(\frac{k}{D} \right) C_8 Ra^{C_9}, \quad (9)$$

where D = diameter of the package,
 C₈ = constant (see Table 2), and
 C₉ = constant (see Table 2).

Insolation

The following insolation (incident solar radiation) data is required for NCT per 10 CFR 71.71(c)(1):^[1]

Form and location of surface	Total insolation for a 12-hour period (cal/cm ²)
Flat surfaces transported horizontally	
Base	None
Other surfaces	800
Flat surfaces not transported horizontally	200
Curved surfaces	400

The total insolation values specified in the previous table are for a 12-hour period. For analytical purposes, these values are “time-averaged” over the entire 12-hour period (i.e., divided by 12).

Therefore, the incident solar heat fluxes ($q''_{\text{solar},i}$) used in the analyses for NCT and cool-down following the HAC fire are as follows:

During NCT, the drum is in an upright (vertical) orientation; therefore, the following heat fluxes are applied to the external surfaces of the drum to represent insolation:

$$\text{Top} \quad q''_{\text{solar},i} = 775.3 \text{ W/m}^2, \quad (10)$$

$$\text{Sides} \quad q''_{\text{solar},i} = 387.7 \text{ W/m}^2, \quad (11)$$

$$\text{Bottom} \quad q''_{\text{solar},i} = 0. \quad (12)$$

During the cool-down period following the HAC 30-minute fire, the drum is assumed to be in a horizontal orientation; therefore, the following heat fluxes are applied to the external surfaces of the drum to represent insolation:

$$\text{Top} \quad q''_{\text{solar},i} = 193.83 \text{ W/m}^2, \quad (13)$$

$$\text{Sides} \quad q''_{\text{solar},i} = 387.7 \text{ W/m}^2, \quad (14)$$

$$\text{Bottom} \quad q''_{\text{solar},i} = 193.83 \text{ W/m}^2. \quad (15)$$

The insolation is applied as a square-wave function (i.e., alternating on and off in 12-hour periods) in the thermal analysis. The heat flux values presented in Eqs. 10–15 represent the insolation absorbed by the package surface since a drum absorptivity of 1.0 was conservatively assumed. An analytical study has been performed on a similar shipping package that investigated three methods of applying the insolation.^[6] The three methods consisted of 1) performing a steady-state analysis assuming the insolation is applied continuously by distributing the heat flux evenly throughout a 24-hour period, 2) performing a transient analysis assuming the insolation is represented by a step function (i.e., applied and then not applied in 12-hour cycles, and 3) performing a transient analysis where the incident insolation is represented by a sinusoidal function that varies throughout the day. The results of the study indicate that the method used in applying the insolation has a significant effect on the temperatures of the outermost portions of the package. However, since the total insolation over any 24-hour period is the same for all cases, internal package temperatures are relatively unaffected by the way in which the insolation is applied. Since containment vessel O-ring temperatures are of primary concern in this report, the step function method for applying the insolation is suitable.

Heat Transfer Across Gaps in the Package

Heat transfer across all gaps in the package is modeled by a combination of radiant exchange and conduction. Natural convection heat transfer is not included across the gaps in the model. Scoping studies performed for a similar shipping package indicate that the heat transfer due to natural convection in relatively small gaps is approximately a factor of 6 times less than the heat transfer due to radiant exchange.^[6] These calculations assumed a temperature difference of 5°C across the gap. Based on these previous calculations, the effect of neglecting the natural convection in the gap regions is minimal. P/VIEWFACTOR^[7] was used to calculate the view factors in all enclosures.

Content Heat Load

In order to simulate the decay heat generated by the ES-3100 shipping container contents, a uniform heat flux is applied to the inner surfaces of the elements representing the containment vessel in the model. Content heat loads of 0.4, 20, and 30 W as well as no content heat load are investigated in this report. The uniform heat flux (q''_{source}) for a given content heat load is calculated using the following equation:

$$q''_{\text{source}} = \frac{Q}{2\left(\frac{\pi D_i^2}{4}\right) + \pi(D_i)(H)}, \quad (16)$$

where Q = content heat load,
 D_i = inside diameter of the containment vessel (0.12802 m),
 H = height of the containment vessel cavity (0.78867 m).

Using Eq. 16, a content heat load of 0.4 W results in a uniform heat flux of 1.1664 W/m², a content heat load of 20 W results in a uniform heat flux of 58.32 W/m², and a content heat load of 30 W results in a uniform heat flux of 87.48 W/m².

DISCUSSION OF ANALYTICAL RESULTS

All thermal analyses discussed in this report were performed using MSC.Patran Thermal (2004 Version 12.0.044)^[8] on an Intel Pentium 4-based Microsoft Windows 2000 computer. Temperatures are monitored at selected locations in the model as shown in Figure 2.

Steady-state Conditions Analyses Results

Steady-state thermal analyses are performed on the finite element model of the ES-3100 shipping container for three cases having content heat loads of 0.4, 20, and 30 W. The temperature distribution results from these analyses are used as the starting temperature distribution within the model when performing the transient thermal analyses for NCT and the HAC 30-minute fire. The boundary conditions for these steady-state analyses include a combination of thermal radiation exchange and natural convection applied to the top and sides of the drum using an ambient temperature of 37.8°C (100°F). The bottom of the drum is modeled as an adiabatic surface (i.e., no heat transfer). Additionally, the content heat load is simulated by applying a uniform heat flux to the internal surfaces of the elements representing the containment vessel. The calculated steady-state temperature distribution with the model of the ES-3100 shipping container for content heat loads of 0.4, 20, and 30 W is presented in Table 4.

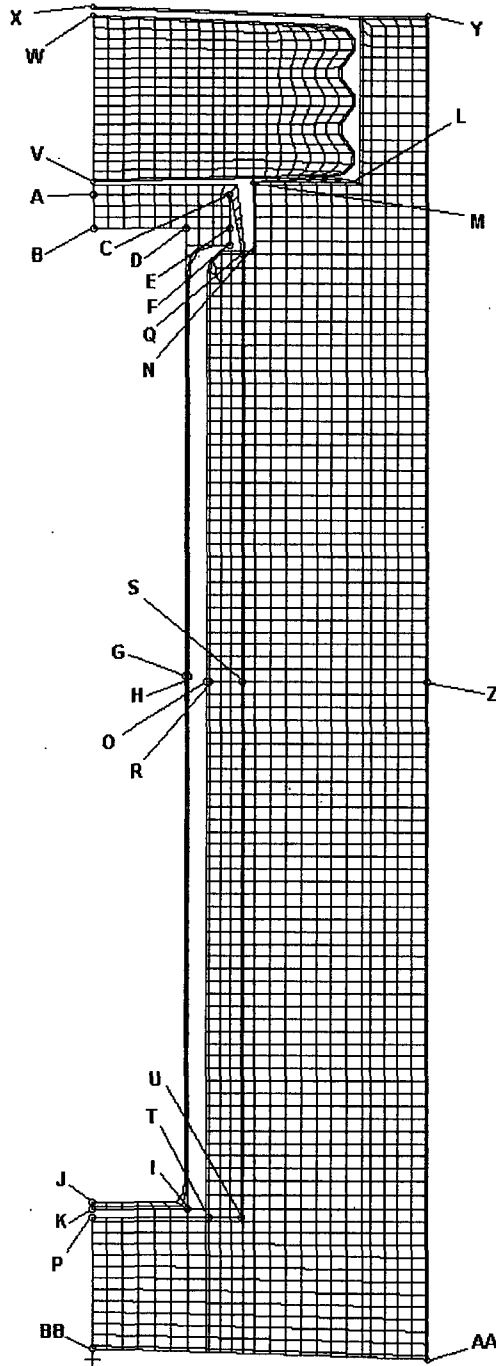


Figure 2. MSC.Patran axisymmetric finite element model of the ES-3100 shipping container—nodal locations of interest (elements representing air not shown for clarity).

Table 4. ES-3100 shipping container steady-state temperatures (37.8°C ambient temperature, no insolation).

Node ^(a)	Location	Steady-state temperature, °C (°F)		
		0.4 W	20 W	30 W
A	CV lid, top, center	38.09 (100.56)	56.06 (132.90)	64.65 (148.37)
B	CV lid, bottom, center	38.09 (100.56)	56.16 (133.08)	64.79 (148.63)
C	CV lid, top, outer	38.09 (100.55)	55.82 (132.47)	64.30 (147.73)
D	CV flange at interface, inner ^(b)	38.09 (100.57)	56.17 (133.10)	64.81 (148.66)
E	CV flange at interface, outer ^(b)	38.09 (100.56)	56.06 (132.90)	64.65 (148.37)
F	CV flange, bottom, outer	38.09 (100.56)	56.05 (132.88)	64.63 (148.34)
G	CV shell, mid-height, inner	38.36 (101.04)	69.36 (156.85)	83.91 (183.04)
H	CV shell, mid-height, outer	38.36 (101.04)	69.35 (156.83)	83.90 (183.01)
I	CV bottom, outer	38.18 (100.72)	59.56 (139.20)	69.97 (157.94)
J	CV bottom, center, inner	38.18 (100.72)	59.65 (139.38)	70.11 (158.20)
K	CV bottom, center, outer	38.18 (100.72)	59.64 (139.35)	70.09 (158.17)
L	Drum liner, plug cavity, outer	37.85 (100.13)	43.26 (109.87)	45.81 (114.46)
M	Drum liner, plug cavity, inner	37.91 (100.25)	46.93 (116.47)	51.29 (124.33)
N	Drum liner, CV flange cavity, outer	37.97 (100.34)	49.87 (121.77)	55.70 (132.26)
O	Drum liner, CV cavity, mid-height, inner	38.07 (100.52)	55.08 (131.15)	63.53 (146.36)
P	Drum liner, CV cavity, bottom, inner	38.12 (100.62)	56.87 (134.37)	66.02 (150.83)
Q	Borobond4, top, outer	37.97 (100.35)	50.31 (122.55)	56.35 (133.43)
R	Borobond4, mid-height, inner	38.07 (100.52)	55.08 (131.14)	63.53 (146.35)
S	Borobond4, mid-height, outer	38.12 (100.50)	54.45 (130.02)	62.59 (144.66)
T	Borobond4, bottom, inner	38.08 (100.55)	54.95 (130.91)	63.21 (145.79)
U	Borobond4, bottom, outer	38.07 (100.52)	54.16 (129.48)	62.05 (143.69)
V	Drum plug liner, bottom, center	37.82 (100.07)	41.36 (106.46)	42.96 (109.34)
W	Drum plug liner, top, center	37.98 (100.37)	50.51 (122.93)	56.59 (133.87)
X	Drum lid, top, center	37.79 (100.03)	39.82 (103.67)	40.67 (105.20)
Y	Drum lid, top, outer	37.79 (100.03)	40.08 (104.14)	41.06 (105.90)
Z	Drum, mid-height, outer	37.84 (100.11)	41.60 (106.88)	43.26 (109.86)
AA	Drum bottom, outer	37.85 (100.13)	41.94 (107.50)	43.76 (110.76)
BB	Drum bottom, center	37.91 (100.23)	45.14 (113.25)	48.51 (119.33)

Notes: (a) See Figure 2.
 (b) Approximate location of the CV O-ring.

Normal Conditions of Transport Analyses Results

Transient thermal analyses are performed on the finite element model of the ES-3100 shipping container to simulate NCT with content heat loads of 0, 0.4, 20, and 30 W. The insolation required for NCT per 10 CFR 71.71(c)(1)^[1] is applied to the top and sides of the drum in alternating 12-hour periods (i.e., 12 hours on and 12 hours off) with the drum bottom remaining adiabatic during the transient thermal analysis. An ambient temperature of 37.8°C (100°F) as stipulated in 10 CFR 71 is used in the NCT analysis. The initial temperature distribution within the package for the NCT transients was determined from steady-state analyses (with radiation and natural convection boundary conditions applied to the top and sides of the drum) for each internal heat load. For the case with no internal heat source (0 W), the initial temperature distribution within the package was assumed to be at a uniform 37.8°C (100°F).

The transient thermal analyses simulate a five-day period of cyclic solar loading with 12 hours of insolation being applied at the beginning of each day (i.e., onset of sunrise) followed by 12 hours in which there is no insolation to end the day (i.e., onset of sunset). This five-day period allows for “quasi

steady-state” conditions to be reached. While the temperature of a particular node within the model changes with respect to time in the transient analyses, the maximum temperature that node reaches from day-to-day does not change once a “quasi steady-state” condition is reached. In particular, the maximum temperature of the key location on the containment vessel (i.e., at the O-ring) on day 5 is within 0.01°C of the maximum temperature of the same location on day 4.

The maximum temperatures of several locations within the model are summarized in Table 5 and Table 6 for content heat loads of 0, 0.4, 20, and 30 W and Kaolite densities of 30 (maximum density) and 19.4 lbm/ft³ (minimum density), respectively. The maximum temperatures reported in Table 5 and Table 6 represent “quasi steady-state.” Temperature-history plots of several locations within the model are also depicted graphically in Figure 3 through Figure 10 for various content heat loads and Kaolite density. Additionally, temperature contours of the model at sunrise (0 hours) and sunset (12 hours) for day 5 of the transient are presented in Figure 11 through Figure 18 for various content heat loads and Kaolite density. The elements representing the air between the drum liner and containment vessel and between the drum liner and top plug liner are not shown in the temperature contours presented in these figures so that the containment vessel temperature contours can be more easily viewed.

The maximum temperature in the model occurs at the top center of the drum lid. This maximum temperature is 118.01°C (244.42°F), 118.03°C (244.45°F), 118.77°C (245.79°F), and 119.15°C (246.47°F) for content heat loads of 0, 0.4, 20, and 30 W, respectively, and occurs at sunset in each case (see Table 6, Kaolite density of 19.4 lbm/ft³). The maximum temperature at the containment vessel O-ring is 88.25°C (190.84°F), 88.56°C (191.41°F), 103.87°C (218.96°F), and 111.42°C (232.55°F) for content heat loads of 0, 0.4, 20, and 30 W, respectively, and occurs at approximately 1 hour after sunset in each case (see Table 6, Kaolite density of 19.4 lbm/ft³).

Table 5. Maximum “quasi steady-state” temperatures during NCT for the ES-3100 shipping container with various content heat loads (see Figure 2 for node locations)—Kaolite density of 30 lbm/ft³.

Node ^(a)	Location	Maximum “quasi steady-state” temperature, °C (°F)			
		0 W	0.4 W	20 W	30 W
A	CV lid, top, center	86.56 (187.81)	86.88 (188.38)	102.98 (215.74)	109.59 (229.26)
B	CV lid, bottom, center	86.56 (187.80)	86.88 (188.38)	102.16 (215.90)	109.71 (229.47)
C	CV lid, top, outer	86.54 (187.78)	86.86 (188.34)	101.89 (215.41)	109.31 (228.75)
D	CV flange at interface, inner ^(b)	86.47 (187.64)	86.79 (188.21)	102.09 (215.77)	109.67 (229.40)
E	CV flange at interface, outer ^(b)	86.44 (187.59)	86.76 (188.16)	102.00 (215.61)	109.53 (229.15)
F	CV flange, bottom, outer	86.42 (187.56)	86.74 (188.13)	101.99 (215.58)	109.51 (229.12)
G	CV shell, mid-height, inner	81.52 (178.74)	82.09 (179.76)	109.01 (228.21)	121.98 (251.57)
H	CV shell, mid-height, outer	81.52 (178.74)	82.09 (179.76)	109.00 (228.19)	121.97 (251.55)
I	CV bottom, outer	81.32 (178.37)	81.71 (179.08)	100.57 (213.02)	109.99 (229.99)
J	CV bottom, center, inner	81.37 (178.47)	81.77 (179.18)	100.73 (213.31)	110.21 (230.38)
K	CV bottom, center, outer	81.37 (178.47)	81.77 (179.18)	100.72 (213.29)	110.19 (230.34)
L	Drum liner, plug cavity, outer	97.74 (207.93)	97.82 (208.07)	101.65 (214.96)	103.59 (218.47)
M	Drum liner, plug cavity, inner	92.91 (199.23)	93.06 (199.50)	100.40 (212.72)	104.13 (219.43)
N	Drum liner, CV flange cavity, outer	87.69 (189.84)	87.90 (190.21)	98.09 (208.57)	103.27 (217.43)
O	Drum liner, CV cavity, mid-height, inner	81.30 (178.35)	81.61 (178.90)	96.82 (206.27)	104.13 (219.43)
P	Drum liner, CV cavity, bottom, inner	81.52 (178.74)	81.86 (179.35)	98.30 (208.94)	106.56 (223.80)
Q	Borobond4, top, outer	87.36 (189.25)	87.58 (189.64)	98.19 (208.74)	103.57 (218.43)
R	Borobond4, mid-height, inner	81.30 (178.35)	81.61 (178.90)	98.81 (206.26)	104.58 (220.24)
S	Borobond4, mid-height, outer	81.37 (178.46)	81.66 (178.99)	96.24 (205.23)	103.69 (218.64)
T	Borobond4, bottom, inner	81.67 (179.01)	81.98 (179.56)	96.73 (206.12)	104.19 (219.55)
U	Borobond4, bottom, outer	81.78 (179.21)	82.07 (179.72)	96.11 (205.00)	103.23 (217.81)
V	Drum plug liner, bottom, center	111.30 (232.35)	111.34 (232.42)	113.25 (235.85)	114.21 (237.57)
W	Drum plug liner, top, center	90.70 (195.26)	90.92 (195.66)	101.53 (214.76)	106.87 (224.36)
X	Drum lid, top, center	117.74 (243.93)	117.75 (243.96)	118.50 (245.30)	118.88 (245.98)
Y	Drum lid, top, outer	107.04 (224.68)	107.06 (224.71)	107.94 (226.29)	108.39 (227.10)
Z	Drum, mid-height, outer	91.86 (197.36)	91.90 (197.41)	93.42 (200.15)	94.18 (201.53)
AA	Drum bottom, outer	91.00 (195.79)	91.04 (195.86)	92.92 (199.26)	93.87 (200.96)
BB	Drum bottom, center	87.21 (188.97)	87.31 (189.15)	92.26 (198.07)	94.74 (202.54)

Notes: (a) See Figure 2.
(b) Approximate location of the CV O-ring.

Table 6. Maximum “quasi steady-state” temperatures during NCT for the ES-3100 shipping container with various content heat loads (see Figure 2 for node locations)—Kaolite density of 19.4 lbm/ft³.

Node ^(a)	Location	Maximum “quasi steady-state” temperature, °C (°F)			
		0 W	0.4 W	20 W	30 W
A	CV lid, top, center	88.30 (190.95)	88.62 (191.52)	103.84 (218.91)	111.35 (232.42)
B	CV lid, bottom, center	88.28 (190.90)	88.60 (191.48)	103.90 (219.03)	111.45 (232.62)
C	CV lid, top, outer	88.32 (190.97)	88.63 (191.54)	103.61 (218.50)	111.00(231.80)
D	CV flange at interface, inner ^(b)	88.24 (190.83)	88.56 (191.41)	103.87 (218.96)	111.42 (232.55)
E	CV flange at interface, outer ^(b)	88.25 (190.84)	88.56 (191.41)	103.77 (218.78)	111.27 (232.28)
F	CV flange, bottom, outer	88.24 (190.82)	88.55 (191.39)	103.75 (218.75)	111.25 (232.24)
G	CV shell, mid-height, inner	83.04 (181.47)	83.61 (182.50)	110.50 (230.89)	123.46 (254.23)
H	CV shell, mid-height, outer	83.04 (181.47)	83.61 (182.50)	110.49 (230.88)	123.45 (254.21)
I	CV bottom, outer	83.36 (182.04)	83.75 (182.74)	102.58 (216.64)	111.99 (233.59)
J	CV bottom, center, inner	88.37 (182.07)	83.76 (182.77)	102.70 (216.86)	112.17 (233.91)
K	CV bottom, center, outer	88.37 (181.07)	83.76 (182.77)	102.69 (216.84)	112.15 (233.87)
L	Drum liner, plug cavity, outer	98.72 (209.70)	98.80 (209.85)	102.63 (216.73)	104.58 (220.24)
M	Drum liner, plug cavity, inner	94.43 (201.97)	94.58 (202.24)	101.92 (215.46)	105.65 (222.16)
N	Drum liner, CV flange cavity, outer	89.43 (192.97)	89.63 (193.34)	99.83 (211.70)	105.01 (221.02)
O	Drum liner, CV cavity, mid-height, inner	83.12 (181.62)	83.43 (182.18)	98.63 (209.54)	106.40 (223.52)
P	Drum liner, CV cavity, bottom, inner	83.62 (182.52)	83.96 (183.13)	100.36 (212.65)	108.60 (227.48)
Q	Borobond4, top, outer	88.82 (191.88)	89.04 (192.27)	99.65 (211.38)	105.04 (221.07)
R	Borobond4, mid-height, inner	83.12 (181.62)	83.43 (182.18)	98.63 (209.53)	106.39 (223.51)
S	Borobond4, mid-height, outer	83.03 (181.46)	83.33 (182.00)	97.91 (208.23)	105.36 (221.65)
T	Borobond4, bottom, inner	83.55 (182.39)	83.85 (182.93)	98.58 (209.45)	106.03 (222.86)
U	Borobond4, bottom, outer	83.51 (182.31)	83.80 (182.83)	97.82 (208.07)	104.90 (238.82)
V	Drum plug liner, bottom, center	112.01 (233.62)	112.05 (233.69)	113.95 (237.11)	114.90 (238.82)
W	Drum plug liner, top, center	92.09 (197.77)	92.31 (198.16)	102.93 (217.27)	108.26 (226.87)
X	Drum lid, top, center	118.01 (244.42)	118.03 (244.45)	118.77 (245.79)	119.15 (246.47)
Y	Drum lid, top, outer	107.33 (225.19)	107.34 (225.22)	108.22 (226.80)	108.67 (227.60)
Z	Drum, mid-height, outer	92.27 (198.08)	92.30 (198.14)	93.81 (200.86)	94.58 (202.24)
AA	Drum bottom, outer	91.70 (197.06)	91.74 (197.13)	93.61 (200.49)	94.54 (202.18)
BB	Drum bottom, center	88.82 (191.88)	88.93 (192.07)	93.84 (200.91)	96.30 (205.35)

Notes: (a) See Figure 2.
 (b) Approximate location of the CV O-ring.

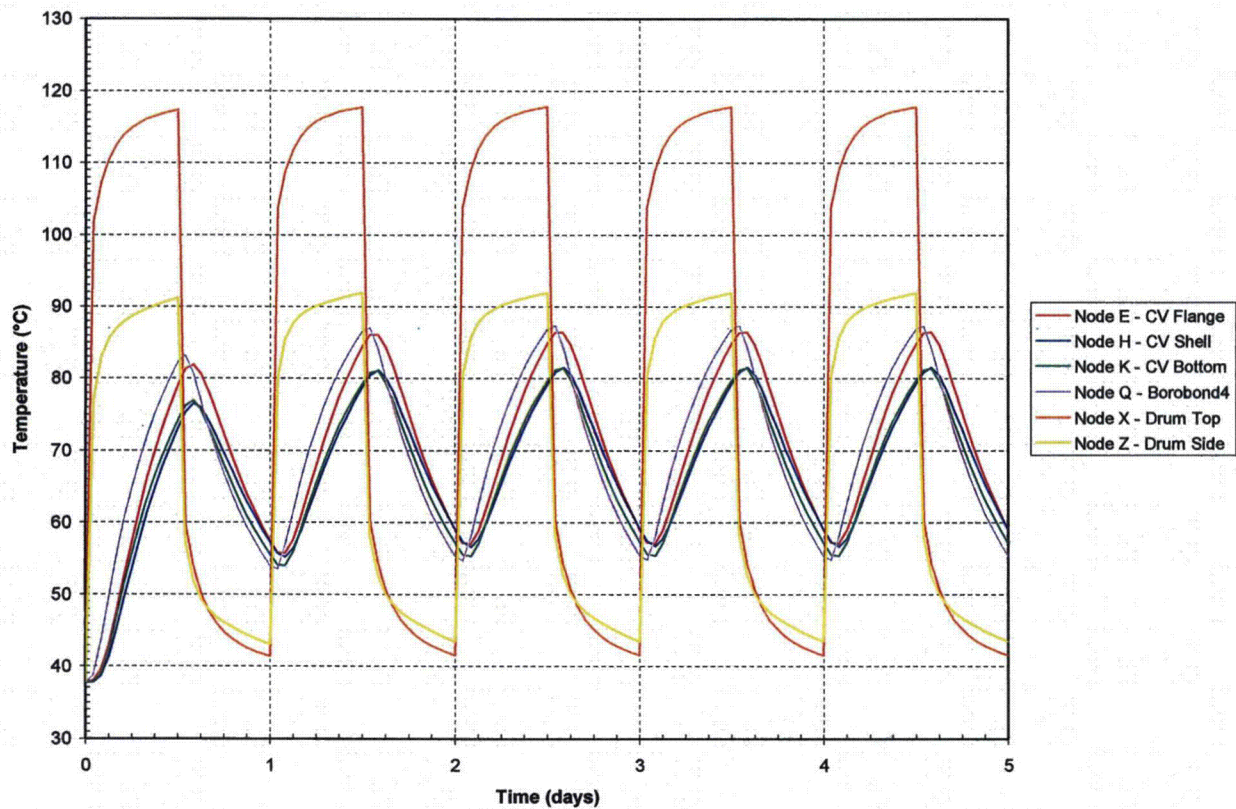


Figure 3. Transient temperatures of the ES-3100 shipping container for NCT (no content heat load) Kaolite density of 30 lbm/ft³ (see Figure 2 for node locations).

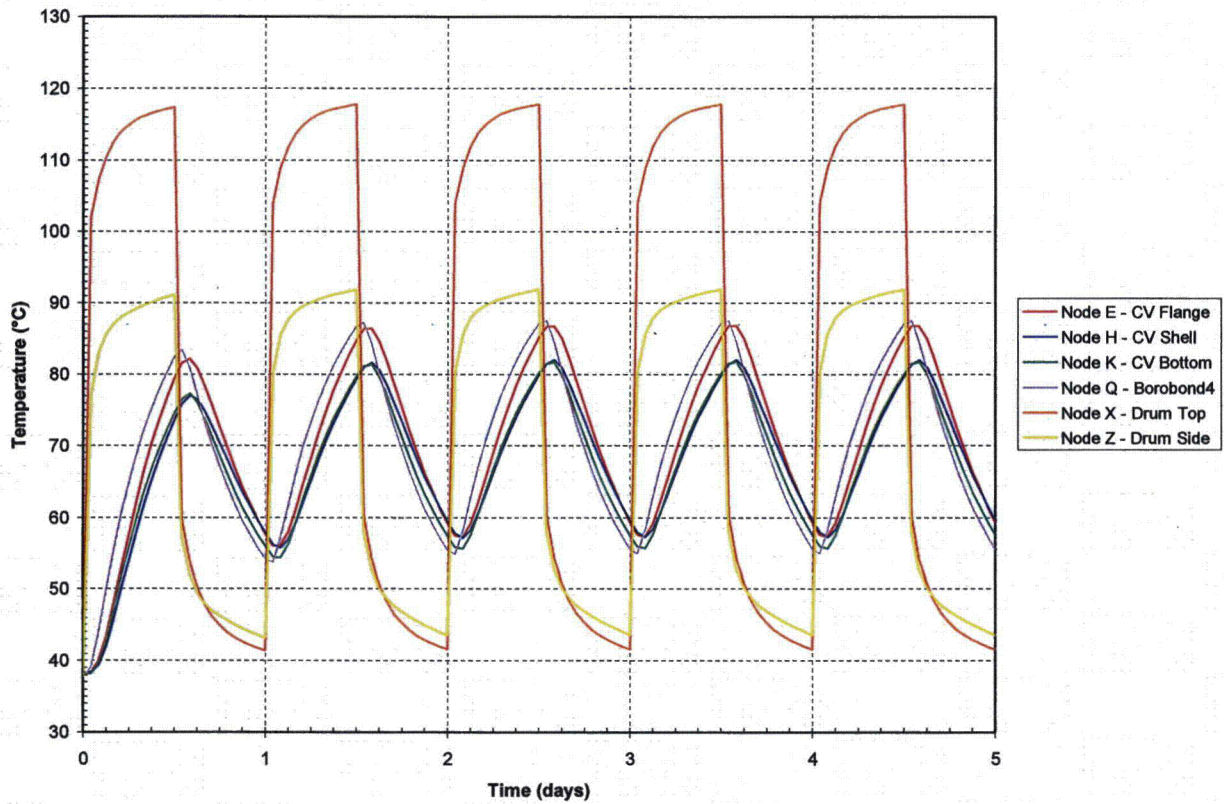


Figure 4. Transient temperatures of the ES-3100 shipping container for NCT (0.4 W content heat load) Kaolite density of 30 lbm/ft³ (see Figure 2 for node locations).

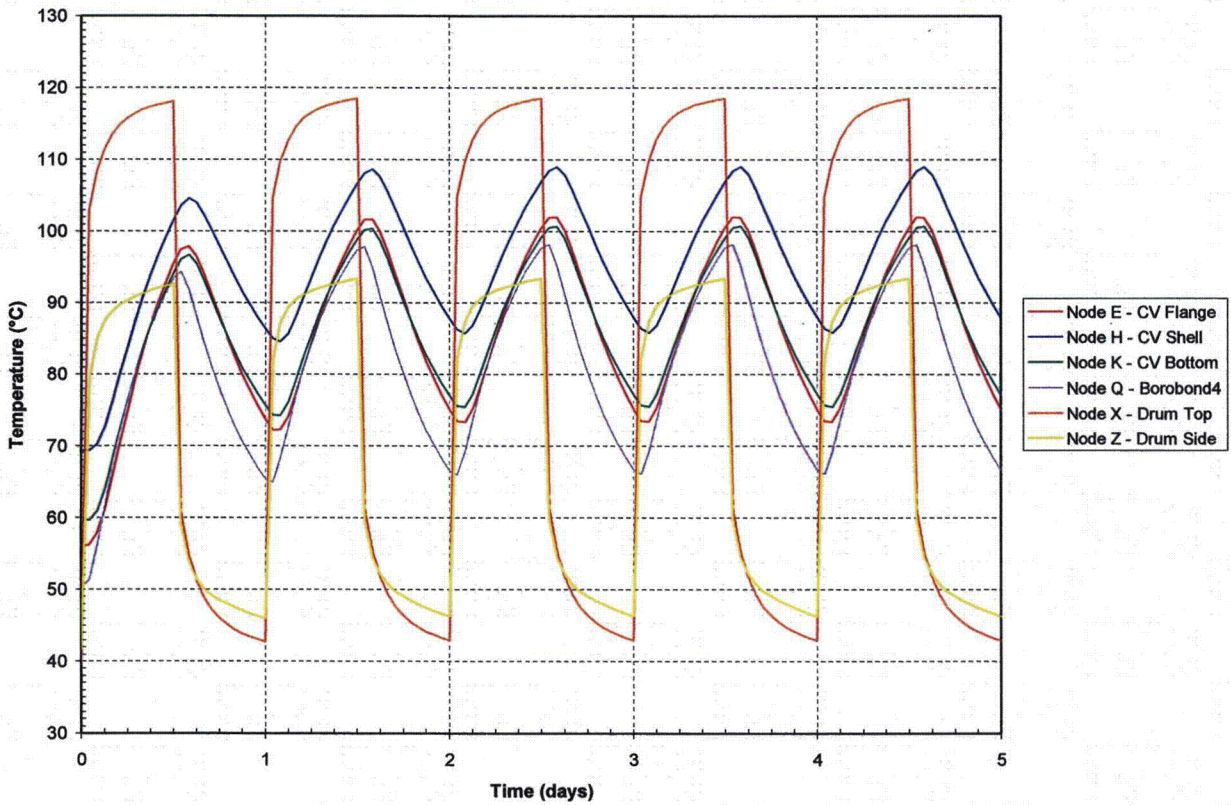


Figure 5. Transient temperatures of the ES-3100 shipping container for NCT (20 W content heat load) Kaolite density of 30 lbm/ft³ (see Figure 2 for node locations).

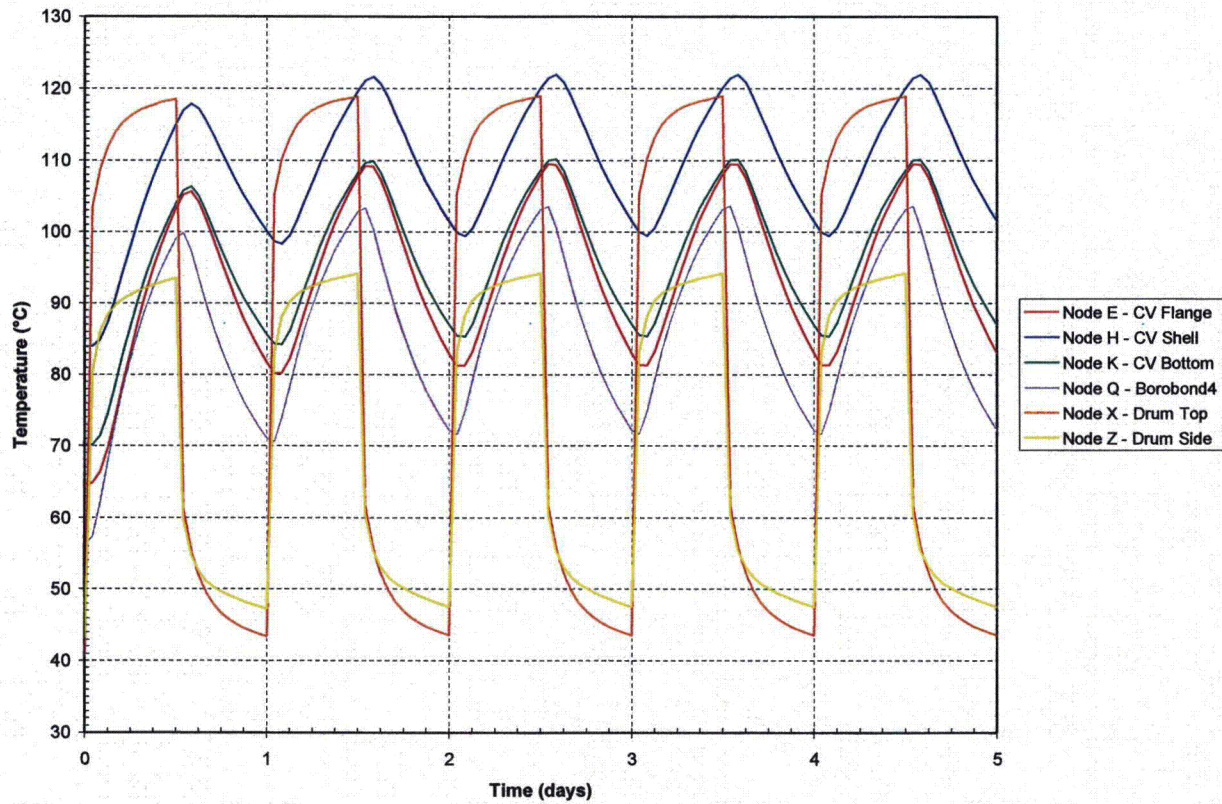


Figure 6. Transient temperatures of the ES-3100 shipping container for NCT (30 W content heat load)Kaolite density of 30 lbm/ft³ (see Figure 2 for node locations).

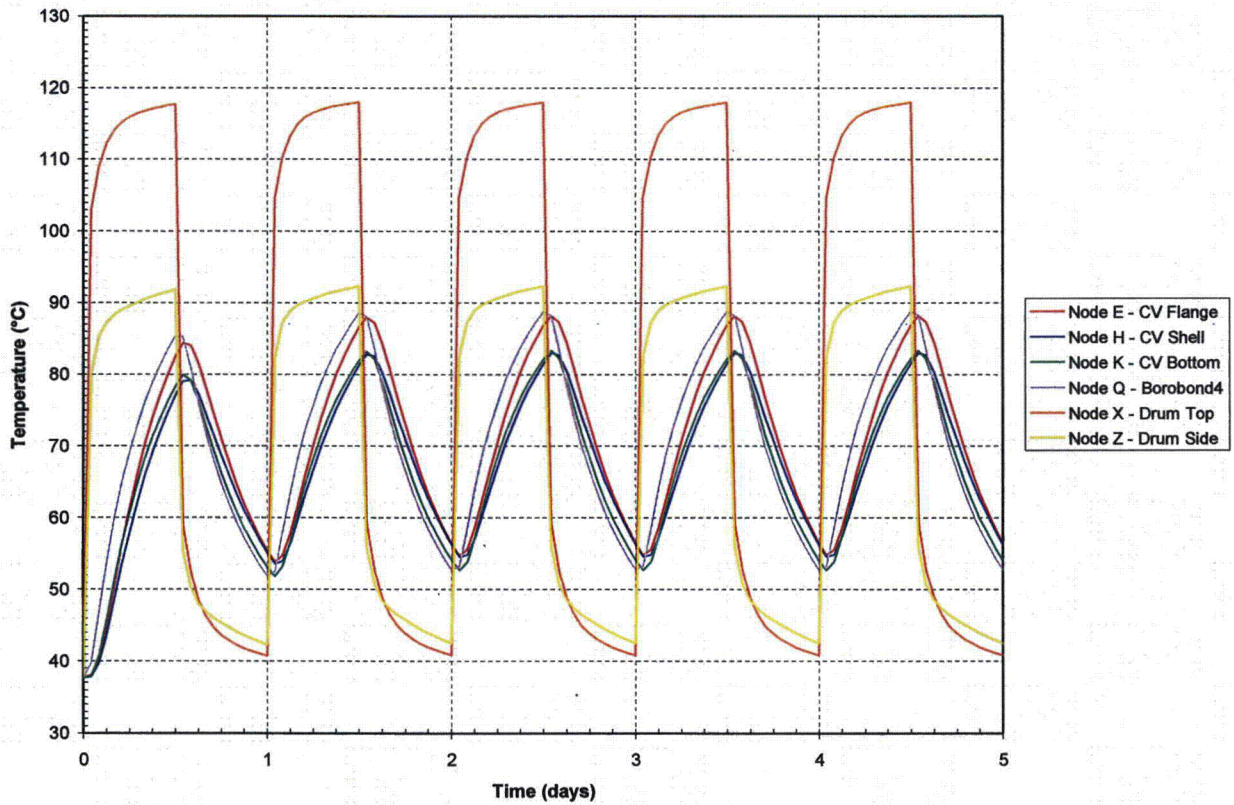


Figure 7. Transient temperatures of the ES-3100 shipping container for NCT (no content heat load) Kaolite density of 19.4 lbm/ft³ (see Figure 2 for node locations).

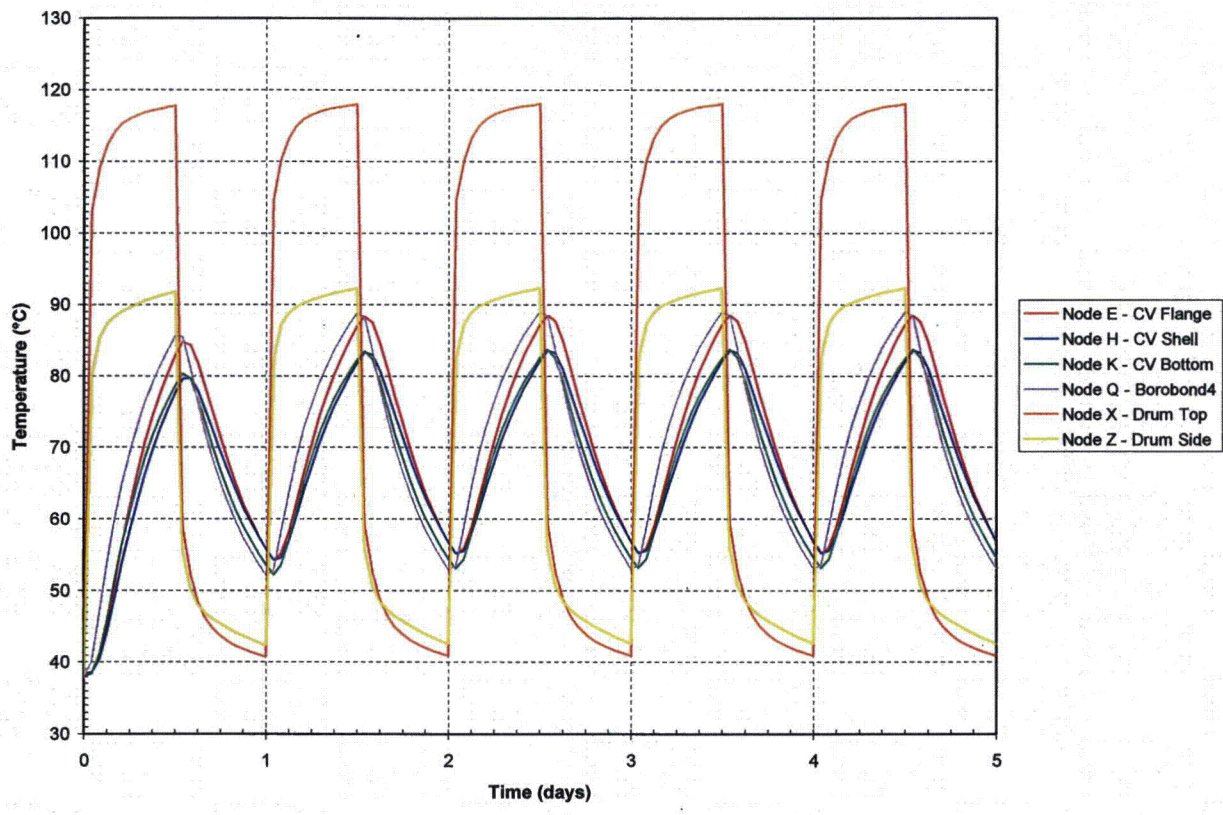


Figure 8. Transient temperatures of the ES-3100 shipping container for NCT (0.4 W content heat load) Kaolite density of 19.4 lbm/ft³ (see Figure 2 for node locations).

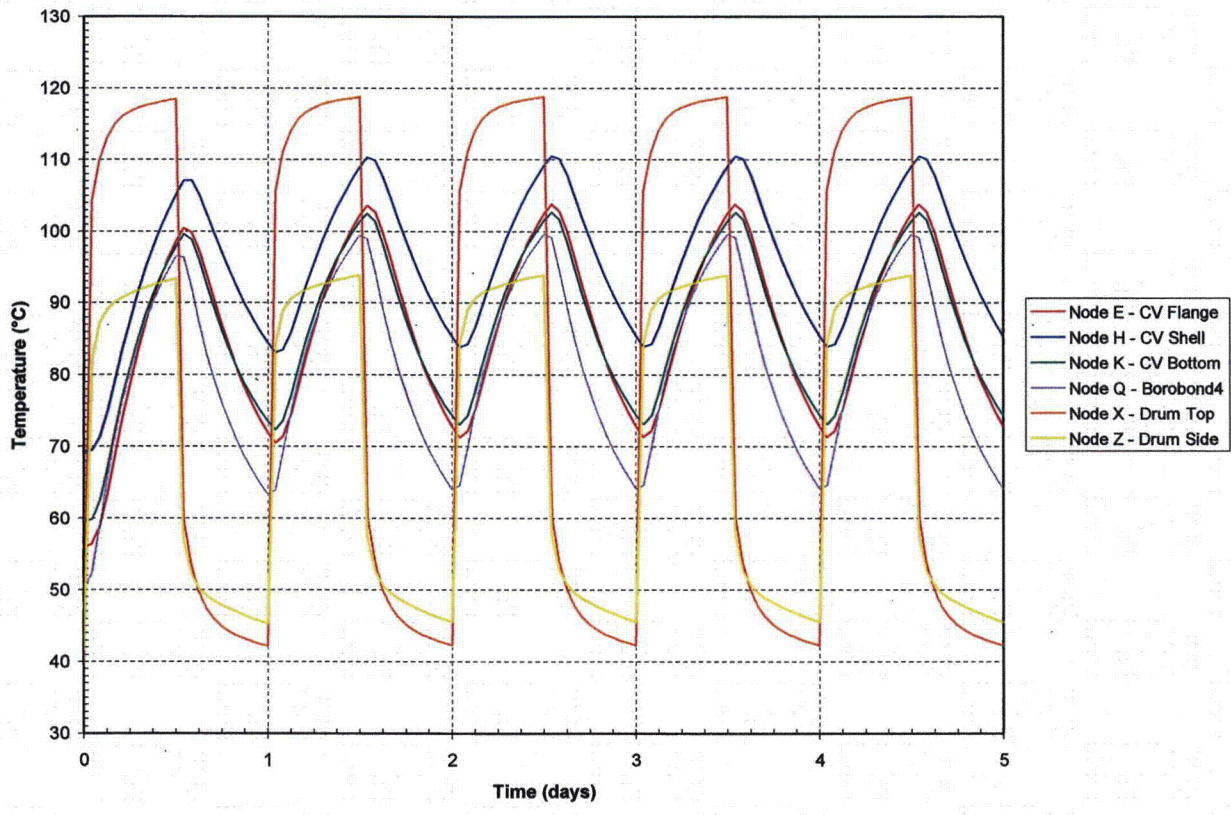


Figure 9. Transient temperatures of the ES-3100 shipping container for NCT (20 W content heat load) Kaolite density of 19.4 lbm/ft³ (see Figure 2 for node locations).

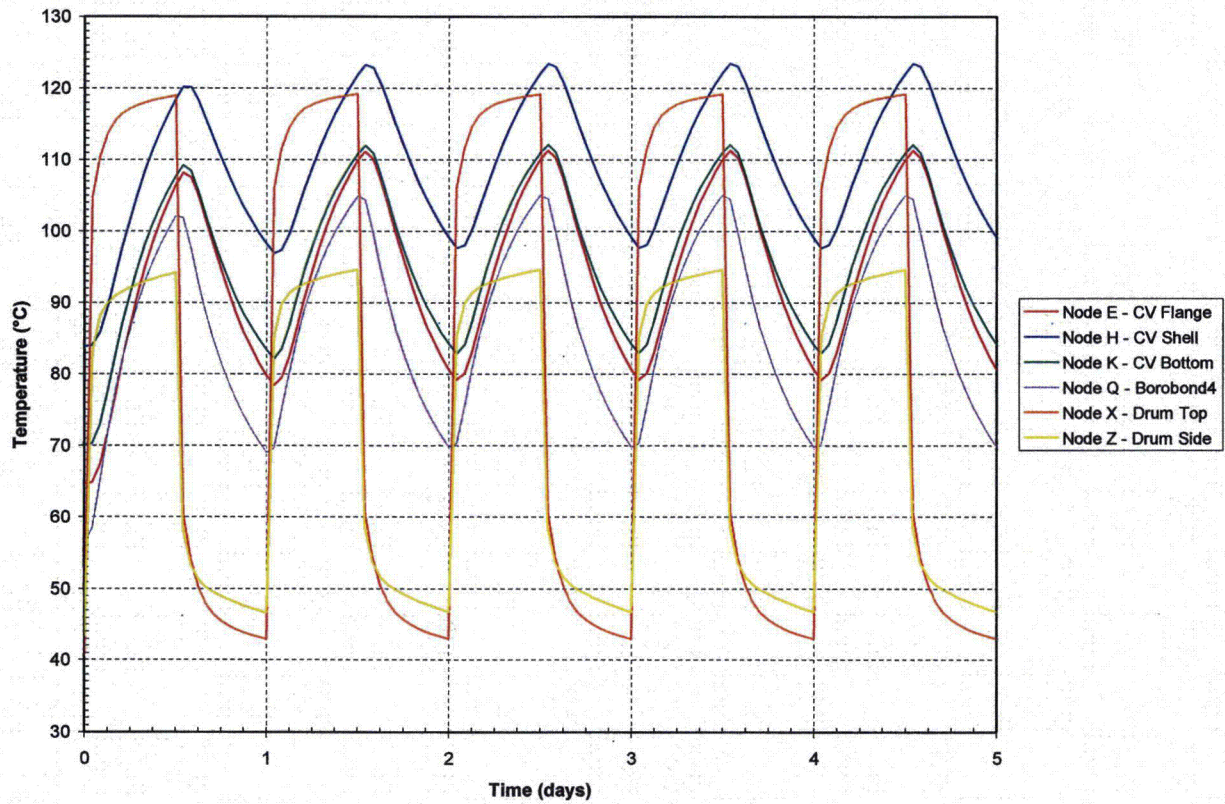


Figure 10. Transient temperatures of the ES-3100 shipping container for NCT (30 W content heat load) Kaolite density of 19.4 lbm/ft³ (see Figure 2 for node locations).

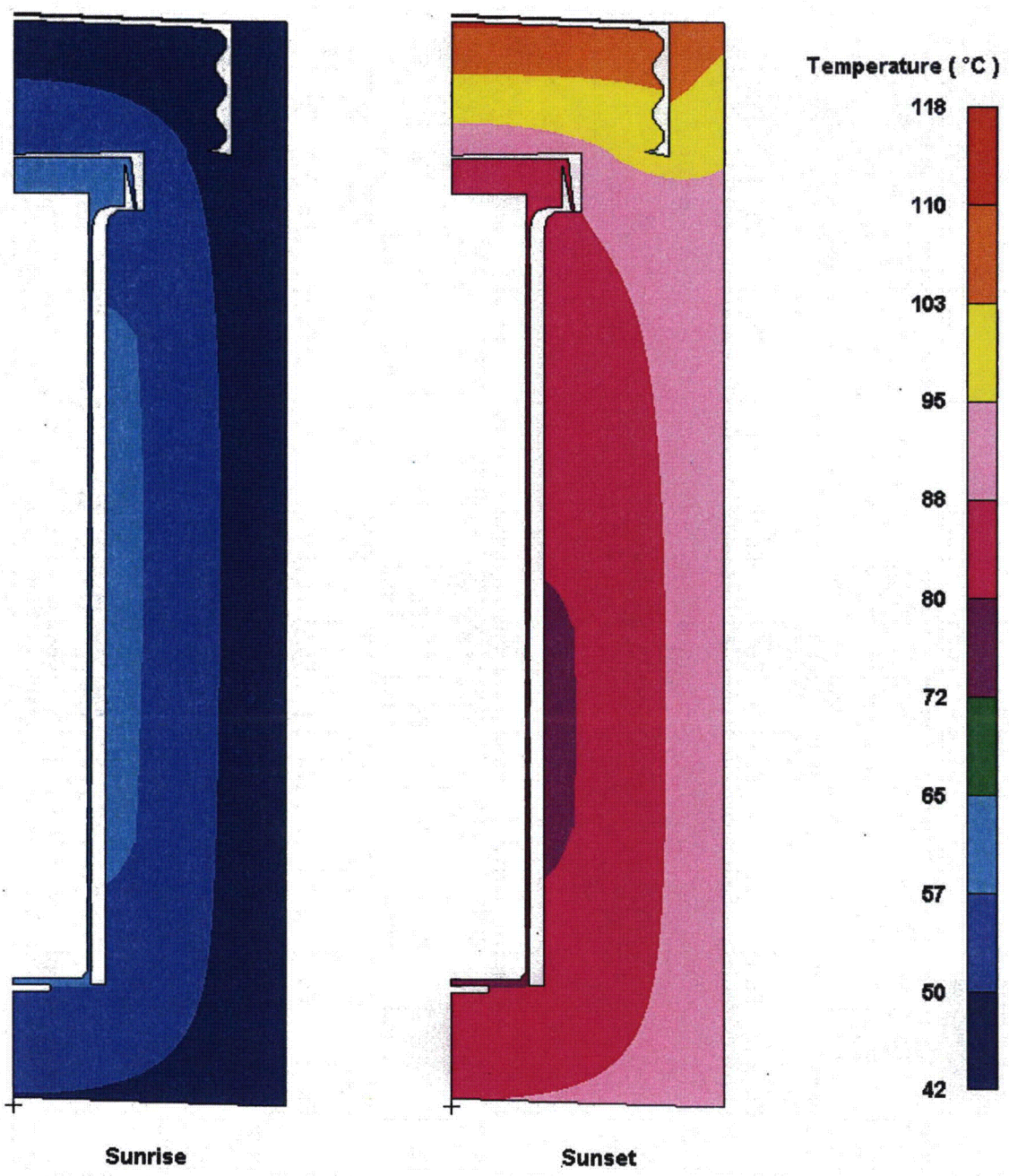


Figure 11. Temperature distribution in the ES-3100 shipping container for NCT (no content heat load)—Kaolite density of 30 lbm/ft³—day 5 of transient analysis (elements representing air not shown for clarity).

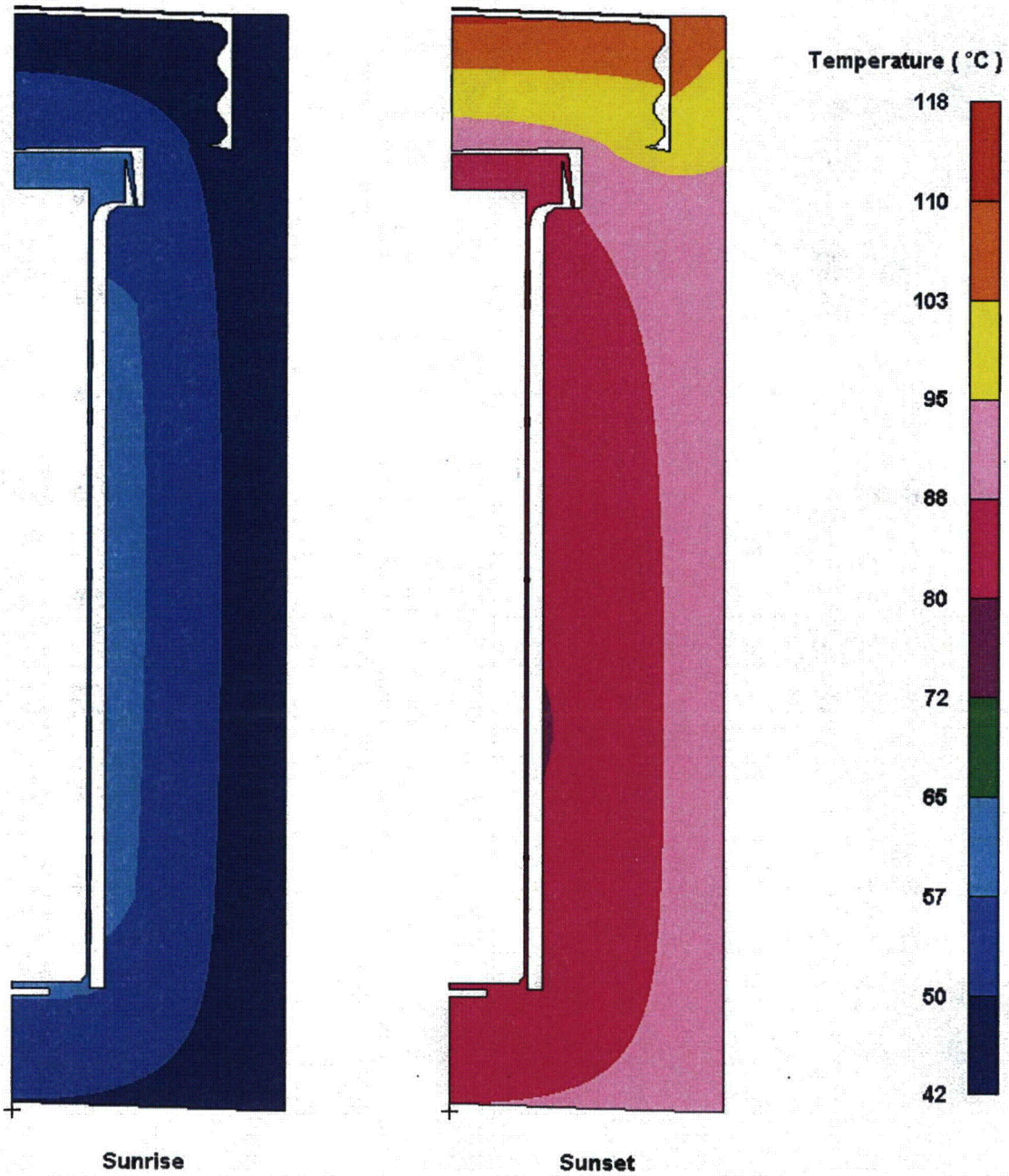


Figure 12. Temperature distribution in the ES-3100 shipping container for NCT (0.4 W content heat load)—Kaolite density of 30 lbm/ft³—day 5 of transient analysis (elements representing air not shown for clarity).

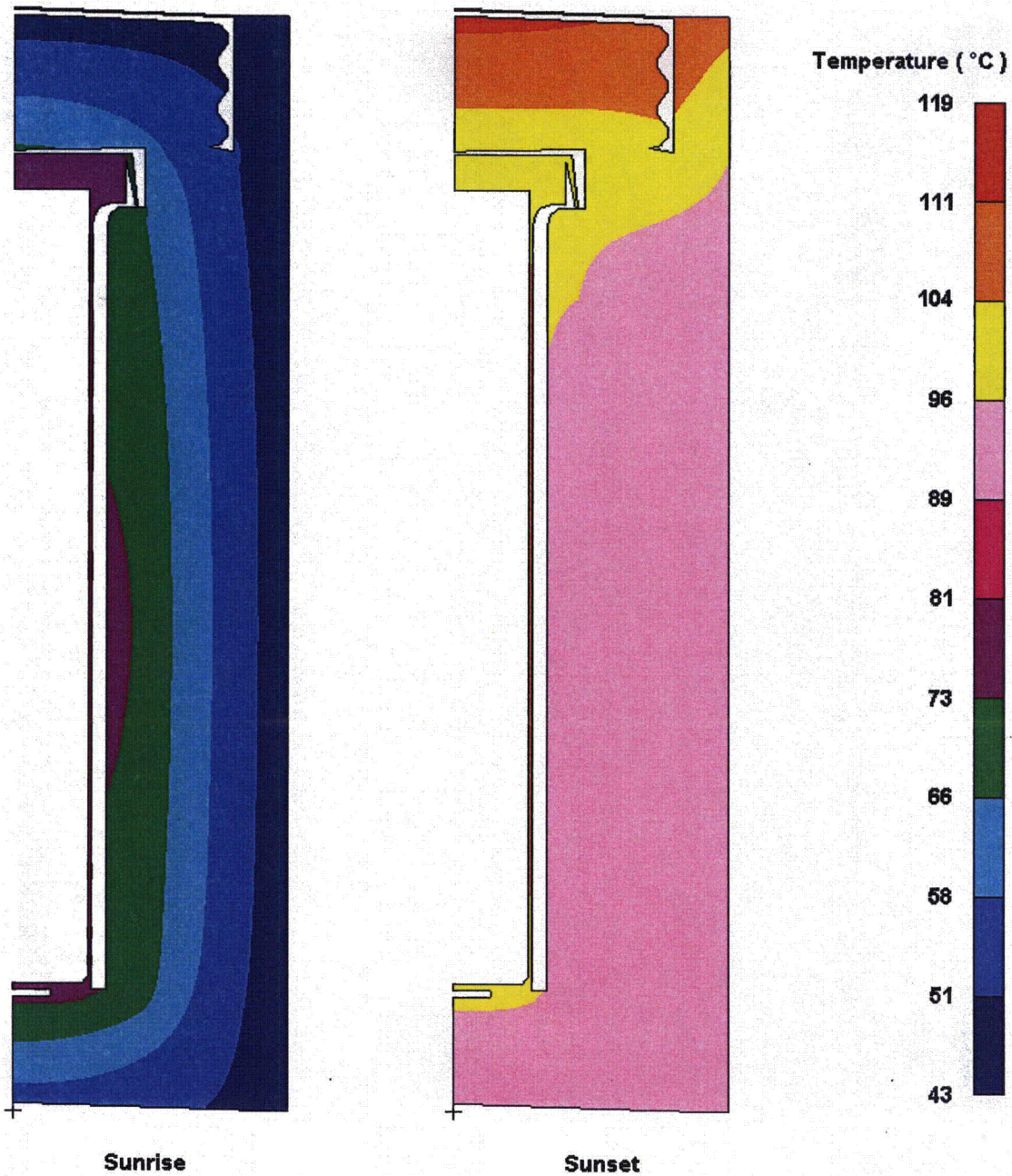


Figure 13. Temperature distribution in the ES-3100 shipping container for NCT (20 W content heat load)—Kaolite density of 30 lbm/ft³—day 5 of transient analysis (elements representing air not shown for clarity).

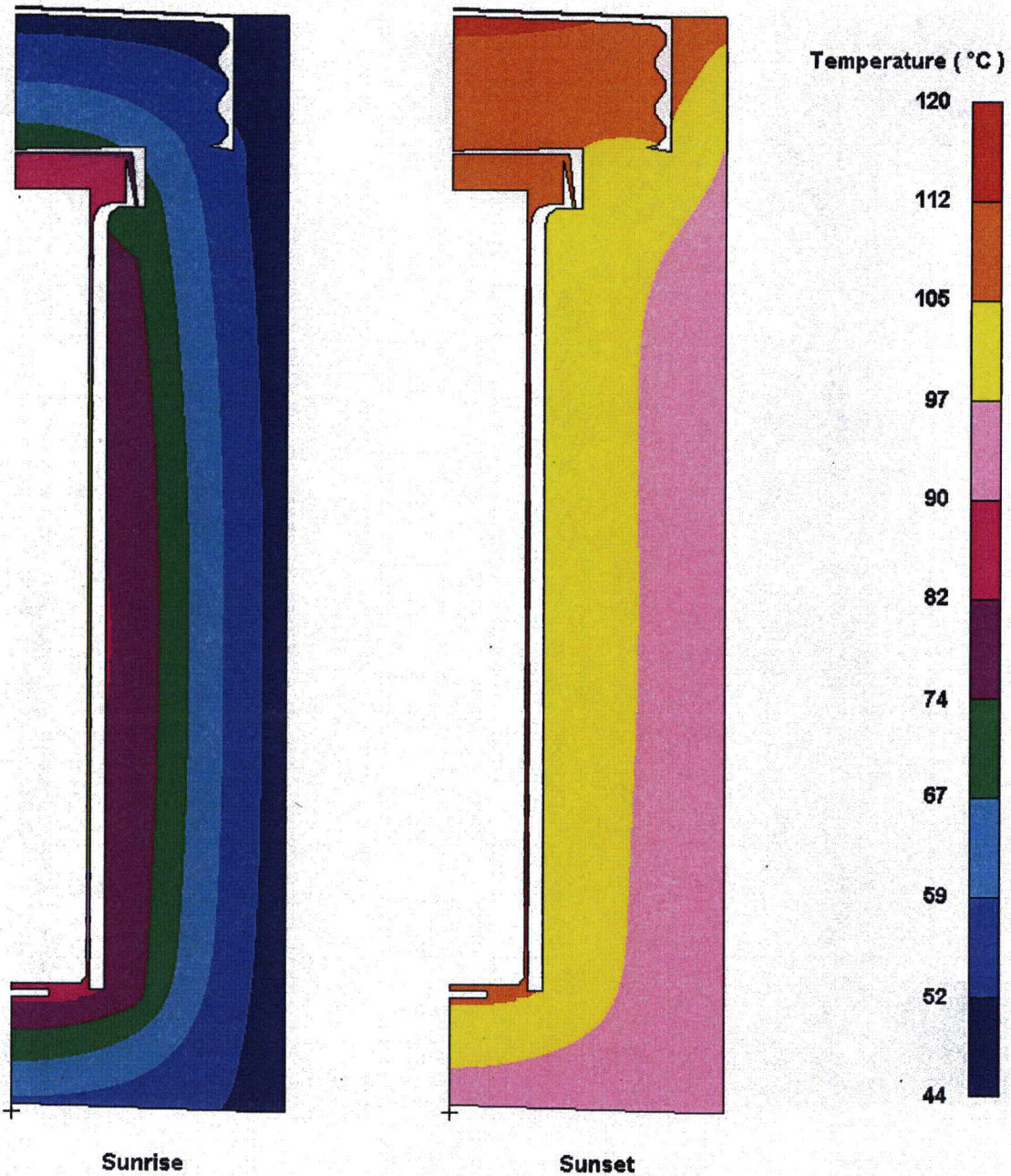


Figure 14. Temperature distribution in the ES-3100 shipping container for NCT (30 W content heat load)—Kaolite density of 30 lbm/ft³—day 5 of transient analysis (elements representing air not shown for clarity).

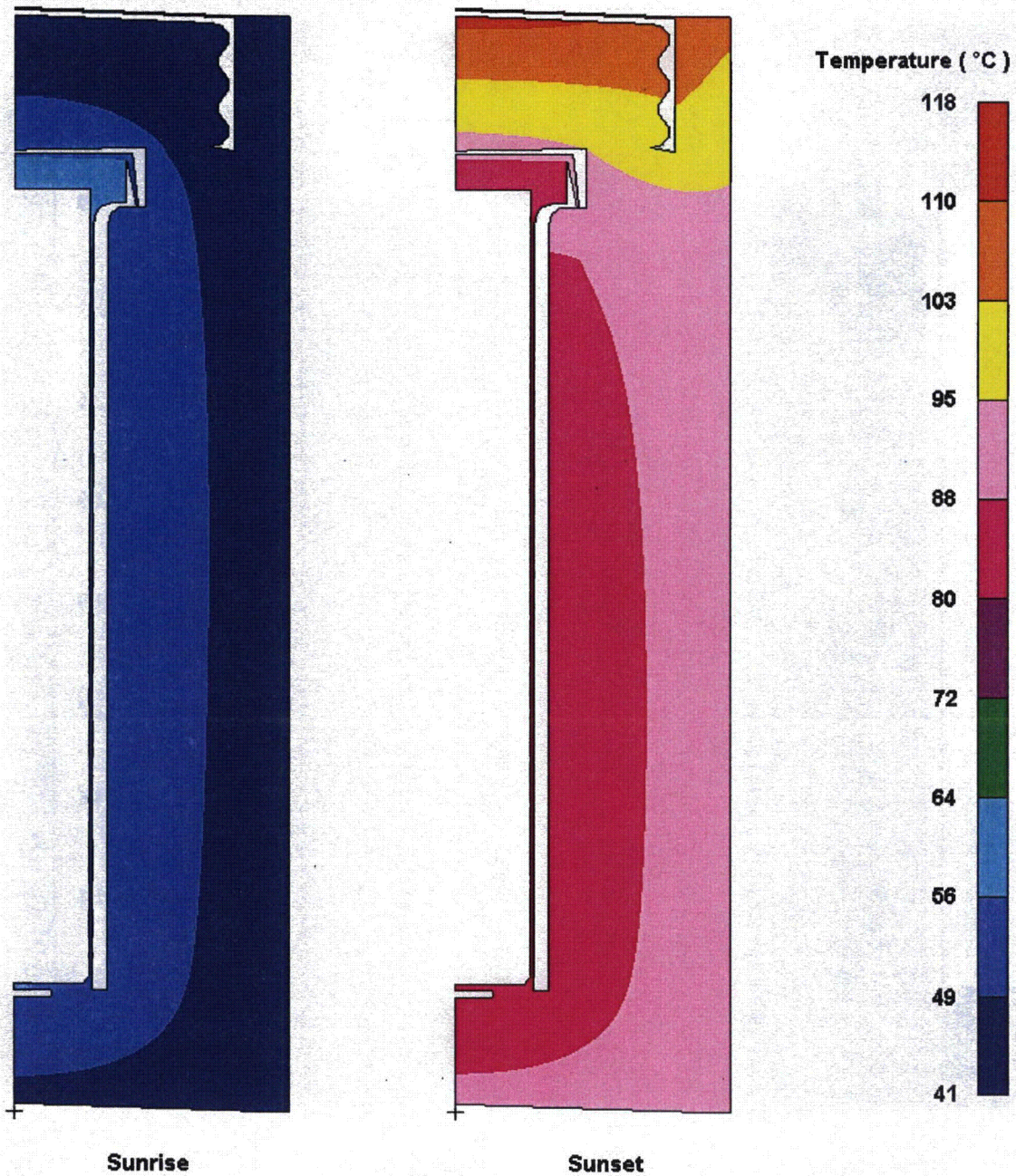


Figure 15. Temperature distribution in the ES-3100 shipping container for NCT (no content heat load)—Kaolite density of 19.4 lbm/ft³—day 5 of transient analysis (elements representing air not shown for clarity).

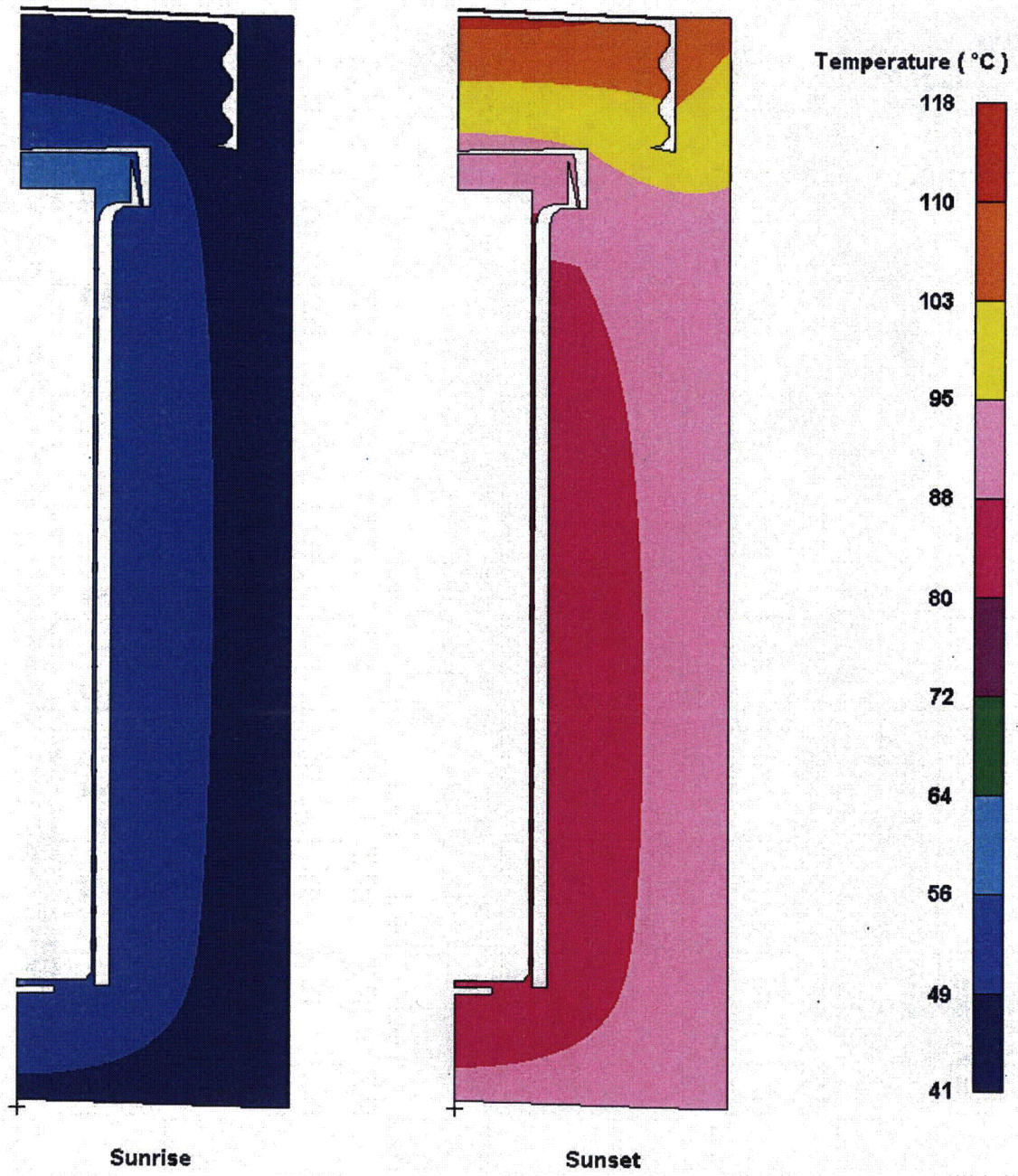


Figure 16. Temperature distribution in the ES-3100 shipping container for NCT (0.4 W content heat load)—Kaolite density of 19.4 lbm/ft³—day 5 of transient analysis (elements representing air not shown for clarity).

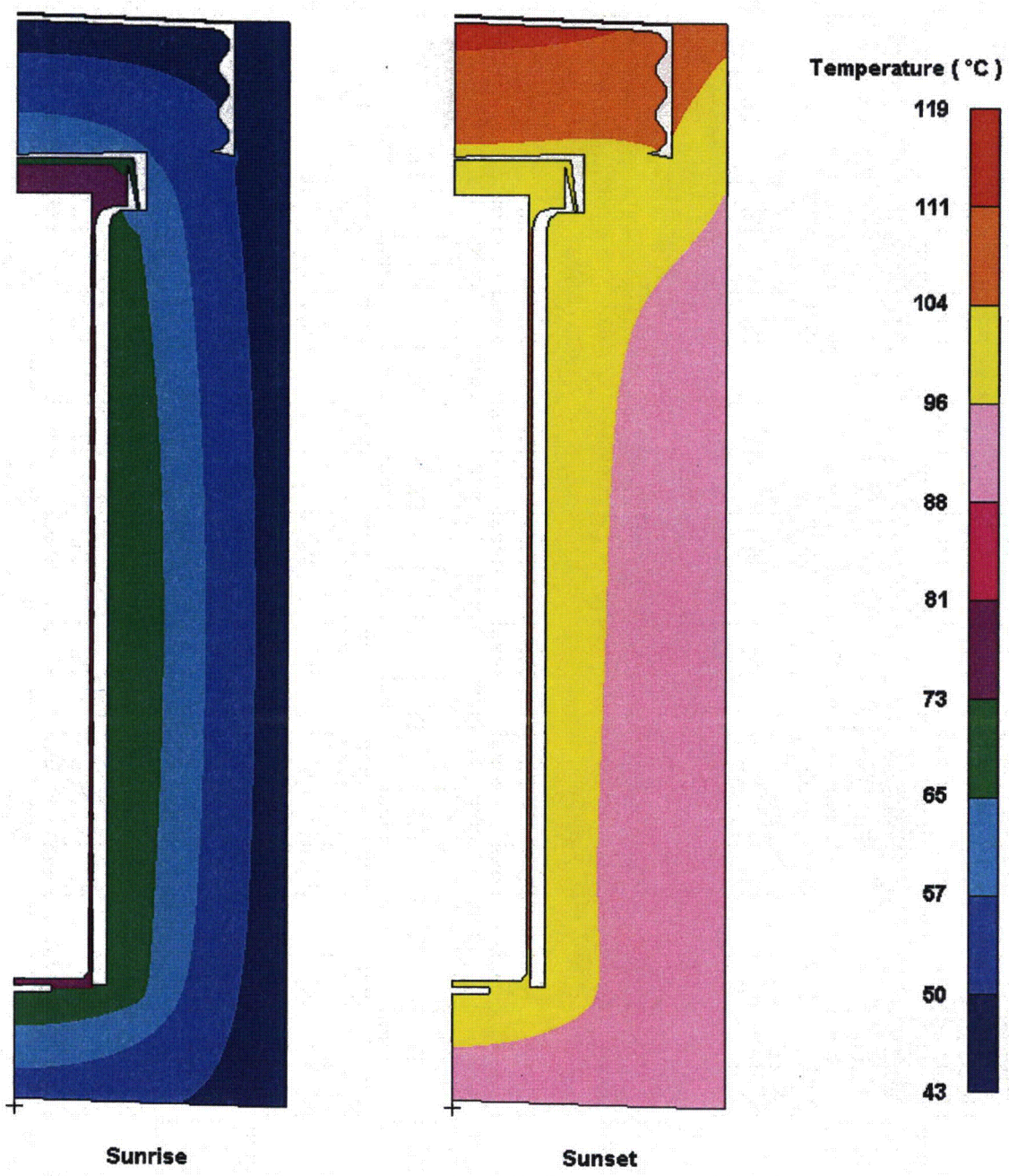


Figure 17. Temperature distribution in the ES-3100 shipping container for NCT (20 W content heat load)—Kaolite density of 19.4 lbm/ft³—day 5 of transient analysis (elements representing air not shown for clarity).

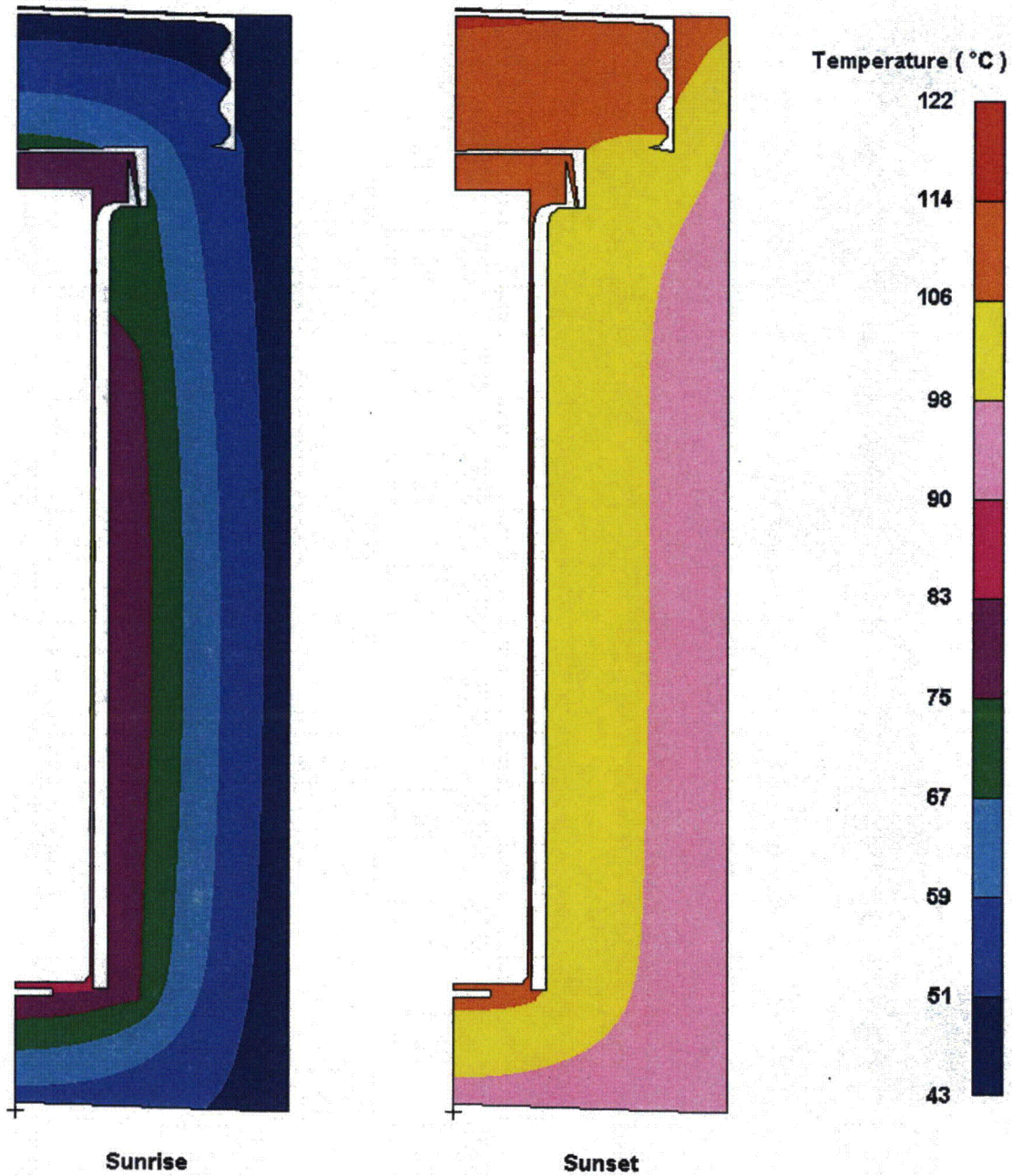


Figure 18. Temperature distribution in the ES-3100 shipping container for NCT (30 W content heat load)—Kaolite density of 19.4 lbm/ft³—day 5 of transient analysis (elements representing air not shown for clarity).

Hypothetical Accident Conditions Analyses Results

Transient thermal analyses are performed on the finite element model of the ES-3100 shipping container (undamaged configuration) to simulate HAC as prescribed by 10 CFR 71.73(c)(4).^[1] A 30-minute fire of 800°C (1472°F) is simulated by applying natural convection and radiant exchange boundary conditions to all external surfaces of the drum (assuming the drum is in a horizontal orientation) with content heat loads of 0, 0.4, 20, and 30 W and Kaolite densities of 30 (maximum density) and 19.4 lbm/ft³ (minimum density). No heat flux boundary conditions simulating insolation are applied to the model during the 30-minute fire. The initial temperature distribution within the package having content heat loads of 0.4, 20, and 30 W is obtained from their respective steady-state analyses. The initial temperature distribution within the package having no content heat load (0 W) is assumed to be at a uniform temperature equal to the ambient temperature of 37.8°C (100°F).

Following the 30-minute fire transient analyses, 48-hour cool-down transient thermal analyses are performed using the temperature distribution at the end of the fire as the initial temperature distribution. During post-fire cool-down, natural convection and radiant exchange boundary conditions are applied to all external surfaces of the drum (assuming the drum is in a horizontal orientation). Additionally, cases are analyzed in which insolation is included during the post-fire cool-down. For the cases in which insolation is applied to the model during cool-down, insolation is applied during the first 12-hour period following the 30-minute fire, then alternated (off, then on) as was done for NCT.

The maximum temperatures calculated for the ES-3100 shipping container for HAC are summarized in Table 7 for the analyses using a Kaolite density of 30 lbm/ft³ and Table 8 for the analyses using a Kaolite density of 19.4 lbm/ft³. Temperature-history plots of several locations within the model are also depicted graphically in Figure 19 through Figure 22 for content heat loads of 0, 0.4, 20, and 30 W and a Kaolite density of 19.4 lbm/ft³ (the graphs for the cases having a Kaolite density of 30 lbm/ft³ are not shown because of their similarity to the presented graphs).

Table 7. ES-3100 shipping container HAC maximum temperatures—Kaolite density of 30 lbm/ft³.

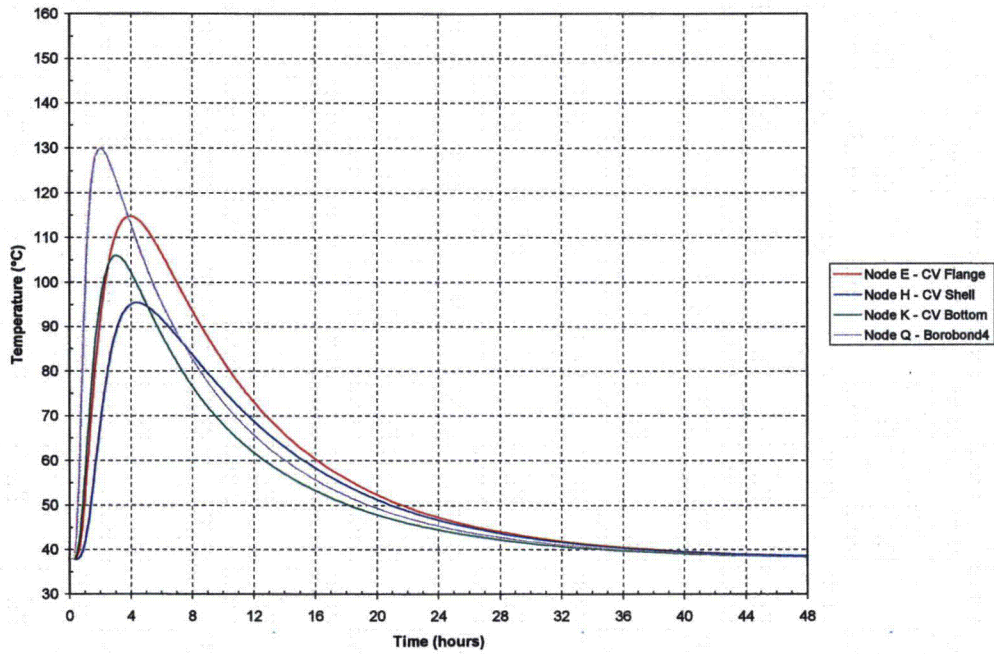
Content heat load (W)	Insolation during cool-down	Maximum temperature, °C (°F)						
		Node A ^(a) CV lid	Node E ^(a) CV flange at O-ring	Node H ^(a) CV shell (mid-elevation)	Node K ^(a) CV bottom (center)	Node Q ^(a) Borobond4 (top)	Node S ^(a) Borobond4 (mid-elevation)	Node T ^(a) Borobond4 (bottom)
0	No ^(b)	109.61 (229.29)	109.34 (228.81)	92.21 (197.98)	99.71 (211.47)	118.48 (245.26)	90.42 (194.76)	102.07 (215.73)
	Yes	116.91 (242.43)	116.74 (242.12)	104.22 (219.59)	106.13 (223.04)	122.46 (252.43)	103.28 (217.90)	107.63 (225.73)
0.4	No	109.93 (229.87)	109.66 (229.38)	92.78 (199.00)	100.11 (212.19)	118.69 (245.64)	90.73 (195.31)	102.38 (216.29)
	Yes	117.22 (243.00)	117.05 (242.68)	104.77 (220.58)	106.52 (223.74)	122.67 (252.81)	103.58 (218.45)	107.93 (226.28)
20	No	126.14 (259.05)	125.85 (258.53)	120.27 (248.48)	119.75 (247.56)	130.06 (266.11)	106.49 (223.67)	117.92 (244.25)
	Yes	133.07 (271.52)	132.85 (271.17)	131.38 (268.48)	125.90 (258.91)	134.05 (273.28)	118.96 (246.13)	123.31 (253.95)
30	No	134.00 (273.20)	133.69 (272.56)	133.41 (272.14)	129.43 (264.97)	135.69 (276.23)	114.38 (237.89)	125.62 (258.11)
	Yes	140.79 (285.42)	140.58 (285.05)	144.22 (291.59)	135.47 (275.85)	139.68 (283.42)	126.76 (260.17)	130.95 (267.71)

Notes: (a) See Figure 2 for node locations.
 (b) Baseline case for ΔT comparisons.

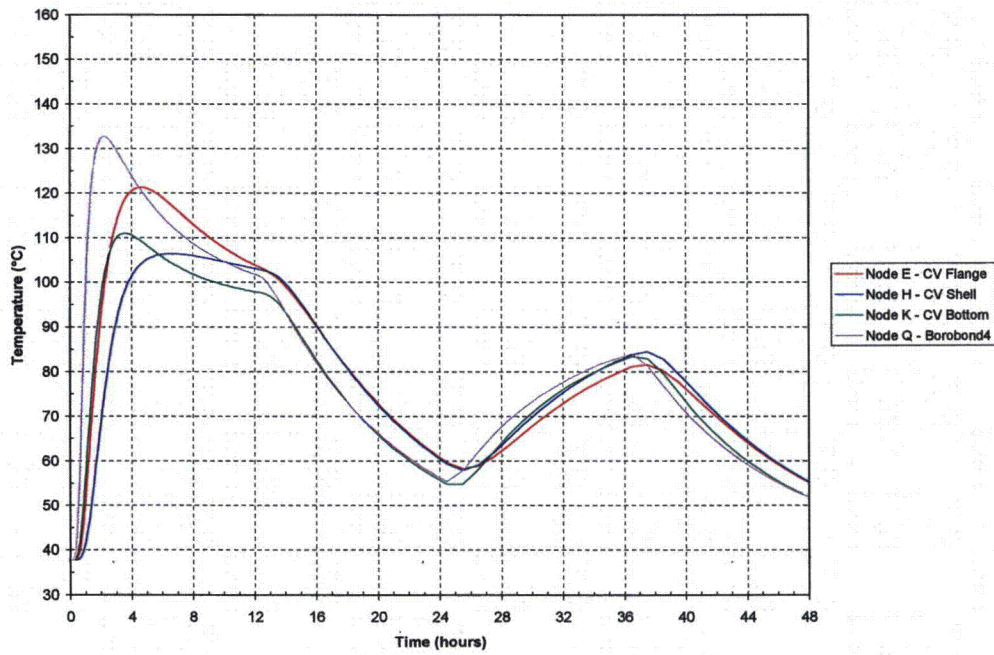
Table 8. ES-3100 shipping container HAC maximum temperatures—Kaolite density of 19.4 lbm/ft³.

Content heat load (W)	Insolation during cool-down	Maximum temperature, °C (°F)						
		Node A ^(a) CV lid	Node E ^(a) CV flange at O-ring	Node H ^(a) CV shell (mid-elevation)	Node K ^(a) CV bottom (center)	Node Q ^(a) Borobond4 (top)	Node S ^(a) Borobond4 (mid-elevation)	Node T ^(a) Borobond4 (bottom)
0	No ^(b)	114.95 (238.92)	114.69 (238.43)	95.48 (203.86)	105.98 (222.77)	129.89 (265.79)	93.95 (201.11)	109.65 (229.36)
	Yes	121.44 (250.60)	121.27 (250.28)	106.43 (223.58)	111.02 (231.83)	132.73 (270.92)	105.10 (221.19)	113.62 (236.51)
0.4	No	115.27 (239.49)	115.00 (239.00)	96.04 (204.87)	106.37 (223.47)	130.09 (266.17)	94.25 (201.65)	109.95 (229.91)
	Yes	121.75 (251.16)	121.58 (250.85)	106.97 (224.57)	111.41 (232.53)	132.94 (271.30)	105.41 (221.73)	113.92 (237.06)
20	No	131.51 (268.71)	131.22 (268.19)	123.43 (254.17)	126.00 (258.80)	141.29 (286.32)	109.98 (229.96)	125.44 (257.80)
	Yes	137.69 (279.84)	137.49 (279.48)	133.54 (272.37)	130.83 (267.49)	144.13 (291.44)	120.84 (249.51)	129.33 (264.79)
30	No	139.39 (282.90)	139.08 (282.25)	136.53 (277.75)	135.66 (276.19)	146.82 (296.28)	117.85 (244.14)	133.11 (271.60)
	Yes	145.45 (293.82)	145.24 (293.44)	146.35 (295.43)	140.42 (284.75)	149.67 (301.41)	128.65 (263.57)	136.97 (278.55)

Notes: (a) See Figure 2 for node locations.
 (b) Baseline case for ΔT comparisons.

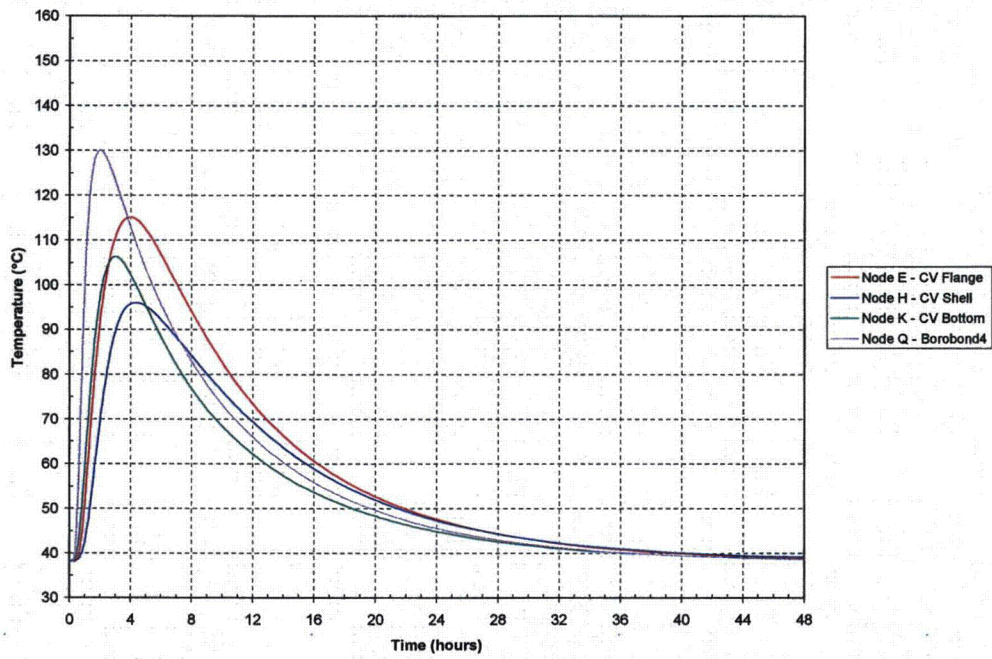


(a) No insolation during post-fire cool-down.

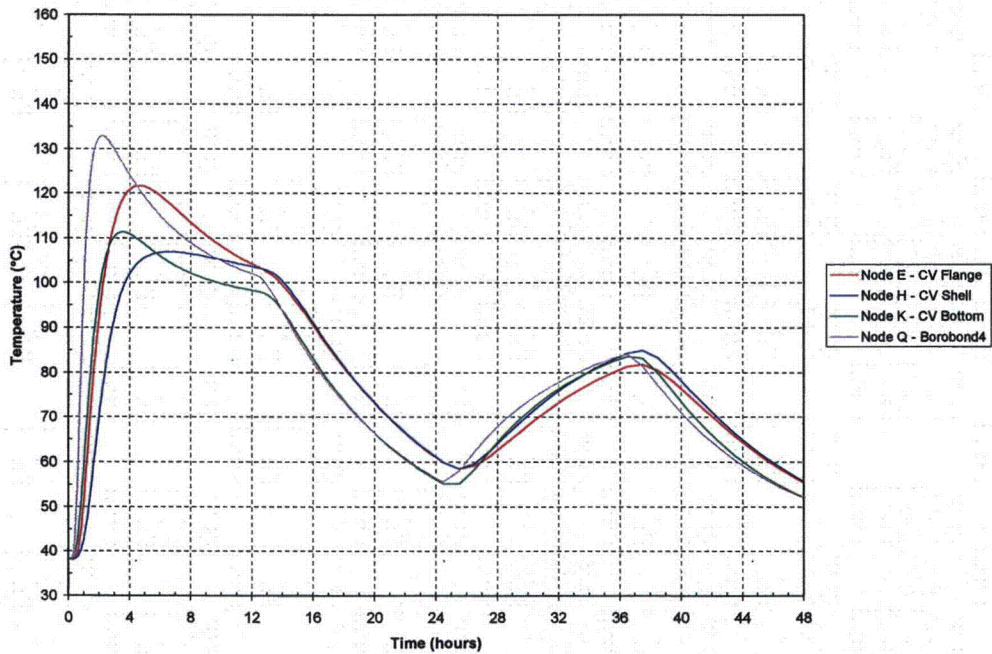


(b) Insolation during post-fire cool-down.

Figure 19. ES-3100 shipping container transient temperatures for HAC (no content heat load) Kaolite density of 19.4 lbm/ft³ (see Figure 2 for node locations).

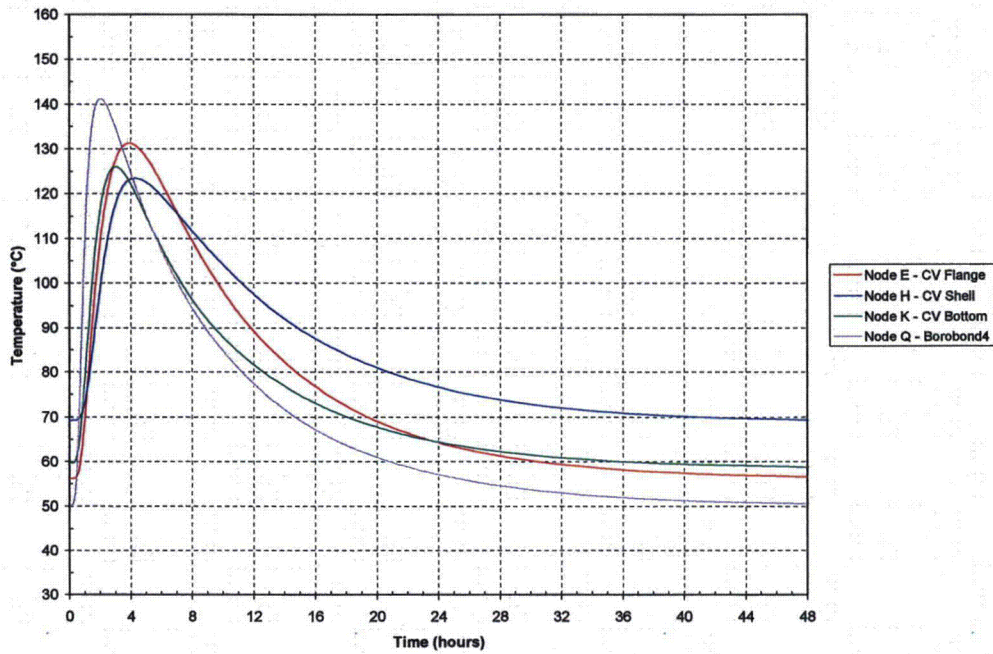


(a) No insulation during post-fire cool-down.

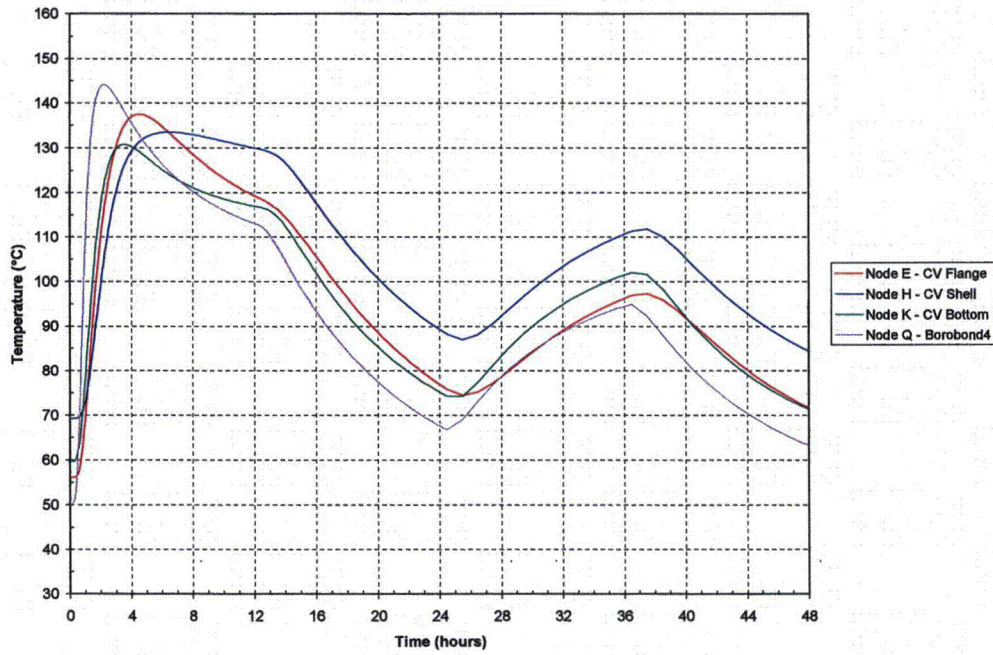


(b) Insulation during post-fire cool-down.

Figure 20. ES-3100 shipping container transient temperatures for HAC (0.4 W content heat load) Kaolite density of 19.4 lbm/ft³ (see Figure 2 for node locations).

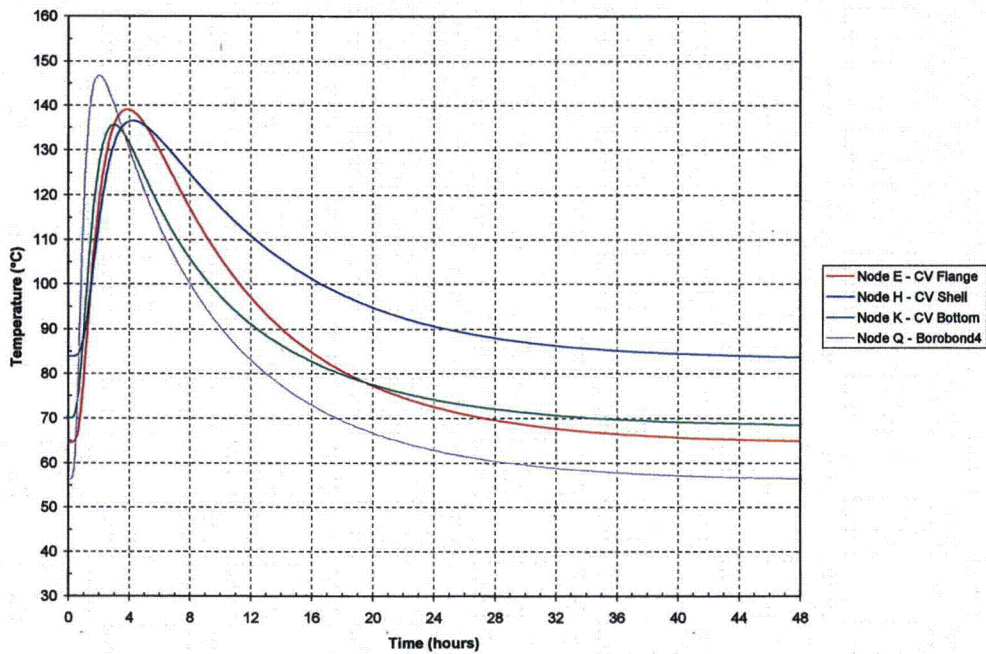


(a) No insulation during post-fire cool-down.

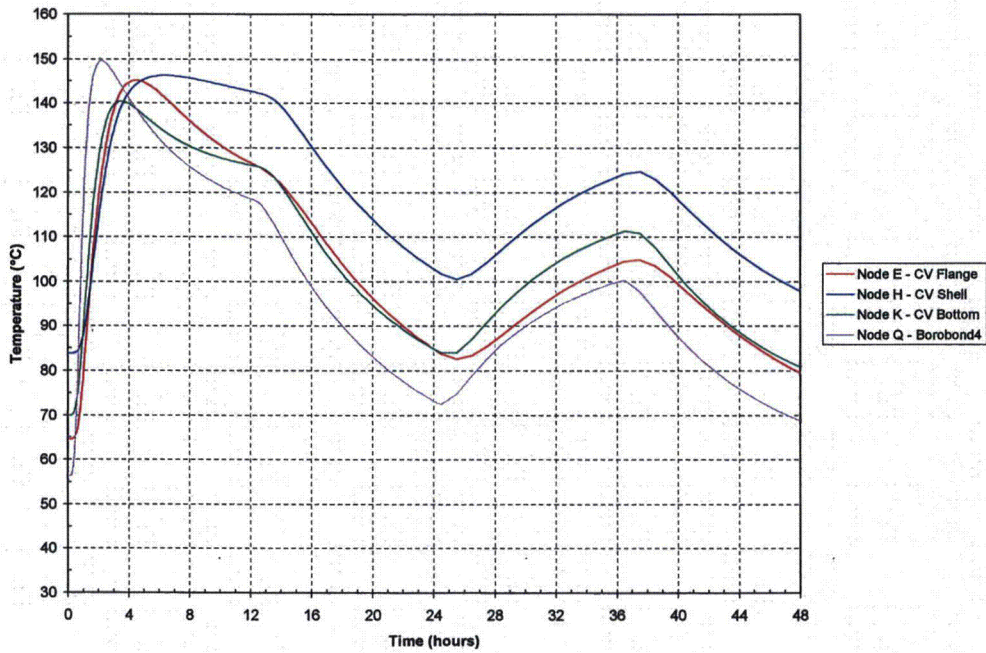


(b) Insulation during post-fire cool-down.

Figure 21. ES-3100 shipping container transient temperatures for HAC (20 W content heat load) Kaolite density of 19.4 lbm/ft³ (see Figure 2 for node locations).



(a) No insulation during post-fire cool-down.



(b) Insulation during post-fire cool-down.

Figure 22. ES-3100 shipping container transient temperatures for HAC (30 W content heat load) Kaolite density of 19.4 lbm/ft³ (see Figure 2 for node locations).

APPENDIX 3.6.1 REFERENCES

1. *Packaging and Transportation of Radioactive Materials*, U.S. Nuclear Regulatory Commission, Code of Federal Regulations, Title 10 – Energy, Part 71, 2003.
2. MSC.Patran 2004 Version 12.0.044, MacNeal Schwendler Corporation, 2004.
3. R. Siegel and J. R. Howell, *Thermal Radiation Heat Transfer*, Second Edition, Hemisphere Publishing Corporation, 1981.
4. F. P. Incropera and D. P. DeWitt, *Fundamentals of Heat and Mass Transfer*, Second Edition, John Wiley & Sons, New York, 1985.
5. *MSC.Patran 2003, Thermal User's Guide Volume 1, Thermal/Hydraulic Analysis*, MSC.Software Corporation, Santa Ana, CA, 2003.
6. J. C. Anderson and M. R. Feldman, *Thermal Modeling of Packages for Normal Conditions of Transport with Insolation*, Proceedings of the ASME Heat Transfer Division, HTD-Vol. 317-2, 1995, International Mechanical Engineering Congress and Exposition, November 1995.
7. P/VIEWFACTOR, Version 12.0.044, MacNeal Schwendler Corporation, 2004.
8. MSC.Patran Thermal, Version 12.0.044, MacNeal Schwendler Corporation, 2004.



Appendix 3.6.2

**THERMAL EVALUATION OF THE ES-3100 SHIPPING CONTAINER FOR NCT AND HAC
(FINAL DESIGN WITH CATALOG 277-4 NEUTRON ABSORBER)**

Appendix 3.6.2

THERMAL EVALUATION OF THE ES-3100 SHIPPING CONTAINER FOR NCT AND HAC (FINAL DESIGN WITH CATALOG 277-4 NEUTRON ABSORBER)

INTRODUCTION

Thermal analyses of the ES-3100 shipping container are performed to determine the temperature distribution within the packaging during Normal Conditions of Transport (NCT) as specified in 10 CFR 71.71(c)(1).^[1] Transient thermal analyses are performed by treating the problem as a cyclic transient with the incident heat flux due to solar radiation applied and not applied in alternating 12-hour periods.

Additionally, thermal analyses of the ES-3100 shipping container are performed to determine the thermal response of the packaging to Hypothetical Accident Conditions (HAC) as specified in 10 CFR 71.73(c)(4).^[1] Since physical testing of the ES-3100 shipping container was conducted with no internal heat source or insolation during cool-down,^[2] temperature increases due to internal heat loads of 0.4, 20, and 30 W as well as temperature increases due to the application of insolation during cool-down following the HAC fire are calculated. Although earlier revisions of 10 CFR 71 specifically state that insolation does not need to be evaluated before, during, or after HAC, the current version of 10 CFR 71 and associated guidance are unclear regarding the need for consideration following HAC testing. Since the Nuclear Regulatory Commission (NRC) has taken the position that insolation must be considered and evaluated following fire testing, analyses are conducted to determine the effect of insolation following the HAC fire on the ES-3100 shipping container. The predicted temperature increases may be used to adjust physical test data for those loads not included in the physical tests.

FINITE ELEMENT MODEL DESCRIPTION

A two-dimensional axisymmetric finite element model of the ES-3100 shipping container is constructed using MSC.Patran^[3] and imported as an orphaned mesh into ABAQUS/CAE^[4] for application of boundary conditions, interactions, and loads. The model is constructed of DCAX4 (four-node linear axisymmetric heat transfer quadrilateral) and DCAX3 (3-node linear axisymmetric heat transfer triangular) elements for evaluation for NCT and HAC. The actual contents of the ES-3100 shipping container are not specifically modeled—instead, the content source heat load (if desired) is modeled by applying a uniform heat flux to the inner surfaces of the containment vessel. This is a conservative approach in that package temperatures will not be reduced in a transient analysis by the heat capacity of the contents. A schematic of the finite element model is presented in Figure 1 with details of the upper and lower portions of the model shown in Figure 2 and Figure 3, respectively. The model consists of five materials: stainless steel (drum, liners, and containment vessel), Kaolite, neutron absorber, silicone rubber, and air in the gaps between the drum liner and containment vessel and between the drum liner and top plug. Degree-of-freedom “ties” are made at the interfaces of the different material regions in order to allow the heat to flow through the model. Thermal properties of the materials used in the analysis are presented in Table 1.

Heat is transferred to the model from the contents (i.e., decay heat of the contents) via heat flux boundary conditions applied to the inner surface of the elements representing the containment vessel. Additionally, solar heat fluxes are applied to the model during NCT and HAC post-fire cool-down via heat flux boundary conditions. The heat applied to the model via the boundary conditions is transferred through the model via conduction and thermal radiation. Heat is rejected from the external surfaces of the model via natural convection and thermal radiation boundary conditions.

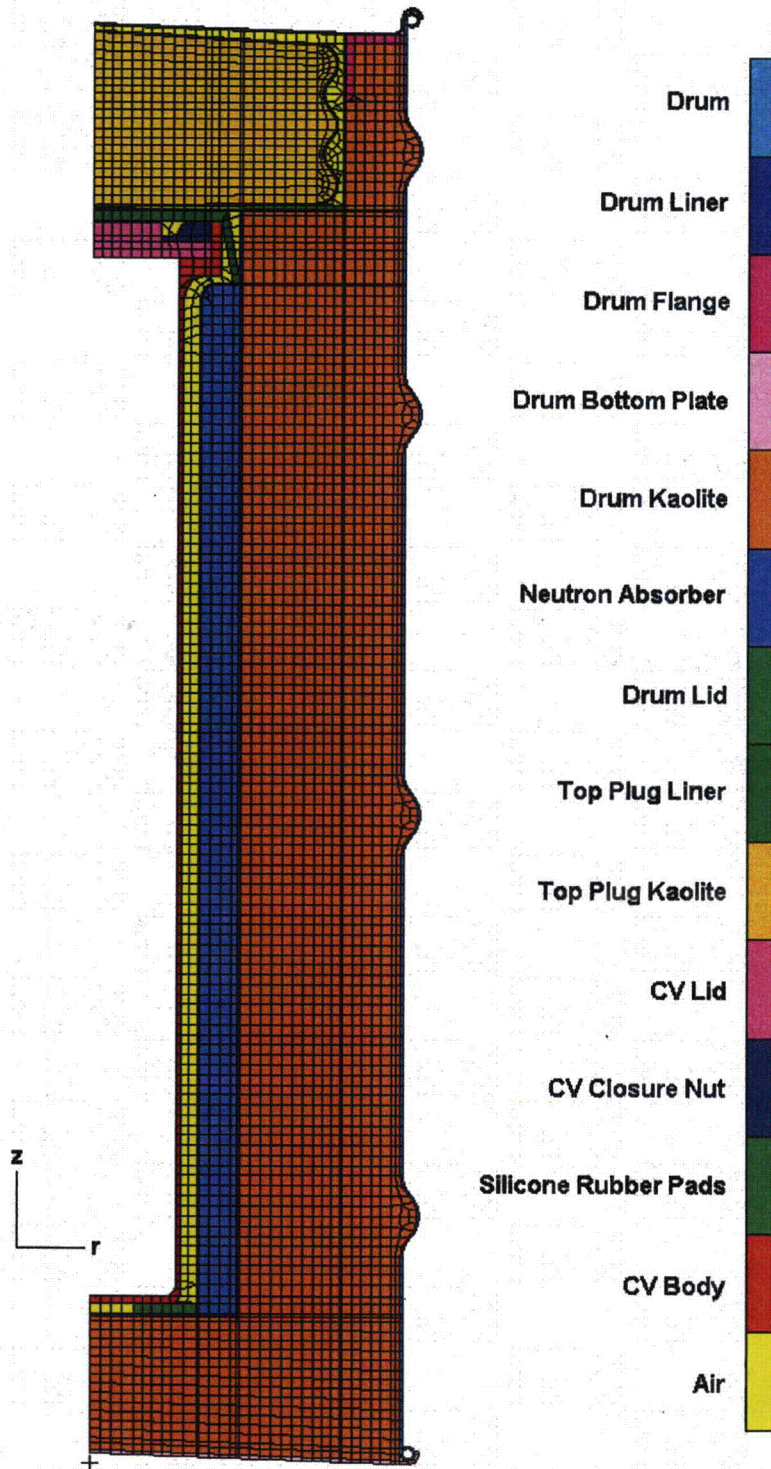


Figure 1. MSC.Patran axisymmetric finite element model of the ES-3100 shipping container.

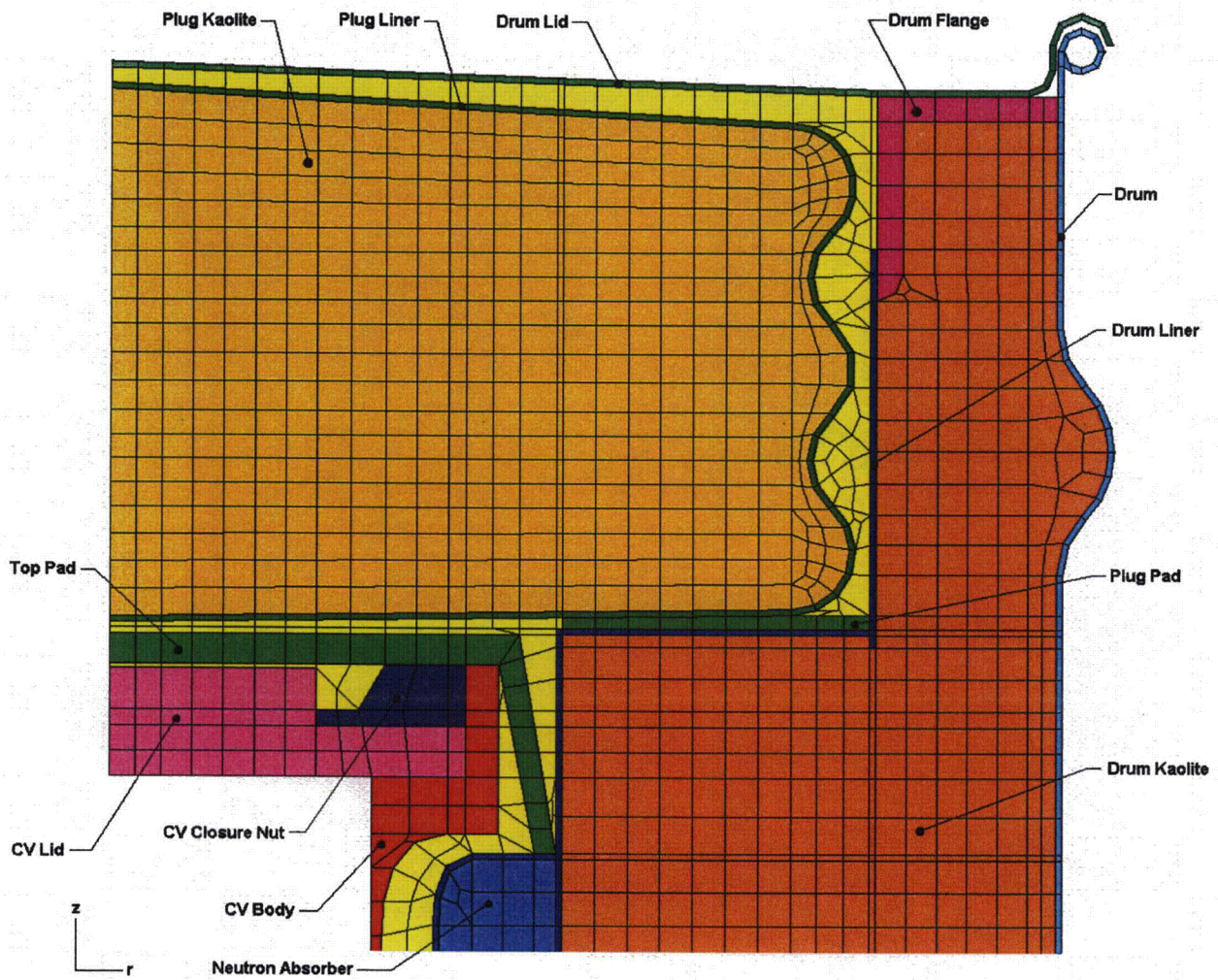


Figure 2. MSC.Patran axisymmetric finite element model of the ES-3100 shipping container (upper portion detail).

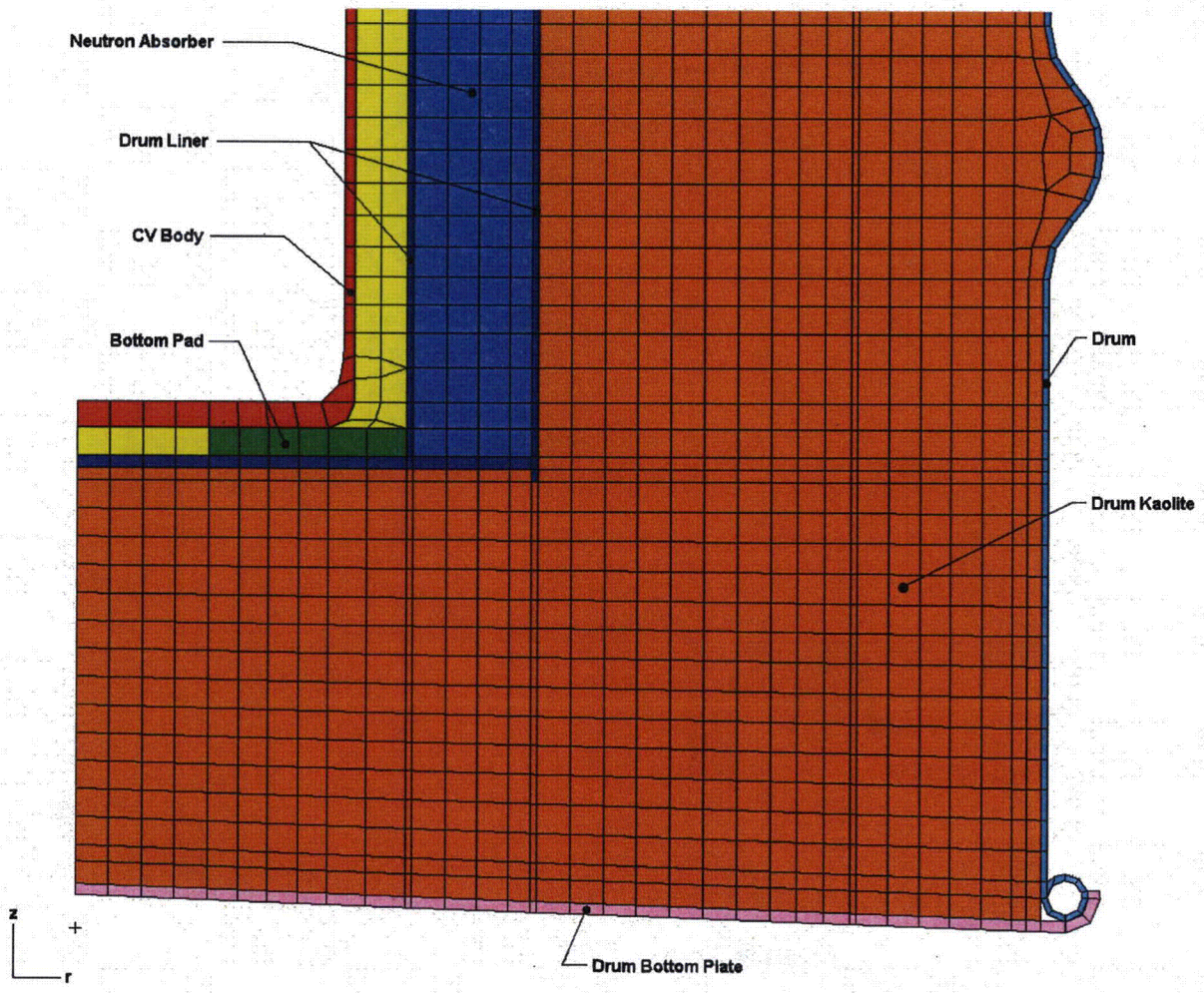


Figure 3. MSC.Patran axisymmetric finite element model of the ES-3100 shipping container (lower portion detail).

Table 1. Thermal properties of the materials used in the thermal analyses.

Material	Temperature (°F)	Thermal Conductivity (Btu/h-in.-°F)	Density (lbm/in. ³)	Specific heat (Btu/lbm-°F)	Emissivity
Stainless steel	-279.67	0.443 ^(a)	0.285 ^(a)	0.065 ^(a)	0.22 ^(a)
	-99.67	0.607	—	0.096	—
	260.33	0.799	—	0.123	—
	620.33	0.953	—	0.133	—
	980.33	1.088	—	0.139	—
	1340.33	1.223	—	0.146	—
	1700.33	1.348	—	0.153	—
	2240.33	1.526	—	0.163	—
Kaolite 1600	68	0.0093 ^(b)	0.011 ^(c)	0.2 ^(d)	—
	212	0.0091	—	—	—
	392	0.0081	—	—	—
	572	0.0072	—	—	—
	1112	0.0082	—	—	—
Neutron absorber (Catalog No. 277-4)	-31	0.0457 ^(e)	0.0579 ^(f)	0.125 ^(e)	—
	73.4	0.0485	—	0.186	—
	140	0.0400	—	0.239	—
	212	0.0295	—	0.242	—
	302	0.0305	—	0.291	—
Silicone rubber	—	0.0161 ^(g)	0.047 ^(g)	0.300 ^(g)	1.0 ^(h)
Air	-9.67	1.074×10 ^{-3(a)}	4.064×10 ^{-5(a),(i)}	0.240 ^(a)	—
	80.33	1.266×10 ⁻³	—	0.241	—
	170.33	1.445×10 ⁻³	—	0.241	—
	260.33	1.628×10 ⁻³	—	0.242	—
	350.33	1.796×10 ⁻³	—	0.244	—
	440.33	1.960×10 ⁻³	—	0.246	—
	530.33	2.114×10 ⁻³	—	0.248	—
	620.33	2.258×10 ⁻³	—	0.251	—
	710.33	2.393×10 ⁻³	—	0.254	—
	800.33	2.523×10 ⁻³	—	0.257	—
	890.33	2.644×10 ⁻³	—	0.260	—
	980.33	2.759×10 ⁻³	—	0.263	—
	1070.33	2.870×10 ⁻³	—	0.265	—
	1160.33	2.985×10 ⁻³	—	0.268	—
	1250.33	3.096×10 ⁻³	—	0.270	—
	1340.33	3.212×10 ⁻³	—	0.273	—
1520.33	3.443×10 ⁻³	—	0.277	—	

- Notes:
- (a) F. P. Incropera and D. P. DeWitt, *Fundamentals of Heat and Mass Transfer*, 2nd edition, John Wiley & Sons, New York, 1985.
 - (b) Hsin Wang, *Thermal Conductivity Measurements of Kaolite*, ORNL/TM-2003/49.
 - (c) Based on a baked density of 19.4 lbm/ft³ (0.011 lbm/in.³). Specification JS-YMN3-801580-A003 requires a baked density of 22.4 ± 3 lbm/ft³. Using a lower value for the Kaolite density results in higher temperatures on the containment vessel because the heat capacity of the Kaolite is minimized—allowing more heat to flow to the containment vessel; therefore, the thermal analyses are performed using a low-end density of 19.4 lbm/ft³. The HAC analyses also consider a high-end density of 30 lbm/ft³.
 - (d) FAX communication from J. W. Breuer of Thermal Ceramics, Engineering Department, August 11, 1995.
 - (e) W. D. Porter and H. Wang, *Thermophysical Properties of Heat Resistant Shielding Material*, ORNL/TM-2004/290, ORNL, Dec. 2004. Specific heat values are presented in MJ/m³-K in ORNL/TM-2004/290—converted to mass-based units using a density of 105 lbm/ft³.
 - (f) Based on a cured density of density of 100 lbm/ft³ (0.0579 lbm/in.³). B. F. Smith and G. A. Byington, *Mechanical Properties of 277-4*, Y/DW-1987, January 19, 2005 presents a range of measured densities between approximately 100 and 110 lbm/ft³ for Catalog No. 277-4. Therefore, in order to minimize the heat capacity of the material and allow more heat to be transferred to the containment vessel, the lower-bound value is used. The HAC analyses also consider a high-end density of 110 lbm/ft³.
 - (g) THERM 1.2, thermal properties database by R. A. Bailey.
 - (h) Conservatively modeled as 1.0.
 - (i) Constant density value evaluated at 100°F.

MODELED HEAT TRANSFER MECHANISMS

The heat transfer mechanisms included in the thermal model such, as thermal radiation, natural convection, and insolation (solar heat flux) are described in detail in the following sections.

Heat Transfer Between Package Exterior and Ambient

The heat transfer between the exterior of the package and the ambient (or fire) is modeled as a combination of radiant heat transfer and natural convection. The heat transfer due to radiant exchange with the environment is calculated as:^[5]

$$q''_{\text{rad}} = \sigma F_e (T_s^4 - T_a^4), \quad (1)$$

where σ = Stefan-Boltzmann constant,
 F_e = overall exchange factor,
 T_s = container outer surface temperature (absolute), and
 T_a = ambient or fire temperature (absolute).

The overall interchange factor is calculated as:^[5]

$$F_e = \left[\frac{1}{\frac{1}{\epsilon_p} + \frac{A_p}{A_s} \left(\frac{1}{\epsilon_s} - 1 \right)} \right], \quad (2)$$

where ϵ_p = emissivity of package surface,
 A_p = surface area of the package,
 A_s = surface area of the surroundings, and
 ϵ_s = emissivity of surroundings.

For NCT and the cool-down period following the HAC fire, the area of the surroundings is assumed to be much larger than the surface area of the package; therefore, Eq. 2 reduces to:

$$F_e \approx \epsilon_p. \quad (3)$$

An emissivity value of 0.22,^[6] which is typical of clean stainless steel, is assumed for the outer surfaces of the drum during NCT and during the cool-down period following the HAC fire. In reality, the outer surfaces of the drum will have a much higher emissivity following the HAC fire; therefore, this assumption is conservative.

During the HAC fire, the area of the surroundings is assumed to be approximately equal to the surface area of the drum; therefore, Eq. 2 reduces to:

$$F_e = \left[\frac{1}{\frac{1}{\epsilon_p} + \frac{1}{\epsilon_s} - 1} \right]. \quad (4)$$

During the HAC 30-minute fire, an emissivity of 0.8 is assumed for the drum, and an emissivity of 0.9 is assumed for the fire per the guidance of 10 CFR 71.74(c)(4).^[1] This results in an overall exchange factor of 0.7347 during the HAC fire using Eq. 4.

The natural convection heat transfer from the package surface to the ambient air is calculated as:

$$q''_{\text{convection}} = h(T_s - T_a). \quad (5)$$

where h = natural convection heat transfer coefficient,
 T_s = container outer surface temperature, and
 T_a = ambient or fire temperature.

During the NCT transient thermal analyses and the steady-state thermal analyses (used to obtain the starting temperature distribution in the package for NCT and HAC when a content heat load is present), the shipping container is assumed to be in an upright (vertical) orientation. The top of the drum is modeled as a heated horizontal flat plate facing up using the following correlation.^[6]

$$h = \left(\frac{k}{L} \right) C_1 Ra^{C_2}, \quad (6)$$

where k = thermal conductivity of air,
 L = characteristic length (= $D/4$ per Ref. 6),
 D = diameter of the package,
 Ra = Rayleigh number,
 C_1 = constant (see Table 2), and
 C_2 = constant (see Table 2).

The Rayleigh number in Eq. 6 is defined as:

$$Ra = \frac{g \beta \Delta T L^3}{\nu \alpha}, \quad (7)$$

where g = acceleration of gravity,
 β = coefficient of thermal expansion,
 ΔT = temperature difference,
 ν = kinematic viscosity [μ/ρ],
 μ = absolute viscosity,
 α = thermal diffusivity [$k/(\rho C_p)$],
 ρ = density of air, and
 C_p = specific heat of air.

The properties of air used in the natural convection calculations are presented in Table 3.

Table 2. Coefficients for natural convection correlations.

Coefficient	Rayleigh Number Range	Value
C ₁	10 ⁴ < Ra < 10 ⁷	0.54
	10 ⁷ < Ra < 10 ¹¹	0.15
C ₂	10 ⁴ < Ra < 10 ⁷	0.25
	10 ⁷ < Ra < 10 ¹¹	1/3
C ₃	Ra < 10 ⁹	0.680
	Ra > 10 ⁹	0.825
C ₄	Ra < 10 ⁹	0.670
	Ra > 10 ⁹	0.387
C ₅	Ra < 10 ⁹	0.25
	Ra > 10 ⁹	1/6
C ₆	Ra < 10 ⁹	4/9
	Ra > 10 ⁹	8/27
C ₇	Ra < 10 ⁹	1
	Ra > 10 ⁹	2

Source: F. P. Incropera and D. P. DeWitt, *Fundamentals of Heat and Mass Transfer*, 2nd ed., John Wiley & Sons, New York, 1985.

Table 3. Properties of air used in natural convection calculations.

Temperature (°F)	Thermal Conductivity (Btu/h-in.-°F)	Density (lbm/in. ³)	Specific Heat (Btu/lbm-°F)	Kinematic Viscosity (in. ² /h)	Thermal Diffusivity (in. ² /h)	Prandtl Number
-9.67	1.074×10 ⁻³	5.039×10 ⁻⁵	0.240	6.384×10 ¹	8.872×10 ¹	0.720
80.33	1.266×10 ⁻³	4.196×10 ⁻⁵	0.241	8.867×10 ¹	1.255×10 ²	0.707
170.33	1.445×10 ⁻³	3.595×10 ⁻⁵	0.241	1.167×10 ²	1.668×10 ²	0.700
260.33	1.628×10 ⁻³	3.147×10 ⁻⁵	0.242	1.474×10 ²	2.137×10 ²	0.690
350.33	1.796×10 ⁻³	2.796×10 ⁻⁵	0.244	1.807×10 ²	2.634×10 ²	0.686
440.33	1.960×10 ⁻³	2.516×10 ⁻⁵	0.246	2.164×10 ²	3.164×10 ²	0.684
530.33	2.114×10 ⁻³	2.286×10 ⁻⁵	0.248	2.543×10 ²	3.722×10 ²	0.683
620.33	2.258×10 ⁻³	2.097×10 ⁻⁵	0.251	2.940×10 ²	4.291×10 ²	0.685
710.33	2.393×10 ⁻³	1.935×10 ⁻⁵	0.254	3.360×10 ²	4.871×10 ²	0.690
800.33	2.523×10 ⁻³	1.797×10 ⁻⁵	0.257	3.800×10 ²	5.468×10 ²	0.695
890.33	2.644×10 ⁻³	1.677×10 ⁻⁵	0.260	4.261×10 ²	6.082×10 ²	0.702
980.33	2.759×10 ⁻³	1.573×10 ⁻⁵	0.263	4.739×10 ²	6.696×10 ²	0.709
1070.33	2.870×10 ⁻³	1.480×10 ⁻⁵	0.265	5.234×10 ²	7.310×10 ²	0.716
1160.33	2.985×10 ⁻³	1.397×10 ⁻⁵	0.268	5.742×10 ²	7.979×10 ²	0.720
1250.33	3.096×10 ⁻³	1.324×10 ⁻⁵	0.270	6.261×10 ²	8.649×10 ²	0.723
1340.33	3.212×10 ⁻³	1.258×10 ⁻⁵	0.273	6.802×10 ²	9.374×10 ²	0.726
1520.33	3.443×10 ⁻³	1.144×10 ⁻⁵	0.277	7.912×10 ²	1.088×10 ³	0.728

Source: F. P. Incropera and D. P. DeWitt, *Fundamentals of Heat and Mass Transfer*, 2nd ed., John Wiley & Sons, New York, 1985.

During the NCT transient thermal analyses and the steady-state thermal analyses, the sides of the drum are modeled as a vertical flat plate using the following correlation:^[6]

$$h = \left(\frac{k}{L} \right) \left[C_3 + \frac{C_4 Ra^{C_5}}{\left(1 + \left[\frac{0.492}{Pr} \right]^{9/16} \right)^{C_6}} \right]^{C_7}, \quad (8)$$

where L = characteristic length = the drum height,
 C_3 = constant (see Table 2),
 C_4 = constant (see Table 2),
 C_5 = constant (see Table 2),
 C_6 = constant (see Table 2),
 C_7 = constant (see Table 2), and
 Pr = Prandtl number.

The bottom of the drum is conservatively modeled as adiabatic during the NCT transient analyses and the steady-state analyses.

During the HAC 30-minute fire and the post-fire cool-down, the shipping container is assumed to be in a horizontal orientation (as it is during furnace testing). As such, the top and bottom of the drum are modeled as vertical flat plates using Eq. 8 having a characteristic length, L, equivalent to the drum diameter, and the sides of the drum are modeled as a horizontal cylinder using the following correlation ($10^{-5} < Ra < 10^{12}$):^[6]

$$h = \left(\frac{k}{D} \right) \left[0.60 + \frac{0.387 Ra^{1/6}}{\left(1 + \left[\frac{0.559}{Pr} \right]^{9/16} \right)^{8/27}} \right]^2, \quad (9)$$

where D = diameter of the package,

The calculated natural convection film coefficients used in the thermal analyses of the ES-3100 are presented graphically in Figure 4 and Figure 5 for NCT and HAC, respectively.

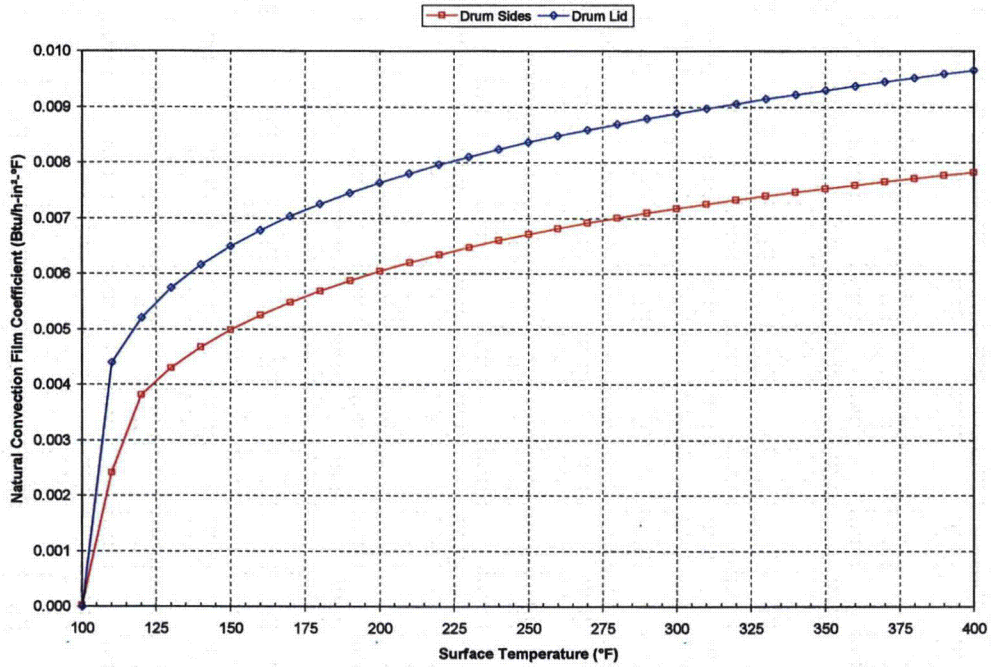


Figure 4. Natural convection film coefficients applied to the drum surfaces during NCT and steady-state conditions.

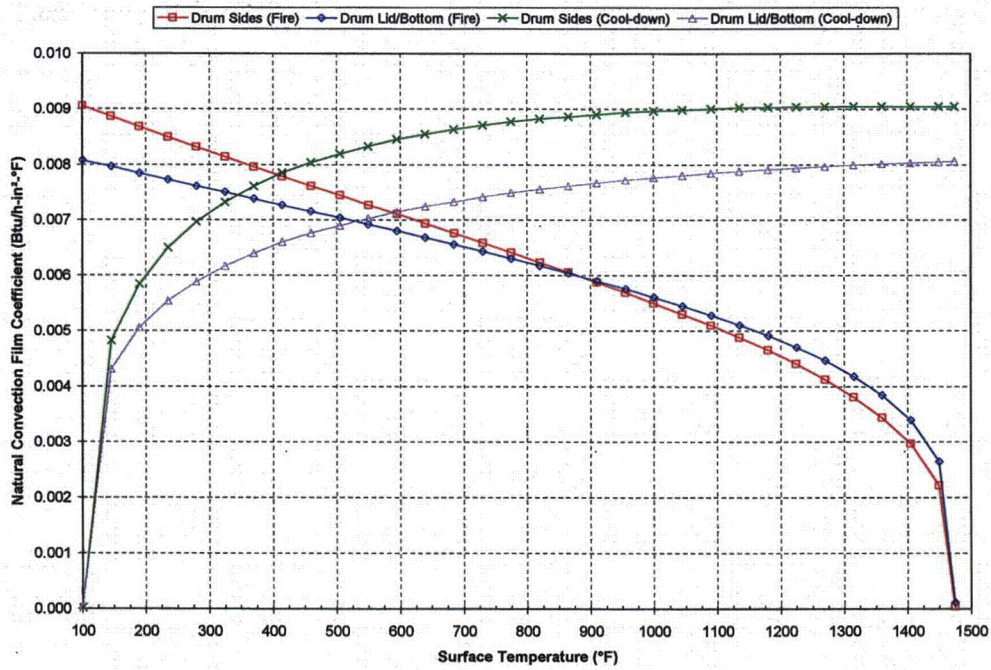


Figure 5. Natural convection film coefficients applied to the drum surfaces during HAC.

Insolation

The following insolation (incident solar radiation) data is required for NCT per 10 CFR 71.71(c)(1):^[1]

Form and location of surface	Total insolation for a 12-hour period (cal/cm ²)
Flat surfaces transported horizontally	
Base	None
Other surfaces	800
Flat surfaces not transported horizontally	200
Curved surfaces	400

The total insolation values specified in the previous table are for a 12-hour period. For analytical purposes, these values are "time-averaged" over the entire 12-hour period (i.e., divided by 12). Therefore, the incident solar heat fluxes ($q''_{\text{solar},i}$) used in the analyses for NCT and cool-down following the HAC fire are as follows:

During NCT, the drum is in an upright (vertical) orientation; therefore, the following heat fluxes are applied to the external surfaces of the drum to represent insolation:

$$\text{Top} \quad q''_{\text{solar},i} = 1.7074 \text{ Btu/h} - \text{in.}^2, \quad (10)$$

$$\text{Sides} \quad q''_{\text{solar},i} = 0.8537 \text{ Btu/h} - \text{in.}^2, \quad (11)$$

$$\text{Bottom} \quad q''_{\text{solar},i} = 0. \quad (12)$$

During the cool-down period following the HAC 30-minute fire, the drum is assumed to be in a horizontal orientation; therefore, the following heat fluxes are applied to the external surfaces of the drum to represent insolation:

$$\text{Top} \quad q''_{\text{solar},i} = 0.4269 \text{ Btu/h} - \text{in.}^2, \quad (13)$$

$$\text{Sides} \quad q''_{\text{solar},i} = 0.8537 \text{ Btu/h} - \text{in.}^2, \quad (14)$$

$$\text{Bottom} \quad q''_{\text{solar},i} = 0.4269 \text{ Btu/h} - \text{in.}^2. \quad (15)$$

The insolation is applied as a square-wave function (i.e., alternating on and off in 12-hour periods) in the thermal analysis. The heat flux values presented in Eqs. 10–15 represent the insolation absorbed by the package surface since a drum absorptivity of 1.0 was conservatively assumed. An analytical study has been performed on a similar shipping package that investigated three methods of applying the insolation.^[7] The three methods consisted of 1) performing a steady-state analysis assuming the insolation is applied continuously by distributing the heat flux evenly throughout a 24-hour period, 2) performing a transient analysis assuming the insolation is represented by a step function (i.e., applied and then not applied in 12-hour cycles, and 3) performing a transient analysis where the incident insolation is represented by a sinusoidal function that varies throughout the day. The results of the study indicate that the method used in applying the insolation has a significant effect on the temperatures of the outermost portions of the package. However, since the total insolation over any 24-hour period is the same for all cases, internal package temperatures are relatively unaffected by the way in which the insolation is applied. Since the containment vessel O-ring temperatures are of primary concern in this evaluation, the step function method for applying the insolation is suitable.

Heat Transfer Across Gaps in the Package

Heat transfer across all gaps in the package is modeled by a combination of radiant exchange and conduction. Natural convection heat transfer is not included across the gaps in the model. Scoping studies performed for a similar shipping package indicate that the heat transfer due to natural convection in relatively small gaps is approximately a factor of 6 times less than the heat transfer due to radiant exchange.^[7] These calculations assumed a temperature difference of 9°F across the gap. Based on these previous calculations, the effect of neglecting the natural convection in the gap regions is minimal. The emissivity values used in the analysis for all internal radiating surfaces in the model are presented in Table 1.

Radiant exchange across gaps is modeled using the cavity radiation feature of ABAQUS/Standard.^[8] For each cavity (or enclosure), radiation surfaces are defined as shown in Figure 6 and Figure 7.

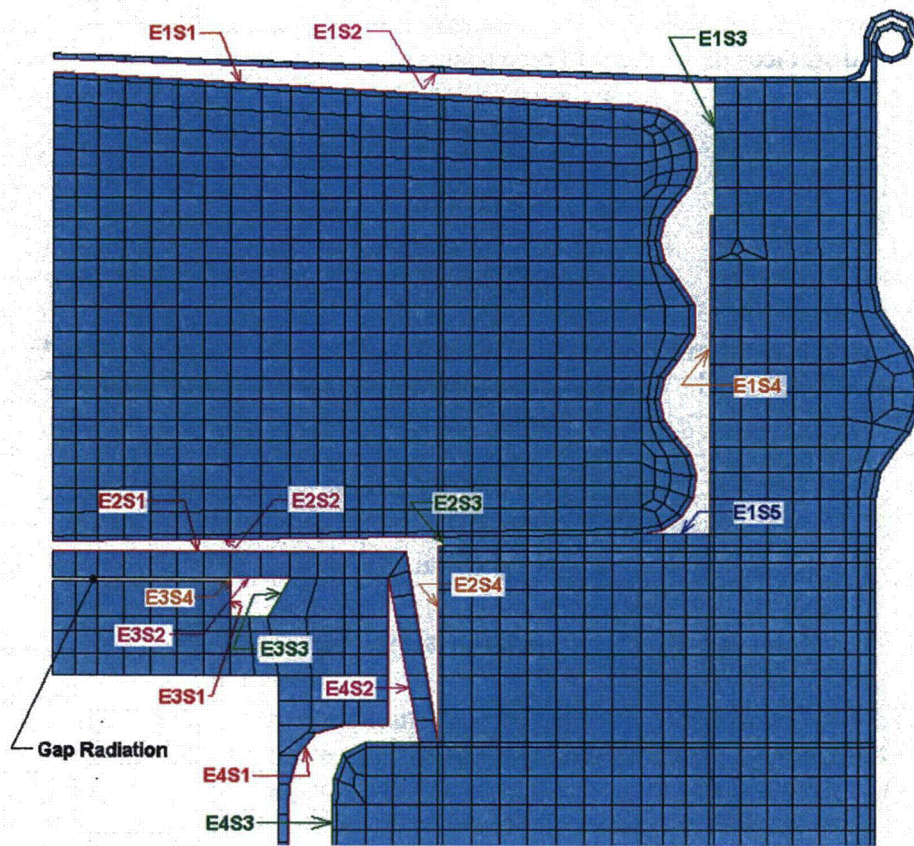


Figure 6. Radiation cavity surface definitions (top portion of the model).

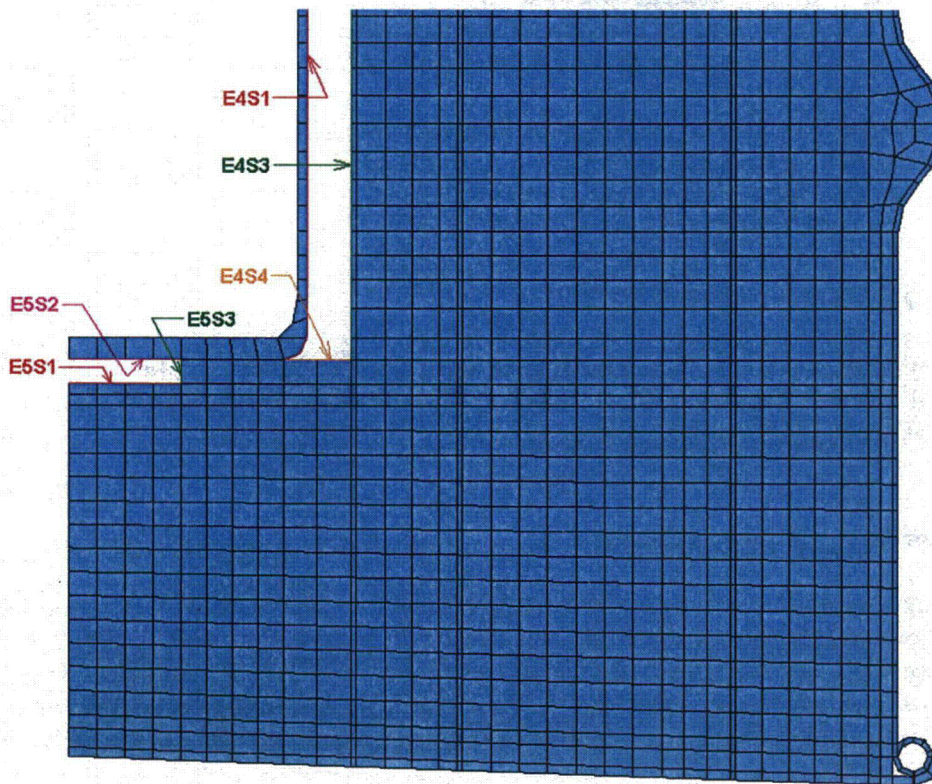


Figure 7. Radiation cavity surface definitions (bottom portion of the model).

As shown in Figure 6 and Figure 7, the various gaps in the model are divided into five separate cavities (designated 'E1' through 'E5' in the figures) with between three and five surfaces (designated 'S1' through 'S5' in the figures) in each cavity for radiation calculations. Because the gap between the CV lid and top pad is small in relation to its characteristic length, radiation exchange is modeled using the gap radiation feature in ABAQUS/Standard with a view factor of 1.0 assigned. As a result, a shell element (type DSAX1) is defined in the model with the radiation surface E3S4 (see Figure 6) superimposed to close off cavity 3. The DSAX1 element is assigned the properties of air, and surface E3S4 is assigned a small emissivity value of 0.01 since it is an imaginary surface used to close the cavity.

Content Heat Load

In order to simulate the decay heat generated by the ES-3100 shipping container contents, a uniform heat flux is applied to the element edges representing the inner surface of the containment vessel in the model. Content heat loads of 0, 0.4, 20, and 30 W are investigated in this report. The uniform heat flux (q''_{source}) for a given content heat load is calculated using the following equation:

$$q''_{\text{source}} = \frac{Q \times 3.4123}{2 \left(\frac{\pi D_i^2}{4} \right) + \pi (D_i)(H)}, \quad (16)$$

where, Q = content heat load (W),
 D_i = inside diameter of the containment vessel (5.06 in.),
 H = height of the containment vessel cavity (31.00 in.).

Using Eq. 16, a content heat load of 0.4 W results in a uniform heat flux of 2.5608×10^{-3} Btu/h-in.², a content heat load of 20 W results in a uniform heat flux of 0.12804 Btu/h-in.², and a content heat load of 30 W results in a uniform heat flux of 0.19206 Btu/h-in.².

DISCUSSION OF ANALYTICAL RESULTS

All thermal analyses discussed in this report were performed using ABAQUS/Standard^[8] on an Intel Pentium 4-based Microsoft Windows 2000 computer. Temperatures are monitored at selected locations in the model as shown in Figure 8 through Figure 11.

Steady-state Conditions Analyses Results

Steady-state thermal analyses are performed on the finite element model of the ES-3100 shipping container for three cases having content heat loads of 0.4, 20, and 30 W. The temperature distribution results from these analyses are used as the starting temperature distributions within the model when performing the transient thermal analyses for NCT and the HAC 30-minute fire. The boundary conditions for these steady-state analyses include a combination of thermal radiation exchange and natural convection applied to the top and sides of the drum using an ambient temperature of 100°F. The bottom of the drum is modeled as an adiabatic surface (i.e., no heat transfer). Additionally, the content heat load is simulated by applying a uniform heat flux to the surfaces of the elements representing the inner surface of the containment vessel. The calculated steady-state temperature distribution within the model of the ES-3100 shipping container for content heat loads of 0.4, 20, and 30 W is presented in Table 4.

As presented in Table 4, the maximum accessible surface temperature of the package when exposed to an ambient temperature of 100°F in the shade is 100.43°F (38.02°C), 114.39°F (45.77°C), and 120.08°F (48.93°C) for content heat loads of 0.4, 20, and 30 W, respectively.

Normal Conditions of Transport Analyses Results

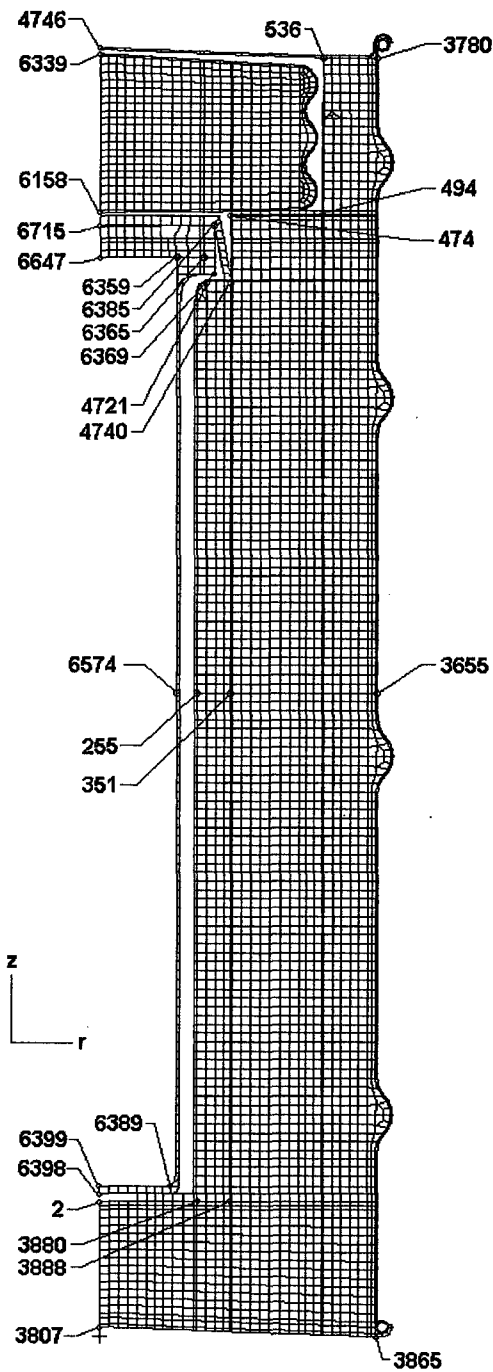
Transient thermal analyses are performed on the finite element model of the ES-3100 shipping container to simulate NCT with content heat loads of 0, 0.4, 20, and 30 W. The insolation required for NCT per 10 CFR 71.71(c)(1)^[1] is applied to the top and sides of the drum in alternating 12-hour periods (i.e., 12 hours on and 12 hours off) with the drum bottom remaining adiabatic during the transient thermal analysis. An ambient temperature of 100°F as stipulated in 10 CFR 71 is used in the NCT analysis. The initial temperature distribution within the package for the NCT transients was determined from steady-state analyses (with radiation and natural convection boundary conditions applied to the top and sides of the drum) for each internal heat load. For the case with no internal heat source (0 W), the initial temperature distribution within the package was assumed to be at a uniform 100°F. As with the steady-state analyses discussed previously, applying a uniform heat flux to the internal surfaces of the elements representing the containment vessel simulates the content heat load.

The transient thermal analyses simulate a five-day period of cyclic solar loading with 12 hours of insolation being applied at the beginning of each day (i.e., sunrise) followed by 12 hours in which there is no insolation to end the day (i.e., sunset). This five-day period allows for "quasi steady-state" conditions

to be reached. While the temperature of a particular node within the model changes with respect to time in the transient analyses, the maximum temperature that node reaches from day-to-day does not change once a "quasi steady-state" condition is reached. In particular, the maximum temperature of the key location on the containment vessel (i.e., at the O-ring) on day 5 is within 0.004°F of the maximum temperature of the same location on day 4.

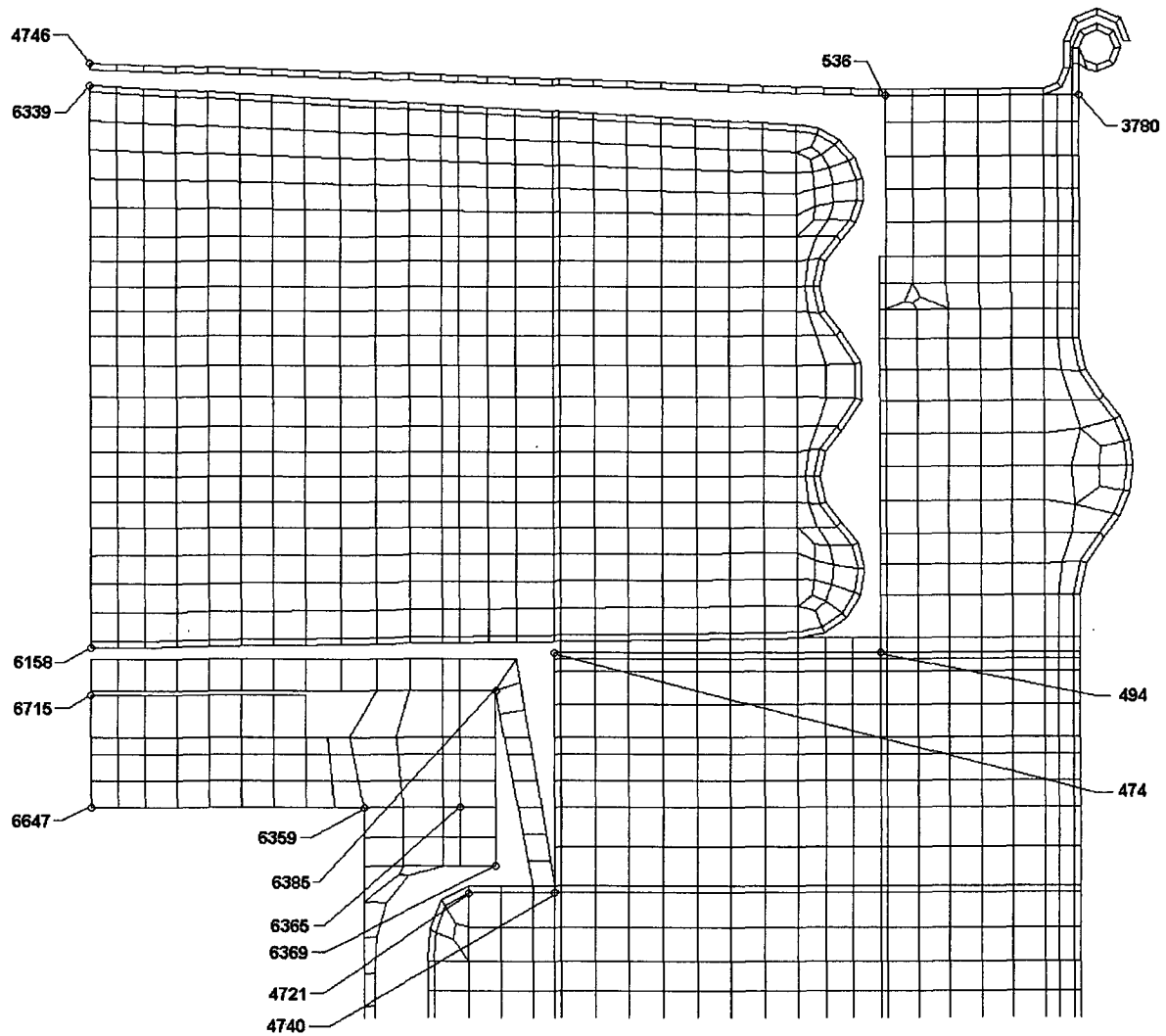
The maximum temperatures of several locations within the model are summarized in Table 5 for content heat loads of 0, 0.4, 20, and 30 W. The maximum temperatures reported in Table 5 represent "quasi steady-state" conditions. Temperature-history plots of several locations within the model are also depicted graphically in Figure 12 through Figure 15 for various content heat loads. Additionally, temperature contours of the model at sunrise (0 hours), sunset (12 hours), and 68 to 70 minutes after sunset for a typical day (after the package temperatures reach "quasi steady-state") of the transient are presented in Figure 16 through Figure 19 for various content heat loads. The temperature contours at 68 to 70 minutes after sunset are presented because the temperature of the CV flange (i.e., O-ring location) peaks at this time. The elements representing the air between the drum liner and containment vessel and between the drum liner and top plug liner are not shown in the temperature contours presented in these figures so that the containment vessel temperature contours can be more easily viewed.

The maximum temperature in the model occurs at the top center of the drum lid in most instances. The drum lid maximum temperature is 243.86°F (117.70°C), 243.89°F (117.72°C), 245.32°F (118.51°C), and 246.03°F (118.91°C) for content heat loads of 0, 0.4, 20, and 30 W, respectively, and occurs at sunset in each case (see Table 5). For the case with a content heat load of 30 W, the maximum temperature in the model occurs in the sidewall of the CV approximately 80 minutes after sunset and is 252.87°F (122.71°C). The maximum temperature at the containment vessel O-ring is 189.28°F (87.38°C), 189.90°F (87.72°C), 217.07°F (102.82°C), and 230.51°F (110.28°C) for content heat loads of 0, 0.4, 20, and 30 W, respectively, and occurs at approximately 68 to 70 minutes after sunset in each case (see Table 5).



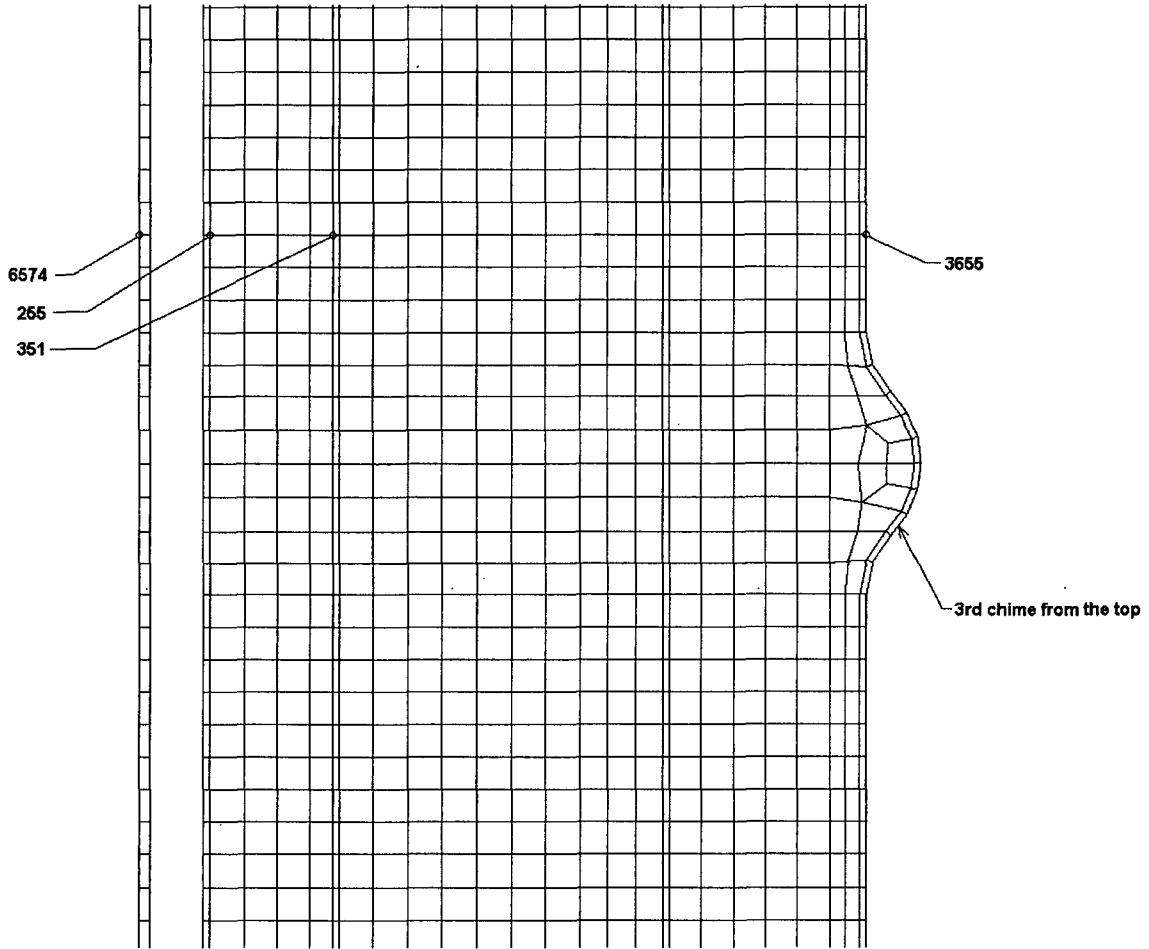
Node	r (in.)	z (in.)
2	0.000	4.505
255	3.180	21.528
351	4.300	21.528
474	4.300	37.535
494	7.325	37.535
536	7.385	42.755
3655	9.185	21.528
3780	9.185	42.755
3807	0.000	0.320
3865	9.185	0.008
3880	3.178	4.505
3888	4.300	4.505
4721	3.500	35.275
4740	4.300	35.275
4746	0.000	43.065
6158	0.000	37.579
6339	0.000	42.859
6369	2.530	36.075
6365	3.425	36.075
6369	3.750	35.525
6385	3.750	37.175
6389	2.310	5.025
6398	0.000	4.775
6399	0.000	5.025
6574	2.530	21.528
6647	0.000	36.075
6715	0.000	37.135

Figure 8. ABAQUS axisymmetric finite element model of the ES-3100 shipping container—nodal locations of interest (elements representing air not shown for clarity).



Node	r (in.)	z (in.)
474	4.300	37.535
494	7.325	37.535
536	7.385	42.755
3780	9.185	42.755
4721	3.500	35.275
4740	4.300	35.275
4746	0.000	43.065
6158	0.000	37.579
6339	0.000	42.859
6359	2.530	36.075
6365	3.425	36.075
6369	3.750	35.625
6385	3.750	37.175
6647	0.000	36.075
6715	0.000	37.135

Figure 9. ABAQUS axisymmetric finite element model of the ES-3100 shipping container—nodal locations of interest (elements representing air not shown for clarity), upper portion detail.



Node	r (in.)	z (in.)
255	3.180	21.528
351	4.300	21.528
3655	9.185	21.528
6574	2.530	21.528



Figure 10. ABAQUS axisymmetric finite element model of the ES-3100 shipping container—nodal locations of interest (elements representing air not shown for clarity), middle portion detail.

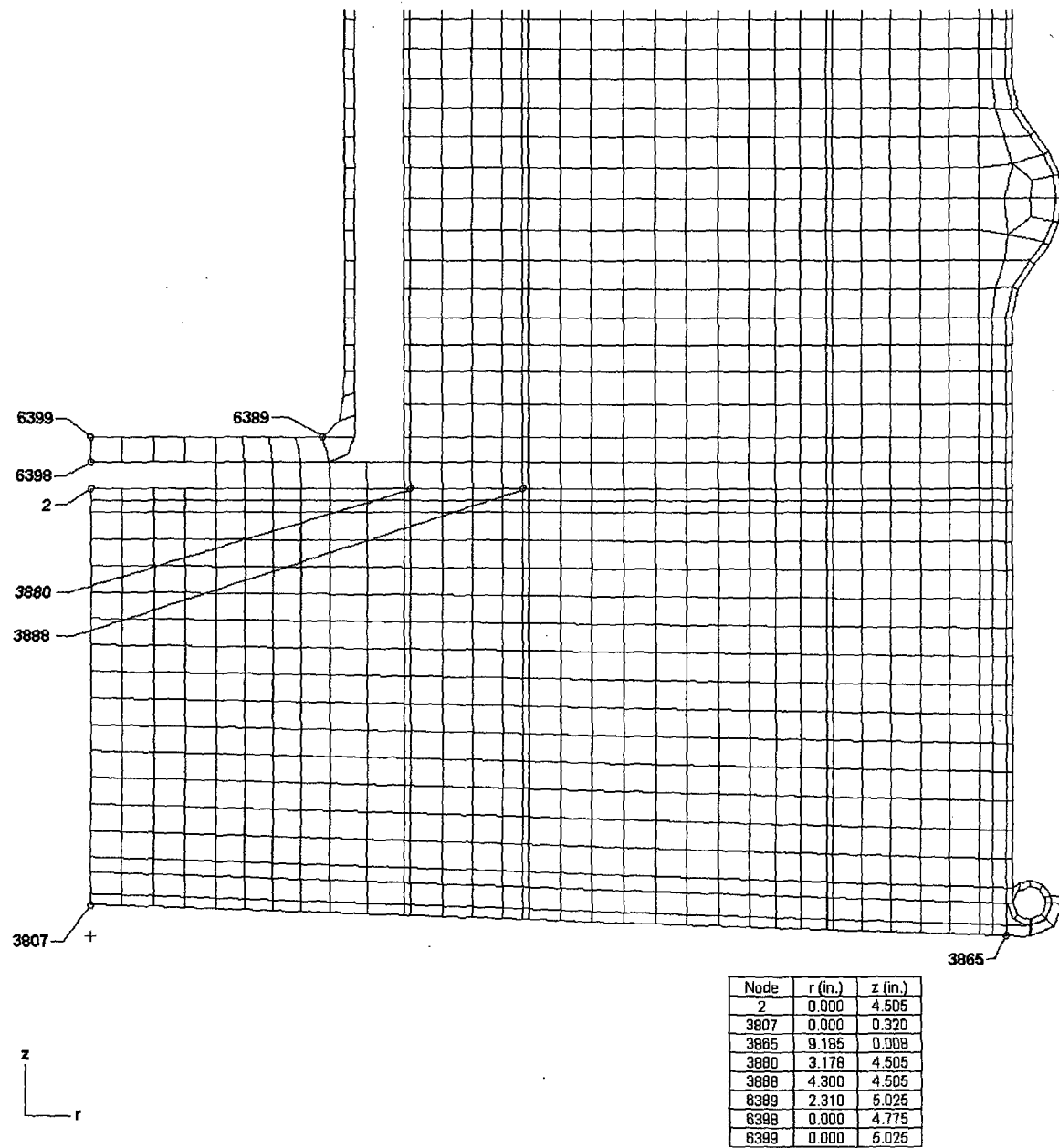


Figure 11. ABAQUS axisymmetric finite element model of the ES-3100 shipping container—nodal locations of interest (elements representing air not shown for clarity), lower portion detail.

Table 4. ES-3100 shipping container steady-state temperatures (100°F ambient temperature, no insolation).

Node map ^(a)	Node coordinates (in.)			Maximum steady-state temperature (°F)		
	No.	r	z	0.4 W	20 W	30 W
	2	0.000	4.505	100.83	134.54	150.15
	255	3.180	21.528	100.75	131.57	146.21
	351	4.300	21.528	100.71	129.45	142.87
	474	4.300	37.535	100.46	117.90	125.67
	494	7.325	37.535	100.32	110.87	115.19
	536	7.385	42.755	100.21	105.50	107.19
	3655 ^(b)	9.185	21.528	100.28	107.58	109.92
	3780 ^(b)	9.185	42.755	100.21	105.29	106.89
	3807 ^(b)	0.000	0.320	100.43	114.39	120.08
	3865 ^(b)	9.185	0.008	100.32	108.97	111.97
	3880	3.178	4.505	100.74	130.48	144.23
	3888	4.300	4.505	100.71	128.60	141.42
	4721	3.500	35.275	100.59	124.08	134.90
	4740	4.300	35.275	100.57	122.92	133.15
	4746 ^(b)	0.000	43.065	100.20	104.99	106.43
	6158	0.000	37.579	100.57	123.14	133.42
	6339	0.000	42.859	100.25	107.42	110.04
	6359 ^(c)	2.530	36.075	100.80	133.51	148.56
	6365 ^(c)	3.425	36.075	100.79	133.33	148.28
	6369	3.750	35.525	100.79	133.27	148.20
	6385	3.750	37.175	100.78	132.85	147.58
	6389	2.310	5.025	100.97	141.27	160.06
	6398	0.000	4.775	100.96	140.91	159.55
	6399	0.000	5.025	100.96	140.94	159.60
	6574	2.530	21.528	101.33	157.70	183.56
	6647	0.000	36.075	100.80	133.56	148.63
	6715	0.000	37.135	100.79	133.40	148.40

Notes: (a) See Figure 8 through Figure 11 for details of node locations.
 (b) These are nodes at the accessible surfaces of the package (i.e., the drum, drum lid, and drum bottom plate).
 (c) Approximate location of the CV O-ring.

Table 5. ES-3100 shipping container maximum “quasi steady-state” temperatures during NCT with various content heat loads.

Node map ^(a)	Node coordinates (in.)			Maximum “quasi steady-state” temperature (°F)			
	No.	r	z	0 W	0.4 W	20 W	30 W
	2	0.000	4.505	180.59	181.23	210.15	224.69
	255	3.180	21.528	179.33	179.93	207.32	221.43
	351	4.300	21.528	179.59	180.14	204.73	217.27
	474	4.300	37.535	198.88	199.20	212.72	219.58
	494	7.325	37.535	207.40	207.56	214.40	217.87
	536	7.385	42.755	226.44	226.49	228.31	229.24
	3655	9.185	21.528	198.09	198.15	200.81	202.16
	3780	9.185	42.755	223.47	223.51	225.13	225.95
	3807	0.000	0.320	190.48	190.70	199.84	204.43
	3865	9.185	0.008	195.87	195.97	199.91	201.90
	3880	3.178	4.505	180.72	181.28	206.65	219.52
	3888	4.300	4.505	181.03	181.55	205.08	217.01
	4721	3.500	35.275	189.45	189.90	209.53	219.47
	4740	4.300	35.275	190.56	190.98	209.37	218.68
	4746	0.000	43.065	243.86	243.89	245.32	246.03
	6158	0.000	37.579	198.42	198.84	217.12	226.32
	6339	0.000	42.859	233.98	234.06	237.32	238.95
	6359 ^(b)	2.530	36.075	189.28	189.90	217.07	230.51
	6365 ^(b)	3.425	36.075	189.27	189.88	216.88	230.23
	6369	3.750	35.525	189.23	189.85	216.79	230.12
	6385	3.750	37.175	189.39	190.00	216.57	229.72
	6389	2.310	5.025	179.94	180.70	215.75	233.27
	6398	0.000	4.775	179.99	180.76	215.52	232.92
	6399	0.000	5.025	179.99	180.76	215.55	232.96
	6574	2.530	21.528	179.27	180.35	229.19	252.87
	6647	0.000	36.075	189.40	190.02	217.24	230.72
	6715	0.000	37.135	189.44	190.06	217.14	230.54

Notes: (a) See Figure 8 through Figure 11 for details of node locations.
 (b) Approximate location of the CV O-ring.

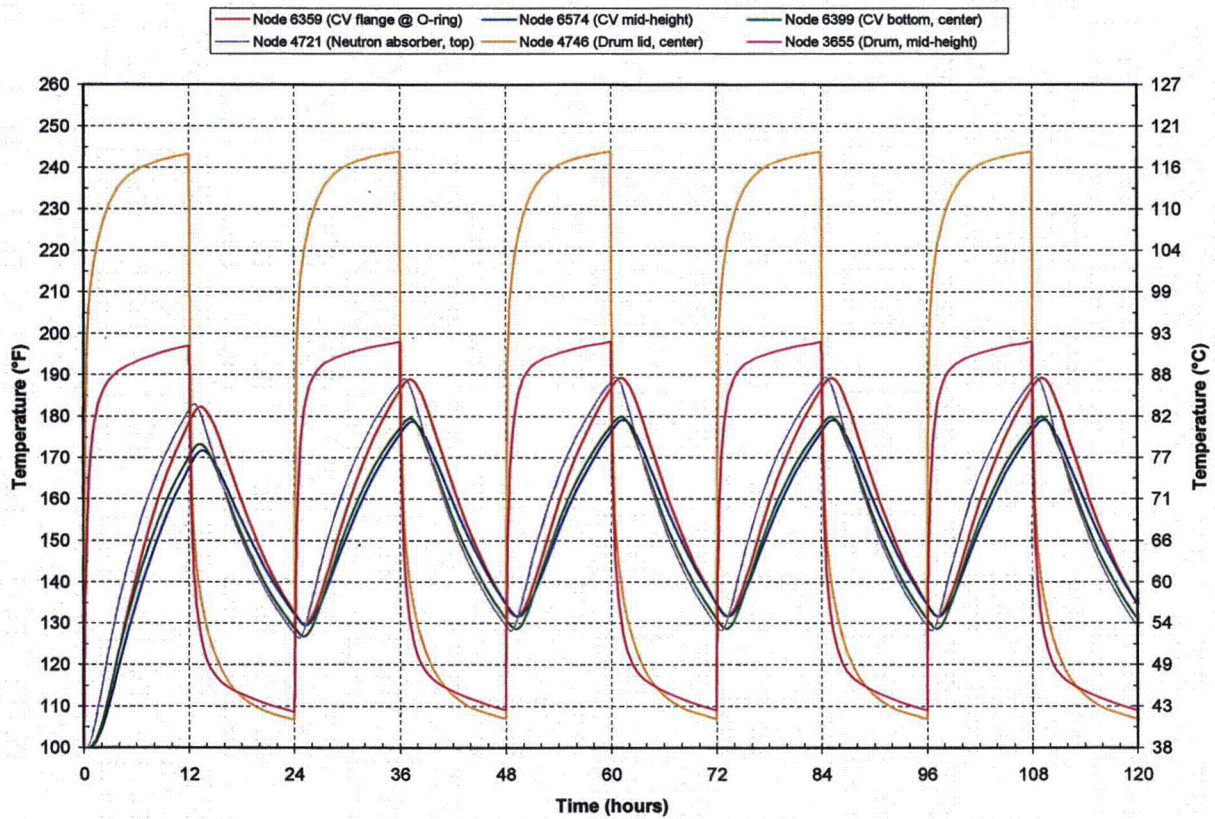


Figure 12. Transient temperatures of the ES-3100 shipping container for NCT (no content heat load) see Figure 8 through Figure 11 for node locations.

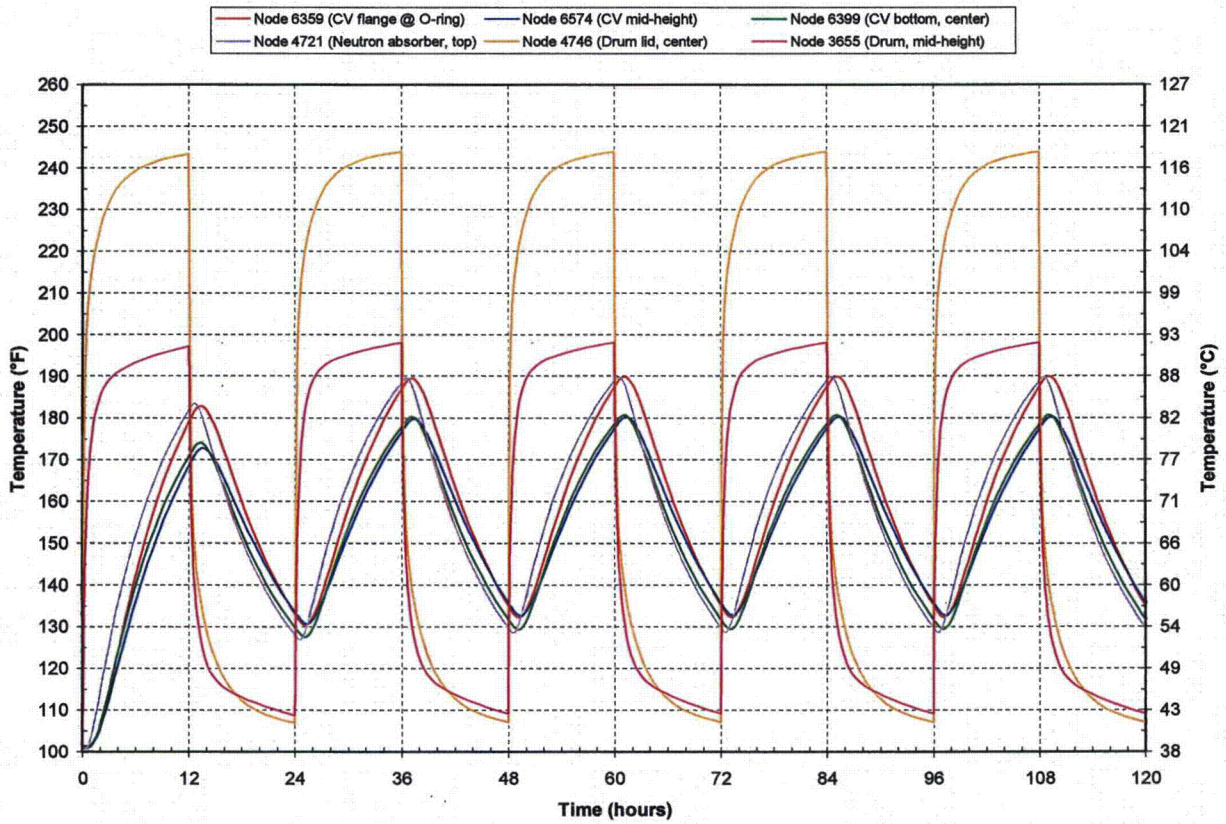


Figure 13. Transient temperatures of the ES-3100 shipping container for NCT (0.4 W content heat load) see Figure 8 through Figure 11 for node locations.

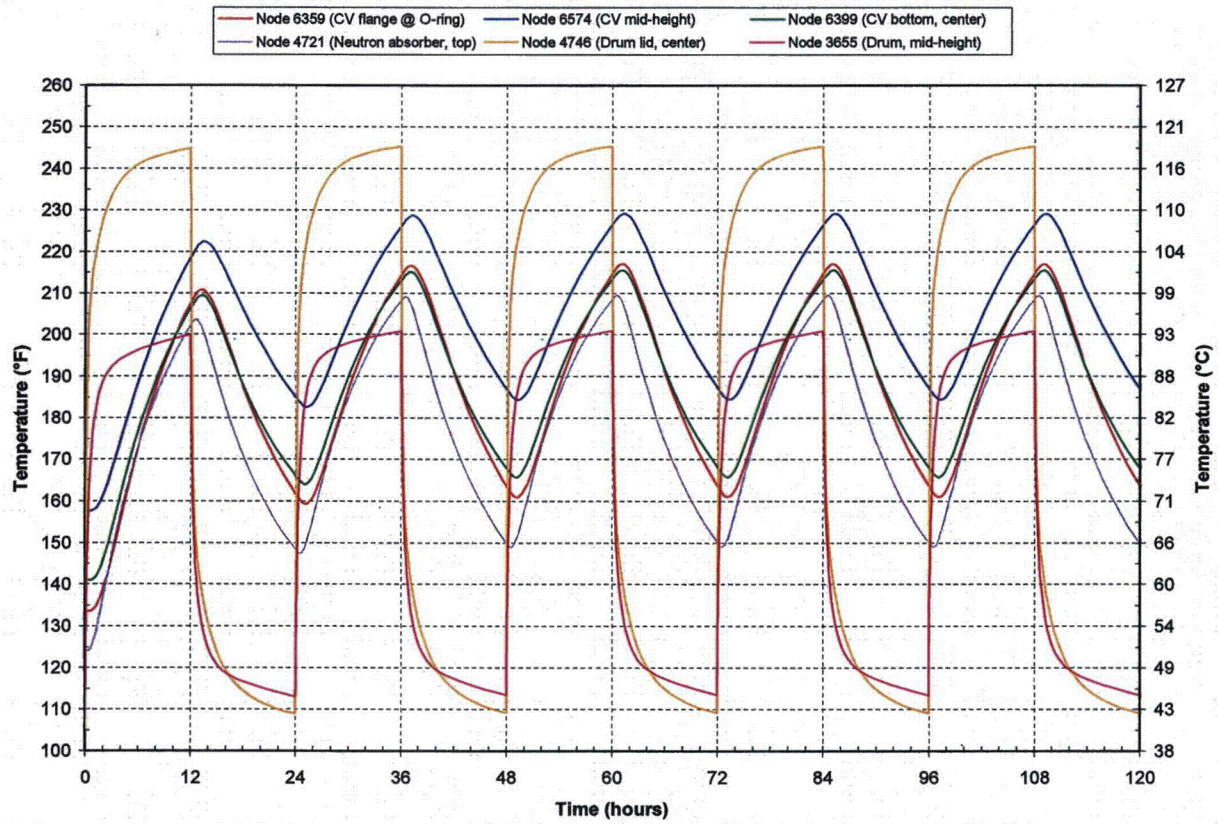


Figure 14. Transient temperatures of the ES-3100 shipping container for NCT (20 W content heat load) see Figure 8 through Figure 11 for node locations.

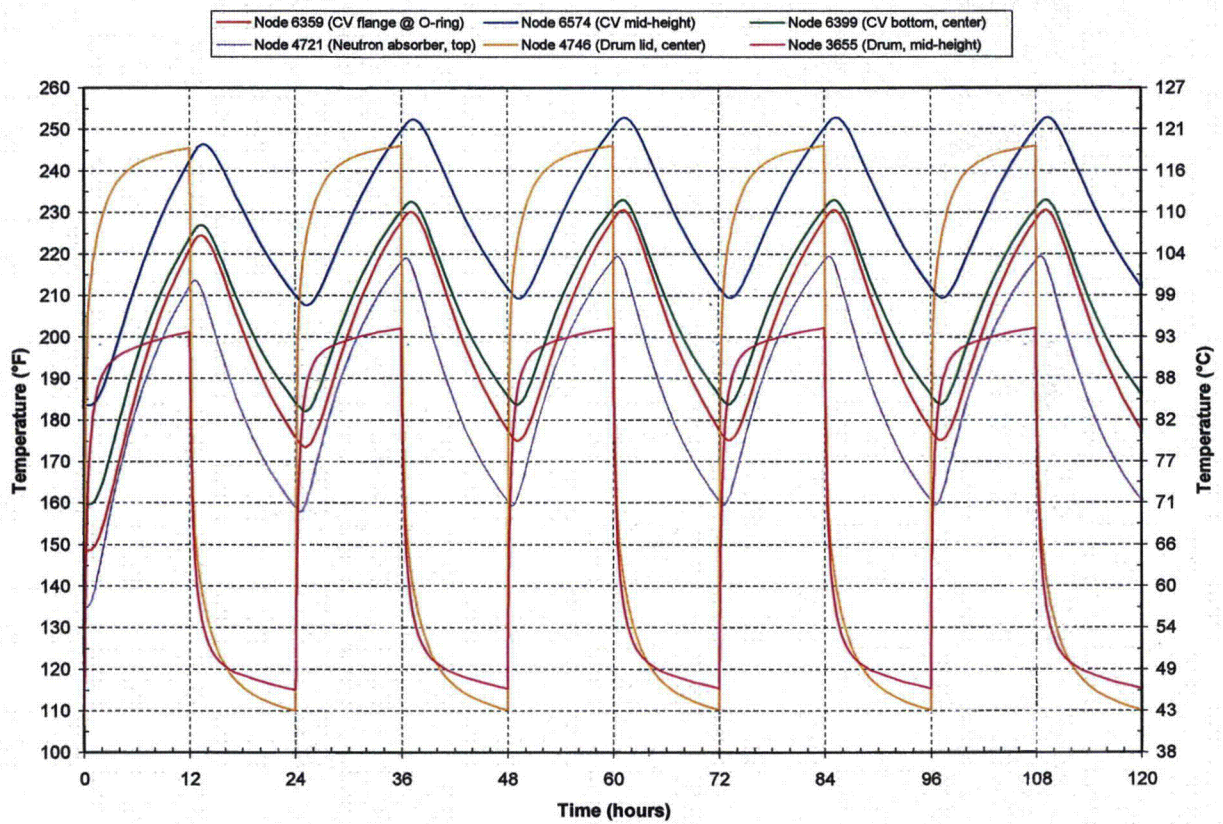


Figure 15. Transient temperatures of the ES-3100 shipping container for NCT (30 W content heat load) see Figure 8 through Figure 11 for node locations.

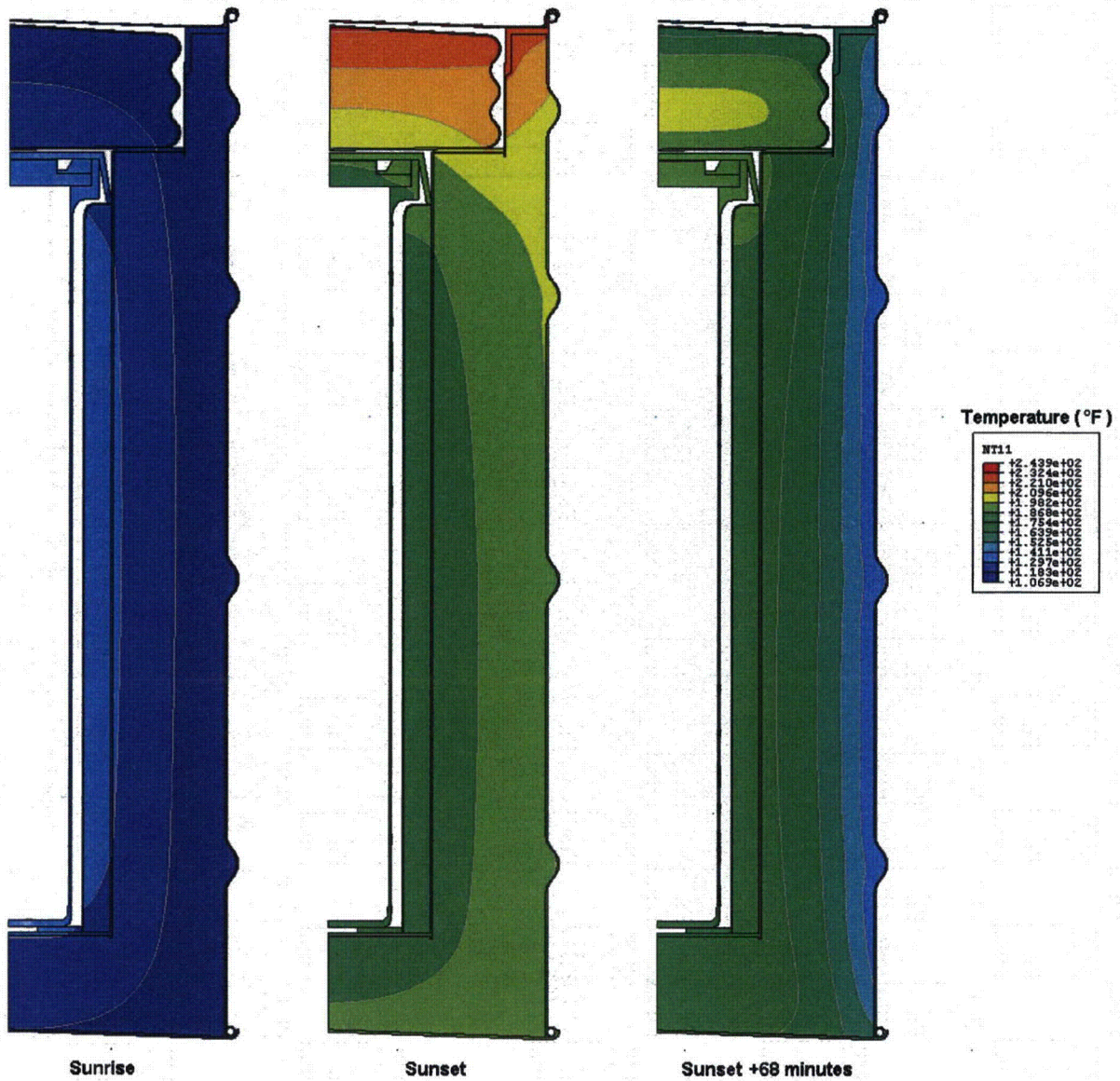


Figure 16. Temperature distribution in the ES-3100 shipping container for NCT (no content heat load) typical day of transient analysis (elements representing air not shown for clarity).

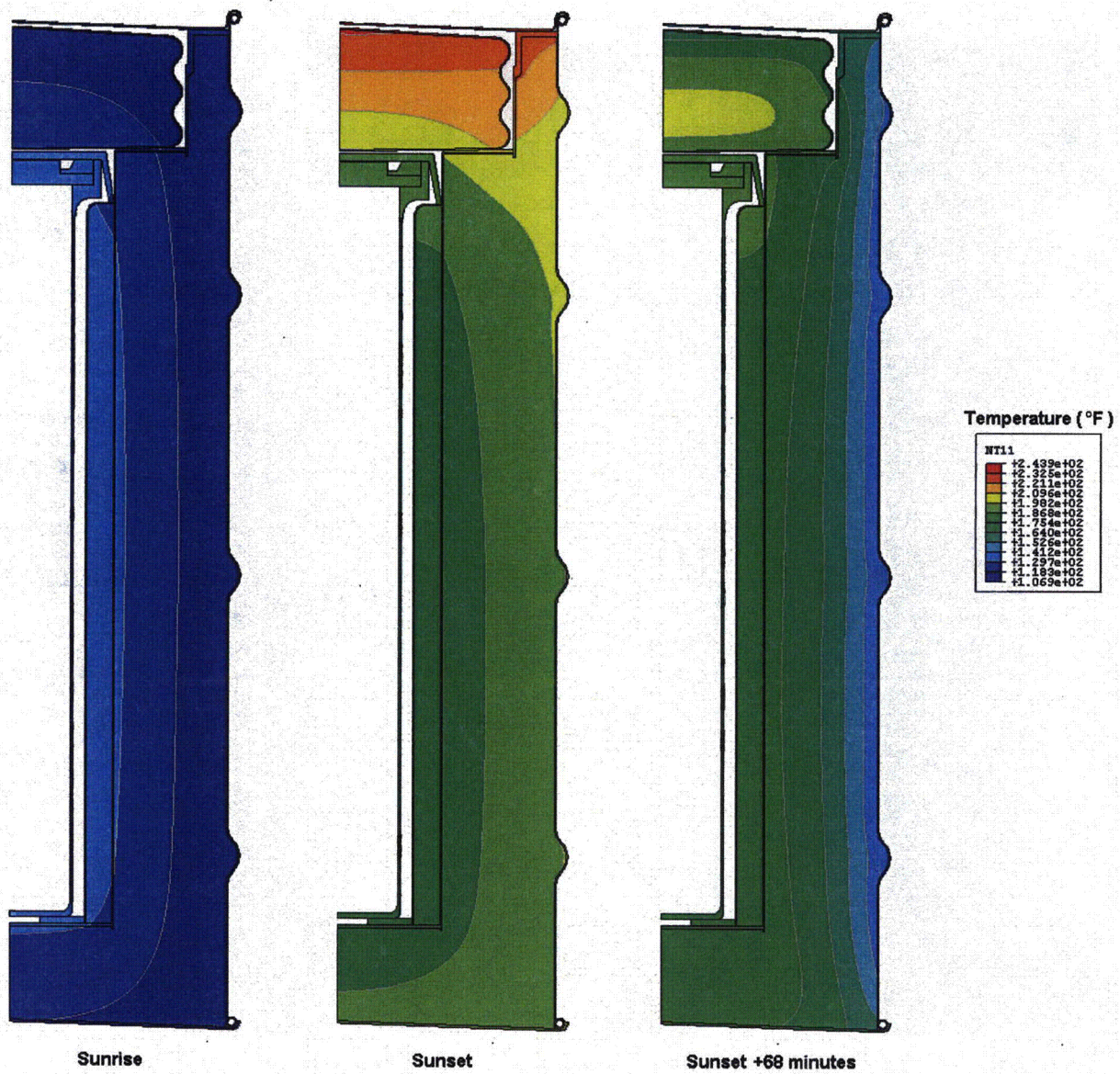


Figure 17. Temperature distribution in the ES-3100 shipping container for NCT (0.4 W content heat load) typical day of transient analysis (elements representing air not shown for clarity).

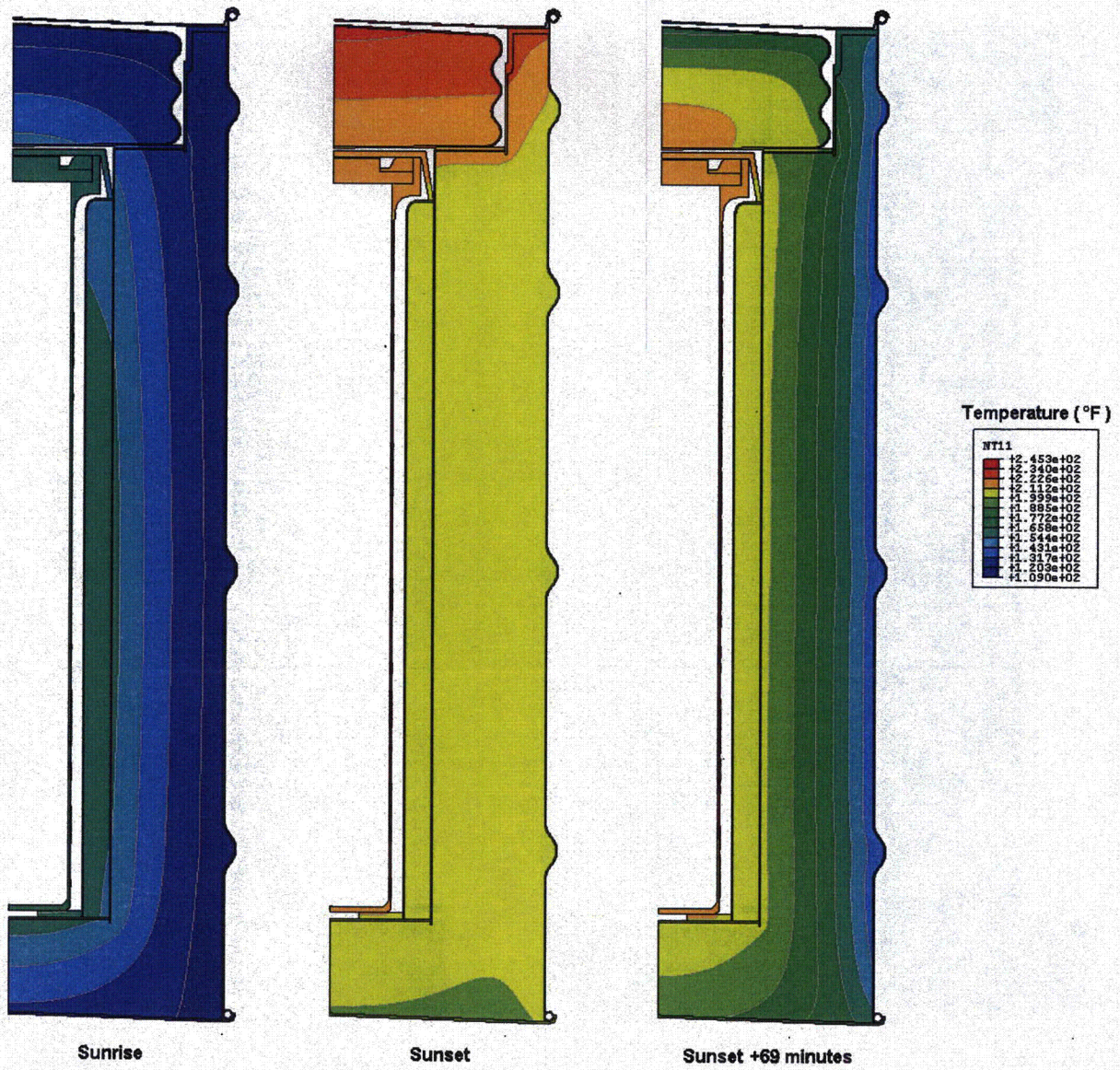


Figure 18. Temperature distribution in the ES-3100 shipping container for NCT (20 W content heat load) typical day of transient analysis (elements representing air not shown for clarity).

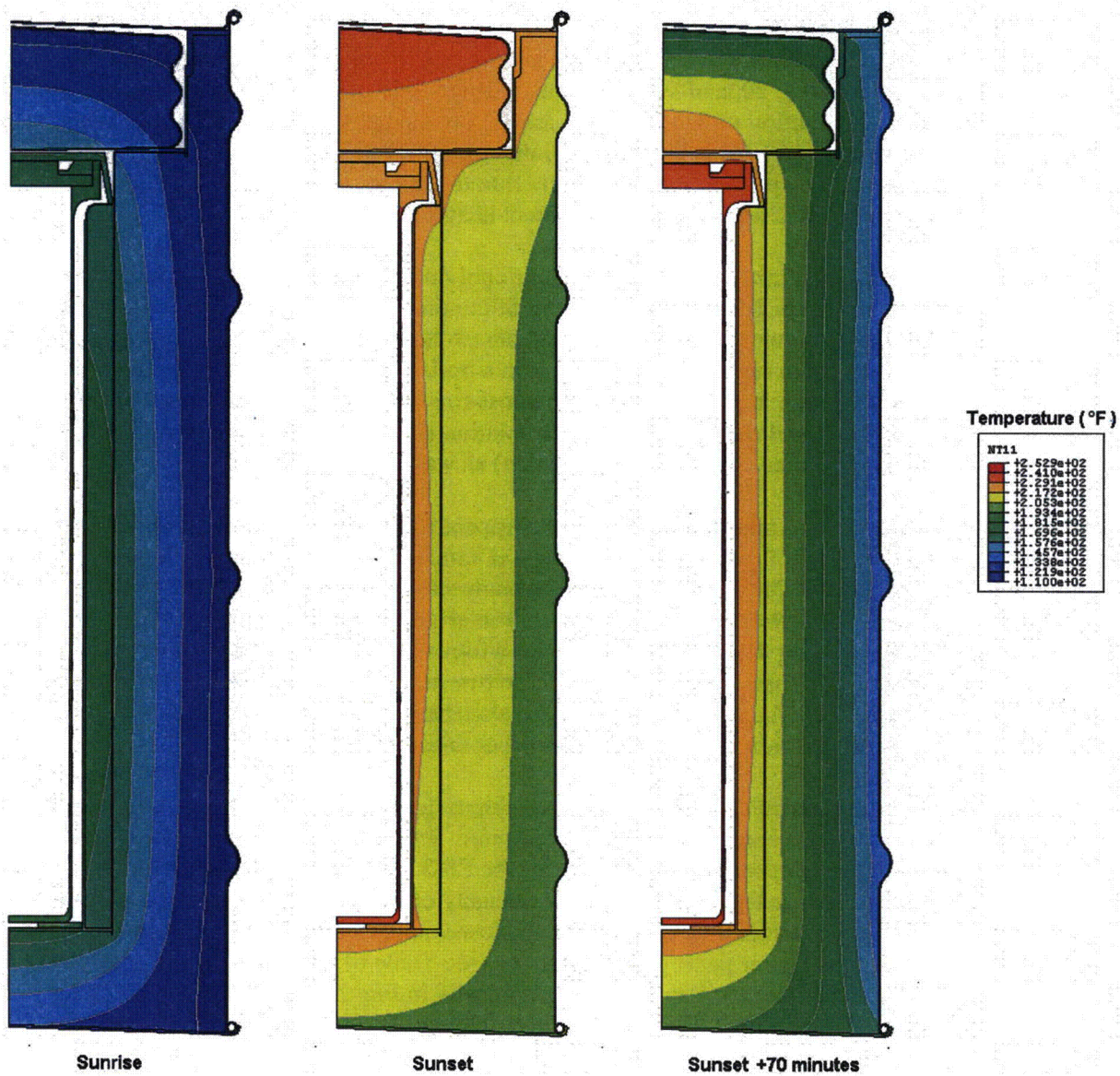


Figure 19. Temperature distribution in the ES-3100 shipping container for NCT (30 W content heat load) typical day of transient analysis (elements representing air not shown for clarity).

Hypothetical Accident Conditions Analyses Results

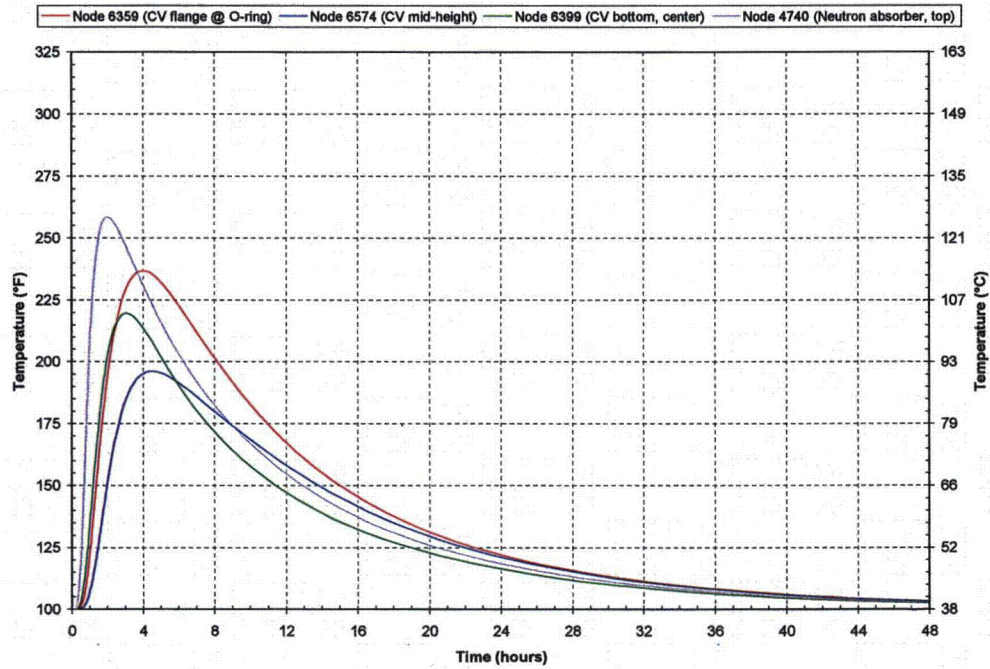
Transient thermal analyses are performed on the finite element model of the ES-3100 shipping container (undamaged configuration) to simulate HAC as prescribed by 10 CFR 71.73(c)(4).^[1] A 30-minute fire of 1475°F (800°C) is simulated by applying natural convection and radiant exchange boundary conditions to all external surfaces of the drum (assuming the drum is in a horizontal orientation) with content heat loads of 0, 0.4, 20, and 30 W. There are no heat flux boundary conditions simulating insolation applied to the model before and during the 30-minute fire. The initial temperature distribution within the package having content heat loads of 0.4, 20, and 30 W is obtained from their respective steady-state analyses. The initial temperature distribution within the package having no content heat load (0 W) is assumed to be at a uniform temperature equal to the ambient temperature of 100°F (37.8°C). As with the steady-state analyses discussed previously, applying a uniform heat flux to the internal surfaces of the elements representing the containment vessel simulates the content heat load.

Following the 30-minute fire transient analyses, 48-hour cool-down transient thermal analyses are performed using the temperature distribution at the end of the fire as the initial temperature distribution. During post-fire cool-down, natural convection and radiant exchange boundary conditions are applied to all external surfaces of the drum (assuming the drum is in a horizontal orientation). Additionally, cases are analyzed in which insolation is included during the post-fire cool-down. For the cases in which insolation is applied to the model during cool-down, insolation is applied during the first 12-hour period following the 30-minute fire, then alternated (off, then on) as was done for NCT.

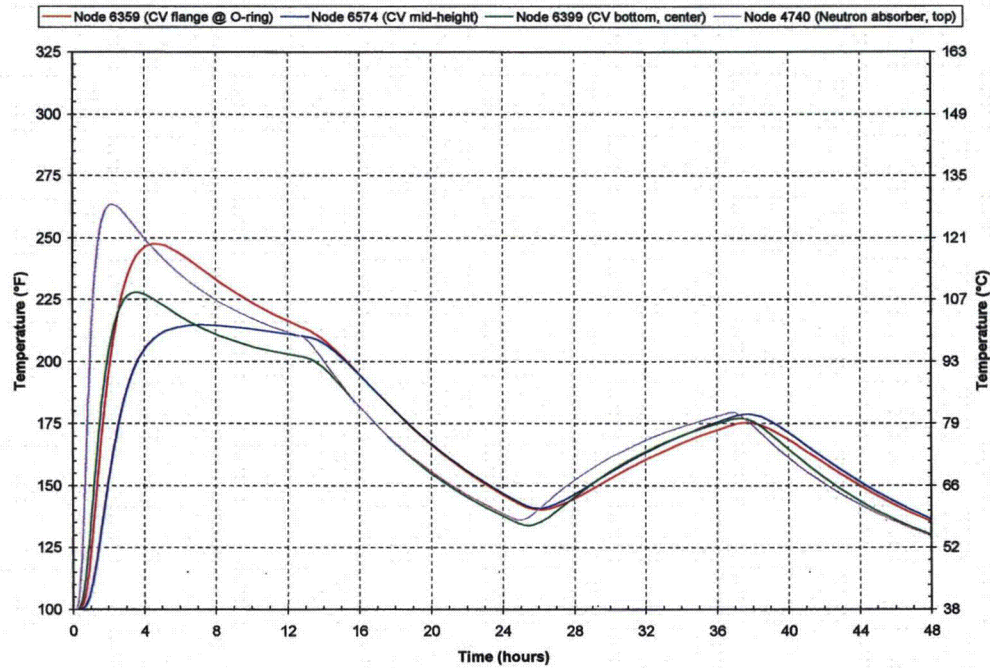
Based on previous analyses of a similar package^[9] (see Appendix 3.6.1), it was noted that using the low-end density of Kaolite results in higher containment vessel temperatures than using the high-end density of Kaolite. For this reason, the NCT and HAC thermal analyses were run using a density of 19.4 lbm/ft³ (see Table 1). Similarly, the low-end density of the neutron absorber (100 lbm/ft³) was also used in these analyses. However, while using these low-end densities will result in higher temperatures to the containment vessel, using the high-end densities for these two materials will result in higher temperature differences from the baseline HAC case. Thus, runs are also made for heat loads of 0, 0.4, 20, and 30 W using a Kaolite density of 30 lbm/ft³ and a neutron absorber density of 110 lbm/ft³.

The maximum temperatures calculated for the ES-3100 shipping container for HAC are summarized in Table 6 for the analyses using a Kaolite density of 19.4 lbm/ft³ and a neutron absorber density of 100 lbm/ft³. The maximum temperatures calculated for the ES-3100 shipping container for HAC are summarized in Table 7 for the analyses using a Kaolite density of 30 lbm/ft³ and a neutron absorber density of 110 lbm/ft³. The thermal analyses that use the low-end density values for Kaolite and the neutron absorber achieve the higher package temperatures (see Table 6). Temperature-history plots of several locations within the model are also depicted graphically in Figure 20 through Figure 23 for content heat loads of 0, 0.4, 20, and 30 W for the analyses using a Kaolite density of 19.4 lbm/ft³ and a neutron absorber density of 100 lbm/ft³.

The HAC thermal analyses presented in this report are performed using a finite element model that represents an undamaged ES-3100 shipping container. While the cumulative damage from NCT and HAC drop tests, crush tests, and puncture tests, must be considered when evaluating the performance of the package to HAC, the temperature differences (i.e., adjustments) calculated from the data presented in Table 6 and Table 7 are of value when combined with the physical test data when making this assessment.

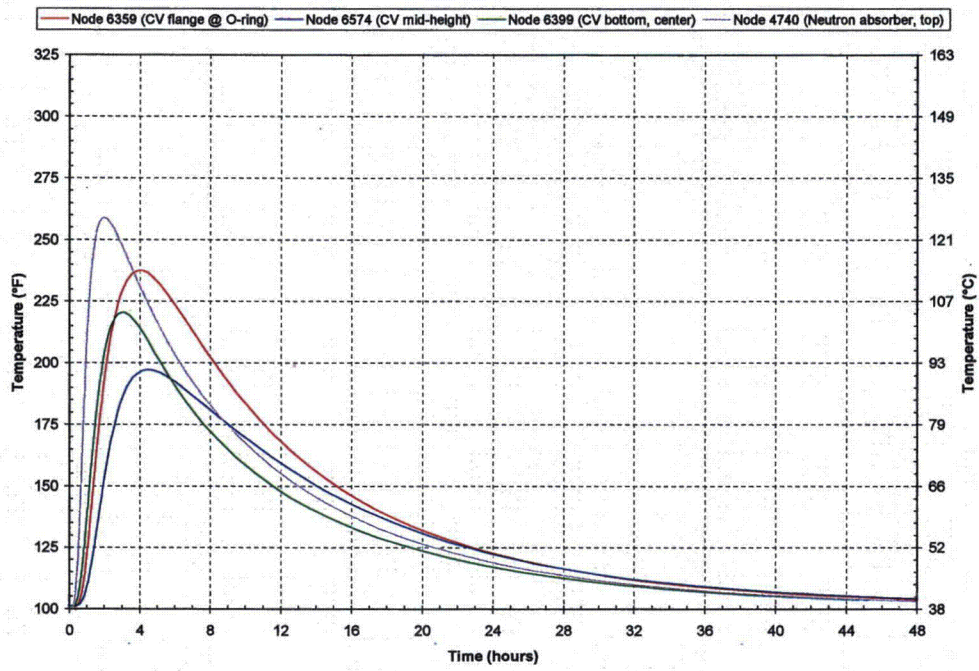


(a) No insolation during post-fire cool-down.

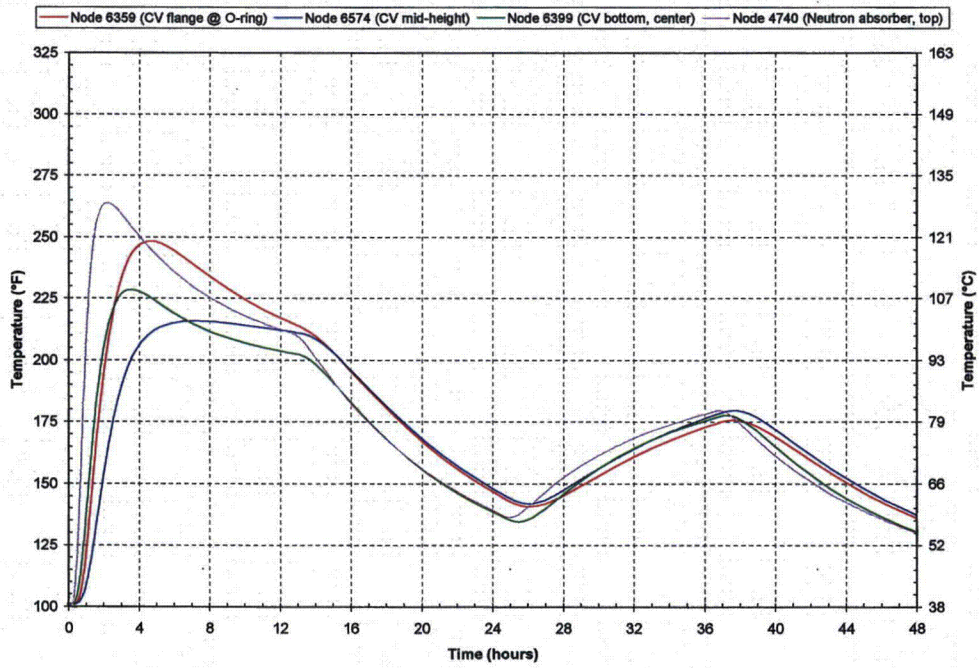


(b) Insolation during post-fire cool-down.

Figure 20. ES-3100 shipping container transient temperatures for HAC—no content heat load and lower bound Kaolite and neutron absorber densities (see Figure 8 through Figure 11 for node locations).

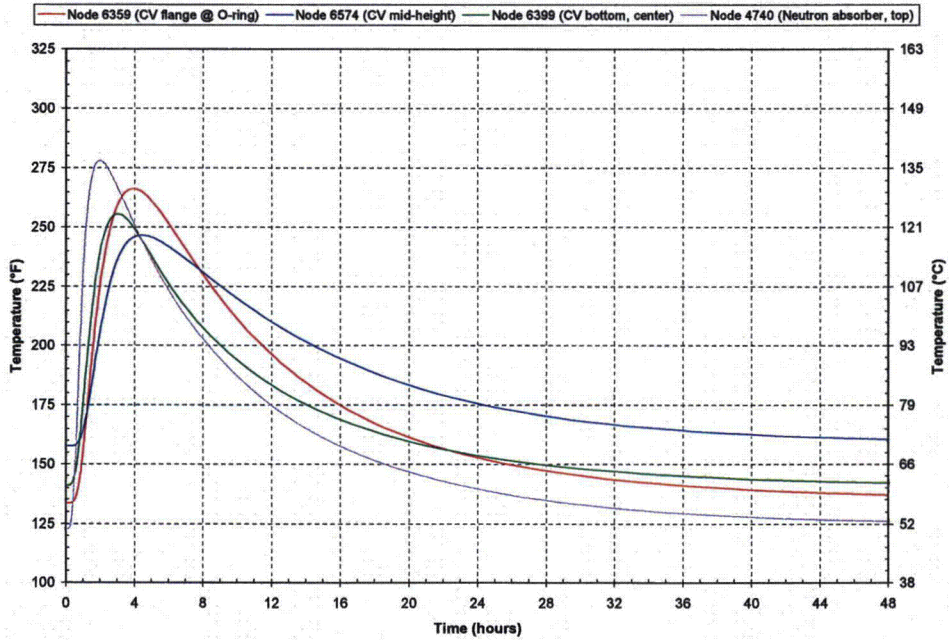


(a) No insulation during post-fire cool-down.

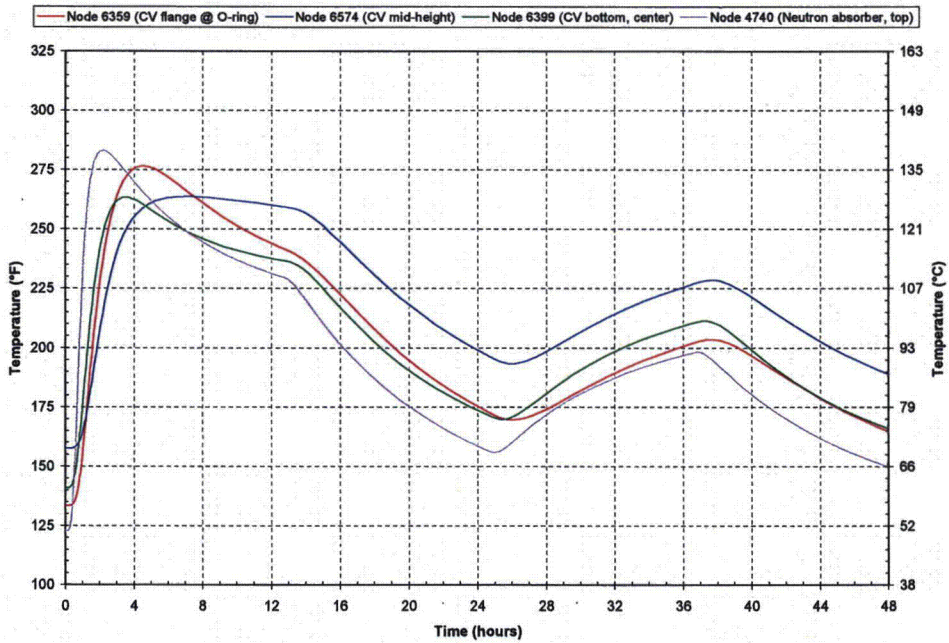


(b) Insulation during post-fire cool-down.

Figure 21. ES-3100 shipping container transient temperatures for HAC, 0.4 W content heat load and lower bound Kaolite and neutron absorber densities (see Figure 8 for through Figure 11 for node locations).

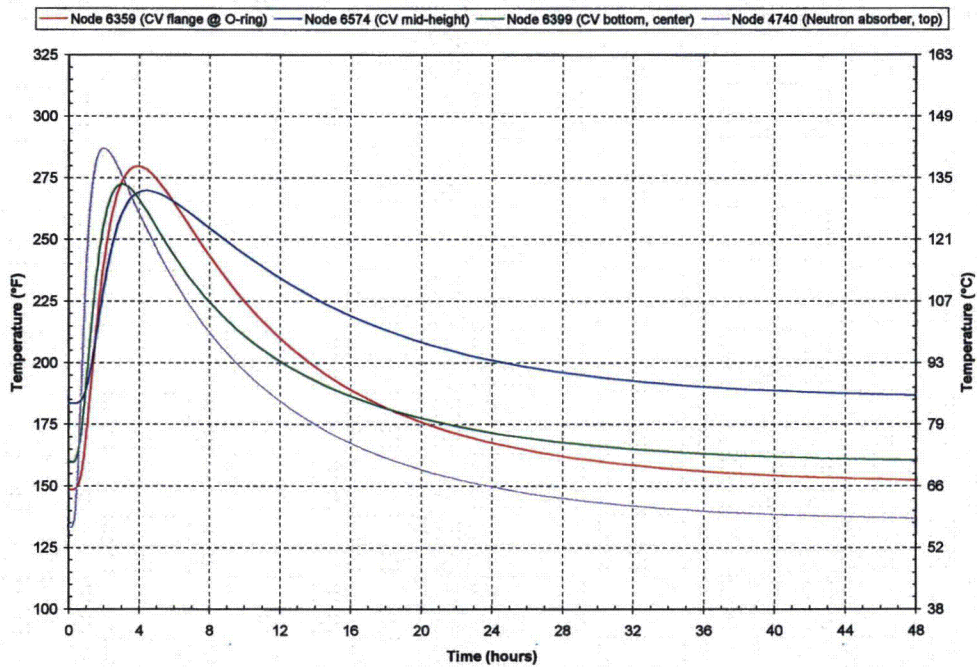


(a) No insolation during post-fire cool-down.

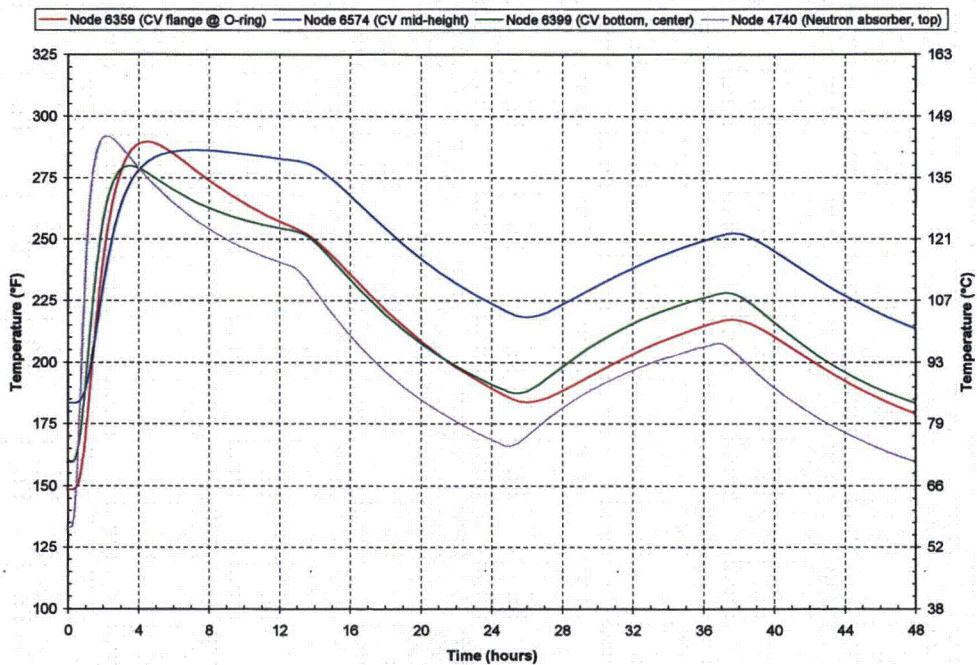


(b) Insolation during post-fire cool-down.

Figure 22. ES-310 shipping container transient temperatures for HAC, 20 W content heat load and lower bound Kaolite and neutron absorber densities (see Figure 8 through Figure 11 for node locations).



(a) No insulation during post-fire cool-down.



(b) Insulation during post-fire cool-down.

Figure 23. ES-3100 shipping container transient temperatures for HAC, 30 W content heat load and lower bound Kaolite and neutron absorber densities (see Figure 8 through Figure 11 for node locations)

APPENDIX 3.6.2 REFERENCES

1. *Packaging and Transportation of Radioactive Materials*, U.S. Nuclear Regulatory Commission, Code of Federal Regulations, Title 10 – Energy, Part 71, January 1, 2004.
2. L. S. Dickerson, M. R. Feldman, and R. D. Michaelhaugh, *Test Report of the ES-3100 Package*, Volumes 1–3, ORNL/NTRC-013, Rev. 0, Nuclear Science and Technology Division, Oak Ridge National Laboratory, Oak Ridge, Tennessee, September 10, 2004.
3. MSC. Patran 2004, Version 12.0.044, MacNeal Schwendler Corporation, 2004.
4. ABAQUS/CAE, Version 6.4-1, Build ID: 2003_09_29-11.18.28 46457, Abaqus, Inc., 2003.
5. R. Siegel and J. R. Howell, *Thermal Radiation Heat Transfer*, Second Edition, Hemisphere Publishing Corporation, 1981.
6. F. P. Incropera and D. P. DeWitt, *Fundamentals of Heat and Mass Transfer*, Second Edition, John Wiley & Sons, New York, 1985.
7. J. C. Anderson and M. R. Feldman, *Thermal Modeling of Packages for Normal Conditions of Transport with Insolation*, Proceedings of the ASME Heat Transfer Division, HTD-Vol. 317-2, 1995, International Mechanical Engineering Congress and Exposition, November 1995.
8. ABAQUS/Standard, Version 6.4-1, 2003_09_29-11.18.28 46457, Abaqus, Inc. , 2003.
9. P. A. Bales, *Thermal Analyses of the ES-3100 Shipping Container for NCT and HAC*, DAC-PKG-801699-A001, Rev. 1, BWXT Y-12, December 30, 2004.

Appendix 3.6.3

**THERMAL STRESS EVALUATION OF THE ES-3100 SHIPPING CONTAINER
DRUM BODY ASSEMBLY FOR NCT (FINAL DESIGN
WITH CATALOG 277-4 NEUTRON ABSORBER)**

Appendix 3.6.3

THERMAL STRESS EVALUATION OF THE ES-3100 SHIPPING CONTAINER DRUM BODY ASSEMBLY FOR NCT (FINAL DESIGN WITH CATALOG 277-4 NEUTRON ABSORBER)

INTRODUCTION

Static stress analyses of the ES-3100 shipping container are performed to determine the maximum thermal stresses within the packaging when exposed to Normal Conditions of Transport (NCT) as specified in 10 CFR 71.71(c)(1).^[1] Transient thermal analyses were previously performed^[2] (see Appendix 3.6.2) on the ES-3100 shipping container to determine its response to NCT. The thermal analyses treat the problem as a cyclic transient with the incident heat flux due to solar radiation applied and not applied in alternating 12-hour periods. The calculated temperature distributions within the drum body assembly for NCT at various times are then mapped onto the structural model, and static analyses are performed for each time step in the thermal analyses.

FINITE ELEMENT MODEL DESCRIPTION

A two-dimensional axisymmetric finite element model of the ES-3100 shipping container is constructed using MSC.Patran^[3] and imported as an orphaned mesh into ABAQUS/CAE^[4] for application of boundary conditions, interactions, and loads. The model is constructed of CAX4I (four-node bilinear axisymmetric quadrilateral, incompatible mode) elements for stress evaluation. These elements are chosen because they can accurately capture bending stresses with only one element through the thickness of a structure. A schematic of the finite element model is presented in Figure 1 with details of the upper and lower portions of the model shown in Figure 2 and Figure 3, respectively. The model consists of three materials: stainless steel (drum, drum bottom plate, and drum liner weldment), Kaolite, and neutron absorber. Details of the model are discussed in the following sections.

Surface-to-surface contact interactions are modeled between contacting surfaces in the static stress model. These interactions are shown graphically in Figure 2 and Figure 3. For all interactions, the tangential behavior is modeled as “frictionless” while the normal behavior is modeled as “hard contact.” For the interactions modeled between the bottom of the neutron absorber and the drum liner and between the drum Kaolite bottom and the drum bottom plate, the contacting surfaces are not allowed to separate after contact is made.

The radial degree-of-freedom (U_r) of each node along the centerline of the model is fixed to simulate symmetry. Additionally, the axial degree-of-freedom (U_z) of one node on the drum bottom plate is fixed.

The temperatures calculated for NCT in Appendix 3.6.2 are stored in the ‘NCT.fil’ file for each of the content head loads analyzed. The temperature distribution for each time of interest is mapped onto the static stress model using the ‘*Temperature’ keyword. The specific times of interest from the transient thermal analyses are at each increment in the final day/night cycle (after “quasi steady-state” is reached).

The mechanical properties of the materials used in the static stress analyses are presented in Table 1. The modulus of elasticity of Kaolite presented in Table 1 is calculated from the first two points of the compressive stress-strain assuming a Poisson’s ratio of 0.01.^[5]

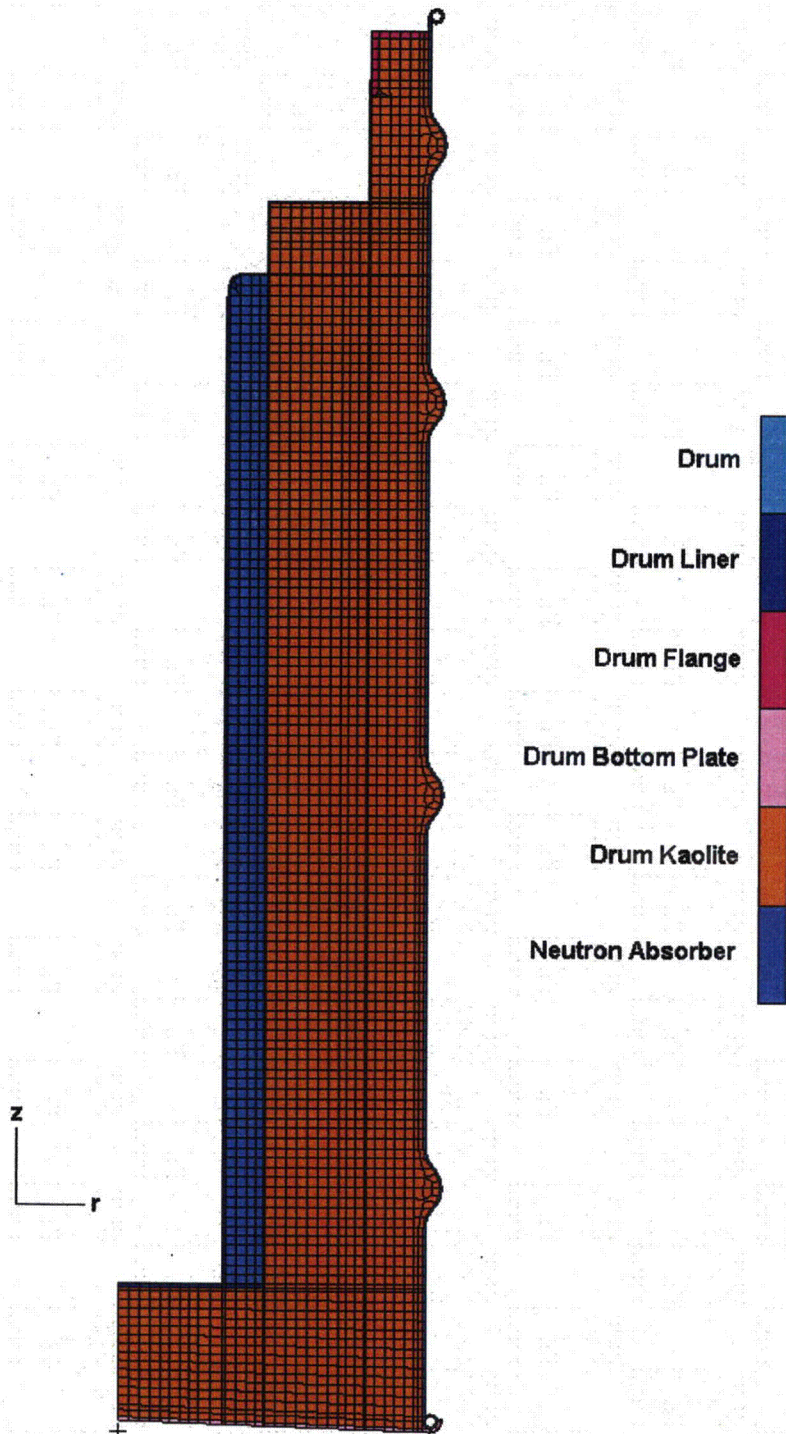


Figure 1. MSC.Patran axisymmetric finite element model of the ES-3100 shipping container drum body assembly.

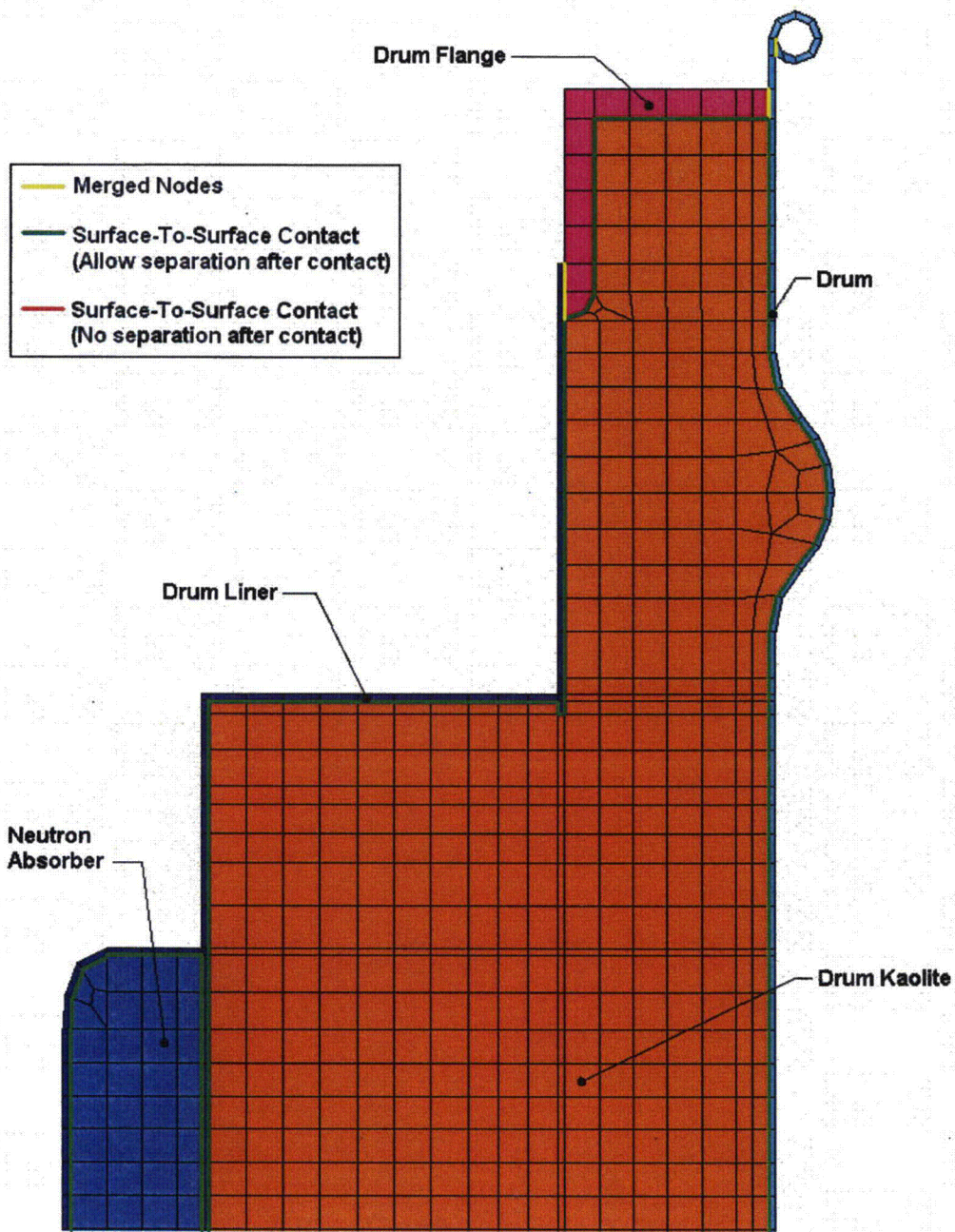


Figure 2. MSC.Patran axisymmetric finite element model of the ES-3100 shipping container drum body assembly (upper portion detail).

- Merged Nodes
- Surface-To-Surface Contact (Allow separation after contact)
- Surface-To-Surface Contact (No separation after contact)
- ▶ Fixed radial degree-of-freedom
- ▲ Fixed axial degree-of-freedom

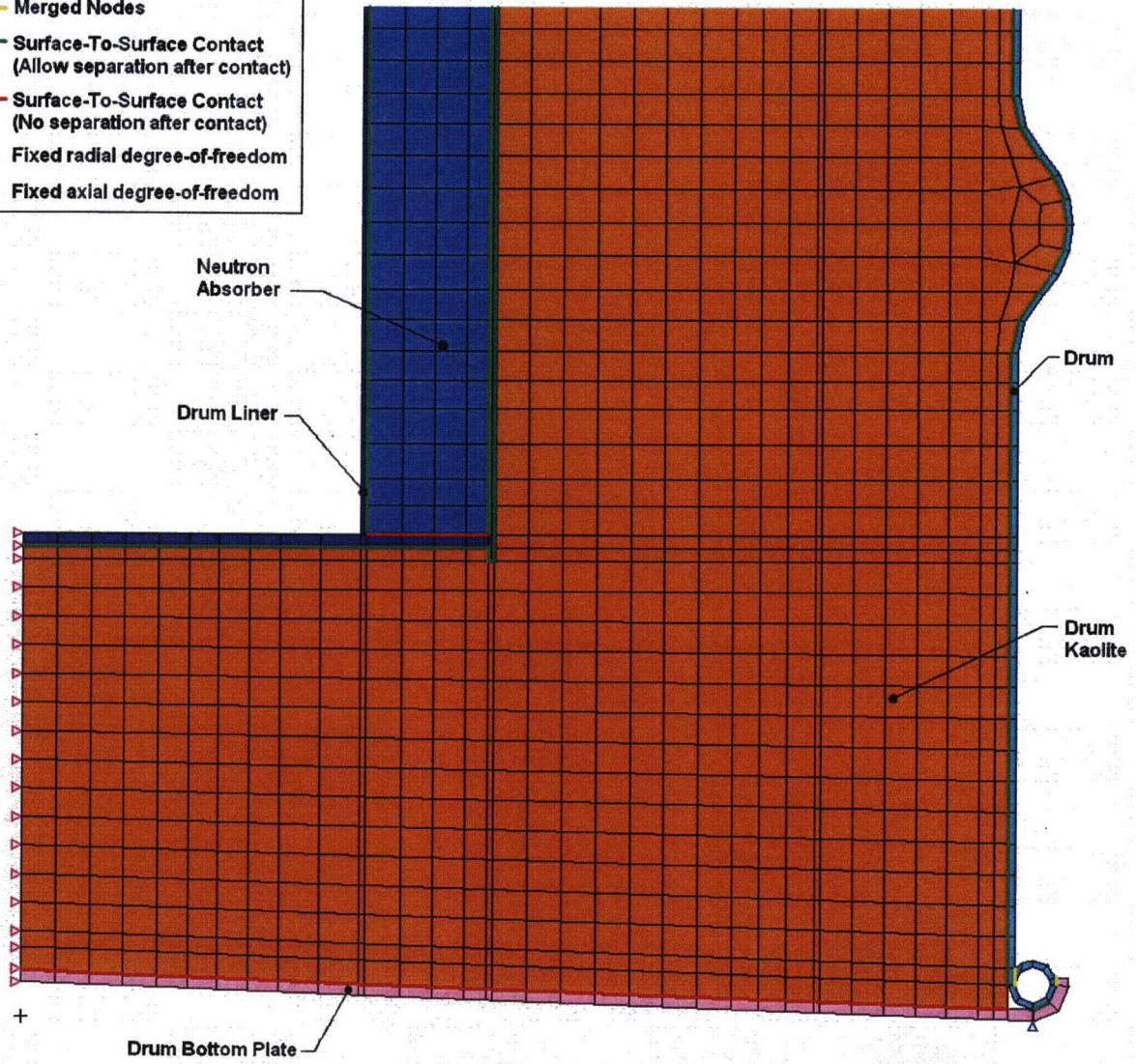


Figure 3. MSC.Patran axisymmetric finite element model of the ES-3100 shipping container drum body assembly (lower portion detail).

Table 1. Mechanical properties of the materials used in the static stress analyses.

Material	Temperature (°F)	Modulus of elasticity (psi)	Poisson's ratio	Density (lbm/in ³)	Coefficient of thermal expansion (in./in./°F)
Stainless Steel	-40	28.6×10 ⁶ (a)	0.29 (b)	0.285 (c)	8.2×10 ⁻⁶ (e)
	100	28.14×10 ⁶	—	—	8.6×10 ⁻⁶
	200	27.6×10 ⁶	—	—	8.9×10 ⁻⁶
	300	27.0×10 ⁶	—	—	9.2×10 ⁻⁶
Kaolite	—	29,210 (d)	0.01 (d)	0.013 (f)	5.04×10 ⁻⁶ (g)
Neutron Absorber	-40	1.991×10 ⁶ (h)	0.33 (h)	0.0608 (h)	7.056×10 ⁻⁶ (i)
	-4	—	—	—	7.222×10 ⁻⁶
	32	—	—	—	7.222×10 ⁻⁶
	70	0.984×10 ⁶	0.28	—	—
	100	0.403×10 ⁶	0.25	—	—
	104	—	—	—	7.000×10 ⁻⁶
	140	—	—	—	6.444×10 ⁻⁶
	176	—	—	—	5.778×10 ⁻⁶
	212	—	—	—	5.389×10 ⁻⁶
	248	—	—	—	5.056×10 ⁻⁶
	284	—	—	—	4.889×10 ⁻⁶
302	—	—	—	4.833×10 ⁻⁶	

- Notes: (a) ASME Boiler and Pressure Vessel Code, Sect. II, Part D, Subpart 2, Tables TE-1, B column, and TM-1.
 (b) R. A. Bailey, *Strain – A Material Database*, Lawrence Livermore National Laboratory, 1989.
 (c) F. P. Incropera and D. P. DeWitt, *Fundamentals of Heat and Mass Transfer*, 2nd edition, John Wiley & Sons, New York, 1985.
 (d) K. D. Handy, *Impact Analysis of ES3100 Design Concepts Using Borobond*, DAC-EA-801699-A001, BWXT Y-12, Oct. 2004. The Poisson's ratio of Kaolite is assumed to be a small value of 0.1.
 (e) *Metallic Materials and Elements for Aerospace Vehicle Structures*, MIL-HDBK-5E, May 1986.
 (f) Specification JS-YMN3-801580-A003 requires a baked density of 22.4 ± 3 lbm/ft³.
 (g) E-mail communication, Ken Moody (Thermal Ceramics, Inc.) to Paul Bales (BWXT Y-12), 12/9/04.
 (h) B. F. Smith and G. A. Byington, *Mechanical Properties of 277-4*, Y/DW-1987, January 19, 2005.
 (i) W. D. Porter and H. Wang, *Thermophysical Properties of Heat Resistant Shielding Material*, ORNL/TM-2004/290, ORNL, Dec. 2004. Coefficient of thermal expansion at each temperature taken as the maximum of values for Runs #2, #3, and #5.

DISCUSSION OF ANALYTICAL RESULTS

All static stress analyses discussed in this report were performed using ABAQUS/Standard^[6] on an Intel Pentium 4–based Microsoft Windows 2000 computer. These analyses are sequential-coupled thermal/structural analyses.

As previously stated, the nodal temperature results for the final day/night cycle of the transient thermal analyses of the ES-3100 shipping container were stored in results files (NCT.fil) for each content heat load analyzed. Because automatic time-stepping was used in the transient thermal analyses, the number of increments stored in each 'NCT.fil' file differs for each content heat load analyzed. The static stress analyses of the ES-3100 are performed for each time increment analyzed in the thermal analyses for the final day/night cycle during NCT by copying the 'NCT.fil' and 'NCT.prt' files from the thermal analysis of interest to the directory where the stress analysis is being performed and entering the '*Temperature' keyword with the proper syntax for the time of interest. For example, for a content heat load of 0.4 W, the thermal stresses for time = 14.127 hours after sunrise (2.127 hours after sunset) on the final day/night

cycle (i.e., step = 11, increment = 29) are analyzed by entering the following keyword syntax via the keyword editor in ABAQUS/CAE:

```
*Temperature, file=NCT, bstep=11, binc=29, estep=11, einc=29
```

A separate static analysis is performed for each time step in the final day/night cycle of each thermal analysis for each content heat load.

The results of the static stress analyses for content heat loads of 0.4, 20, and 30 W are presented in Figure 4 through Figure 6. The stresses presented in these figures are the maximum nodal Mises stresses of each component at each point in time—as such, they don't necessarily occur at the same node location during the duration of the time period analyzed. The x-axes (i.e., time) are scaled in these figures such that the onset of sunrise on the final day/night cycle from the thermal analyses begins at time = 0 hours. Additionally, the stress (Mises) contours of the components of the finite element model are shown at various times in Figure 7 through Figure 11 for the case with a content heat load of 0.4 W. The time chosen for each stress contour plot coincides with the time that particular component reaches its maximum stress during the day/night cycle. The stress contours for the other heat loads investigated are similar to the 0.4 W case.

In addition to the static stress analyses performed for NCT, a static stress analysis is performed for exposure of the package to a -40°F ambient temperature (i.e., cold condition). A transient thermal analysis (24 hours in duration) is performed on the ES-3100 thermal model described in Appendix 3.6.2 to obtain the temperature distribution within the drum body assembly for exposure to cold conditions (see Appendix C for details). The package is assumed to be at an initial uniform temperature of 77°F, and no content heat load is applied. The natural convection coefficients (applied to the top and sides of the drum) are calculated for a -40°F ambient as described in Appendix 3.6.2 and are shown in Figure 12. A schematic of the thermal model showing several node locations for which the temperatures are tracked is presented in Figure 13. The transient temperatures calculated for cold conditions are presented in Figure 14 for several node locations. The maximum thermal stresses are presented in Figure 15 for this cold condition. Additionally, stress contours of the drum liner weldment, drum, and drum bottom plate are presented in Figure 16 through Figure 18 for the cold conditions at various times.

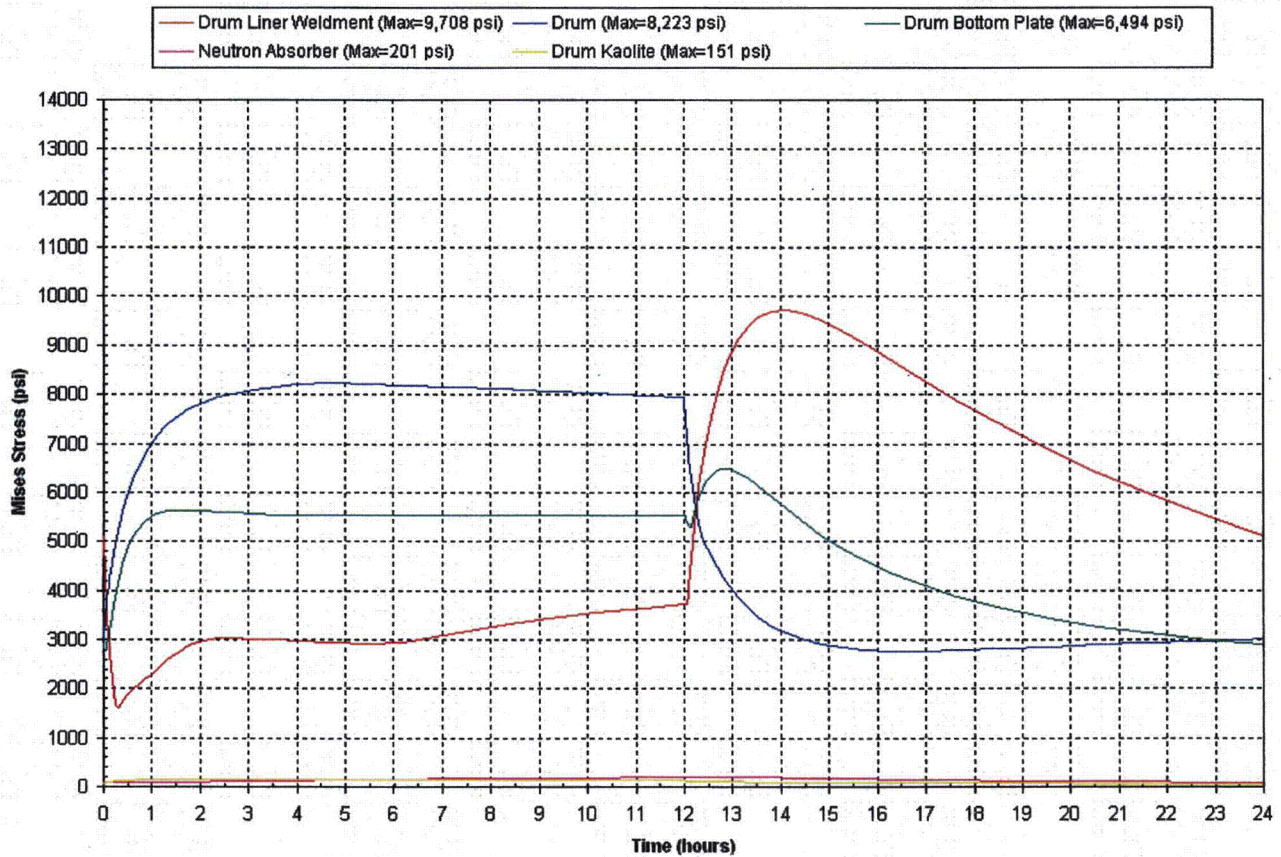


Figure 4. Thermal stresses (Mises) in the ES-3100 shipping container drum body assembly during a typical NCT day/night cycle—0.4 W content heat load.

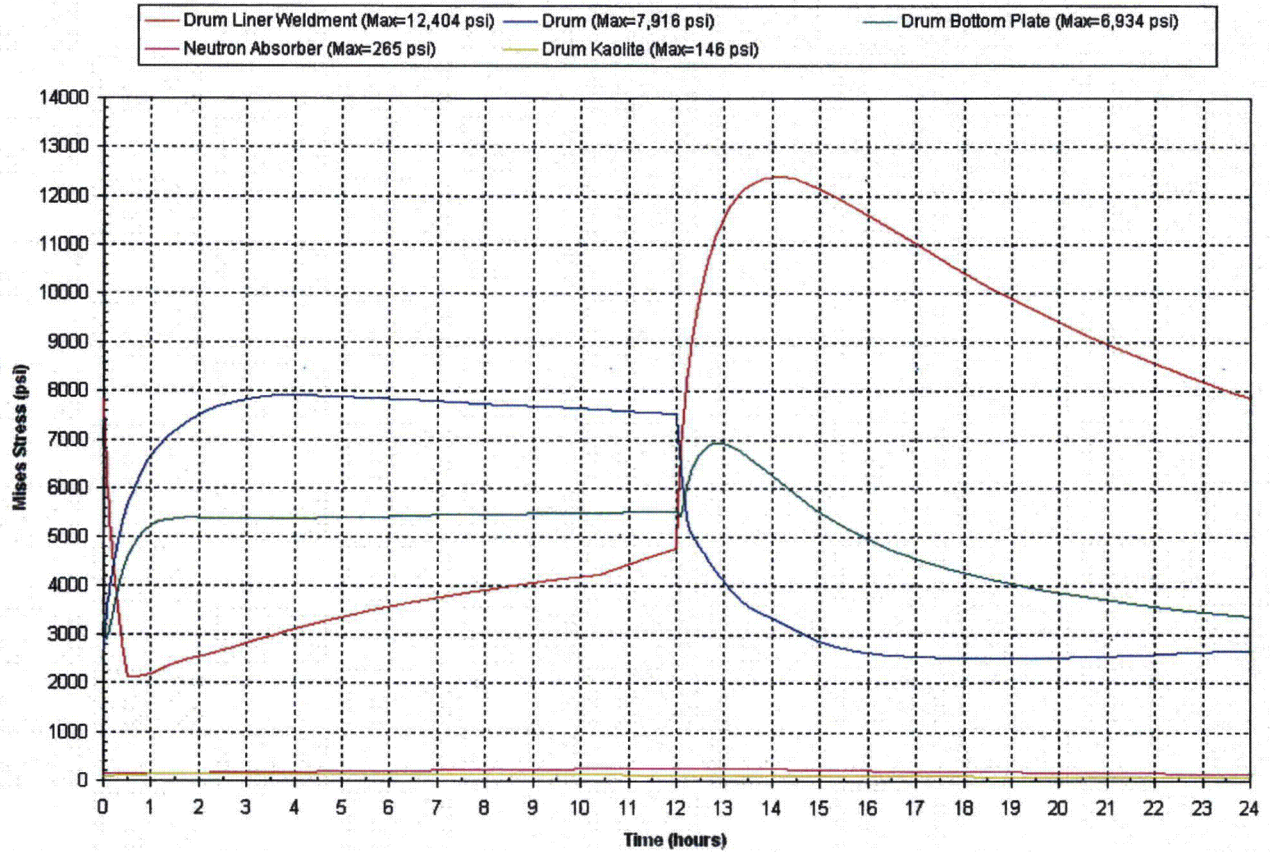


Figure 5. Thermal stresses (Mises) in the ES-3100 shipping container drum body assembly during a typical NCT day/night cycle—20 W content heat load.

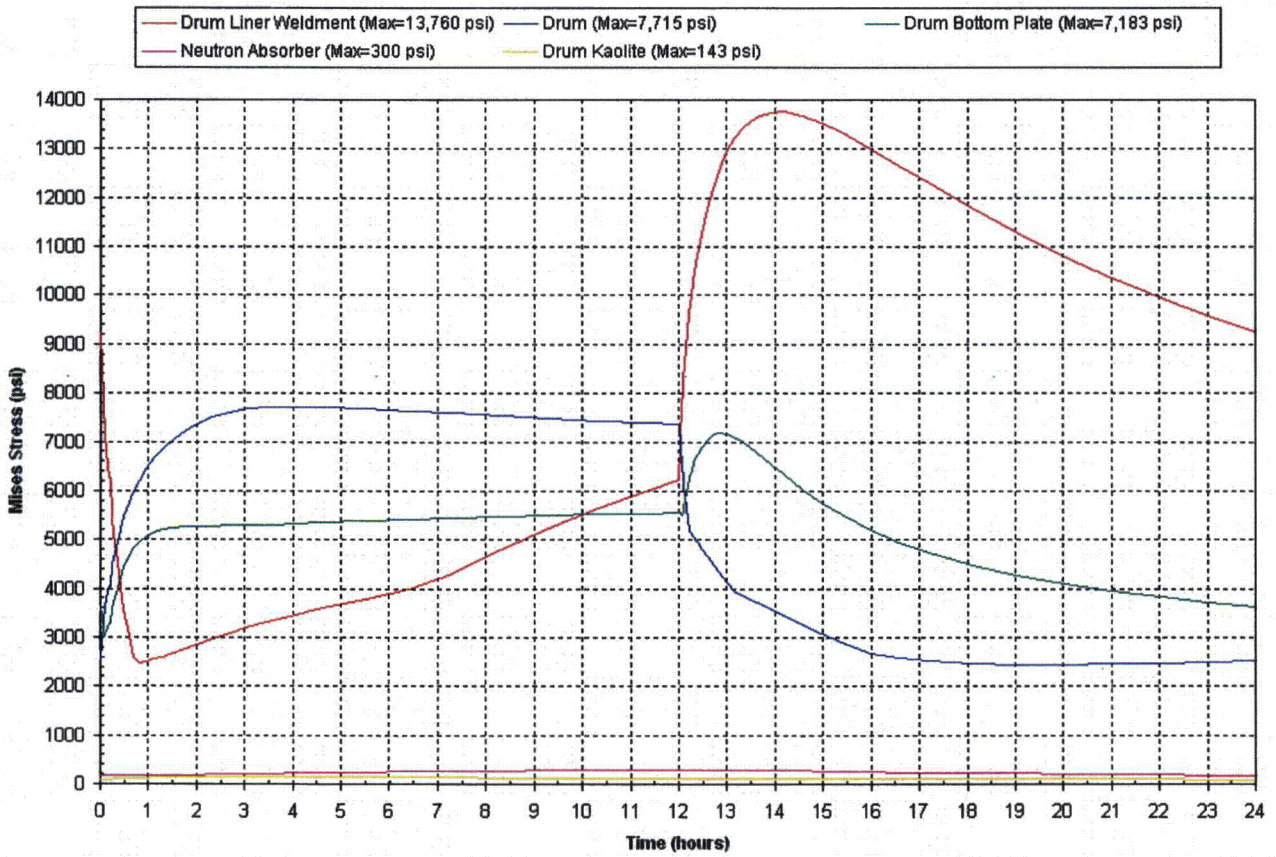


Figure 6. Thermal stresses (Mises) in the ES-3100 shipping container drum body assembly during a typical NCT day/night cycle—30 W content heat load.

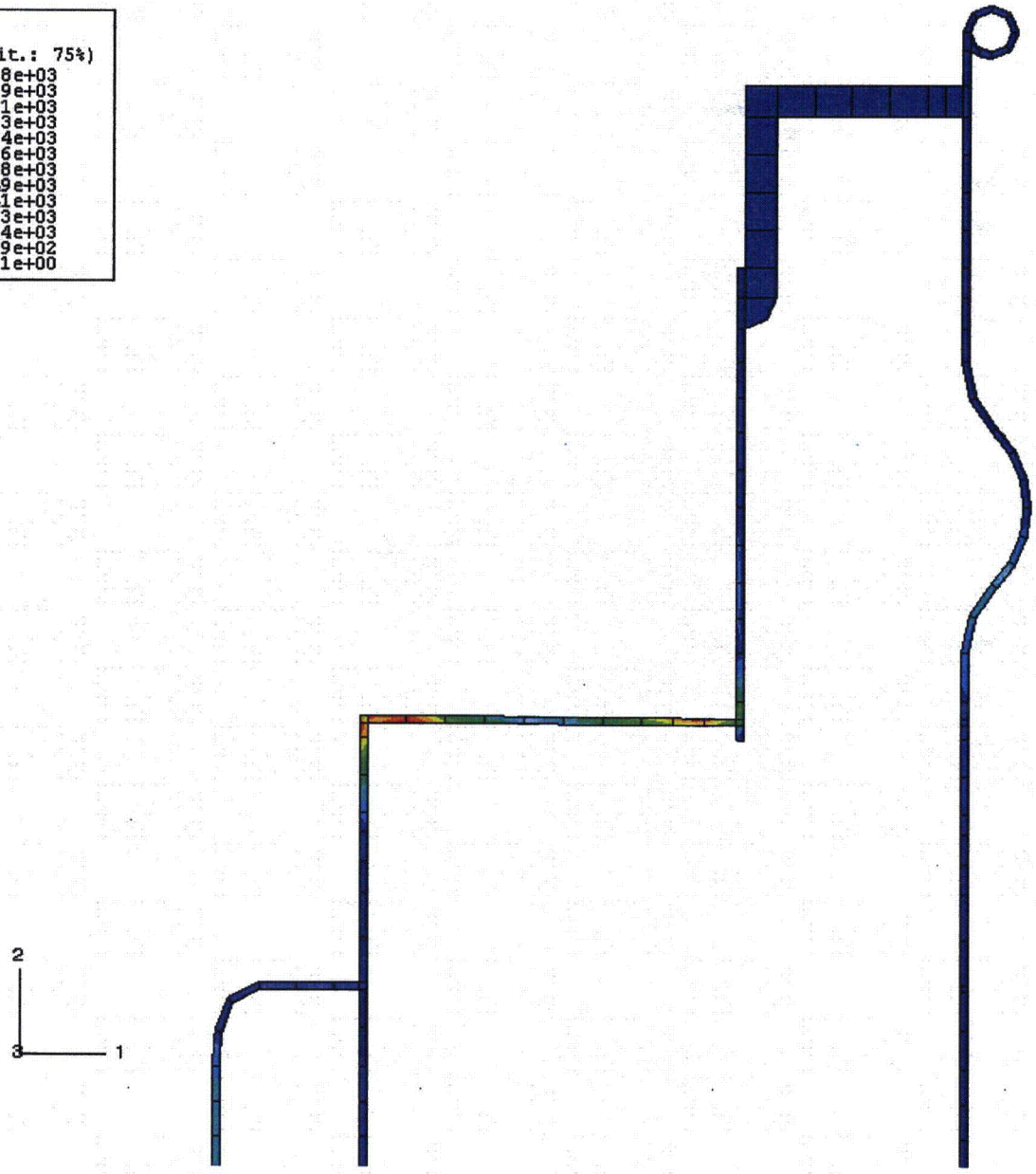
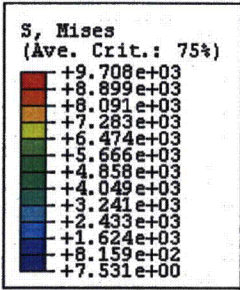


Figure 7. Drum/drum liner weldment Mises stresses (psi) during NCT at t = 14.127 hours (+2.127 hours after sunset)—0.4 W content heat load.

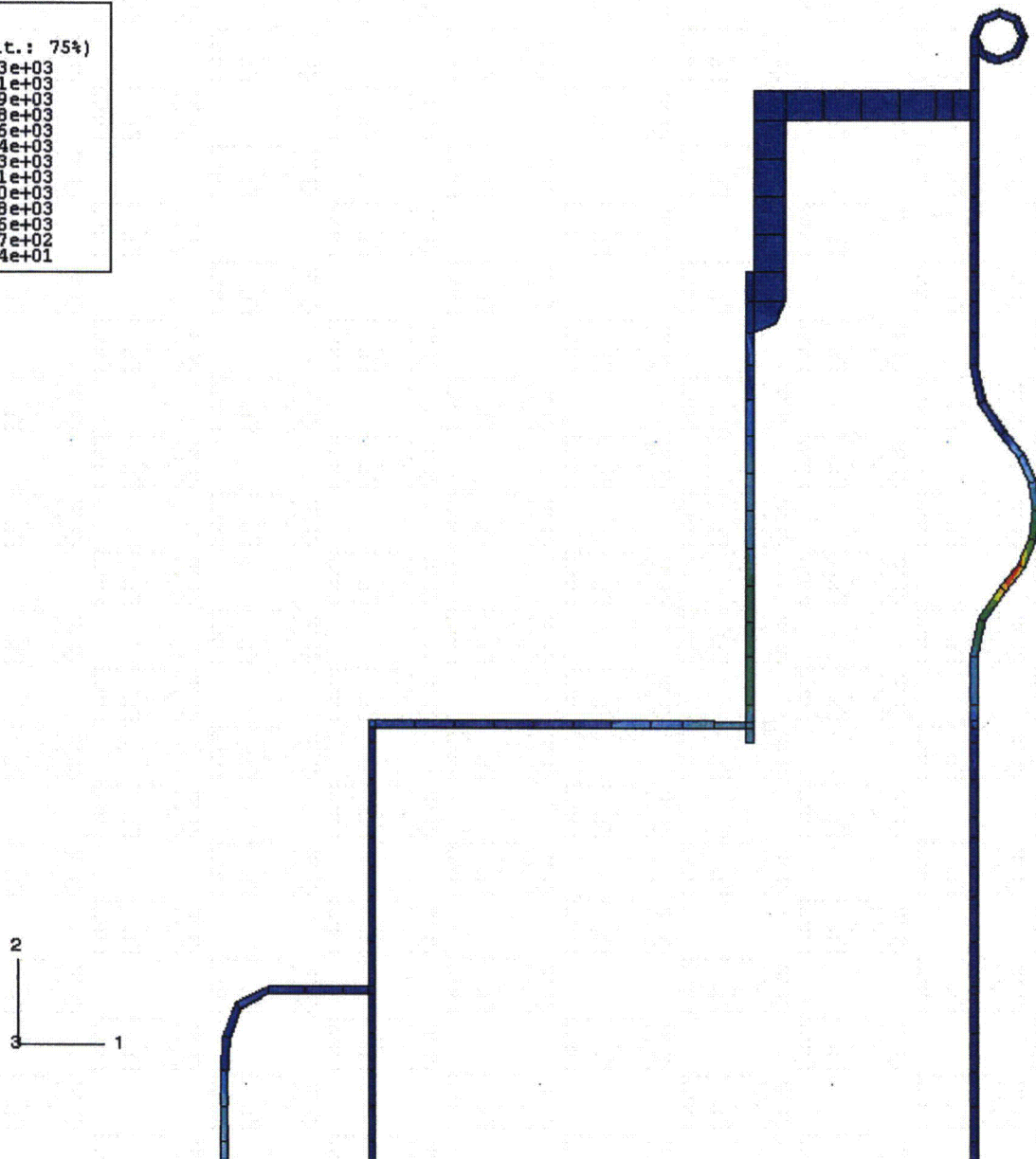
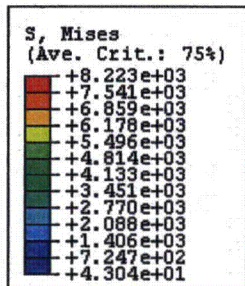


Figure 8. Drum/drum liner weldment Mises stresses (psi) during NCT at t = 4.724 hours (+4.724 hours after sunrise)—0.4 W content heat load.

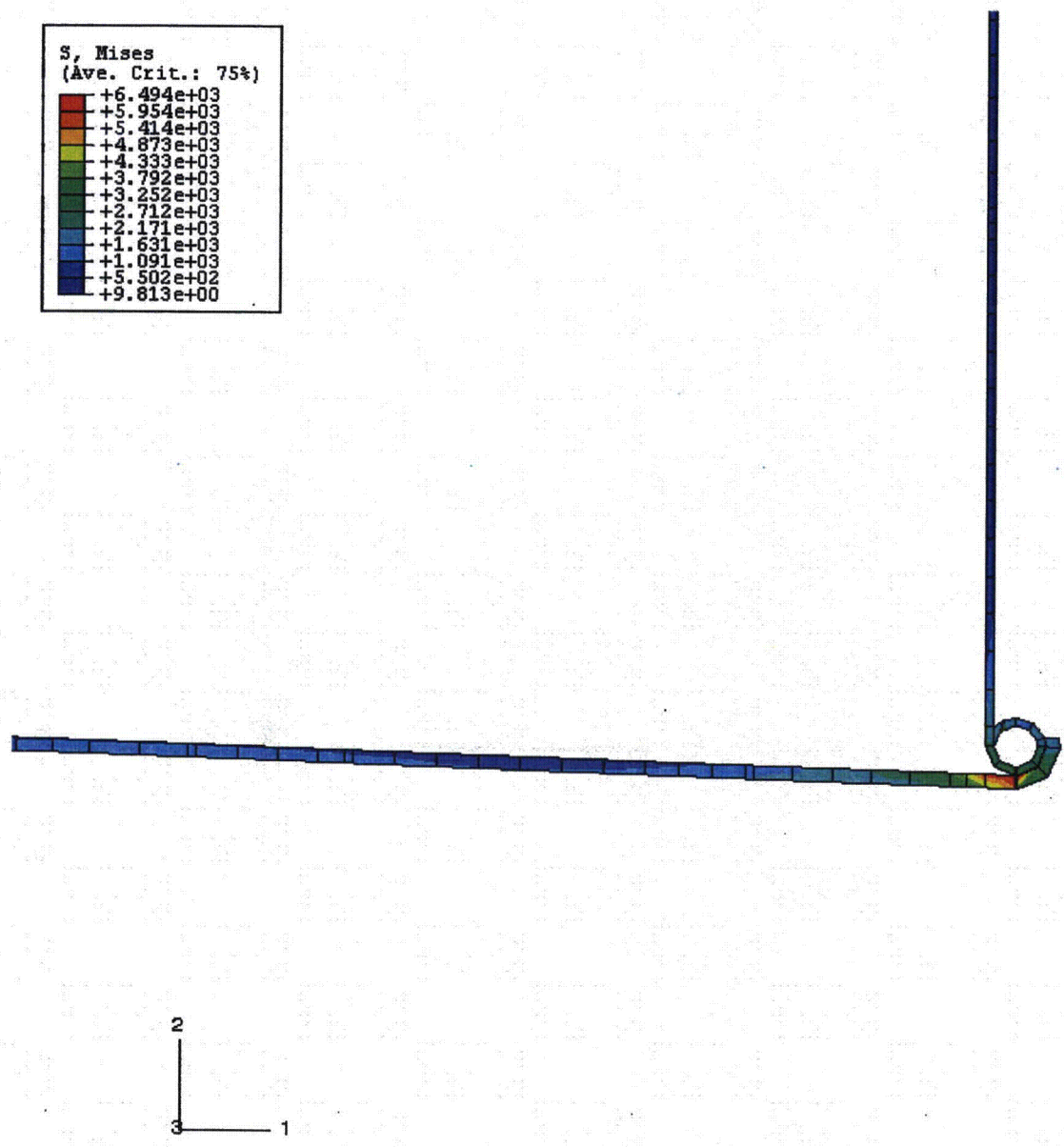


Figure 9. Drum/drum bottom plate Mises stresses (psi) during NCT at t = 12.814 hours (+0.814 hours after sunset)—0.4 W content heat load.

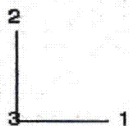
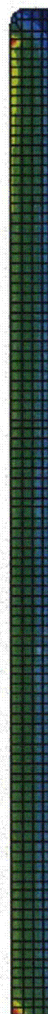
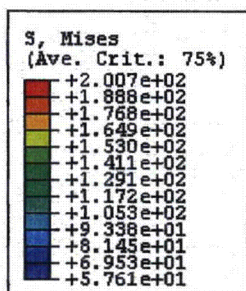


Figure 10. Neutron absorber Mises stresses (psi) during NCT at $t = 12.867$ hours (+0.867 hours after sunset)—0.4 W content heat load.

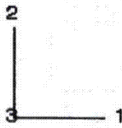
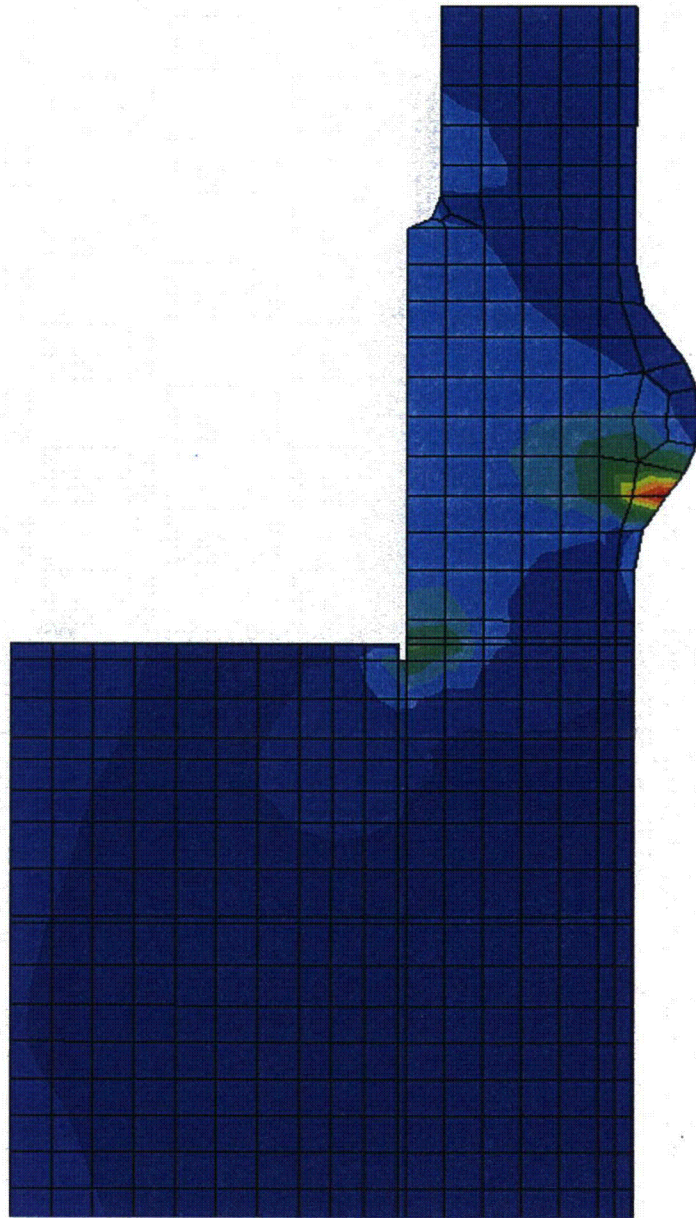
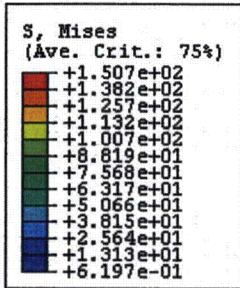


Figure 11. Drum Kaolite Mises stresses (psi) during NCT at t = 3.992 hours (+3.992 hours after sunrise)—0.4 W content heat load.

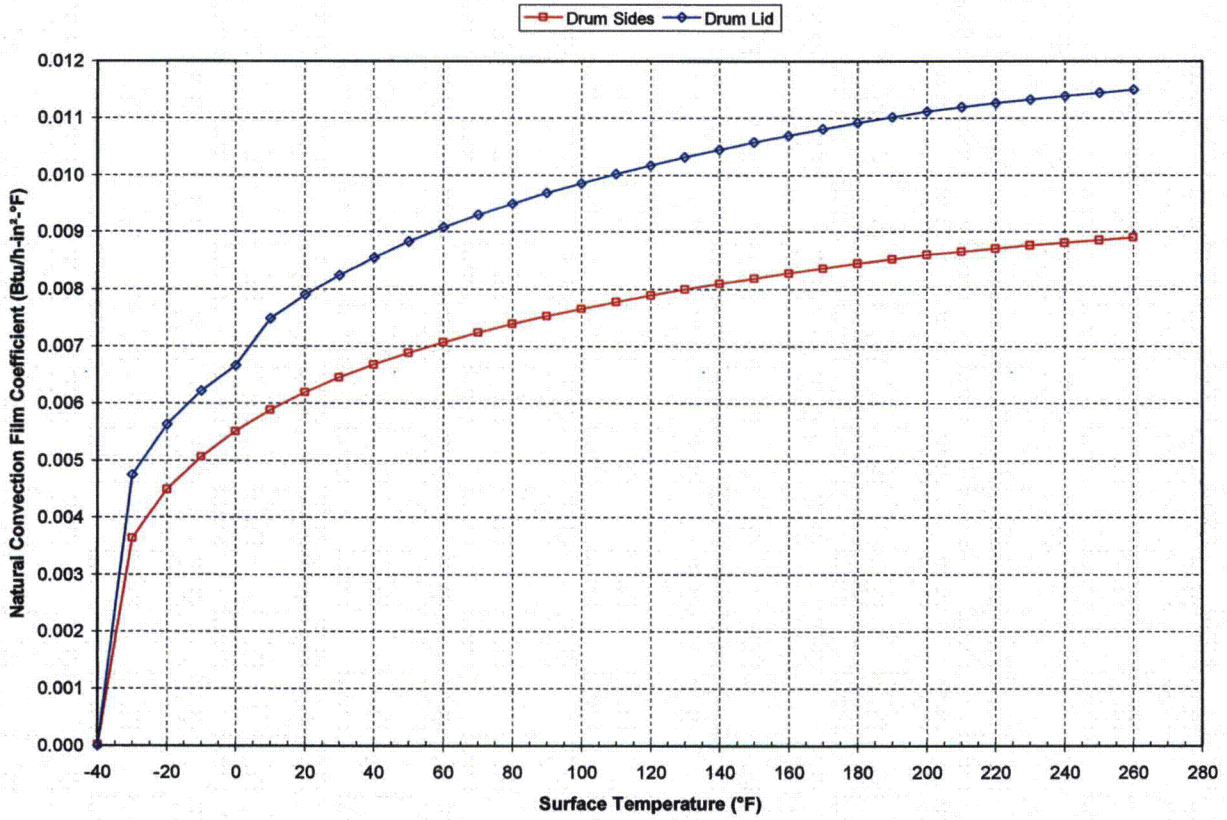


Figure 12. Natural convection film coefficients applied to the drum surfaces during cold conditions.

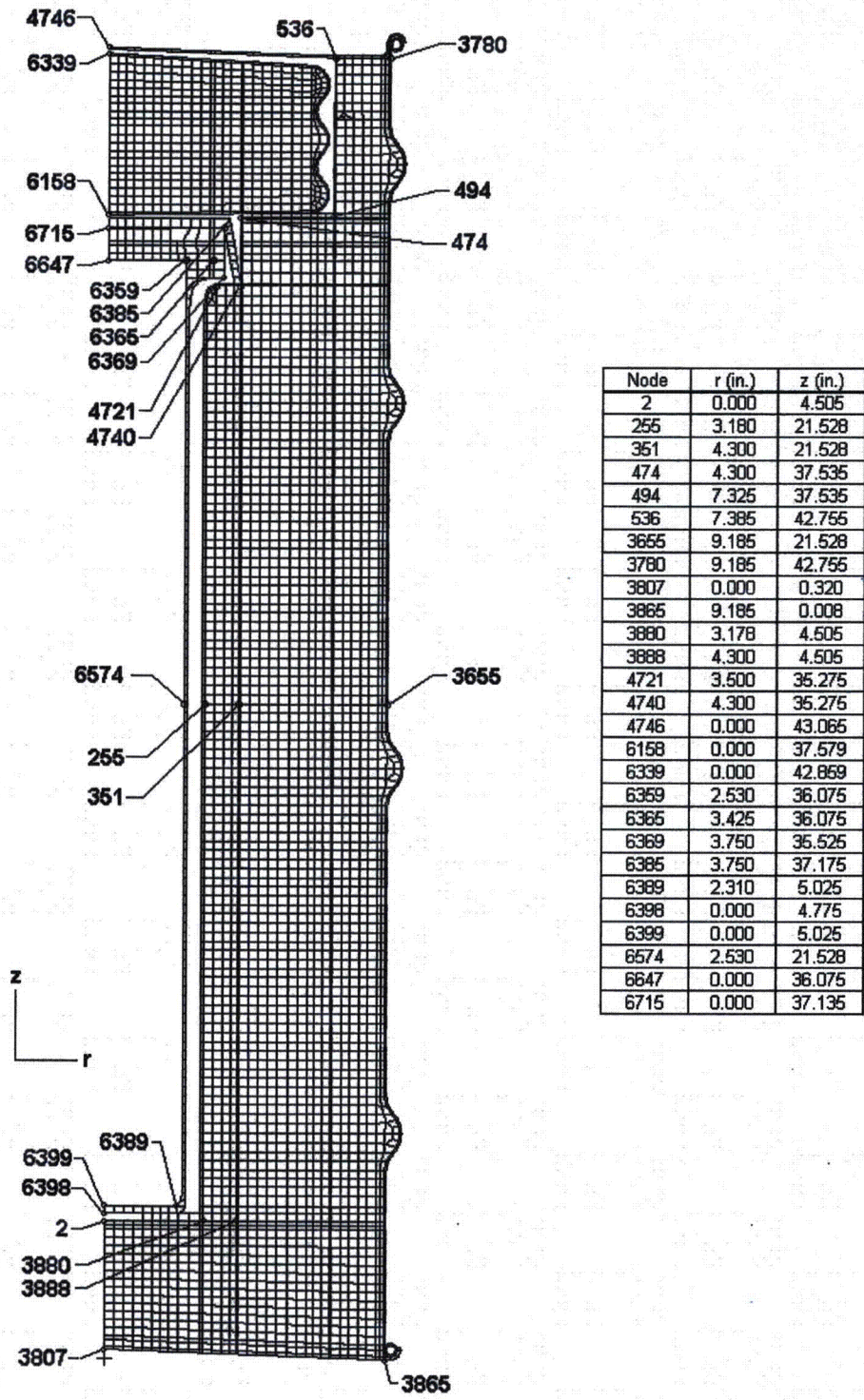


Figure 13. ABAQUS axisymmetric finite element thermal model of the ES-3100 shipping container—nodal locations of interest (elements representing air not shown for clarity).

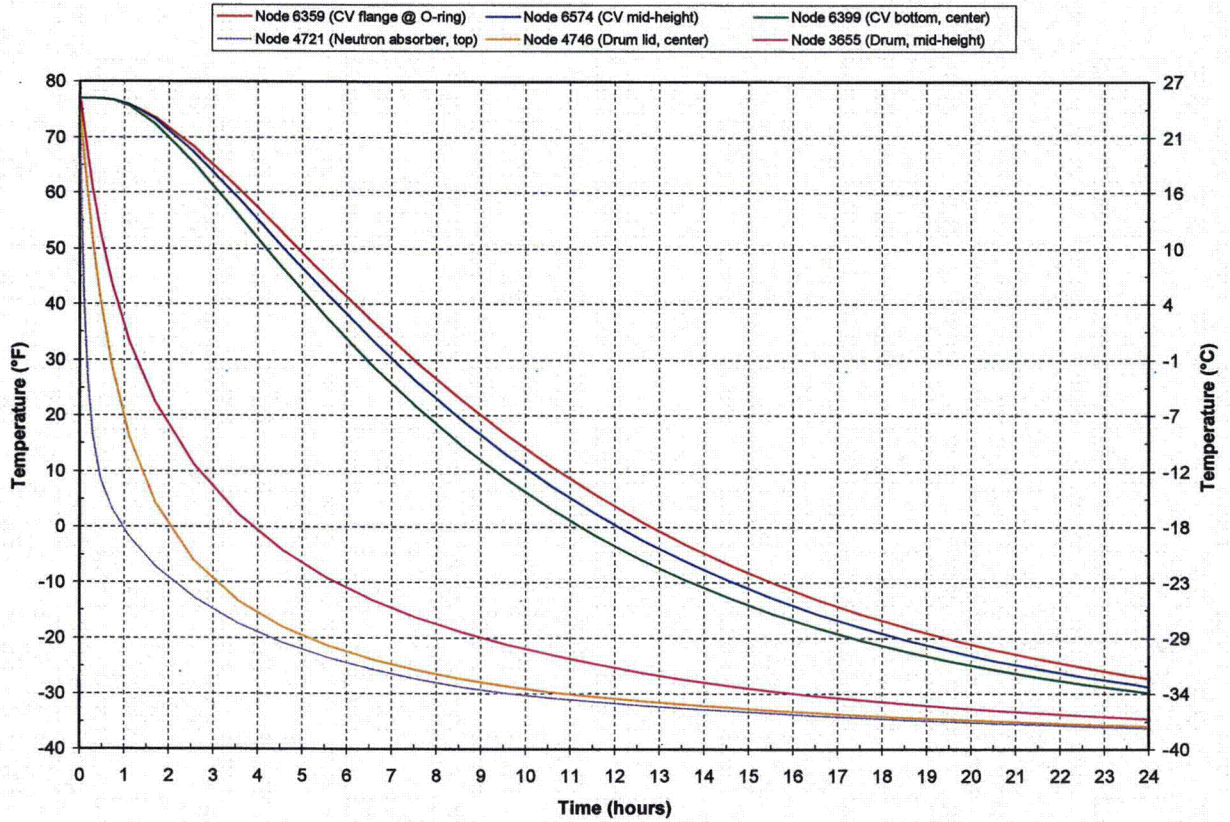


Figure 14. Transient temperatures of the ES-3100 shipping container for cold conditions (no content heat load) see Figure 13 for node locations.

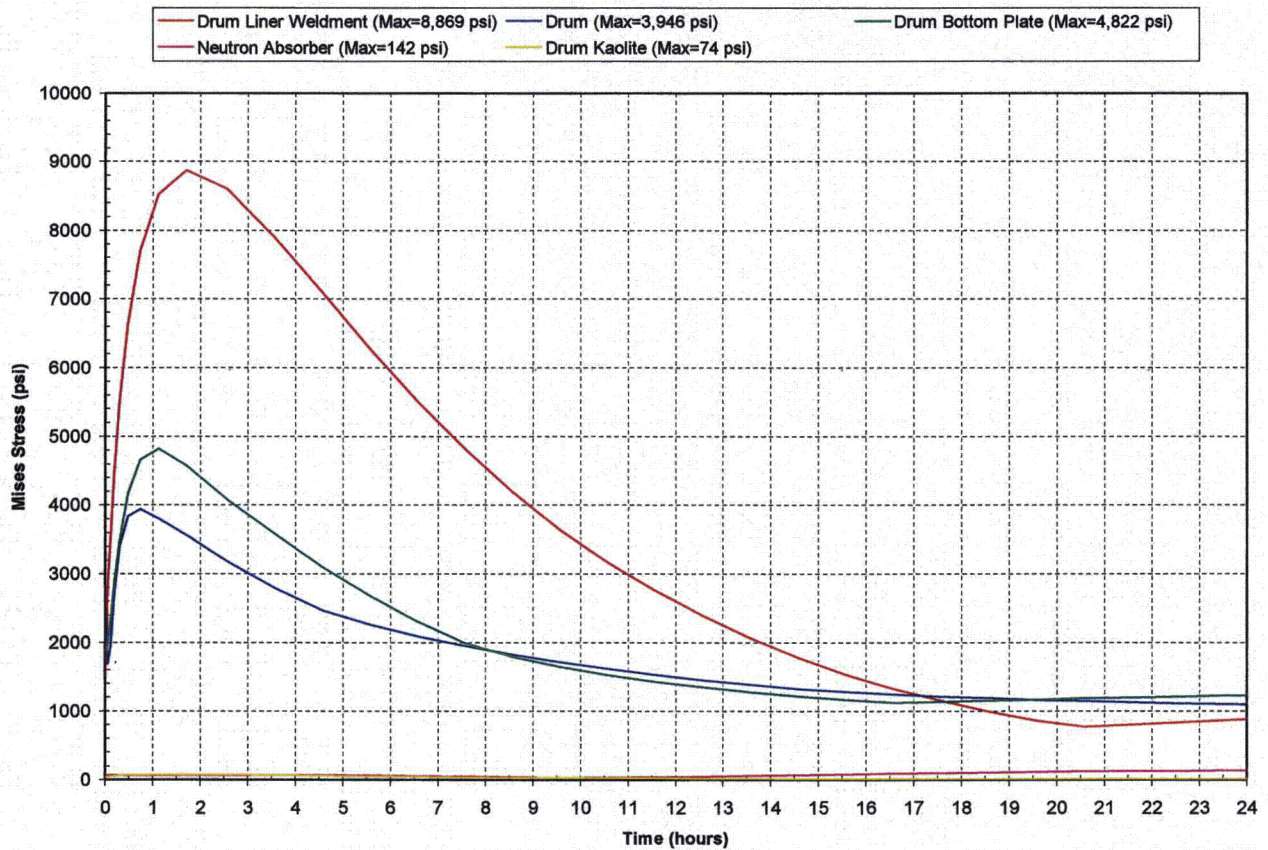


Figure 15. Thermal stresses (Mises) in the ES-3100 shipping container drum body assembly during cold conditions (-40°F ambient temperature)—no content heat load.

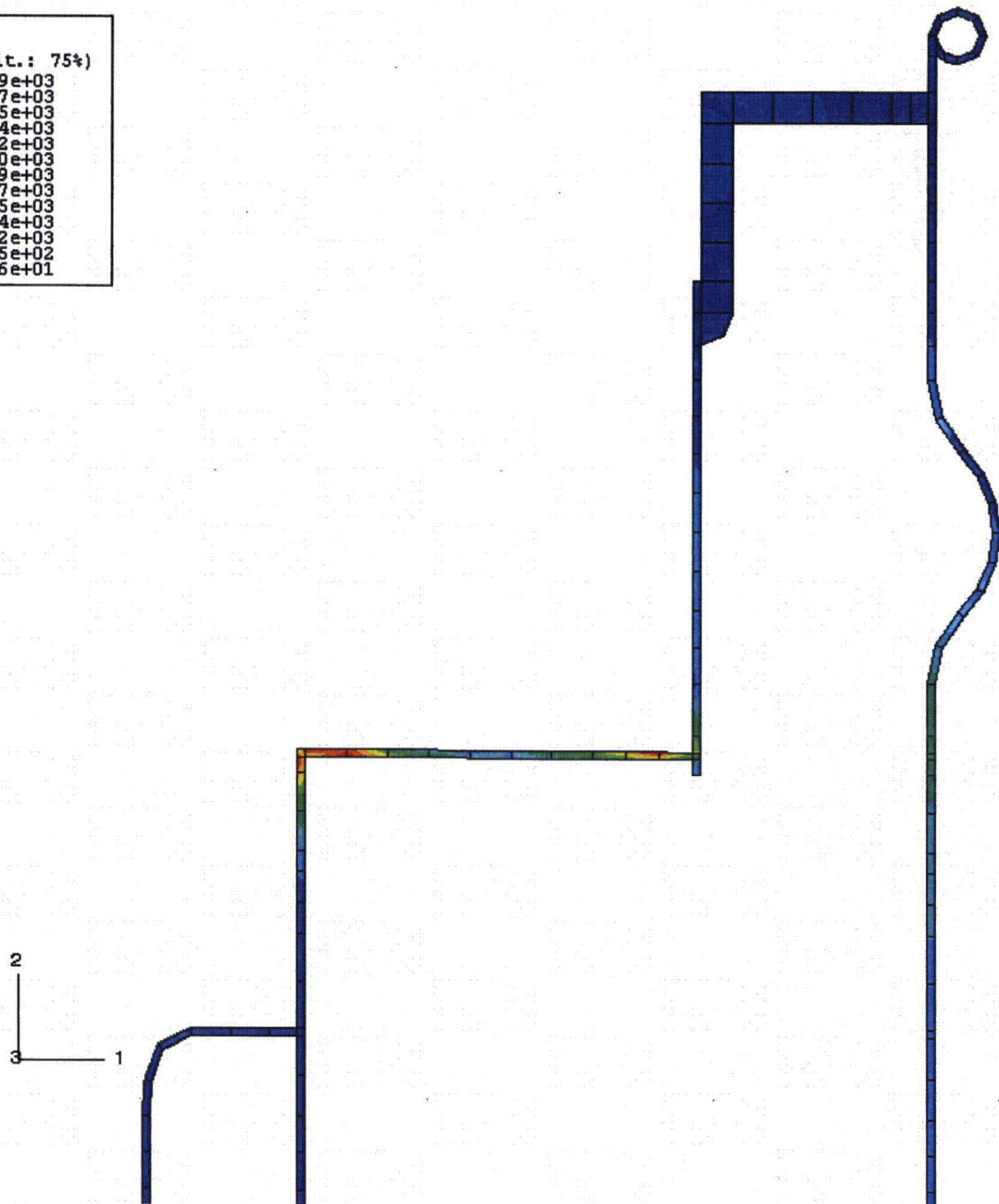
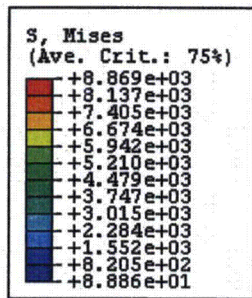


Figure 16. Drum/drum liner weldment Mises stresses (psi) during cold conditions at $t = 1.698$ hours—no content heat load.

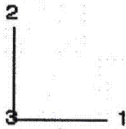
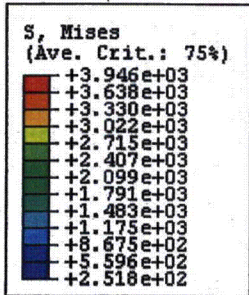
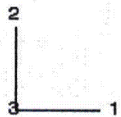
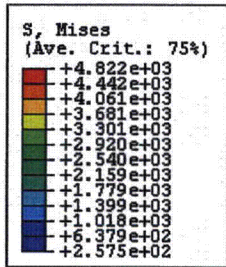


Figure 17. Drum Mises stresses (psi) during cold conditions at $t = 0.726$ hours — no content heat load.



**Figure 18. Drum bottom plate Mises stresses (psi) during cold conditions at $t = 1.115$ hours—
no content heat load.**

APPENDIX 3.6.3 REFERENCES

1. *Packaging and Transportation of Radioactive Materials*, U.S. Nuclear Regulatory Commission, Code of Federal Regulations, Title 10 – Energy, Part 71, January 1, 2004.
2. P. A. Bales, *Thermal Analyses of the ES-3100 Shipping Container for NCT and HAC (Final Design with 277-4 Neutron Absorber)*, DAC-PKG-801699-A002, Rev. 0, BWXT Y-12, January 31, 2005.
3. MSC. Patran 2004, Version 12.0.044, MacNeal Schwendler Corporation, 2004.
4. ABAQUS/CAE, Version 6.4-1, Build ID: 2003_09_29-11.18.28 46457, Abaqus, Inc., 2003.
5. K. D. Handy, *Impact Analysis of ES3100 Design Concepts Using Borobond*, DAC-EA-801699-A001, BWXT Y-12, Oct. 2004.
6. ABAQUS/Standard, Version 6.4-1, 2003_09-11.18.28 46457, Abaqus, Inc.

Appendix 3.6.4

**CONTAINMENT VESSEL PRESSURE DUE TO
NORMAL CONDITIONS OF TRANSPORT FOR THE PROPOSED CONTENTS**

Prepared by: M. L. Goins
B&W Y-12
December 2007

Reviewed by: Paul Bales
B&W Y-12
January 2008

Appendix 3.6.4

CONTAINMENT VESSEL PRESSURE DUE TO NORMAL CONDITIONS OF TRANSPORT FOR THE PROPOSED CONTENTS

The following calculations determine the pressure of the containment vessel when subjected to the tests and conditions of Normal Condition of Transport per 10 CFR 71.71 for the most restrictive convenience can arrangements shipped in the ES-3100. The following packaging arrangements are evaluated for shipment:

1. one shipment will contain six cans with external dimensions of 4.25-in. diameter by 4.875-in. high;
2. one shipment will contain five cans with external dimensions of 4.25-in. diameter by 4.875-in. high and three can spacers, top can will be empty;
3. one shipment will contain three cans with external dimension of 4.25-in. diameter by 8.75-in. high and two can spacers;
4. one shipment will contain three cans with external dimension of 4.25-in. diameter by 10-in. high; and
5. one shipment will contain six cans with external dimension of 3.00-in. diameter by 4.75-in. high;
6. one shipment will contain three polyethylene bottles with external dimensions of 4.94-in. diameter by 8.7-in. high;
7. one shipment will contain three Teflon FEP bottles with external dimensions of 4.69-in. diameter by 9.4-in. high;
8. one shipment will contain a brazed assembly of two cans with final external dimensions of 4.25 in. diameter by 17.50 in. high. An empty can with external dimensions of 4.25 in. diameter by 8.75 in. high will be placed on top of the 17.50 in. high can;
9. one shipment will contain fuel rods, or tubes, or plates greater than 17.00 in. in length. These items are bundled together and protected on both ends with an open-ended can with external dimensions of ≤ 5.0 in. diameter by ≤ 8.75 in. high. Total assembly height will be ≤ 30.5 in. If space is available inside the containment vessel, stainless-steel metal scrubbers will be added on the bottom and top of this assembly or an empty convenience can will be placed on top of the assembly; and
10. one shipment will contain three cans brazed together with external dimensions of 4.25-in. diameter by ~ 30 in. high.

To determine this pressure, the following assumptions have been made:

1. The HEU contents are loaded into convenience cans which are placed inside the ES-3100 containment vessel at standard temperature (T_{amb}) and pressure (P_c) [25°C (77°F) and 101.35 kPa (14.7 psia)] with air at a maximum relative humidity of 100%.
2. The convenience cans are assumed to be sealed, which minimizes the void volume inside the containment vessel.
3. Polyethylene bagging of contents and/or convenience cans is limited to 500 g per containment vessel shipping arrangement.

4. If metal convenience cans are used, the total amount of polyethylene bagging and lifting slings is limited to 500 g per containment vessel shipping arrangement.
5. All offgassing material (polyethylene bagging or bottles, Teflon bottles, silicone pads, lifting slings) is limited to 1490 g for containment vessel arrangement #7 and 845 g for containment vessel arrangement #6.

Applying Dalton's law concerning a mixture of gases, the properties of each component are considered as though each component exists separately at the volume and temperature of the mixture. Therefore, the molar quantities of each constituent inside the containment vessel (i.e., dry air, water vapor, polyethylene bagging, and silicone rubber) must be calculated individually.

To calculate these molar properties, the void volume of the containment vessel must be determined. The volume inside an empty ES-3100 containment vessel was determined from Algor finite element software to be 637.18 in.³ (10,441.51 cm³).

I. Molar quantity determination for dry air and water vapor

According to *Fundamentals of Classical Thermodynamics*,

“Relative humidity (Φ) is defined as the ratio of the mole fraction in the mixture to the mole fraction of vapor in a saturated mixture at the same temperature and total pressure.”

Since the vapor is considered an ideal gas, the definition reduces to the ratio of the partial pressure of the vapor (P_v) as it exists in the mixture to the saturation pressure of the vapor (P_g) at the same temperature.

Therefore,

$$\Phi = P_v / P_g .$$

From the above equation and interpolating the values given in Table A.1.1 of *Fundamentals of Classical Thermodynamics*, the partial pressure of the water vapor at saturation is:

$$\begin{aligned} P_v &= 1.0 (0.464) \text{ psia,} \\ P_v &= 0.464 \text{ psia.} \end{aligned}$$

The partial pressure of the dry air (P_a) in the volume:

$$\begin{aligned} P_a &= P_t - P_v \\ &= 14.7 - 0.464 \\ &= 14.236 \text{ psia.} \end{aligned}$$

From the ideal gas law, the number of water vapor moles and dry air moles in the void volume (V_v) for each containment vessel arrangement (CVA) is calculated as follows:

$$n_v = \frac{P_v \cdot V_v}{R_u \cdot T_{amb} \cdot 12}, \quad n_a = \frac{P_a \cdot V_v}{R_u \cdot T_{amb} \cdot 12}$$

To determine the number of moles, the void volume of the air mixture must be determined. The void volume (V_v) in the containment vessel for each CVA is calculated as follows:

$$V_v = V_{ECV} - V_{SP} - V_{PB} - V_{CC} - V_{CS} - V_{CH}$$

where

- V_{ECV} = volume inside an empty containment vessel,
- V_{SP} = silicone pad volume,
- V_{PB} = polyethylene bagging or lifting sling volume,
- V_{CC} = external volume of the convenience cans or bottles,
- V_{CS} = external volume of the can spacers,
- V_{CH} = external volume of the convenience can handles.

A summary for each CVA is shown in Table 1.

Table 1. Containment vessel void volume for each CVA

CVA	V_{ECV} (in. ³)	V_{SP}^a (in. ³)	V_{PB} (in. ³)	V_{CC} (in. ³)	V_{CS} (in. ³)	V_{CH} (in. ³)	V_v (in. ³)
1 Six 4.875-in.-high cans Seven silicone pads Six can handles	637.18	9.35	30.51	380.47	0.00	1.02	215.83
2 Five 4.875-high cans Nine silicone pads Three Cat 277-4 spacers Eight can handles	637.18	12.03	30.51	317.06	60.60	1.36	215.62
3 Three 8.75-in.- high cans Two Cat 277-4 spacers Six silicone pads Five can handles	637.18	8.02	30.51	345.96	40.40	0.85	211.44
4 Three 10-in.-high cans Four silicone pads Three can handles	637.18	5.35	30.51	396.20	0.00	0.51	204.62
5 Six 4.75 in.-high nickel cans	637.18	0.00	30.51	194.38	0.00	1.02	411.27
6 Three 4.94 in. OD polyethylene bottles	637.18	0.00	30.51	465.33	0.00	0.00	141.34
7 Three 4.69 in. OD Teflon FEP bottles	637.18	0.00	30.51	485.52	0.00	0.00	121.15
8 One 17.5-in.-high can loaded One 8.75-in.-high can empty Three silicone pads Two can handles	This configuration is bounded by CVA #3						
9 Two open-ended cans One empty convenience can with height \leq 8.75-in. Three silicone pads Two can handles	This configuration is bounded by CVA #4 ^b						
10 Three 10 in. cans brazed together Two silicone pads One can handle	This configuration is bounded by CVA #4						

^a This assumes that the internal convenience cans, polyethylene or Teflon FEP bottles, and Cat 277-4 spacer cans are sealed.

^b Although CVA #9 may slightly exceed the height of the combined three 25.4 cm (10 in.) can height (CVA #4), the open-ended cans and contents produce a larger void volume and thereby lower overall pressure inside the containment vessel.

Using the above molar equations, the number of moles for water vapor and dry air in the vessel for each CVA is summarized in Table 2.

Table 2. Water vapor and dry air molar summary for each CVA

CVA	P _a (psia)	P _v (psia)	V _v (in. ³)	R _u (ft-lb/lb-mole·R)	T _{amb} (R)	n _v (lb-mole)	n _a (lb-mole)
1	14.236	0.464	215.83	1545.32	537	1.0057E-05	3.0855E-04
2	14.236	0.464	215.63	1545.32	537	1.0047E-05	3.0826E-04
3 or 8	14.236	0.464	211.44	1545.32	537	9.8522E-06	3.0227E-04
4, 9, or 10	14.236	0.464	204.62	1545.32	537	9.5344E-06	2.9252E-04
5	14.236	0.464	411.27	1545.32	537	1.9163E-05	5.8795E-04
6	14.236	0.464	141.34	1545.32	537	6.5858E-06	2.0206E-04
7	14.236	0.464	121.15	1545.32	537	5.6450E-06	1.7320E-04

II. Molar quantity determination due to offgassing for each containment vessel arrangement

The maximum temperature calculated for the containment vessel is 87.81 °C (190.06 °F). This temperature is assumed to be constant throughout the containment vessel and contents. Therefore, the polyethylene bags, polyethylene bottles, Teflon FEP bottles, and silicone rubber can pads are assumed to be at this temperature.

Using the above calculated results and the specific gas generation of polyethylene bags and silicone rubber pad measurements at temperatures up to 170 °C (338 °F) conducted by the Y-12 Development Division, the amount of gas (V_{bo} and V_{po}) generated due to offgassing of the polyethylene bags and bottles, and silicone rubber can pads at any temperature is estimated by first determining the offgassing volume per unit mass at temperature and multiplying that by the total mass of the bags and can supports inside the containment vessel. Based on testing at a temperature of 93.33 °C (200 °F), no recordable offgassing occurred in the polyethylene bags and bottles, or silicone rubber pad material as documented in Y/DZ-2585, Rev. 2 (Appendix 2.10.4). The data showed that the Teflon FEP material offgassing volume per unit mass (V_{tf}) was conservatively assumed to be 0.25 cm³/g@STP (Appendix 2.10.9). These values are used to determine the offgassing volumes as shown below:

$$V_{po} = W_p \times 0.0 / 16.387 \text{ (in.³)} \quad \text{(offgassing volume of silicone rubber pads)}$$

$$V_{bo} = W_b \times 0.0 / 16.387 \text{ (in.³)} \quad \text{(offgassing volume of polyethylene bags and bottles or lifting sling)}$$

$$V_{tf} = W_{tf} \times 0.25 / 16.387 \text{ (in.³)} \quad \text{(offgassing volume of Teflon bottles)}$$

From the ideal gas law, the number of gas moles in the volume at standard temperature and pressure is as follows:

$$n_{io} = \frac{P_v \cdot V_i}{R_u \cdot T_{amb} \cdot 12}$$

A summary of the results obtained using the above equations for each containment vessel arrangement is presented in Tables 3, 4, and 5.

Table 3. Molar quantity of gas generated due to the silicone rubber pad offgassing

CVA	W _p (g)	V _{po} (in. ³)	P _v (psia)	R _u (ft-lb/lb-mole·R)	T _{amb} (R)	n _{po} (lb-mole)
1	186.74	0.00	14.7	1545.32	537	0.0000E+00
2	240.09	0.00	14.7	1545.32	537	0.0000E+00
3 or 8	160.06	0.00	14.7	1545.32	537	0.0000E+00
4, 9, or 10	106.71	0.00	14.7	1545.32	537	0.0000E+00
5	0.00	0.00	14.7	1545.32	537	0.0000E+00
6	0.00	0.00	14.7	1545.32	537	0.0000E+00
7	0.00	0.00	14.7	1545.32	537	0.0000E+00

Table 4. Molar quantity of gas generated due to the polyethylene bag, sling and bottle offgassing

CVA	W _b (g)	V _{bo} (in. ³)	P _v (psia)	R _u (ft-lb/lb-mole·R)	T _{amb} (R)	n _{bo} (lb-mole)
1	500.00	0.00	14.7	1545.32	537	0.0000E+00
2	500.00	0.00	14.7	1545.32	537	0.0000E+00
3 or 8	500.00	0.00	14.7	1545.32	537	0.0000E+00
4, 9, or 10	500.00	0.00	14.7	1545.32	537	0.0000E+00
5	500.00	0.00	14.7	1545.32	537	0.0000E+00
6	845.00	0.00	14.7	1545.32	537	0.0000E+00
7	500.00	0.00	14.7	1545.32	537	0.0000E+00

Table 5. Molar quantity of gas generated due to the Teflon bottle offgassing

CVA	W _{tf} (g)	V _{tf} (in. ³)	P _v (psia)	R _u (ft-lb/lb-mole·R)	T _{amb} (R)	n _{tf} (lb-mole)
7	990.00	15.10	14.7	1545.32	537	2.2296E-05

III. Total pressure due to offgassing and NCT temperatures inside the containment vessel

The total pressure of the mixture at 87.81 °C (190.06 °F), P_T, for each containment vessel arrangement is the sum of each of the previously calculated molar quantities. Table 6 summarizes the molar constituents and total pressure of each containment vessel arrangement. The following equation is used to calculate the final containment vessel pressure:

$$P_{87.81^{\circ}\text{C}} = (\sum n_i \cdot R \cdot T \cdot 12) / V_{\text{GMV}}$$

where

n_i = individual molar quantity for each gas,
 T = average gas temperature = 87.81 °C (190.06 °F),
 V_{GMV} = V_v = gas mixture volume.

Table 6. Total pressure inside the containment vessel at 87.81°C (190.06°F) ^a

CVA	n _a (lb-mole)	n _v (lb-mole)	n _{po} (lb-mole)	n _{bo} (lb-mole)	n _{tf} (lb-mole)	n _T (lb-mole)	P _T (psia)
1	3.0855E-04	1.0057E-05	0.0000E+00	0.0000E+00	0.0000E+00	3.1861E-04	17.786
2	3.0826E-04	1.0047E-05	0.0000E+00	0.0000E+00	0.0000E+00	3.1831E-04	17.786
3 or 8	3.0227E-04	9.8522E-06	0.0000E+00	0.0000E+00	0.0000E+00	3.1212E-04	17.786
4, 9, or 10 ^b	2.9252E-04	9.5344E-06	0.0000E+00	0.0000E+00	0.0000E+00	3.0205E-04	17.786
5	1.9163E-05	5.8795E-04	0.0000E+00	0.0000E+00	0.0000E+00	6.0711E-04	17.786
6	2.0206E-04	6.5858E-06	0.0000E+00	0.0000E+00	0.0000E+00	2.0865E-04	17.786
7	5.6450E-06	1.7320E-04	0.0000E+00	0.0000E+00	2.2296E-05	2.0114E-04	20.004

^a This assumes that the internal convenience cans, polyethylene or Teflon FEP bottles, and Cat 277-4 spacer cans are sealed.

^b Although CVA #9 may slightly exceed the height of the combined three 25.4 cm (10 in.) can height (CVA #4), the open-ended cans and contents produce a larger void volume and thereby lower overall pressure inside the containment vessel.

At -40°C (-40°F), the partial pressure of the water vapor is conservatively assumed to be zero. Therefore, the final pressure of the mixture at -40°C (-40°F) is calculated according to the ideal gas law based solely on the partial pressure of the air.

$$\frac{P_1 V_1}{T_1} = \frac{P_2 V_2}{T_2}$$

where

$$\begin{aligned} P_1 &= 14.236 \text{ psi,} \\ T_1 &= 77^\circ\text{F} &= 536.67 \text{ R,} \\ T_2 &= -40^\circ\text{F} &= 419.67 \text{ R,} \\ V_1 &= V_2. \end{aligned}$$

Rearranging and solving for P₂,

$$\begin{aligned} P_2 &= P_1 (T_2/T_1), \\ P_2 &= (14.236)(419.67/536.67) = 11.13 \text{ psia.} \end{aligned}$$

Appendix 3.6.5

**CONTAINMENT VESSEL PRESSURE DUE TO
HYPOTHETICAL ACCIDENT CONDITIONS FOR THE PROPOSED CONTENTS**

Prepared by: M. L. Goins
B&W Y-12
December 2007

Reviewed by: Paul Bales
B&W Y-12
January 2008

Appendix 3.6.5

CONTAINMENT VESSEL PRESSURE DUE TO HYPOTHETICAL ACCIDENT CONDITIONS FOR THE PROPOSED CONTENTS

The following calculations determine the pressure of the containment vessel when subjected to the tests and conditions of Hypothetical Accident Conditions per 10 CFR 71.73 for the most restrictive convenience can arrangements shipped in the ES-3100 package. The following packaging arrangements are evaluated for shipment:

1. one shipment will contain six cans with external dimensions of 4.25-in. diam by 4.875-in. high;
2. one shipment will contain five cans with external dimensions of 4.25-in. diam by 4.875-in. high and three can spacers, the top can is empty;
3. one shipment will contain three cans with external dimensions of 4.25-in. diam by 8.75-in. high and 2 can spacers;
4. one shipment will contain three cans with external dimensions of 4.25-in. diam by 10-in. high;
5. one shipment will contain six nickel cans with external dimensions of 3.00-in. diam by 4.75-in. high;
6. one shipment will contain three polyethylene bottles with external dimensions of 4.94-in. diam by 8.7-in. high;
7. one shipment will contain three Teflon FEP bottles with external dimensions of 4.69-in. diam by 9.4-in. high;
8. one shipment will contain a brazed assembly of two cans with final external dimensions of 4.25 in. diameter by 17.50 in. high. An empty can with external dimensions of 4.25 in. diameter by 8.75 in. high will be placed on top of the 17.50 in. high can;
9. one shipment will contain fuel rods, or tubes, or plates greater than 17.00 in. in length. These items are bundled together and protected on both ends with an open-ended can with external dimensions of ≤ 5.0 in. diameter by ≤ 8.75 in. high. Total assembly height will be ≤ 30.5 in. If space is available inside the containment vessel, stainless-steel metal scrubbers will be added on the bottom and top of this assembly or an empty convenience can will be placed on top of this assembly; and
10. one shipment will contain three cans brazed together with external dimensions of 4.25-in. diameter by ~ 30 in. high.

To determine this pressure, the following assumptions have been made:

1. The highly enriched uranium (HEU) contents are loaded into convenience cans and placed inside the ES-3100 containment vessel at standard temperature [25°C (77°F)] and at the maximum normal operating pressure (see Table 5 of Appendix 3.6.4) with air at a maximum relative humidity of 100%.

2. The convenience cans are assumed to be sealed to minimize the void volume inside the containment vessel.
3. Polyethylene bagging of contents and/or convenience containers is limited to 500 g per containment vessel shipping arrangement.
4. If metal convenience cans are used, the total amount of polyethylene bagging and lifting slings is limited to 500 g per containment vessel shipping arrangement.
5. All offgassing material (polyethylene bagging or bottles, Teflon bottles, silicone pads, lifting slings) is limited to 1490 g for containment vessel arrangement #7 and 845 g for containment vessel arrangement #6.

Applying Dalton's law concerning a mixture of gases, the properties of each component are considered as though each component exists separately at the volume and temperature of the mixture. Therefore, the molar quantities of each constituent inside the containment vessel (i.e., dry air, water vapor, polyethylene bagging and bottles, silicone rubber pads, and teflon bottles) must be calculated individually.

To calculate these molar properties, the void volume of the containment vessel must be determined. The volume inside an empty ES-3100 containment vessel was determined from Algor finite element software to be 637.18 in.³ (10,441.51 cm³).

I. Molar quantity determination based on MNOP

Table 1. Total pressure inside the containment vessel at 87.81 °C (190.06 °F) ^a

CVA	n _a (lb-mole)	n _v (lb-mole)	n _{po} (lb-mole)	n _{bo} (lb-mole)	n _{tr} (lb-mole)	n _T (lb-mole)	P _T (psia)
1	3.0855E-04	1.0057E-05	0.0000E+00	0.0000E+00	0.0000E+00	3.1861E-04	17.786
2	3.0826E-04	1.0047E-05	0.0000E+00	0.0000E+00	0.0000E+00	3.1831E-04	17.786
3	3.0227E-04	9.8522E-06	0.0000E+00	0.0000E+00	0.0000E+00	3.1212E-04	17.786
4	2.9252E-04	9.5344E-06	0.0000E+00	0.0000E+00	0.0000E+00	3.0205E-04	17.786
5	1.9163E-05	5.8795E-04	0.0000E+00	0.0000E+00	0.0000E+00	6.0711E-04	17.786
6	2.0206E-04	6.5858E-06	0.0000E+00	0.0000E+00	0.0000E+00	2.0865E-04	17.786
7	5.6450E-06	1.7320E-04	0.0000E+00	0.0000E+00	2.2296E-05	2.0114E-04	20.004
8	This configuration is bounded by CVA #3						
9	This configuration is bounded by CVA #4 ^b						
10	This configuration is bounded by CVA #4						

^a This assumes that the internal convenience cans, polyethylene or Teflon FEP bottles, and Cat 277-4 spacer cans are sealed.

^b Although CVA #9 may slightly exceed the height of the combined three 25.4 cm (10 in.) can height (CVA #4), the open-ended cans and contents produce a larger void volume and thereby lower overall pressure inside the containment vessel.

To use the maximum normal operating pressure at standard temperature, the number of lb-mole of gas needs to be increased using the following equation:

$$n_{\text{MNOP}} = \frac{P_T \cdot V_v}{R_u \cdot T_{\text{amb}} \cdot 12}$$

Using the above molar equations, the total number of moles is summarized in Table 2.

Table 2. Molar summary at MNOP and 25°C (77°F)

CVA	P _T (psia)	V _v (in. ³)	R _u (ft-lb/lb-mole·R)	T _{amb} (R)	n _{MNOP} (lb-mole)
1	17.786	215.83	1545.32	537	3.8549E-04
2	17.786	215.63	1545.32	537	3.8514E-04
3 or 8	17.786	211.44	1545.32	537	3.7765E-04
4, 9, or 10	17.786	204.62	1545.32	537	3.6547E-04
5	17.786	411.27	1545.32	537	7.3457E-04
6	17.786	141.34	1545.32	537	2.5245E-04
7	20.004	121.15	1545.32	537	2.4337E-04

II. Molar quantity determination due to offgassing for each containment vessel arrangement

To determine the maximum pressure inside the containment vessel as a result of thermal testing, the average adjusted gas temperature must be calculated based on the results shown in Sect. 3.5.3. The approach used is to divide the containment vessel volume into three distinct equal regions and then average the three together. The first volume is represented by the gas adjacent to the containment vessel lid and flange region and the top most convenience can. Based on the temperature recorded near the O-rings [116.11°C (241°F)] and the temperature recorded on the external surface of the convenience can [98.89°C (210°F)], the average temperature of the gas in this region is 107.50°C (225.50°F). Using the temperature adjustment of 25.11°C (45.20°F) for this region, the adjusted average temperature in the first region is 132.61°C (270.70°F). The second volume is represented by the gas adjacent to the second convenience can from the top. Based on the temperature recorded on the containment vessel wall and convenience can [92.78°C (199°F)], the average temperature of gas in this region is 92.78°C (199°F). Using the temperature adjustment of 27.89°C (50.20°F) for this region, the adjusted average temperature in the second region is 120.67°C (249.20°F). The third and final volume is represented by the gas adjacent to the bottom convenience can. Again, based on the convenience can temperature [87.78°C (190°F)] and the containment vessel end cap temperature [98.89°C (210°F)], the average temperature of gas in this region is 93.33°C (200°F). Using the temperature adjustment of 24.94°C (44.90°F) for this region, the adjusted average temperature in the third region is 118.28°C (244.90°F). Averaging these three temperatures, an average adjusted gas temperature of 123.85°C (254.93°F) is determined for the containment vessel.

Using the above calculated results and the specific gas generation of polyethylene bags and silicone rubber pads measurements at temperatures up to 170°C (338°F) conducted by the Y-12 Development Division (Appendix 2.10.4), the amount of gas generated due to offgassing of the silicone rubber can pads, the polyethylene bags and bottles, and the Teflon FEP bottles at 123.85°C (254.93°F), (V_{po}, V_{bo}, and V_{tf}) is estimated by first determining the offgassing volume per unit mass at temperature

and multiplying that by the total mass of the bags, bottles, slings, and silicone rubber can supports inside the containment vessel. Based on testing at an approximate temperature of 141.11 °C (286.00 °F), values of ~7.0 and ~0.8 cm³/g @STP for the polyethylene bagging and bottles, and silicone rubber pads, respectively, were taken from the curves for the offgassing volume per unit mass as documented in Y/DZ-2585, Rev. 2 (Appendix 2.10.4). The data showed that the Teflon FEP material offgassing volume per unit mass (V_{tf}) was conservatively assumed to be 0.25 cm³/g@STP (Appendix 2.10.9). These values are used to determine the offgassing volume as shown below:

$$V_{po} = W_p \times 0.8 / 16.387 \text{ (in.}^3\text{)} \quad \text{(offgassing volume of silicone rubber pads)}$$

$$V_{bo} = W_b \times 7.0 / 16.387 \text{ (in.}^3\text{)} \quad \text{(offgassing volume of polyethylene bags, bottles, and lifting sling)}$$

$$V_{tf} = W_{tf} \times 0.25 / 16.387 \text{ (in.}^3\text{)} \quad \text{(offgassing bottles of Teflon FEP bottles)}$$

From the ideal gas law, the number of gas moles in the volume is as follows:

$$n_i = \frac{P_v \cdot V_i}{R_u \cdot T_{amb} \cdot 12}$$

A summary of the results obtained using the above equations for each containment vessel arrangement is presented in Tables 3, 4, and 5.

Table 3. Molar quantity of gas generated due to the silicone rubber pad offgassing

CVA	W_p (g)	V_{po} (in. ³)	P_v (psia)	R_u (ft-lb/lb-mole-R)	T_{amb} (R)	n_{po} (lb-mole)
1	186.74	9.12	14.7	1545.32	537	1.3458E-05
2	240.09	11.72	14.7	1545.32	537	1.7302E-05
3 or 8	160.06	7.81	14.7	1545.32	537	1.1535E-05
4, 9, or 10	106.71	5.21	14.7	1545.32	537	7.6901E-06
5	0.00	0.00	14.7	1545.32	537	0.0000E+00
6	0.00	0.00	14.7	1545.32	537	0.0000E+00
7	0.00	0.00	14.7	1545.32	537	0.0000E+00

Table 4. Molar quantity of gas generated due to polyethylene bag, sling, and bottle offgassing

CVA	W_b (g)	V_{bo} (in. ³)	P_v (psia)	R_u (ft-lb/lb-mole-R)	T_{amb} (R)	n_{bo} (lb-mole)
1	500.00	213.58	14.7	1545.32	537	3.1529E-04
2	500.00	213.58	14.7	1545.32	537	3.1529E-04
3 or 8	500.00	213.58	14.7	1545.32	537	3.1529E-04
4, 9, or 10	500.00	213.58	14.7	1545.32	537	3.1529E-04
5	500.00	213.58	14.7	1545.32	537	3.1529E-04
6	845.00	360.96	14.7	1545.32	537	5.3284E-04
7	500.00	213.58	14.7	1545.32	537	3.1529E-04

Table 5. Molar quantity of gas generated due to the Teflon FEP bottle offgassing

CVA	W _{tr} (g)	V _{tr} (in. ³)	P _v (psia)	R _u (ft-lb/lb-mole·R)	T _{amb} (R)	n _{tr} (lb-mole)
7	990.00	15.10	14.7	1545.32	537	2.2296E-05

III. Total pressure due to offgassing and HAC temperatures inside the containment vessel

The total pressure of the mixture at 123.85°C (254.93°F), P_T, for each containment vessel arrangement is the sum of each of the previously calculated molar quantities. Table 6 summarizes the molar constituents and total pressure of each containment vessel arrangement. The following equation is used to calculate the final containment vessel pressure:

$$P_{123.85^{\circ}\text{C}} = (\sum n_i \cdot R \cdot T \cdot 12) / V_{\text{GMV}}$$

where

- n_i = individual molar quantity for each gas,
- T = average gas temperature = 123.85°C (254.93°F),
- V_{GMV} = V_v = gas mixture volume.

Table 6. Total pressure inside the containment vessel at 123.85°C (254.93°F) ^a

CVA	n _{MNOP} (lb-mole)	n _{po} (lb-mole)	n _{bo} (lb-mole)	n _{tr} (lb-mole)	n _T (lb-mole)	P _T (psia)
1	3.8549E-04	1.3458E-05	3.1529E-04	0.0000E+00	7.1424E-04	43.852
2	3.8514E-04	1.7302E-05	3.1529E-04	0.0000E+00	7.1773E-04	44.110
3 or 8	3.7765E-04	1.1535E-05	3.1529E-04	0.0000E+00	7.0448E-04	44.151
4, 9, or 10 ^b	3.6547E-04	7.6901E-06	3.1529E-04	0.0000E+00	6.8845E-04	44.585
5	7.3457E-04	0.0000E+00	3.1529E-04	0.0000E+00	1.0499E-03	33.829
6	2.5245E-04	0.0000E+00	5.3284E-04	0.0000E+00	7.8529E-04	73.625
7	2.4337E-04	0.0000E+00	3.1529E-04	2.2296E-05	5.8096E-04	63.545

^a This assumes that the internal convenience cans, polyethylene or Teflon FEP bottles, and Cat 277-4 spacer cans are sealed.

^b Although CVA #9 may slightly exceed the height of the combined three 25.4 cm (10 in.) can height (CVA #4), the open-ended cans and contents produce a larger void volume and thereby lower overall pressure inside the containment vessel.

Appendix 3.6.6

SILICONE RUBBER THERMAL PROPERTIES FROM THERM 1.2 DATABASE

The thermal properties for silicone rubber used in the thermal analyses of the ES-3100 shipping container were obtained from the THERM 1.2 Thermal Properties Database by R. A. Bailey. Since THERM 1.2 is not a publicly available program, screen captures from THERM 1.2 of the data for silicone rubber are presented in Figures 1 and 2 in English and SI units, respectively.

silicone rubber, medium k (see ref 5)		
Density	.04696548	lb/in**3
Specific Heat	.3	Btu/lb°F
Conductivity	.01612725	Btu/hr in°F
Maximum Material Temp.	545.0	°F
silicone rubber, medium k (see ref 5)		
References:		
fleming p	private collection of plastics data	1968
	materials engr matl selector issue	1967
	metals handbook 8th ed	1961
moyer j	private collection of thermal data	1968
Material properties quality		
Density	-	Good data, or no way of estimating quality.
Specific Heat	-	Poor or conflicting data. Used best or average.
Conductivity	-	Poor or conflicting data. Used best or average.
Transition Temperature	-	Good data, or no way of estimating quality.
Latent Heat	-	No data. Made no estimate.
Specific Heat Tables	-	No data. Made no estimate.
Conductivity Tables	-	No data. Made no estimate.

Figure 1. Silicone rubber thermal properties from Therm 1.2 (English units).

silicone rubber, medium k (see ref 5)		

Density	1300.0	kg/m**3
Specific Heat	1255.2	J/kg°K
Conductivity	.33472	J/sec m°K
Maximum Material Temp	558.15	°K
silicone rubber, medium k (see ref 5)		

References:		
fleming p	private collection of plastics data	1968
	materials engr matl selector issue	1967
	metals handbook 8th ed	1961
moyer j	private collection of thermal data	1968
Material properties quality		
Density	-	Good data, or no way of estimating quality.
Specific Heat	-	Poor or conflicting data. Used best or average.
Conductivity	-	Poor or conflicting data. Used best or average.
Transition Temperature	-	Good data, or no way of estimating quality.
Latent Heat	-	No data. Made no estimate.
Specific Heat Tables	-	No data. Made no estimate.
Conductivity Tables	-	No data. Made no estimate.

Figure 2. Silicone rubber thermal properties from Therm 1.2 (SI units).

SECTION 3 REFERENCES

10 CFR 71, *Packaging and Transportation of Radioactive Material*, Jan. 1, 2007.

ABAQUS/Standard, Version 6.4-1, 2003-09-29-11.18.28 46457, Abaqus, Inc., 2003.

ASME Boiler and Pressure Vessel Code, An American National Standard, Materials, Sect. II, *Materials*, Part D, American Society of Mechanical Engineers, New York, 2001 ed. with 2002 and 2003 addenda.

ASME Boiler and Pressure Vessel Code, An American National Standard, Rules for Construction of Nuclear Power Facility Components, Sect. III, Div. 1, Subsection NB, American Society of Mechanical Engineers, New York, 2001 ed. with 2002 and 2003 addenda.

ASME Boiler and Pressure Vessel Code, An American National Standard, Welding and Brazing Qualifications, Sect. IX, American Society of Mechanical Engineers, New York, 2001 ed. with 2002 and 2003 addenda.

ASTM D-2000, *Standard Classification System for Rubber Products in Automotive Applications*, American Society for Testing and Materials, Philadelphia, current revision.

ASTM E-2230-02, *Standard Practice for Thermal Qualification of Type B Packages for Radioactive Materials*, ASTM International, West Conshohocken, Pa., 2002.

Bailey, R. A., *Strain—A Material Database*, Lawrence Livermore Natl. Lab., Nov. 18, 1987.

Bailey, R. A., *THERM 1.2, A Thermal Properties DataBase for the IBM PC*, Lawrence Livermore Natl. Lab., Nov. 18, 1987.

Byington, G. A., *Vibration Test Report of the ES-2M Shipping Package*, GAB1296-2, Lockheed Martin Energy Systems, Inc., Oak Ridge Y-12 Plant, Sept. 3, 1997.

Incropera, F. P., and D. P. DeWitt, *Fundamentals of Heat and Mass Transfer*, 2nd ed., John Wiley & Sons, New York, 1985.

MIL-HDBK-5H, *Metallic Materials and Elements for Aerospace Vehicle Structures*, Dec. 1 1998.

MSC.Patran, Version 12.0.044, MacNeal Schwendler Corp., 2004.

OO-PP-986, rev. D, *Procurement Specification for 70A Durometer Preformed Packing (O-rings)*, Lockheed Martin Energy Systems, Inc., Oak Ridge Y-12 Plant, Jan. 26, 1999.

Parker O-ring Handbook, Catalog ORD 5700A/US, Parker Hannifin Corp., O-ring Div., Lexington, Ky., 2001.

SG 140.1, *Combination Test Analysis/Method Used to Demonstrate Compliance to DOE Type B Packaging Thermal Test Requirements (30 Minute Fire Test)*, U.S. DOE, Albuquerque Field Office, Nuclear Explosive Safety Division, Feb. 10, 1992.

Van Wylen, G. J., and R. E. Sonntag, *Fundamentals of Classical Thermodynamics*, 2d ed., John Wiley & Sons, Inc., New York, 1973.

